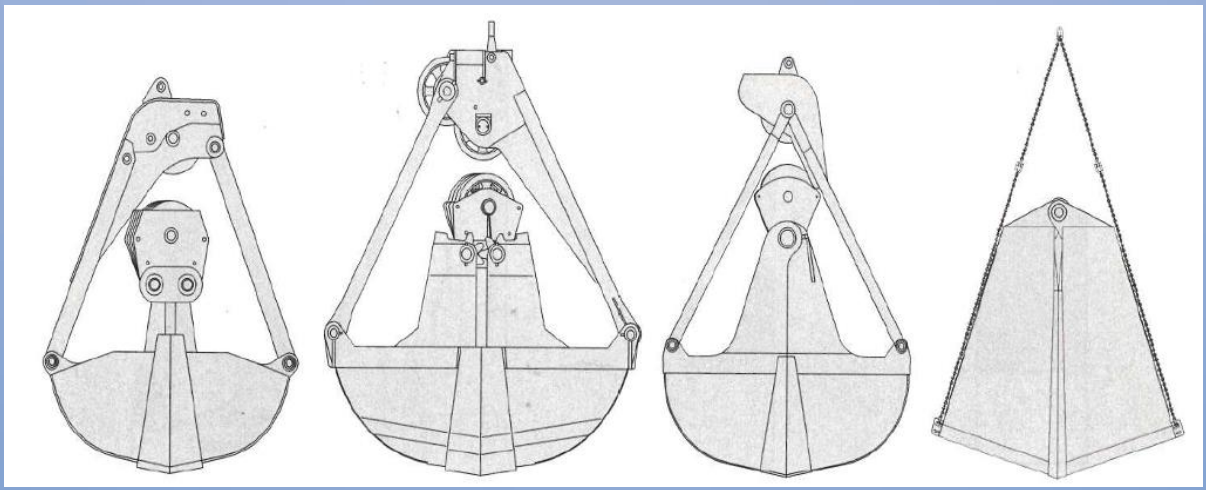

Clamshell Dredge bucket improvement for Clay Production

Clamshell bucket concepts and adhesive strength study of natural field clays

BSc. Thomas A. A. Combe
May 25th, 2015
Great Lakes Dredge & Dock and Delft University of Technology

Preface

This study has been a challenging and exciting to have done. Starting in May of 2014 and completing it in May of 2015. The time spend in States and Chicago area have changed me for life and I'm very thank full for the opportunity granted by Great Lakes Dredge & Dock and the support and supervision of Robert Ramsdall, Sape Miedema and Cees van Rhee. I have evolved over time in academic level, but also on personal level.

At Great Lakes Dredge & Dock I have had the possibility to work with professional and nice people. The technical drawings of the adhesive test-up were made by Justin Rench. Without him my experiments at University Texas A&M would not have been possible.

Also my thanks goes out to all that have supported me at University Texas A&M and wanted to mention Bob Randell, John Reed, Yuanzhe Zhi, Madhuri Murali and Ryan Beemer for their help in the Ocean Engineering laboratory and Geotechnical laboratory.

I want to dedicate my first paper to my mother, Leonie van der Bruggen, for years of support and unconditional love. The completion of my bachelors and masters at Delft University of Technology has been supported by my aunt and uncle, José van der Burggen and Wybe Taekema. Without them my time as a student would be still searching for the right direction to sail in and deciding where to focus on.

Abstract

Especially for the dredging industry in the United States of America and the leading dredging company Great Lakes Dredge & Dock Company the clamshell dredge is a commonly used dredge tool. The aim of this study was production [m^3/s] optimization of the clamshell bucket for stiffer clays. Different aspects of clamshell bucket geometry to clay experiments and bucket concepts are discussed and presented in the report.

The approach of tackling this challenge was first evaluating four main elements of the clamshell bucket. These elements were: bucket geometry, bucket kinematics, the cutting process and the soil properties. Questions arose during the cutting process examination and its normative parameter, cohesion and adhesion. At the transition zone for rock to clay with strength of 400 kPa the adhesive strength is zero, because rock is no adhesion and therefore the adhesion has to decrease to zero. With this boundary condition the prediction was made that with increasing cohesive strength there is a decrease of adhesive strength with clay.

As assessed the adhesive strength property of clay has a dominant role in the clay cutting process. The correlation between increasing cohesive strength and possible decreasing adhesive strength is of importance for fully grasping the clay cutting process with clamshell buckets or other dredging tools. For this an adhesive measuring test set-up has been designed, constructed and used at Texas A&M. The test set-up was able to pull a steel blade out from two layers of clay and measured the resistance force with an inline load cell connected to an electric actuator. A total of 56 experiments were done at two different pulling speeds, 8 and 0.4 mm/s, on three different natural field clays. The natural field clays were retrieved from two project sites. The first is the softer (10 kPa) Delaware River clay from Philadelphia, Pennsylvania and the stiffer grey (17 kPa) and red (87 kPa) clay from Freeport, Texas. Additional testing was done with Atterberg limits, UU-traxial and mineralogy determination.

A clamshell bucket sensitivity analysis was conducted on two existing GLDD buckets to evaluate parameters that influence the production in m^3/s. The GL485, an Anvil-Owen, 16 m^3 and 24.5 ton and the GL484, Hawco, 9 m^3 and 29.5 ton buckets were used. These two grabs were subjected to the variation of the normative parameters: cutting angle, adhesive cutting length, centre point of gravity, bucket weight, bucket span and bucket width. This analysis was done with the Clamshell Closing Simulation software (CCS32). The software can be used to make estimates on bucket payloads, forces, bite profiles in soil and the ability of varying different bucket parameters. These parameters have different results for the two buckets. The GL485's production is mostly increased by increasing the bucket weight, lowering and outward moving of the centre point of gravity and reducing the adhesive cutting length. For the GL484 it is slightly different and the most effect on the production is reducing the adhesive cutting length, followed by increasing the bucket weight and increasing bucket span for increasing the production.

With the acquired data from the adhesive experiments and clamshell bucket sensitivity analysis different clamshell bucket concept designs were created. Of the four clamshell bucket concepts, three (GLX, GLY and GLZ) have their own unique design. These concepts are evaluated with the acquired data of the sensitivity analysis leading to the final concept the GLXYZ. This concept is a combination of GLX, GLY and GLZ and its best features for improving production for every clamshell closing cycle. Each concept is graded with the multi criteria analysis and the concept with the highest overall grade is the best option for new bucket design.

The adhesive test set-up with the approaches to the experimental adhesive data has led to confirming the prediction of adhesive strength development with increasing cohesive strength. With an increasing cohesive strength of the clay, there is a decrease to zero for the adhesive strength. In addition to the decreasing adhesion, there is an increase in the internal friction angle (φ). This can be concluded from the data of the Freeport grey clay of 17 kPa cohesive strength and the stiffer Freeport red clay with a cohesive strength of 89 kPa with a even smaller adhesive strength. The internal friction angle for the Freeport red clay is 30 degrees, however the internal friction angle will have a

limit considering rock has an internal friction angle. This has a major influence on the productions [m^3/s] and production estimates of stiffer clays with clamshell dredges or any other dredging equipment.

Table of Contents

1. Introduction

The world's surface consists of approximately 71% water. Humanity has to live around and cope with this water. The drive to reclaim land and ever-increasing water transportation has demanded maintenance of our waterways and passages. The existing harbours, beaches and waterways will have to endure several influences, such as erosion and sedimentation over time and weather conditions. To properly maintain and reclaim land the dredging industry evolved over the past century.

The dredging industry has different tools to do the job. For the shallow drift, shallow water, confined space or the very deep dredging, the clamshell dredge is a good option (Van Oord, 2015). The clamshell has been a widely used tool for loading and offloading ships in the docks. The clamshell's main purpose is to scoop and move dry material on and off ships in the docks. The bucket design has hardly changed over the past decades; moreover, the bucket design was not developed for other excavated materials like clay. The clamshell dredge has two main closing mechanisms, a cable or hydraulic closing system (Figure 1.1). The cable or mechanical grab is operated by manipulation of the closing and hoisting wires, making it the most dependable type. The digging process consists of lowering the bucket to the sea bottom, releasing the holding wire and pulling on the closing wire. As the grab needs its own weight to penetrate the soil, closing the grab by means of a closing wire could be seen as a disadvantage: the forces in the closing rope tend to lift up the grab, thus decreasing the cutting forces and therefore the production. The hydraulic grab which is closed using hydraulic cylinders has the great advantage of using their full weight for penetrating the soil, the absence of blocks thus prolonging the average rope life, however more risks are involved. One of the main problems is damage to the hydraulic hose. However, improved technologies have brought better cable reeling systems thus alleviating such problems.

Figure 1.1 – Hydraulic (left) and cable (right) clamshell bucket (Mack Manufacturing)

In the United States of America, the leading dredging company Great Lakes Dredge & Dock (GLDD) was founded in 1890 by business partners William A. Lydon and Fred C. Drews. Their first project was to construct an offshore tunnel that extended the water intake at Chicago Avenue to a new Water Crib near Chicago further from the shore. GLDD is a Chicago area based company that adopted its name from its location. GLDD operates not only in the whole United States, but also in the Middle East and it is rapidly expanding. Currently a total revenue of 731 million US dollars in 2013, with their latest project contributing to expantion of the Suez channel in Egypt. The Suez channel project has a total cost of 1.5 billion US dollars. In the US the clamshell dredge is used commonly in dredging projects. However, in Europe only a very small part of the dredging market is covered by clamshell dredges. Together with strict regulations on hydraulic fluid usage in the US, and company profile GLLD owns four cable clamshell dredges with a large number of clamshell buckets. GLDD's goal is to diversify in the following years. This means to do research into the possibilities of trenching in stiffer clay and eventually cutting permafrost with the clamshell bucket. The data of grabs operating in the field are scarce, especially when it concerns the

measurements of the forces working of the shells and the influence of the closing velocity on the production payload.

1.1. Problem description

With this development at GLDD, the interest in taking a close look at the clamshell bucket and all its possibilities was created. The clamshell bucket's particular design is many years old and needs to be closely examined. The closing sequence of a clamshell bucket consists of different phases. The first phase is the soil penetration phase. When penetrating a dry material, the weight of the clamshell bucket is sufficient to have a good penetration. With dredging, the penetration in a saturated soil is smaller, because the soil resistance is larger compared to the dry material. The second phase is the clamshell closing phase. With a dry material, the closing force is normative for the closing cycle. The bucket weight is used to overcome the vertical resistance force and the closing wire for the horizontal resistance force. The centre point of gravity of one half of the bucket during the first part of the closing phase can contribute to overcome the horizontal resistance force. During the closing, the horizontal force becomes three times the vertical force.

Figure 1.2 – Clamshell dredge No. 54 of GLDD

The saturated sand and clay behave very differently compared to the dry material and compared to each other. During the cutting of a soil, different factors contribute to the total resistance force such as: the soil weight (gravity), inertia, cohesion, adhesion, water content, internal and external friction. During a production estimating phase, the information provided concerning clay is limited. The information consists of undrained shear strength (S_u), a grain size distribution and a possible x-ray diffraction. To make an accurate production estimate, the cohesion, adhesion and tensile strength are needed. The undrained shear strength can be measured in different ways: with an UU-traxial

test, Torvane or penetrometer. UU-traxial is by far the most accurate and reliable.The coshesion can be determined from the UU-traxial test if the internal friction angle (φ) is known. The adhesion and tensile strength are never provided, because very little is known about these properties. During clay cutting, the cohesion and adhesion are the normative parameters determining the total forces. Therefore determining the correlation between the cohesive and adhesive properties of the clay is inevitable. The contact surface between the steel blade and cut clay creates the resistance force (adhesion). If the contact area between steel and clay is submerged, this will have an effect on the cutting process. When the clay surface is constantly wet, a suction effect may occur during the cutting and lifting up the bucket. The last phase of the clamshell closing cycle is hoisting the bucket by retracting the hoisting cable.

1.2. Research Objective

The current study is on optimization of the clamshell bucket (or grab) cubic meter [m^3] production per cycle [s] for stiffer clays. There are different elements to consider based on the clamshell cycle. The phases of a bucket cycle are soil penetration, bucket closing and bucket hoisting. These phases have four main parameters that determine the clamshell closing cycle: the bucket kinematics, bucket geometry, clay cutting process and the clay properties. Each input has its challenges and hurdles to overcome. The bucket kinematics are the equations of motion of a clamshell. During the closing of the grab, the clay is cut similar to cutting the clay with a steel blade. The cutting process is described with a formula that has a set of parameters as input to determine the total force needed to cut the clay: the cohesion (internal shear strength) and the adhesion (external shear strength) are the normative clay cutting parameters. The cohesion is a property of clay that can be determined tourgh a UU-traxial test and internal friction angle, however the adhesion or internal shear strength is not easy to determine. To complete the clamshell bucket optimization data on the adhesive properties have to be acquired by means of designing an adhesive test set-up. With the goal set, a proper approach is needed to tackle this challenge.

1.3. Approach

Before jumping into a dark hole with equations and unknown variables, information on the clamshell and clay needs to be found to get a better understanding of the current situation. The background information on the clamshell has to be found in bucket geometry, kinematics and clamshell closing cycle. The soil mechanics of clay and its properties will be very useful for conducting this study on clamshell buckets. This also includes information on the cutting of clay processes and its parameters contributing to the process.

During the closing phase of the grab, the clay cutting processes commence when the grab is closed. The forces created by the cutting process have influence on the bucket design and possibly on any other modification. The cutting theory for sand and clay was developed in 1987 by Miedema. The clay cutting process is a simplification of the sand cutting equation. The clay cutting theory is simplified with the $\varphi = 0$ concept or the internal friction (φ) is zero. In clay there is theory no internal friction and internal friction angle under undrainded conditions. With this concept, the dominant factors in clay cutting are the cohesion or internal shear strength and adhesion or external shear strength. The relationship between cohesion and adhesion is expressed in the way that the adhesion is a percentage of the cohesion. This percentage varies from 100% for soft clays to 60% for hard clays the relationship between cohesion and adhesion will be investigated (API, 1993).

With the created interest on the adhesive and cohesive behaviour, a study must be conducted. To be able to measure, a test set-up will be designed with the main purpose to measure the adhesive strength of the clay. This will be done at different speeds to examine the speed effect on the adhesive properties of clay. The testing clays acquired from the field will have to undergo some additional testing to determine all its properties. The additional UU-traxial test is done to determine the strength of the clay or cohesion. Moreover, the Atterberg test and mineralogy are also done to evaluate the strength of the clay and to determine if any phenomenon can be discovered within the clay's consistency. The adhesive test set-up will be designed, constructed and used in the Ocean Engineering lab at the

University Texas A&M in College Station, Texas. The data can be used for further bucket analysis and possible grab designs.

Before making any modifications to improve the production of the clamshell bucket, a sensitivity analysis will be done. The goal of this sensitivity analysis is determining the parameters for increasing the payload production and this analysis will be executed with a clamshell closing simulation software (CCS32), (Miedema, 1989). This CCS32 software has three components: clamshell kinematics, soil properties and bucket geometry. By varying with COG, adhesive cutting length, bucket lip thickness, bucket weight, number of sheaves etc., the normative parameters can be determined. The simulations will all be ran using the original clay properties with predetermined cohesion, adhesion and tensile strength of the clay. This phase of the study is completed after running all simulations for the 16 m^3 bucket (GL485) and the 9 m^3 heavy duty bucket (GL484) with stiff clay.

With all this information on soil properties, the cutting process, bucket kinematics and bucket geometry, the possible modification on the cable clamshell bucket can be made. The concepts will be subjected to a multi criteria analysis (MCA) taking production payload, closing time, total forces, total weight, footprint, feasibility costs and wear and tear into consideration.

The final part of the study will summarize the possible options for bucket modifications or concepts for production optimization. The study on the relationship between cohesion and adhesion of the field clay will be summerised by comparing it to assumptions made in the literature phase. Also including the possibilities for further stuies on clamshell buckets.

1.4. Report Overview

Chapter 1 **Introduction**

Present chapter introducing the reader to the subject, previous studies and goal of the research.

Chapter 2 **Background information**

This chapter presents and discusses the available related literature and introduces bucket geometry and kinematics, soil properties, the cutting of the soil, and the Clamshell Closing Software 32. This knowledge is vital for a thorough understanding of the subject at hand and for further determination of possible optimization on bucket design

Chapter 3 **Adhesive natural field clay experiments**

With the soil mechanics being an important part of the clamshell study, natural field clays will be tested with a new designed and constructed adhesive test set-up. The approach of the final design, how to calculate the adhesive property of the clays and its possible boundary conditions will be presented.

Chapter 4 **Results of adhesive experiments and additional tests**

In this chapter all the results of the adhesive experiments and the additional tests are presented. The adhesive data acquired from the test set-up is also approached with different methods to check the development between the cohesion, adhesion and internal friction angle. The additional test results are from: UU-Traxial test, Atterberg limits and clay mineralogy.

Chapter 5 **Clamshell bucket sensitivity analysis**

The clamshell bucket sensitivity analysis has different parameters that will be varied. The bucket cutting angles, adhesive cutting length, centre point of gravity, total weight, total span and total

bucket width. This will be done with two bucket (GL484 and GL485) of GLDD that are used for stiffer clays.

Chapter 6 Clamshell bucket concepts

The clamshell bucket concepts are concepts introducing a way of reaching the clamshell optimization on production. Each of the concepts will be graded with use of the multi criteria analysis. The overall highest score is the best solution for bucket optimization.

Chapter 7 Conclusion and recommendation

The conclusion and recommendation have the most valuable and interesting results of the adhesive experiments of the natural field clays. This chapter also presents a summary of the parameters of the clamshell bucket sensitivity analysis.

Chapter 8 Appendices

All the relevant, but superfluous data for fully understanding the story of this report can be found here. These are the adhesive data graphs, AutoCAD drawings of the adhesive test set-up, mineralogy reports, etc.

2. Background information

This background information chapter is to ensure that readers have sufficient technical background during the reading of this report. This includes the cable clamshell geometry, kinematics, soil mechanics and clay cutting and is partially inspired by Wittekoek.

2.1. Historical clamshell bucket study overview

The following historical study overview on the clamshell bucket is based and inspired on the work done by Wittekoek, 1992. The clamshell bucket or grab has some history and a little evolution from first design to the current bucket. The first grab was reportedly designed in the 15th century by Leonardo da Vinci (1452-1519), but was most probably never constructed. Most writings and literature about clamshell buckets describe the handling of dry matter and saturated sand, no reports about the behaviour of grabs digging clay have been found.

The primary research in the field of grabs was done by Pfahl in 1912, (Pfahl, 1912). Pfahl's study concerned the influence of the bucket weight or deadweight (m_g) on the payload (m_f) of 1.00-2.25 m^3 size grabs and also varied the average grain size. Pfahl concluded that the payload is linear to the deadweight, see Figure 2.1.

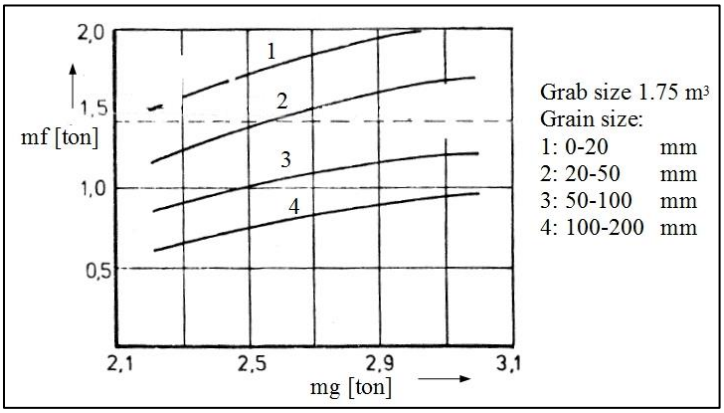

Figure 2.1 – The influence of the dead-weight (m_g) on the payload (m_f) (Pfahl, 1912)

In 1927, Ninnelt conducted similar experiments by varying the deadweight and confirmed Pfahl's (1912) work. Ninnelt also had recommended focusing on the shape of the bucket bowl or grab shell.

Niemann (1935) was the first to do a study with experiments with clamshell bucket models of scale 1:15. He studied the deadweight, the shape of the shells, soil properties, payload and the closing force. Niemann especially focused on the influence of the grab width on the payload stating that with an increase of the footprint of the bucket or grab area (A_0) the payload increased.

Both prototype grabs and models of grabs were used in 1959 by Tauber to study the weight distribution of the shells and the effect of reeving. Like his predecessors, Tauber also found a direct influence of the deadweight on the payload. He concluded that increasing the footprint does not always imply an increase of the payload. He contradicted Niemann and found that the optimum for the ratio of grab width and grab span (Ψ_a) is between the 0.60-0.75. Tauber also applied theories of soil mechanics to grabs and drew some conclusions about the direction of the soil reaction force.

Torke (1962) studied the closing cycle in sand of three 39.5 kg clamshell buckets and discussed the influences of the shape of the bucket bowl or shell, the bucket weight and closing forces. He determined the digging curves by experiments, after which he graphically reconstructed the filing process of each grab, see Figure 2.2.

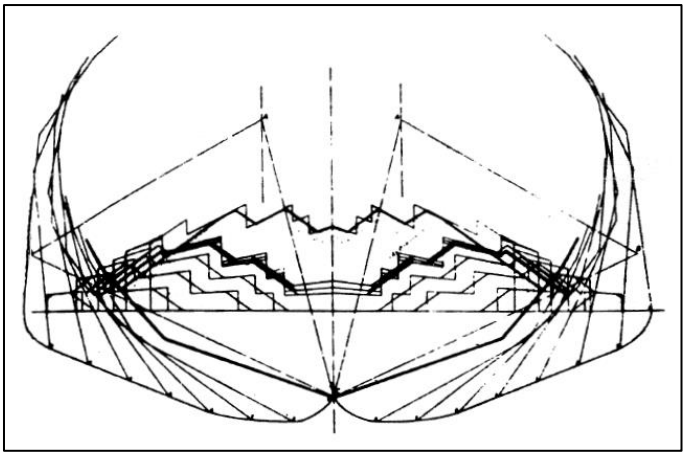

Figure 2.2 – The reconstruction of the clamshell filling process (Torke, 1962)

Shortly after Torke, Wilkinson (1963) performed tests on models and evaluated the practical use of these. Wilkinson's paper claims that wide span grabs are more efficient than original Clamshell buckets design for dry materials. Wilkinson's investigations on the effects of an interaction between variables showed that in spite of the existence of interaction, the differences with the general trends are small. Wilkinson hereafter concluded that existing clamshell buckets are proportioned in about the best way possible. Results of the tests with model grabs suggest that for a maximum payload the shells should exert as high a torque as possible on the soil, especially towards the end of the bucket closing phase. Wilkinson concluded that there were no certain "laws" or bucket model factors and confirmed Niemann's (1935) work by reassuring that the grab efficiency is the highest when the footprint (A_0) is maximal.

Hupe and Schuszter (1965) were the first to investigate the effects of soil properties like an angle of internal friction, see paragraph 2.6.1. They recommended increasing the clamshell bucket size for handling coarse materials like coal.

At the end of the sixties, Dietrich (1969) tested a 0.6 m^3 clamshell bucket and measured the payload for different values of deadweight (bucket weight), grab area/footprint (A_0), cutting angle (α) (angle bucket with respect to soil) and grain size. Dietrich's conclusion was that when digging for coarse materials, 80% of the total closing force is used for penetration of the soil. For penetration of fine materials, however, this values is approximately 30%. Additionally, Dietrich concluded that with an average grain size of 200 mm the optimum width/span ratio (Ψ_a) was equal to 0.6-0.7. Dietrich recommended the cutting knifes or bucket teeth should make an angle of 11-12 degrees with a horizontal axis when the clamshell was closed.

The paper of Gebhardt (1972, written in German) was a study done on the penetration force in materials with a minimum grain size between 30-50 mm. The most noticeable fact is that according to Gebhardt the penetration forces primarily depend on the grain size and grain size distribution. Strangely, the internal friction angle is absent. The theoretical background is neglected, but noteworthy is the influence of the grain size distribution on the cutting force. Gebhardt's tests showed that penetration of soils with a wide grain size distribution is easier than penetration of soils with a narrow size distribution. Moreover, Gebhardt found that the use of teeth to penetrate fine materials increases the penetration force.

In 1972, Scheffler made an inventory of the clamshell buckets dimensions and tendencies of efficient volume, bucket weight, footprint and width/span ration in several eastern European countries. He claimed that the buckets were not used to their full potential and experimented on a grab to determine the penetration force for coarse materials. Scheffler concluded that as much as 80% of the total closing force is needed to penetrate coarse materials.

A cooperation in 1976 between Scheffler, Pajer and Kurth gave a good overall picture of the mechanical side of trimmer, clamshell and other types of mechanical grabs. The reaction force and the behaviour of the soils during the closing phase are however simplified or absent. The researchers state that to get the best bucket efficiency all clamshell bucket parameters should be adapted to the soil properties. The conclusions from previous studies are that the angle of the bucket bowl with the horizontal axis, or the angle of bucket lip with respect to the inside of the bucket bowl, has a great influence on the bucket closing phase whereas the shape of the bucket bowl of minor importance. Likewise, the grain size has a big influence on the filling grade or production payload, not the specific weight. Furthermore, the bucket lips should be placed perpendicular to the soil, thus increasing the initial penetration.

In 1979, Bauerschlag gave a good impression of the literature that is written about clamshell buckets. His study on the grabbing process of ores with an average grain size of 55 mm by means of a motor grab first measured the digging curve and discussed the influence of several forces of the bucket closing phase, like Torke (1962). In Figure 2.3 Bauerschlag's results of the various forces, a total force F_3 consiting of the F_{31} and F_{32} on a shell are plotted. There forces are the reaction force of soil resitance of excavation. An additional study of Bauerschlag added a vibration tool to the bucket.

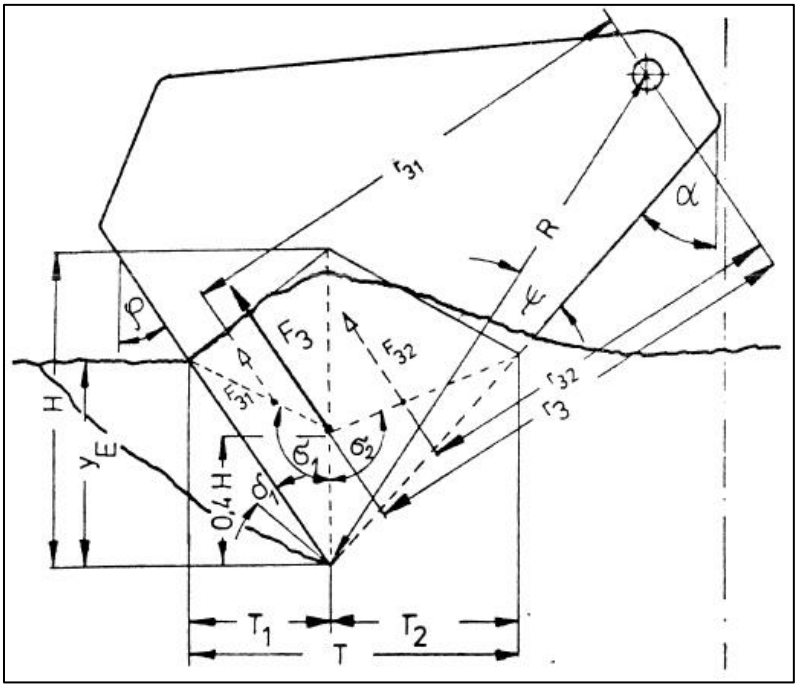

Figure 2.3 – The force on the clamshell bucket bowl by (Bauerslag, 1979)

In 1989, Miedema developed the first clamshell closing simulation software for GLDD to have a tool for production payload prediction. In 1992 at the WODCON in Bombay, India, Becker, Miedema and Wittekoek had written a paper on the closing process of clamshell dredge in water-saturated sand. This research carried out in dry and in water saturated sand, resulted in a verification and validation of the calculation method with respect to the closing

curve, the angular velocity and the pulling force in the closing wire. This paper contained results of a literature survey, the equations of motion of a clamshell grab, background to the sand cutting theory, results of the computer program Clamshell Closing Simulation (CCS32) and gave some of the results of the research carried out with respect to verification and validation of the computer program.

The demand for further research into the clamshell dredge and the cutting of clay with a clamshell bucket has increased in the past few years. This created a new opportunity for cooperation between Great Lakes Dredge & Dock and TU Delft.

2.2. Clamshell geometry

The large variation of cable grab shapes and sizes are seen on the dredge. The grabs are symmetric with two shells, two or four lever arms, an upper and lower sheave block and a closing and a holding wire put together by means of hinges, see Figure 2.4.

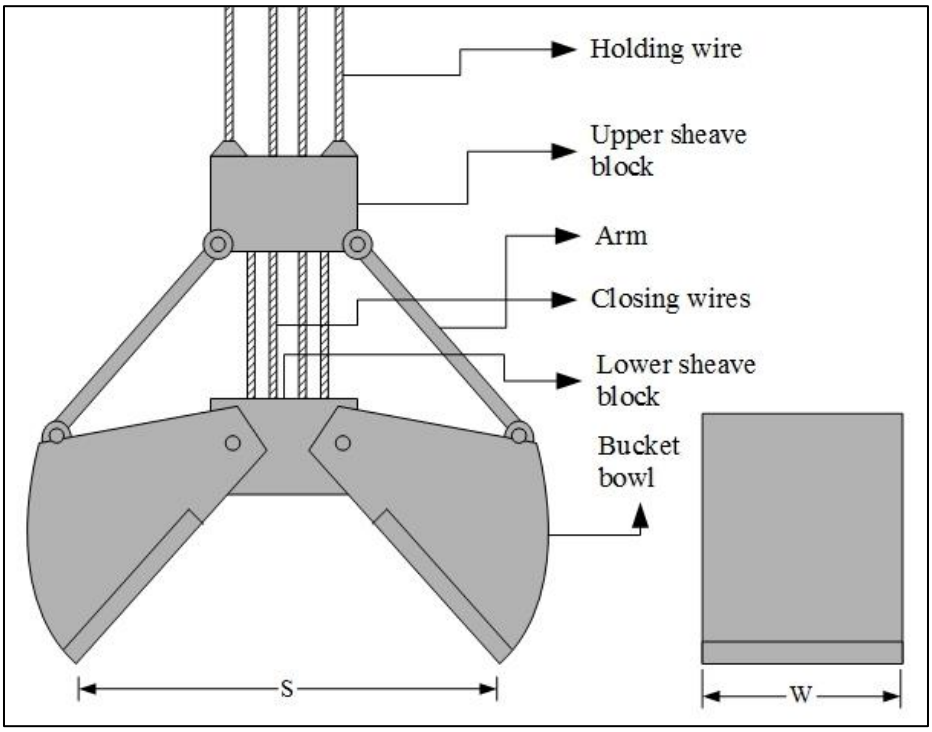

Figure 2.4 – General layout of a cable clamshell bucket

The clamshell is connected to the crane by two reeved wires: the closing wire, which is attached to the lower sheave block and the holding or hoisting wire, attached to the upper one. Closing the grab is done by releasing the holding wire when the grab is placed on the clay, and pulling up the closing wire. The closing wire forces the sheave blocks together, forcing the shells to rotate about the hinge on the lower sheave block, while the arms exert force on the shells. The weight of the lower sheave block and the shells cause the grab to open itself when holding the hoisting and releasing the closing wire. In Figure 2.4, the weight of the left shell (and/or the weight of the lower sheave block) causes a clockwise opening momentum. Likewise, the weight of the right shell opens the right shell with a counter clockwise momentum.

Because most clamshell grabs are symmetrical, the movements of the upper and lower sheave block are vertical if the soil is homogeneous and its surface horizontal. As can be seen in Figure 2.4, the global dimensions of the grab are the shell span S and the shell width W. The ratio of the span S and the width W of the shell is explained in equation 2.2.1.

$$\Psi_a = \frac{W}{S} = \frac{W \cdot S}{S^2} = \frac{A_0}{S^2} \qquad 2.2.1$$

A_0 is the total area of soil covered by the fully opened grab, in other words the footprint of the bucket. The study of the influence of Ψ_a on the payload of model grabs on the optimum ratio has concluded a maximum 0.42 for digging in fine and medium ores, see Figure 2.5 (Wilkinson, 1963). For digging fine, easy to dig sands he found a value of around 0.66. Another study found that the optimum for Ψ_a while excavating fine sand is as high as 0.72 (Tauber, 1958). In general, when a grab is used for excavating hard materials, width (W) of the shells should be small in relation to the span (S). The consequence of this is a greater concentration of weight at the edge of the cutting knife thus increasing initial penetration and available cutting force.

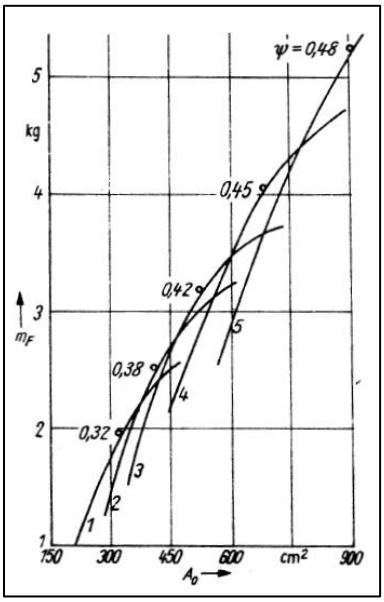

Figure 2.5 – The influence of the footprint (A_0) on the payload (m_f) (Wilkinson, 1963)

2.2.1. Shape of the bucket bowl

The part of the grab that has a great influence on the digging process is the bucket bowl or shell. The variables of the shell shape are the cutting angle (α) and the shape of the bowl or shell, see Figure 2.6. The study done with experiments on three buckets of approximately the same size, but with different types of bowls and cutting angles present the effect on rope force and opening angle, see Table 2.1 (Torke, 1962). In the study, the deadweight of each grab was varied with a counterweight and the filling grade and tension in closing wires were recorded. The filling grade is the percentage of the volume of the soil to the water volume of each grab.

Table 2.1 - Dimensions of experimental grabs on shape shell and cutting angle (Torke, 1962)

Grab number	Deadweight [kg]	Volume [l]	Shape	Cutting angle when closed [degree]
1	39.5	38.2	Triangle	62
2	39.5	42.2	Triangle with bend	70
3	39.5	45.0	Elliptical	90

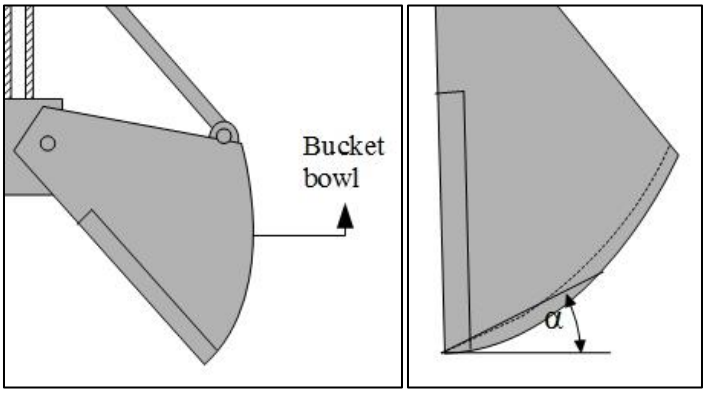

Figure 2.6 – Clamsheel bucket bowl (shell) and cutting angle

The soil used for this study was dry river sand with grain size of 0.5 to 1 mm with a density of 1650 kg/m^3. The shapes of the bucket bowls and the deadweight have great influence on the filling grade. Without the counterweights the filling grades of grab 1 and 2 was 80%, for grab 3 a filling grade of nearly 100%, see Figure 2.7. Torke's main conclusion was that the influence on the bucket bowl and on the digging process was greatly determined by the cutting angel when closed. On the other hand, the shape of the bowl is of minor importance. Experimental grab 3 had the optimal bucket bowl shape for excavating fine river sand.

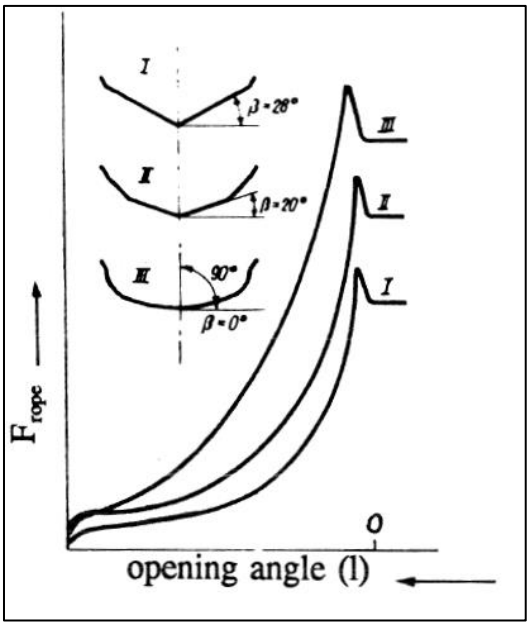

Figure 2.7 – The influence of the shape of the bucket bowl and the deadweight on the filling grade (Torke, 1962)

2.2.2. Bucket openings angle

The digging process of the clamshell bucket starts the moment the bucket lips touch the ground. The distance the grab sinks in the ground due to its own weight is the penetration or phase 1 of clamshell closing cycle. During phase 2 or closing phase the opening angle decreases over distance travelled through the soil. The goal is to get the highest possible initial penetration with the bucket having an openings angle (α_o) equal to almost 90 degrees. The opening angle (Figure 2.8) has influence on the cutting forces created during the grab closing. During the closing of the grab, the bucket bowl has different cutting angles and the shear planes (β) or planes of failure becomes steeper, which also effects the cutting force, see Figure 2.9 and paragraph 2.6.2.

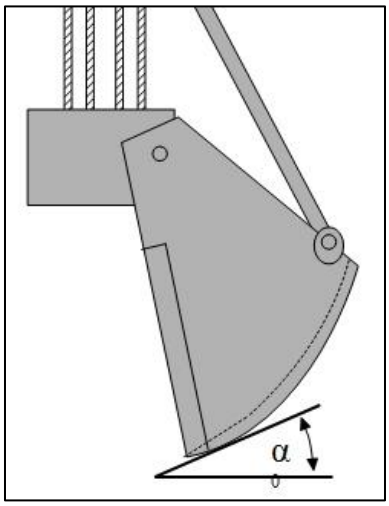

Figure 2.8 – Openings angle of clamshell bucket

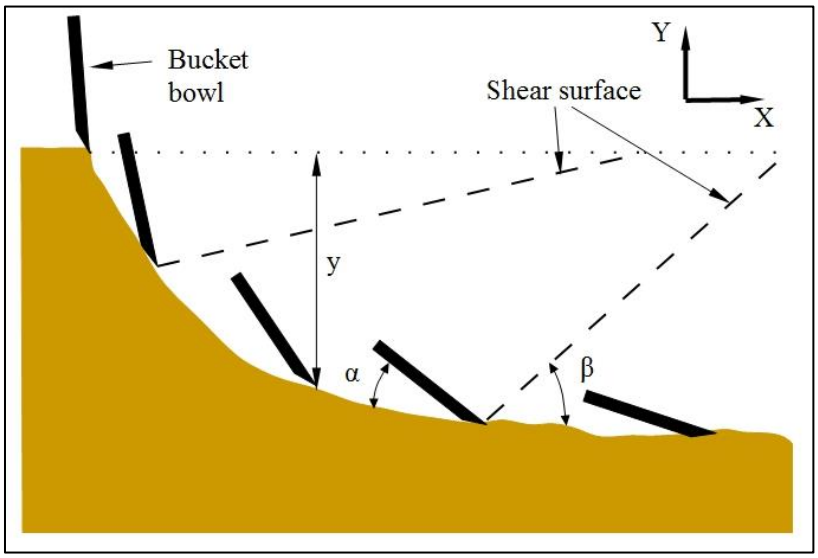

Figure 2.9 – Cutting and shear plane angle development during clamshell closing

The cutting angle changes during closing of the bucket, but so does the ratio between the vertical and horizontal force. The vertical force is much larger during the penetration phase and decreases with decreasing cutting angle, on the other hand the horizontal force increases with decreasing cutting angle, see Figure 2.10. During the second phase of the soil excavation, the horizontal force acts on the both tips of the blade. This reduces penetration because the horizontal force is three times larger than the vertical force.

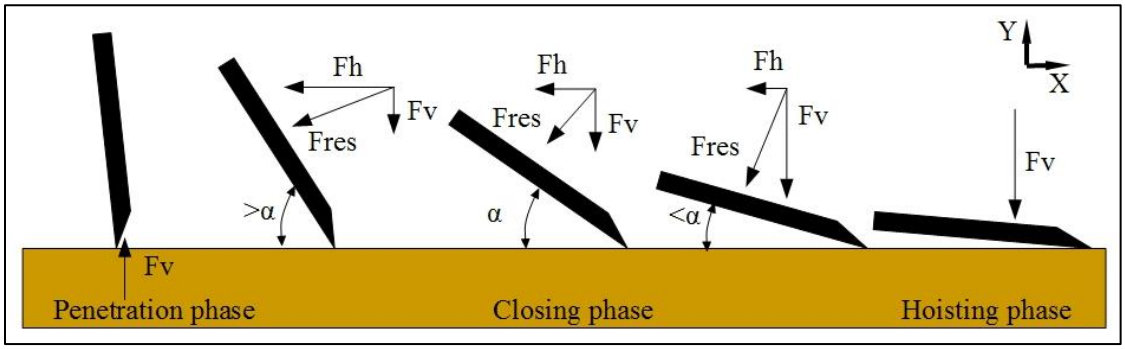

Figure 2.10 – Vertical and horizontal force ratio with decreasing cutting angle

2.3. Clamshell bucket kinematics

The clamshell is symmetrical; therefore only one half will have to be considered. The masses of half of the sheave blocks are M_1 and M_2. The mass of the shell is M_3 with the coordinates (X_3, Y_3), see Figure 2.11. The clamshell kinematics work with a system with two degrees of freedom. With the equations of Lagrange (1813), an output is the motion of the centre point of gravity of the shell during the closing phase, which can be written in equations 2.3.1 and 2.3.2.

$$X_3 = f + s \cdot \sin(\lambda + \varepsilon) \qquad 2.3.1$$

$$Y_3 = Y_1 - s \cdot \cos(\lambda + \varepsilon) \qquad 2.3.2$$

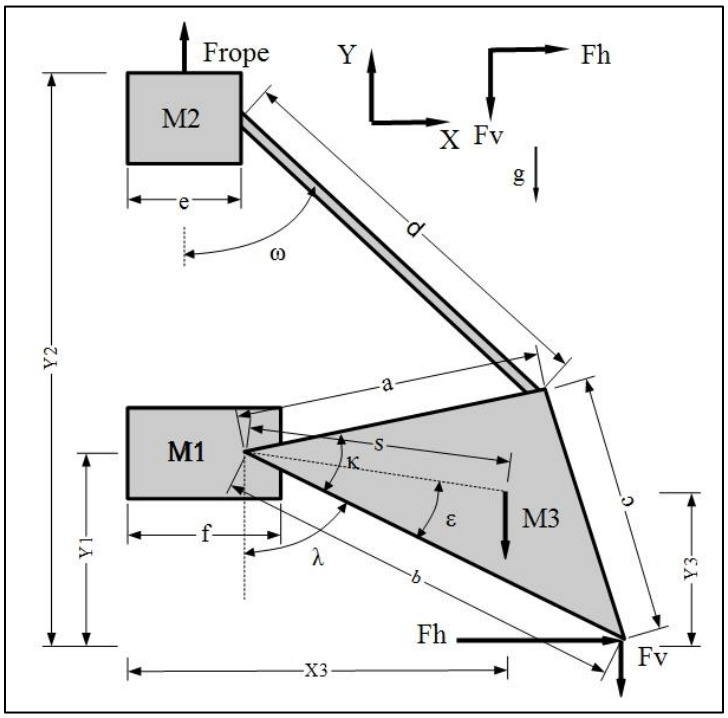

Figure 2.11 – Variables overview of the clamshell equations of motion

Lagrange (1813) developed a theory with which the kinematic equations of systems of many links can be derived. The derivation of the equations of motion according to Lagrange will result in two lengthy differential equations, which will have to be solved numerically. Putting the lower sheave block in a position (Y_1) and with the opening angle (λ) known, it is possible to derive all coordinates. The equations of Lagrange are shown in equations 2.3.3 and 2.3.4 (Rao, 2011).

$$\frac{d}{dt}\left(\frac{\partial T}{\partial \dot{Y}_1}\right) - \frac{\partial T}{\partial Y_1} + \frac{\partial V}{\partial Y_1} = W_{Y_1} \quad \text{2.3.3}$$

$$\frac{d}{dt}\left(\frac{\partial T}{\partial \dot{\lambda}}\right) - \frac{\partial T}{\partial \lambda} + \frac{\partial V}{\partial \lambda} = W_{\lambda} \quad \text{2.3.4}$$

With T being the kinetic energy and V is the potential energy, the W_{y1} and W_{λ} terms are the virtual labour of distance Y_1 and rotation λ. The kinematic energy of the system consists of the translation of the sheave blocks plus the translation and rotation of the shells. The weight of the closing cables may be neglected, because the weight of the closing cables is very small compared to the sheave blocks and bucket bowl.

$$T = \tfrac{1}{2}M_1\dot{Y_1^2} + \tfrac{1}{2}M_2\dot{Y_2^2} + \tfrac{1}{2}I_3\dot{l^2} + \tfrac{1}{2}M_3\left(\dot{X_3^2} + \dot{Y_3^2}\right) \quad \text{2.3.5}$$

And the potential energy equation 2.3.6.

$$V = M_1 g Y_1 + M_2 g Y_2 + M_3 g Y_3 \quad \text{2.3.6}$$

If the number of reeves is equal to z, and the soil forces F_h and F_v result in a moment M_c about the shell/lower sheave block hinge, then the coefficients of the virtual labour of equations 2.3.3 and 2.3.4 can be determined according to equations 2.3.7, 2.3.8 and 2.3.9.

$$W_{y1} = F_{Y_1} \cdot \Delta Y_1 \quad \text{2.3.7}$$

$$W_{\lambda} = M_{\lambda} \cdot \Delta\lambda \quad \text{2.3.8}$$

$$F_{Y_1} \cdot \Delta Y_1 + M_{\lambda} \cdot \Delta\lambda = \Delta(Y_2 - Y_1) \cdot F_{rope} \cdot z + M_c \cdot \Delta\lambda \quad \text{2.3.9}$$

Solving the Lagrange equations, the variables Y_2, X_g and Y_g need to be expressed in Y_1 and l. Y_2 can be limited by means of equation 2.3.10 and 2.3.11.

$$Y_2 = Y_1 + a \cdot \cos(\pi - \kappa - \lambda) + d \cdot \cos(\omega) \quad \text{2.3.10}$$

$$d \cdot \sin(\omega) = f - e + a \cdot \sin(\pi - \kappa - \lambda) \quad \text{2.3.11}$$

The solution of equation 2.3.9 with 2.3.10 and 2.3.11 results in the long equation 2.3.12 with Figure 2.14.

$$I_b \cdot \ddot{\lambda} = -M_3 \cdot s \cdot \sin(\lambda + \varepsilon) + M_3 \cdot (Y_2 - Y_3) \cdot s \cdot \sin(\lambda + \varepsilon) - F_t \cdot \cos(\omega) \cdot a \cdot \sin(\lambda + \kappa) + F_t \cdot \sin(\omega) \cdot a \cdot \cos(\lambda + \kappa) + F_h \cdot b \cdot \cos(\lambda) - F_v \cdot b \cdot \sin(\lambda) - M_e \quad \text{2.3.12}$$

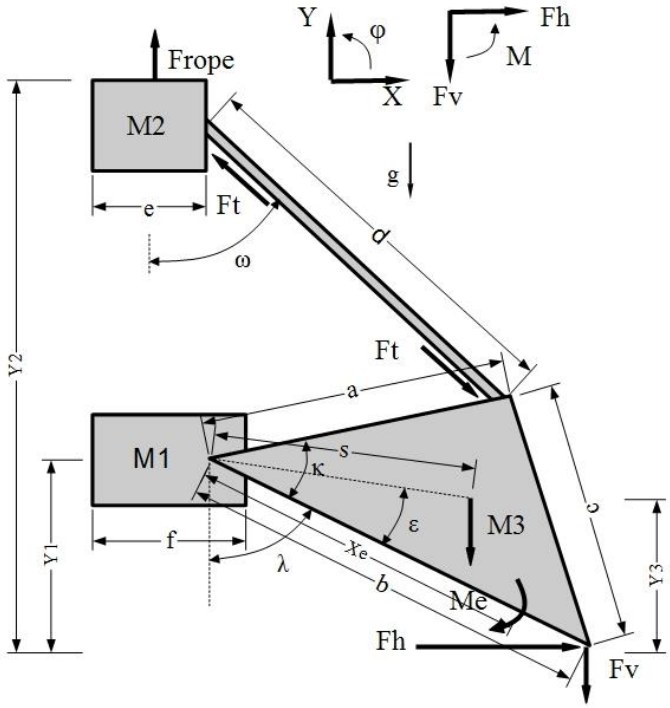

Figure 2.12 – Solution of clamshell bucket kinematics of one half

I_b is the inertia moment times the acceleration $\ddot{\lambda}$. There is a balance between the two bucket halves and each has the same equilibrium, see equation 2.3.12, however for the left half all '-'and '+' signs are interchanged. The interchange of symbols is not for the gravity and vertical forces, but for the momentum and horizontal forces.

The arm force F_t in paragraph 2.4.2, equations 2.4.3, 2.4.4 and 2.4.5. M_e is the momentum from the side edges of the bucket , see paragraph 2.3.1.

2.3.1. Soil penetration

The friction force on the side surfaces of the buckets can be derived by integrating the shear stress over the side surfaces. The initaial penetration of the clamshell with the help of the bearing capacity of shallow footings by Terzaghi (1967). In this theory the maximum laod on a footing is predicted. If it is reversed it can also be used to predict the intial penetration of the edges of a clamshell, for at this pint the soil carris its maxum possible load.

A shallow foundation is defined as one whose depth is equal to or less tis width. It must be underlinded however that the calculations are an approximation of the real value. A general solution for the bearing capacity has not been obtained and sosts of the sum of three componnets.

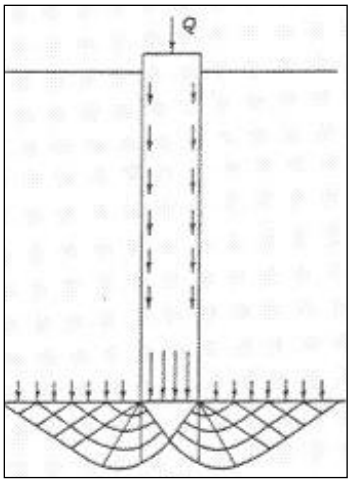

Figure 2.13 – The boundaries of the zone of plastic equilibrium of soil beneat a continuous footing at the poilt of failure (Lambe, 1979)

$$F_e = A_e \cdot \left(c \cdot N_c + \frac{\gamma_t \cdot \delta \cdot N_\gamma}{2} + \gamma_c \cdot h_i \cdot N_q \right) \quad \textbf{2.3.13}$$

$$M_e = X_e \cdot A_e \cdot \left(c \cdot N_c + \frac{\gamma_t \cdot \delta \cdot N_\gamma}{2} + \gamma_c \cdot h_i \cdot N_q \right) \quad \textbf{2.3.14}$$

The list of vertical forces acting on the clamshell bucket:

1. X_e : The arm of bucket side in contact with soil [m].
2. A_e : Bucket side surface in contact with soil [m^2];
3. c : Cohesion [N];
4. N_c : The cohesion and friction of a weightless material carrying no surcharge;
5. N_γ : The friction of a weightless material upon addition of a surcharge q on the ground surface;
6. N_q : the friction of a matrial possessing weight and carrying no surcharge;
7. γ_t : Unit weight of clay [kg/m^3];
8. h_i : thicknes layer of cut soil [m];

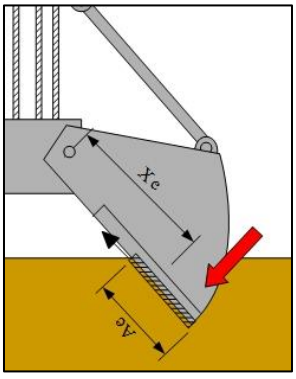

Figure 2.14 – side edges of the bucket creating the resistance momentum

Although the resulting equation for the force on the side edges is empirical, it is based on a combination of Terzaghi's foundation theory and Miedema's cutting theory.

2.4. Forces on clamshell bucket

The digging curve of the bucket depends on the forces on the bucket lips and bowl. The interaction between the bucket and the soil against can be seen as the "resistance" of the soil and will be discussed in paragraph 2.6.2. First, the focus is on the influence of the forces on the shell as a result of the weight of the several parts of the grab and the force in the closing rope. There are horizontal and vertical forces working on the grab and interchange from vertical to horizontal during the closing phase of the bucket. The clamshell bucket parameters that are designed to calculate the closing curve, the weight of the several parts and the effect of reeving will also have to be taken into account. The vertical cutting forces will be determined first.

2.4.1. The vertical forces on clamshell

The force determination will be simplified by assuming that the only force that acts on the bucket is the cutting force. Starting with determining the vertical forces, the forces that influence the vertical cutting force are plotted in Figure 2.15. The weight of the several parts of the grab contributes to the vertical forces. If there are two arms acting on one shell and the centre point of gravity of each arm is situated at the middle point of the arm, the influence of the weight of these two arms is equal to two forces F_a acting on the upper sheave block and the shell.

The vertical cutting force is related to the force in the closing wire and the weight of the grab. The closing wire force can be directly subtracted from the vertical component of the cutting force.

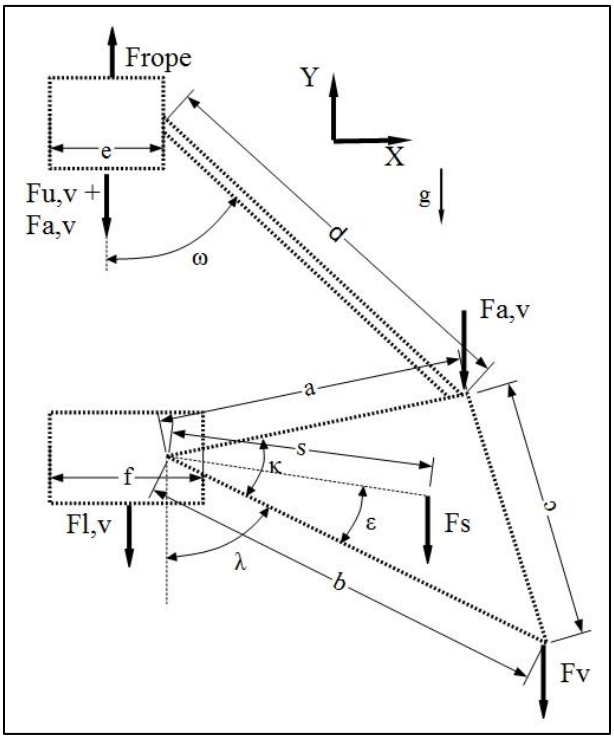

Figure 2.15 – Vertical forces on clamshell bucket during penetration and closing

The list of vertical forces acting on the clamshell bucket:

1. F_{rope} : the tension in the closing rope;
2. $F_{a,v}$: vertical force as a result of the weight of an arm (two or four arms);
3. $F_{u,v}$: vertical force as a result of the weight of half the upper sheave block;
4. $F_{l,v}$: vertical force as a result of the weight of half the lower sheave block;

5. F_s : force as a result of the weight of a shell;
6. F_v : the vertical cutting force;

The equilibrium of these vertical forces are in equation 2.4.1, because equation 2.4.1 equals half the weight of the grab. The total vertical cutting force (F_v) is related to the force in the closing wire (F_{rope}) and the weight of the grab (F_{grab}), see equation 2.4.2. There is a direct relation between the closing rope force and the vertical component of the cutting force. With increasing force on the closing rope comes a decrease of vertical force. This has direct effect on phase one of the clamshell cycle, the penetration phase and closing phase by pulling the grab out of the soil.

$$F_{u,v} + F_{l,v} + F_s + 2 \cdot F_{a,v} + F_v - F_{rope} = 0 \qquad 2.4.1$$

$$F_v = F_{rope} - F_{grab} \qquad 2.4.2$$

2.4.2. The horizontal cutting force

For the horizontal cutting force a larger number of forces have to be taken in account. This makes the calculation of the horizontal cutting forces more complicated, see Figure 2.16.

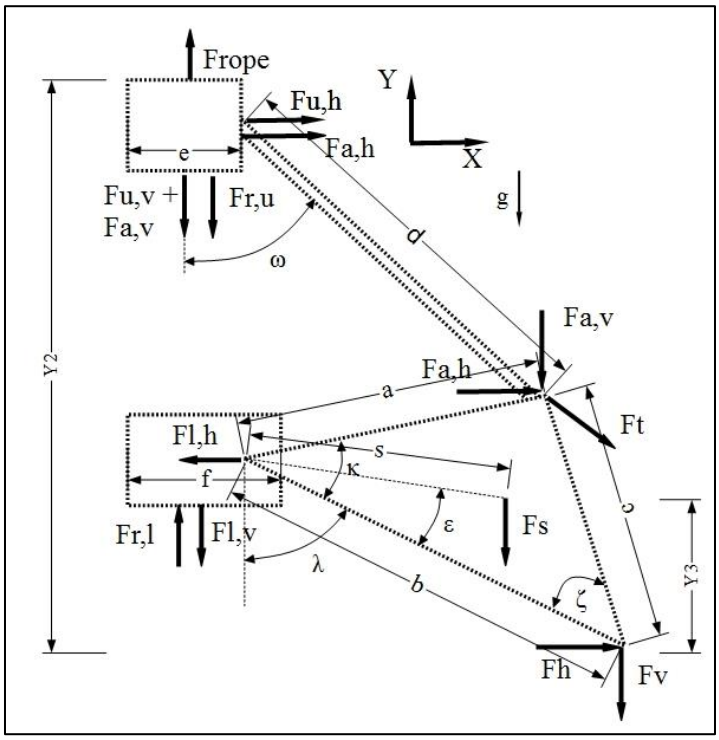

Figure 2.16 – Horizontal forces on clamshell bucket during clamshell closing

The list of horizontal forces acting on the clamshell bucket:

1. F_{rope} : the tension in the closing rope;
2. $F_{a,v}$: vertical force as a result of the weight of an arm (two or four arms);
3. $F_{a,h}$: horizontal force as a result of the weight of an arm (two or four arms);
4. F_t : resulting force of $F_{a,v}$, $F_{a,h}$, $F_{u,v}$ and $F_{r,u}$
5. $F_{u,v}$: vertical force as a result of the weight of half the upper sheave block;
6. $F_{u,h}$: horizontal force as a result of the weight of half the upper sheave block;
7. $F_{r,u}$: force as a result of closing rope on half the upper sheave block;

8. $F_{l,v}$: vertical force as a result of the weight of half the lower sheave block;
9. $F_{l,h}$: horizontal force as a result of the weight of half the lower sheave block
10. $F_{r,l}$: force as a result of closing rope on half the lower sheave block;
11. F_s : force as a result of the weight of a shell;
12. F_v : the vertical cutting force;
13. F_h : the horizontal cutting force;

The vertical forces that contribute to the horizontal cutting force act on the upper sheave block result in a force F_t, see equation 2.4.3.

$$F_t = \frac{\left(F_{u,v} + F_{r,u} + F_{a,v}\right)}{\cos(\omega)} \qquad 2.4.3$$

The force in the closing rope results in two forces $F_{r,u}$ and $F_{r,l}$ that act on the upper and lower sheave block. If the number of ropes that act on the lower sheave block is equal to z and the efficiency of each sheave equals η (η<1), see equation 2.4.4 and 2.4.5.

$$F_{r,u} = F_{rop} \cdot \frac{(\eta - \eta^z)}{(1-\eta)} \qquad 2.4.4$$

$$F_{r,l} = F_{rop} \cdot \frac{(1 - \eta^z)}{(1-\eta)} \qquad 2.4.5$$

The horizontal cutting force can now be determined by calculating the momentum equilibrium around lower sheave block resulting in equation 2.4.6.

$$\begin{aligned}(F_t \cdot \cos(\omega) + F_a) \cdot a \cdot \sin(\lambda + \kappa) - F_t \cdot \sin(\omega) \cdot a \cdot \cos(\lambda + \kappa) \\ -F_h \cdot b \cdot \cos(\lambda) + F_v \cdot b \cdot \sin(\lambda) + F_s \cdot s \cdot \sin(\lambda + \varepsilon) = 0\end{aligned} \qquad 2.4.6$$

This can be rewritten to equation 2.4.7:

$$F_h = \frac{\left((F_t \cdot \cos(\omega) + F_a) \cdot a \cdot \sin(\lambda + \kappa) - F_t \cdot \sin(\omega) \cdot a \cdot \cos(\lambda + \kappa) + F_v \cdot b \cdot \sin(\lambda) + F_s \cdot s \cdot \sin(\lambda + \varepsilon)\right)}{(b \cdot \cos(\lambda))} \qquad 2.4.7$$

Here the distance s and angle ε determine the position of the centre point of gravity of the shell (X_3, Y_3). With equations 2.4.4 and 2.4.5 the horizontal cutting force as a function of the opening angle λ can now be solved if the weight of the several parts of the grab and the tension in the closing wire is known. It is however necessary to calculate the relation between the openings angle (λ) and the arm angle (ω), see equation 2.4.8.

$$\omega = \arctan\left(\frac{\{f + b \cdot \sin(\lambda) - e - c \cdot \sin(\lambda - \zeta)\}}{\{(Y_1 - Y_3) - a \cdot \cos(\pi - \lambda - \kappa)\}}\right) \qquad 2.4.8$$

The clamshell cutting force is at its maximum when fully opened and strongly decreases to its minimum toward the end of the closing process (λ=0). This could be seen as a disadvantage of a clamshell grab: at the end of the closing cycle the required cutting face reaches its maximum value, however the available cutting force is minimal. This is also the reason that most excavating curves show a peak in the middle of the cutting curve. The only way to decrease the big difference in cutting force at the beginning and the end of each cycle is to increase the a/d ratio, the

consequence of doing this however is that the span S decreases. Therefore it is necessary that the best compromise is found between the required cutting force and the span.

2.5. Soil mechanics

Clay is characterized by small particle size, negative electrical charge, plastic behaviour when mixed with water and high weathering resistance (Mitchell & Soga, 2005). There are different types of clay with varying strength, stickiness and structure. The different structures are determined by the molecular order and rearrangement of strings. There are four main clay types: kaolinite, illite, montmorillonite and chlorite. The clay found during processing is a combination of these four types.

Clay has a dense structure due to its small particle size. This is clearly illustrated in Figure 2.17, which shows that clay particle size is < 0.006 mm. Due to the fact the clay has a high density, its permeability is low. Clay's low permeability has important effects on the cutting force. This will be discussed later in this chapter.

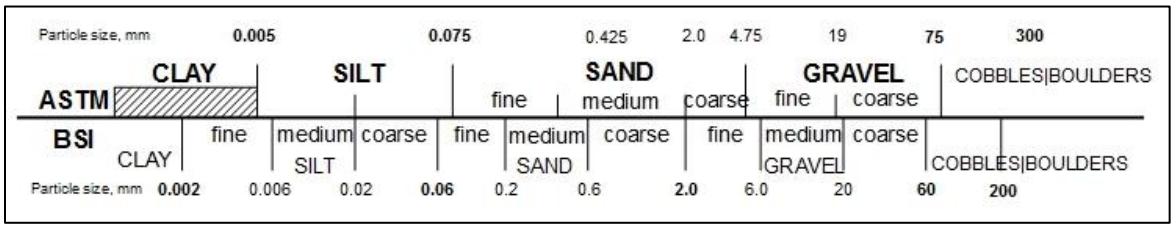

Figure 2.17 - Grain size distribution

2.5.1. Clay Properties

In order to provide a foundation for understanding the strength and structure of clay, it is necessary to discuss the four different types of clay.

2.5.2. Structure of clay minerals

Clay soil consists of a mixture of several kinds of clay minerals. The clay minerals consist of different silica layers stacked in specific configurations. The layers are built from tetrahedron or octahedrons units. The units are composed of silicon, oxygen and different type of cations, such as aluminium and magnesium ions. Figure 2.18 illustrates the structure of the tetrahedron and octahedron.

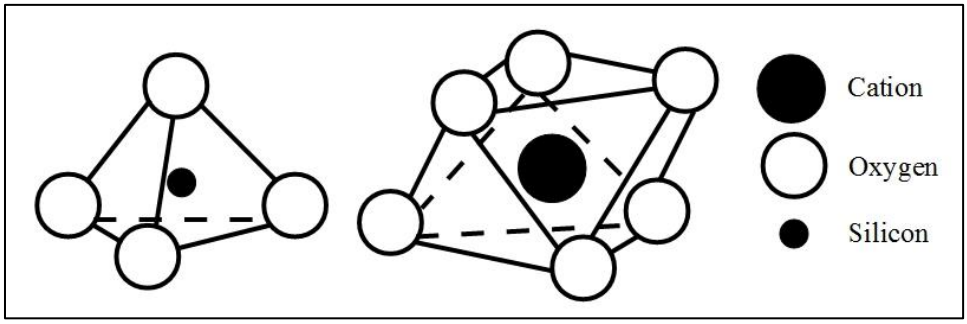

Figure 2.18 – Tetrahedron (left) and Octahedron (right) molecular structure

Tetrahedral and octahedral sheets are created by positioning the basic units in a specific configuration and a silica sheet is formed. The tetrahedrons form the tetrahedral silica sheet by sharing three of their four vertices, the octahedrons form the octahedral silica sheet is formed by sharing all their vertices. The patterns are shown in Figure 2.19.

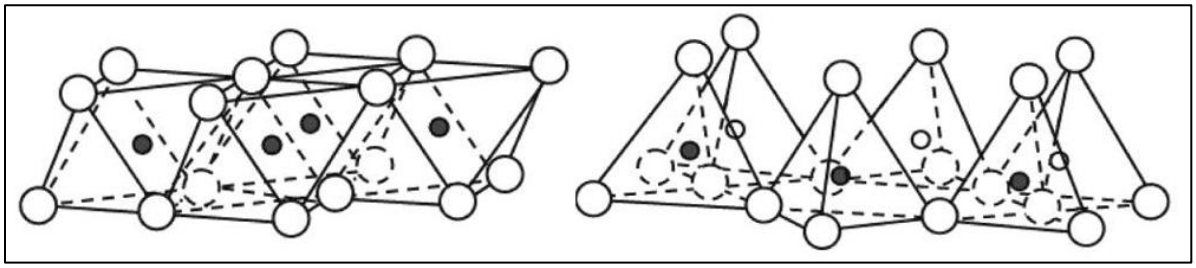

Figure 2.19 - octahedral silica sheet (left) and a tetrahedral silica sheet (right)

2.5.3. Different common clay types

Phyllosilicate minerals consist of four groups: serpentine, clay mineral, mica and chlorite. Kaolinite, montmorillonite (one of the smectite clay mineral) and illite belong to the clay mineral group, whereas chlorite is a group of its own.

Kaolinite is the most common of the clay minerals and is a soft and usually white mineral. It can be found in several parts of the world, including Brazil, Vietnam, India and the United States. The chemical formula for kaolinite as used in mineralogy is $Al_2Si_2O_5(OH)_4$ with a specific gravity between 2.16-2.68. Kaolinite will form under the right chemical-weathering conditions in rocks in hot, moist climates. The structure of kaolinite is such that it has a low shrink-swell capacity. This capacity refers to the extent to which clay will expand when wet and retract when dry. X-ray diffraction analysis has shown that sheets of kaolinite are arranged like pages in a book; this affects the amount of surface area available for holding water or cations like Ca^{2+} or K^{+}. Imagine a closed book with many pages; each page has surface area on the front and back, which might be a lot of surface area. But if the book is closed the pages are so tightly packed the surface area is not available. The only practical surface for water or cations to attach (or "adsorb") to would be the edges of the book, plus the front and back covers.

Because of this arrangement, kaolinite has less external surface area than other clay minerals, no internal surface area and less capacity for holding water and cations. Comparing soils along a gradient towards progressively cooler or drier climates, the proportion of kaolinite decreases, while the proportion of other clay minerals such as illite (in cooler climates) or smectite (in drier climates) increases. Such climatically-related differences in clay mineral content are often used to infer changes in climates in the geological past, where ancient soils have been buried and preserved.

Montmorillonite is soft clay that has a structure composed of microscopic crystals. Montmorillonite belongs to the smectite group and is 2:1 clay. The 2:1 clay structure of this clay consists of three layers: two tetrahedral sheets that sandwich an octahedral sheet see Figure 2.20. The water content of montmorillonite is variable and the clay increases greatly in volume when it absorbs water. Chemically it is known as hydrated sodium-calcium-aluminium-magnesium-silicate-hydroxide (Na,Ca) 0.33 (Al,Mg) 2 $(Si_4O_{10})(OH)_2 \cdot n\ H_2O$. Potassium, iron and other cations are common substitutes; the exact ratio of cations varies with source. It often occurs intermixed with chlorite, muscovite, illite, cookeite and kaolinite. The bonds between the successive layers are Van der Waal's and cationic bonds. Montmorillonite-smectite clay mineral is different from illite clay mineral in that if the water concentration is increased in montmorillonite-smectite clay mineral, its bonds will break, resulting in a great increase in water volume. Similar to many other types of clay, montmorillonite swells with the addition of water. However, some montmorillonites expand considerably more than other clays due to water penetrating the interlayer molecular spaces and concomitant adsorption. The amount of expansion is due largely to the type of exchangeable cation contained in the sample. The presence of sodium as the predominant exchangeable cation can result in the clay swelling to several times its original volume.

Illite clay has a similar particular structure that consists of three layers: tetrahedron – octahedron – tetrahedron (TOT). This structure allows illite clay to absorb water and bond water molecules to its outer layer. The chemical formula is given as (K,H3O) $(Al,Mg,Fe)_2$ $(Si,Al)_4O_{10}$ $[(OH)_2,(H_2O)]$, but there is considerable ion substitution. The specific gravity is between the 2.6-2.9. The clay does not swell after water is absorbed because of poorly hydrated potassium captions between the top and bottom layer.

Chlorite clay has four main molecular compositions: chlinochlore ((Mg5Al)(AlSi3)O10(OH)8), chamosite ((Fe5Al)(AlSi3)O10(OH)8), nimite ((Ni5Al)(AlSi3)O10(OH)8) and pennantite ((Mn,Al)6(Si,Al)4O10(OH)8). The typical general formula is: (Mg,Fe)3(Si,Al)4O10(OH)2·(Mg,Fe)3(OH)6. This formula emphasizes the structure of the group. Chlorites have a 2:1 sandwich structure TOT, this is often referred to as a talc layer. Unlike other 2:1 clay minerals, a chlorite's interlayer space (the space between each 2:1 sandwich filled by a cation) is composed of $(Mg2+, Fe3+)(OH)_6$. This $(Mg2+, Fe3+)(OH)_6$ unit is more commonly referred to as the brucite-like layer, due to its closer resemblance to the mineral brucite $(Mg(OH)_2)$. Therefore, chlorite's structure appears as follows: -t-o-t-brucite-t-o-t-brucite ... Chlorite is so soft that it can be scratched by a finger nail (Wikipedia, 2015).

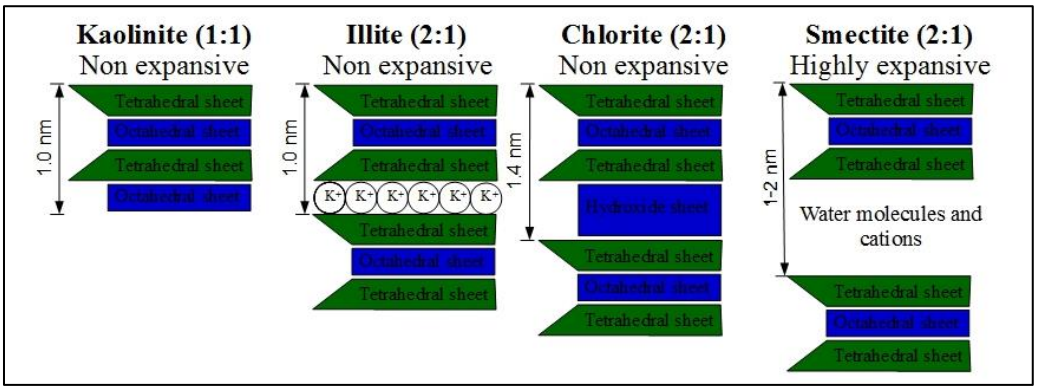

Figure 2.20 – Stacking configurations of common clay types

2.5.4. Clay Strength

There are different strength categories accompanying the different types of clay. Table 2.2 shows an overview of the different clay consistencies. The most important aspect of this table is the SPT N-value column, or blows/ft. This N-value contributes to the estimations for projects involving the clamshell. Lower N-values correspond to increased production, which will increase revenue.

Table 2.2 - Clay undrained shear strength

Undrained Shear Strength S_u					
Consistency	kPa	$\frac{kg}{cm^2}$ or tsf	psf	psi	**Approximate Equivalent N-value [*blows/ft*]**
Very Soft	<12.5	<0.13	<250	<1.75	0-2
Soft	12.5-25	0.13-0.25	250-500	1.75-3.5	2-4
Firm	25-50	0.25-0.50	500-1000	3.5-7	4-8
Stiff	50-100	0.50-1.00	1000-2000	7-14	8-15
Very Stiff	100-200	1.00-2.00	2000-4000	14-28	15-30
Hard	>200	>2.00	>4000	>28	>30

The undrained shear strength (Su) of the clay is property that must not be confused with the cohesive strength or internal shear strength. There is a relation between the undrained shear strength and cohesion, however this is

dependent on the angle of internal friction (phi). If phi=0, than the undrained shear strength of clay is equal to two times the clays cohesive strength (c), see equation 2.5.1 (Miedema, 2014). This only holds if the UU-traxial test executed is under undrained conditions.

$$c = \frac{UCS}{2} \cdot \left(\frac{1 - \sin(\varphi)}{\cos(\varphi)} \right) \qquad c = \frac{UCS}{2} \qquad (2.5.1)$$

Drained condition **Undrained condition**

The focus of this study is on the consistencies stiff , very stiff and hard clay. This is between the 50-400 kPa, where 400 kPa strength can be considered to be rock.

2.5.4.1. Methods of measuring the undrained shear strength of clay

The undrained shear strength (S_u) can be measured with different tests that vary from very accurate and time consuming to a ball park number done in a couple of seconds. For this study, two methods of measuring were applied: the UU-traxial test and Torvane test. There is a third method of clay strength measuring, the Penetrometer and it is similar to the Torvane test, which means a rough number and a quick test, see Figure 2.23.

The UU-traxial test is a very accurate test and consists of different phases, which makes it time consuming. The test set-up consists of the following: a pressure chamber with clay sample, a vertical actuator, a water pressure system and a recording system, see Figure 2.21.

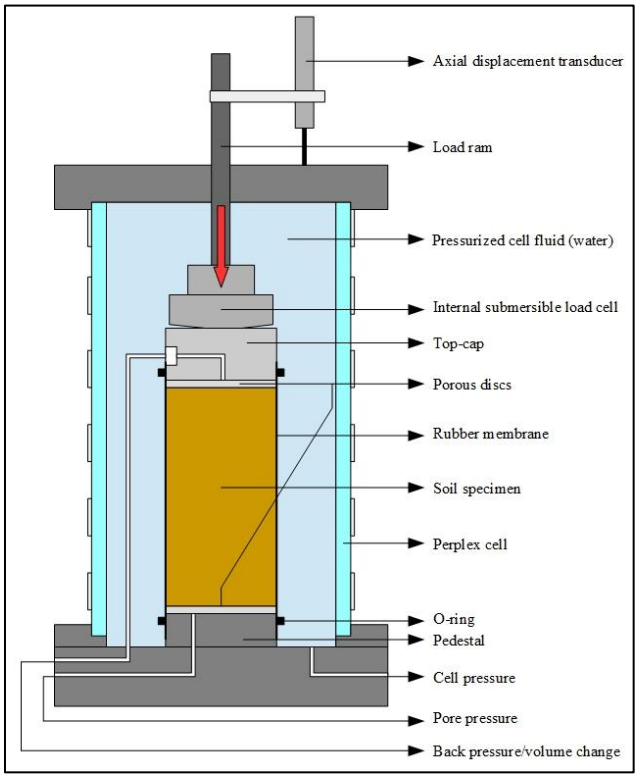

Figure 2.21 – UU-Traxial test set-up

The phases are sample preparation or sample trimming, followed by placing the sample in the pressure chamber and placing it beneath the vertical actuator. The final step before starting the test is filling up the pressure chamber with water and applying the needed pressure.

With this test set-up different types of clay sample testing can be done to reconstruct its "natural habitat" or load cycle. The UU in UU-traxial stands for unconsolidated and undrained, this means there is no possible mass volume change or drainage of water during the test. During the cutting of clay with different dredging tools these circumstances occur. The reconstructions of these circumstances are similar with the UU-traxial test. The standard UU-traxial test time depends on the height of the sample and is approximately three hours or 5% height per hour. Another test is the CU-traxial test or consolidated and undrained traxial test. The CU test is similar to measure how much a bank will dilatate in days, months or even years. This test takes up to three days to recreate the similar circumstances.

The Torvane test, or pocket vane shear tester, is a different method compared to the UU-traxial test. A vane shear tester is used to measure the shear strength of clay. There are many types of vane testers for use in-situ, in the laboratory and hand testers. A pocket vane shear tester (often called a Torvane) is a portable hand-held tester used most commonly in the field at drill sites, but it is also used in the laboratory. Figure 2.22 shows a set of Torvane equipment. This includes the tester with the standard vanes, a large adapter for soft clays, a small adapter for stiff clays and an allen key to attach the adapters.

Figure 2.22 – Torvane

Figure 2.23 – Pocket Penetrometer

2.5.5. Liquid and plastic limits of clay

Liquid and plastic limits are also known as the Atterberg limits. These limits are a basic measure of the nature of a fine-grained soil. Depending on the water content of the soil, it may appear in four states: solid, semi-solid, plastic and liquid. In each state the consistency and behaviour of a soil is different and thus so are its engineering properties. Therefore, the boundary between each state can be defined based on a change in the soil's behaviour. The Atterberg limits can be used to distinguish between silt and clay and it can distinguish between different types of silts and clays. These limits were created by Albert Atterberg. They were later refined by Arthur Casagrande. These distinctions in soil are used in selecting the soils on which structures can be built. These tests are mainly used on clayey or silty soils since these are the soils that expand and shrink due to moisture content. Clays and silts react with the water and thus change sizes and have varying shear strengths. These tests are used widely in the

preliminary stages of building any structure to ensure that the soil will have the correct amount of shear strength and not too much change in volume as it expands and shrinks with different moisture contents.

2.5.5.1. Shrinkage limit

The shrinkage limit (SL) is the water content where further loss of moisture will not result in any more volume reduction. The test to determine the shrinkage limit is ASTM International D4943. The shrinkage limit is much less commonly used than the liquid and plastic limits.

2.5.5.2. Plastic limit

The plastic limit (PL) is the water content where soil transitions between brittle and plastic behaviour. A thread of soil is at its plastic limit when it begins to crumble when rolled to a diameter of 3 mm. To improve test result consistency, a 3 mm diameter rod is often used to gauge the thickness of the thread when conducting the test. The Plastic Limit test is defined by ASTM standard test method D 4318.

2.5.5.3. Liquid limit

The liquid limit (LL) is the water content at which a soil changes from plastic to liquid behaviour. The original liquid limit test of Atterberg involved mixing a part of clay in a round-bottomed porcelain bowl of 10-12cm diameter. A groove was cut through the pat of clay with a spatula and the bowl was then struck many times against the palm of one hand. Casagrande subsequently standardized the apparatus and the procedures to make the measurement more repeatable. Soil is placed into the metal cup portion of the device and a groove is made down its centre with a standardized tool of 13.5 millimetres width. The cup is repeatedly dropped 10mm onto a hard rubber base during which the groove closes up gradually as a result of the impact. The number of blows for the groove to close is recorded. The moisture content at which it takes 25 drops of the cup to cause the groove to close a distance of 13.5 millimetres is defined as the liquid limit. The test is usually run at several moisture contents and the moisture content which requires 25 blows to close the groove is interpolated from the test results. The Liquid Limit test is defined by ASTM standard test method D 4318. The test method also allows running the test at one moisture content where 20 to 30 blows are required to close the groove; then a correction factor is applied to obtain the liquid limit from the moisture content, see Figure 2.24.The following step is when you should record the N in number of blows needed to close this 13.5 millimetres gap. The materials needed to do a liquid limit test are:

- Casagrande cup (liquid limit device)
- Grooving tool
- Soil pat before test
- Soil pat after test

Another method for measuring the liquid limit is the fall cone test. It is based on the measurement of penetration into the soil of a standardized cone of specific mass. Despite the universal prevalence of the Casagrande method, the fall cone test is often considered to be a more consistent alternative because it minimizes the possibility of human variations when carrying out the test.

Figure 2.24 – Atterberg liquid limit set-up

2.5.5.4. Importance of Liquid Limit test

The importance of the liquid limit test is to classify soils. Different soils have varying liquid limits. In addition to this, you need to know the liquid limit and the plastic limit in order to find to find the plasticity index of a soil.

2.5.5.5. Derived limits

The values of these limits are used in a number of ways. There is also a close relationship between the limits and properties of a soil such as compressibility, permeability and strength. This is thought to be very useful because whereas limit determination is relatively simple, it is more difficult to determine these other properties. Thus the Atterberg limits are not only used to identify the soil's classification, but they allow for the use of empirical correlations for some other engineering properties.

2.5.5.6. Plasticity index

The plasticity index (PI) is a measure of the plasticity of a soil. The plasticity index is the size of the range of water contents where the soil exhibits plastic properties. The PI is the difference between the liquid limit and the plastic limit (PI = LL-PL). Soils with a high PI tend to be clay, those with a lower PI tend to be silt and those with a PI of 0 (non-plastic) tend to have little or no silt or clay. PI and their meanings:

- 0 Non-plastic
- (1-5) Slightly Plastic
- (5-10) Low plasticity
- (10-20) Medium plasticity
- (20-40) High plasticity
- >40 Very high plasticity

2.5.5.7. Liquidity index

The liquidity index (LI) is used for scaling the natural water content of a soil sample to the limits. It can be calculated as a ratio of difference between natural water content, plastic limit and plasticity index with equation 2.5.2, where W is the natural water content.

$$LI = \frac{(W - PL)}{(LL - PL)} \qquad 2.5.2$$

2.5.6. Density

The terms density and unit weight are used interchangeably in soil mechanics. The density paragraph is inspired by work done by Miedema. Though not critical, it is important that we know it. Density, bulk density or wet density (ρ_t) are different names for the density of the mixture, i.e. the total mass of air, water and solids divided by the total volume of air, water and solids (the mass of air is assumed to be zero for practical purposes). To find the formula for density, divide the mass of the soil by the volume of the soil. The basic formula for density is:

$$\rho_t = \frac{M_t}{V_t} = \frac{M_s + M_w + M_a}{V_s + V_w + V_a} \qquad 2.5.3$$

With:

1.	M_t	: Mass of the soil, total mass	[kg]
2.	M_s	: Mass of the solids	[kg]
3.	M_w	: Mass of the water	[kg]
4.	M_a	: Mass of the air	[kg]
5.	V_t	: Volume of the soil, total volume	[m^3]
6.	V_s	: Volume of the solids	[m^3]
7.	V_w	: Volume of the water	[m^3]
8.	V_a	: Volume of the air	[m^3]
9.	P_t	: Density of the soil	[kg/m^3]
10.	γ_t	: Unit weight of the soil	[N/m^3]
11.	g	: Gravitational constant (9.81 m/s^2)	[m/s^2]

The unit weight of a soil mass is the ratio of the total weight of soil to the total volume of soil. Unit weight ($\boldsymbol{\gamma_t}$) is usually determined in the laboratory by measuring the weight and volume of a relatively undisturbed soil sample obtained from a brass ring. Measuring the unit weight of soil in the field requires a sand cone test, rubber balloon or nuclear densitometer, the basic formula for unit weight is:

$$\gamma_t = \frac{M_t \cdot g}{V_t} \qquad 2.5.4$$

Dry density (ρ_d) is the mass of solids divided by the total volume of air water and solids:

$$\rho_d = \frac{M_s}{V_t} = \frac{M_s}{V_s + V_w + V_a} \qquad 2.5.5$$

Buoyant density (ρ'), defined as the density of the mixture minus the density of water, is useful if the soil is submerged under water:

$$\rho' = \rho - \rho_w \qquad 2.5.6$$

Table 2.3 - Empirical values for clay ρ_t, of granular soils based on the standard penetration number (GLDD, 2008).

SPT Penetration, N-Value [blows/ foot]	ρ_t [kg/m^3]
0 - 2	< 130
2 - 4	130 - 250
4 - 8	250 - 500
8 – 15	500 - 1000
15 – 30	1000 - 2000
> 30	> 2000

2.6. Cutting Theory

Every soil has its own normative parameters that have to be considered during excavation in order to understand where the forces on the clamshell originate.

2.6.1. General Cutting Process

Figure 2.25 gives an overview of all the forces present during cutting of a soil with a steel blade. Certain forces are dominant depending on the soil that is excavated (Miedema, 2014).

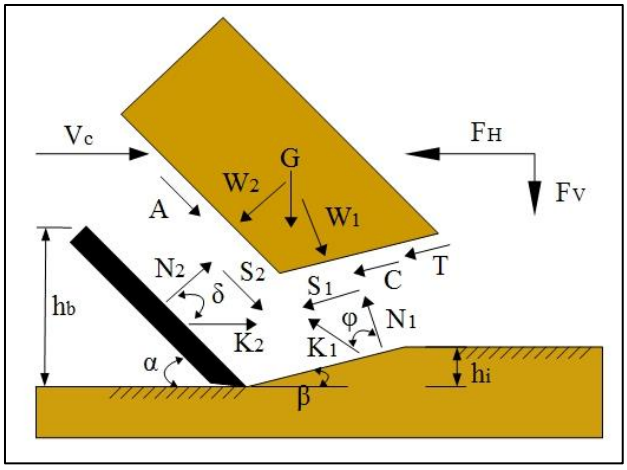

Figure 2.25 - Forces during the cutting of a soil

$$F_h = -W_2 \cdot \sin(\alpha) + K_2 \cdot \sin(\alpha + \delta) + A \cdot \cos(\alpha) \quad \text{2.6.1}$$

$$F_v = -W_2 \cdot \cos(\alpha) + K_2 \cdot \sin(\alpha + \delta) - A \cdot \sin(\alpha) \quad \text{2.6.2}$$

Equations 2.6.1 and 2.6.2 are the horizontal and vertical force on the blade. K_1 is a resulting force between the cut soil shear plane and stationary soil of the normal force N_1 and the shear force S_1. W_1 and W_2 are the water pressure forces present during the cutting, which are created when water is unable to flow out the pores of the soil, creating under pressure. Pressure is translated to the water forces. Similar is the resulting force K_2 between the cutting blade, shear plane with normal force N_2 and shear force S_2. A is the adhesion between the cutting blade and the cut soil. The angles α and δ are the blade angle and the external friction angle, respectively. In order to solve the equations 2.6.1 and 2.6.2, an expression for K_2 is needed.

$$K_2 = \frac{W_2 \cdot \sin(\alpha + \beta + \varphi) + W_1 \cdot \sin(\varphi) + G \cdot \sin(\beta + \varphi) + I \cdot \cos(\varphi) + C \cdot \cos(\varphi) - A \cdot \sin(\alpha + \beta + \varphi)}{\sin(\alpha + \beta + \delta + \varphi)} = 0 \quad \text{2.6.3}$$

$$K_1 = \frac{W_2 \cdot \sin(\delta) + W_1 \cdot \sin(\alpha + \beta + \delta) + G \cdot \sin(\alpha + \delta) - I \cdot \cos(\alpha + \beta + \delta) - C \cdot \cos(\alpha + \beta + \delta) + A \cdot \cos(\alpha)}{\sin(\alpha + \beta + \delta + \varphi)} = 0 \quad \text{2.6.4}$$

There are two normal forces: N_1 on the shear plane and N_2 on the blade.

$$N_2 = \frac{W_2 \cdot \sin(\delta) + W_1 \cdot \sin(\alpha + \beta + \varphi) + G \cdot \sin(\alpha + \delta) - I \cdot \cos(\alpha + \beta + \delta) - C \cdot \cos(\alpha + \beta + \varphi) - A \cdot \sin(\delta)}{\sin(\alpha + \beta + \delta + \varphi)} = 0 \quad \text{2.6.5}$$

$$N_1 = \frac{W_2 \cdot \sin(\alpha + \beta + \varphi) + W_1 \cdot \sin(\varphi) + G \cdot \sin(\beta + \varphi) + I \cdot \cos(\varphi) + C \cdot \cos(\varphi) - A \cdot \cos(\alpha + \beta + \varphi)}{\sin(\alpha + \beta + \delta + \varphi)} = 0 \quad \text{2.6.6}$$

From the forces in Figure 2.25, a balance is created in the horizontal and vertical direction in order to determine the total horizontal and vertical forces on the blade.

$$K_1 \cdot \sin(\beta+\varphi) - W_1 \cdot \sin(\beta) + C \cdot \cos(\beta) + I \cdot \cos(\beta) - A \cdot \cos(\alpha) + W_2 \cdot \sin(\alpha) - K_2 \cdot \sin(\alpha+\delta) = 0 \quad \text{2.6.7}$$

$$-K_1 \cdot \cos(\beta+\varphi) + W_1 \cdot \cos(\beta) + C \cdot \sin(\beta) + I \cdot \sin(\beta) + G + A \cdot \sin(\alpha) + W_2 \cdot \cos(\alpha) - K_2 \cdot \cos(\alpha+\delta) = 0 \quad \text{2.6.8}$$

2.6.2. Clay cutting process

There are two normative parameters in the clay cutting theory, the cohesive force (C) and adhesive force (A). The cohesive strength or internal shear strength is the stickiness between two similar materials, which in our case is clay. The adhesive strength or external shear strength is the stickiness between two different materials, steel and clay. There are no internal and external frictions and the frictions are not the same as the cohesion and adhesion. The horizontal and vertical forces on a blade cutting through clay are given in equations 2.6.9 and 2.6.10.

$$\boldsymbol{F_h = -W_2 \cdot sin(\alpha) + K_2 \cdot sin(\alpha+\delta) + A \cdot cos(\alpha)} \quad \text{2.6.9}$$

$$\boldsymbol{F_v = -W_2 \cdot cos(\alpha) + K_2 \cdot cos(\alpha+\delta) - A \cdot sin(\alpha)} \quad \text{2.6.10}$$

With different K_1 and K_2 to solve equations 2.6.9 and 2.6.10.

$$\boldsymbol{K_1 = \frac{W_2 \cdot \sin(\delta) + W_1 \cdot \sin(\alpha+\beta+\delta) + G \cdot \sin(\alpha+\delta) - I \cdot \cos(\alpha+\beta+\delta) - C \cdot \cos(\alpha+\beta+\delta) + A \cdot \cos(\delta)}{\sin(\alpha+\beta+\delta+\varphi)} = 0} \quad \text{2.6.11}$$

$$K_2 = \frac{W_2 \cdot \sin(\alpha+\beta+\varphi) + W_1 \cdot \sin(\varphi) + G \cdot \sin(\beta+\varphi) + I \cdot \cos(\varphi) + C \cdot \cos(\varphi) - A \cdot \sin(\alpha+\beta+\varphi)}{\sin(\alpha+\beta+\delta+\varphi)} = 0 \quad \text{2.6.12}$$

The α and β are the blade angle and angle in the clay cut area. The adjustment can also be made for the normal forces and is similar to K_1 and K_2 of equations 2.6.11 and 2.6.12. This is because the angles of the internal and external friction are zero (φ = 0 and δ = 0).

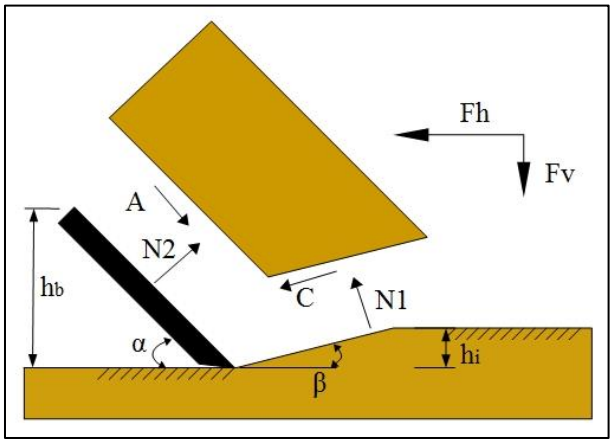

Figure 2.26 – Clay cutting forces with steel blade

The following equations in Table 2.4 elaborate the different failure types associated with different horizontal and vertical forces on the clay-cutting blade. The type of failure is determined by different conditions – I will come back to this in paragraph 2.6.4.

Table 2.4 - Overview of horizontal and vertical cutting force on a steel blade for clay

Type	Vertical Cutting Force [N]	Horizontal Cutting Force [N]
Flow type	$F_{V,f} = w \cdot \frac{\frac{c \cdot h_i}{\sin(\beta)} \cdot \cos(\alpha) - \frac{a \cdot h_b}{\sin(\alpha)} \cdot \cos(\beta)}{\sin(\alpha + \beta)}$	$F_{H,f} = w \cdot \frac{\frac{c \cdot h_i}{\sin(\beta)} \cdot \sin(\alpha) + \frac{a \cdot h_b}{\sin(\alpha)} \cdot \sin(\beta)}{\sin(\alpha + \beta)}$
Shear type	$F_{V,s} = w \cdot \frac{\frac{c \cdot h_i}{\sin(\beta)} \cdot \cos(\alpha) - \frac{a \cdot h_b}{\sin(\alpha)} \cdot \cos(\beta)}{\sin(\alpha + \beta)}$	$F_{H,s} = w \cdot \frac{\frac{c \cdot h_i}{\sin(\beta)} \cdot \sin(\alpha) + \frac{a \cdot h_b}{\sin(\alpha)} \cdot \sin(\beta)}{\sin(\alpha + \beta)}$
Curling type	$F_{V,c} = -c \cdot h_i \cdot w \cdot \frac{\frac{\sin(\alpha)}{\sin(\beta)}}{\cos(\alpha + \beta)}$	$F_{H,c} = c \cdot h_i \cdot w \cdot \frac{\frac{\cos(\alpha)}{\sin(\beta)}}{\cos(\alpha + \beta)}$
Tear type	$F_{V,t} = c' \cdot h_i \cdot w \cdot \frac{\frac{\cos(\alpha + \beta)}{\sin(\beta)} - r \cdot \frac{\cos(\alpha + \beta)}{\sin(\alpha)}}{\sin(\alpha + \beta)}$	$F_{H,t} = c' \cdot h_i \cdot w \cdot \frac{\frac{\sin(\alpha + \beta)}{\sin(\beta)} + r \cdot \frac{\sin(\alpha + \beta)}{\sin(\alpha)}}{\sin(\alpha + \beta + \delta)}$
	$c_m = \left(\frac{\sin(\alpha + \beta)}{r \cdot \frac{\sin(\beta)}{\sin(\alpha)} - \cos(\alpha + \beta) - \sin(\alpha + \beta)} \right) \cdot \sigma_T$	

The c_m is the pseudo cohesion, a scaled form of the cohesion based on the Mohr circle for the tear type, see paragraph 2.6.5. For readers familiar with the cutting theory have noticed that all φ's and δ's symbols are equal to zero and are therefore not present in the equations in Table 2.4, see paragraph 2.7 on why the internal (φ) and external (δ) friction angles are zero with clay cutting.

2.6.3. Soil failure types

The different failure types are dependent on soil properties and forces on the soil that are normative for failure. There are four different failure types for soil, as demonstrated in the figures below.

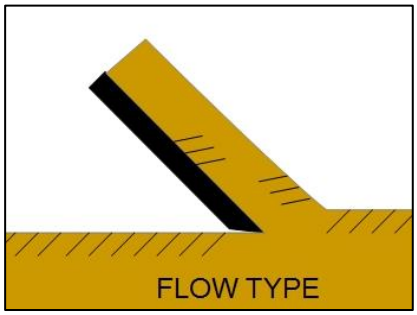

Figure 2.27 - Flow type failure

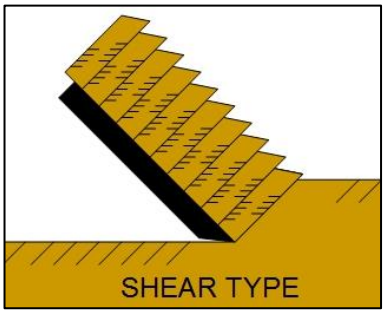

Figure 2.28 - Shear type failure

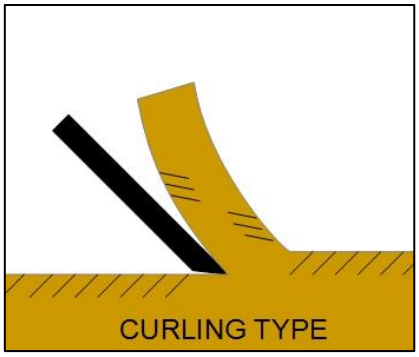

Figure 2.29 - Curling type failure

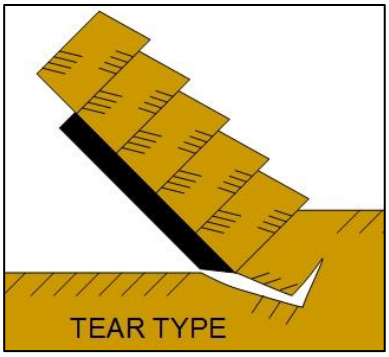

Figure 2.30 - Tear type failure

2.6.4. Clay failure types

Of the four failure types, three failure types occur with clay: the tear, curling, and flow type. The tear type may occur during the cutting of a thick layer of clay with a primary crack followed by a secondary crack, illustrated in Figure 2.31. The tear type is applicable when the clay conditions can be described by equation 2.6.13.

$$\frac{A - C \cdot \cos(\alpha + \beta)}{\sin(\alpha + \beta)} - C \leq T \qquad 2.6.13$$

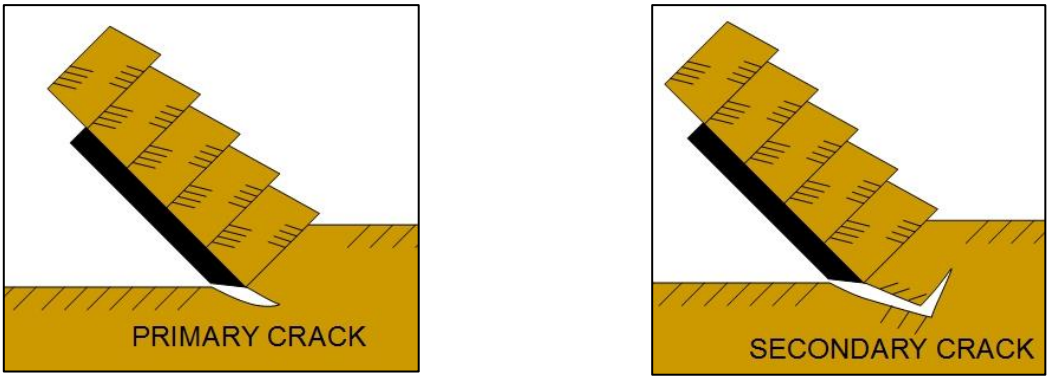

Figure 2.31 - Primary and Secondary crack with the tear type

Curling type may occur when clay conditions are described by equation 2.6.14. As a result of this condition, the clay layer that is cut will be thin.

$$\frac{C - A \cdot \cos(\alpha + \beta)}{\sin(\alpha + \beta)} - A \leq 0 \qquad 2.6.14$$

The flow type is the intermediate failure type between the tear and curling type. In this case, the cut layer must not be too thick or too thin, and therefore neither satisfies both the condition of equation 2.6.13 nor 2.6.14. The clay layer in this case would be medium-thick. This should vary for different clay types with respect to the undrained shear strength of the clay.

With the three failure types there are region when the flow, curling or tear type will occur. To visualise this more both Figure 2.32 and Figure 2.33 display the transition regions for horizontal and vertical cutting forces with the different types. The green lines are the development state and determine the failure type

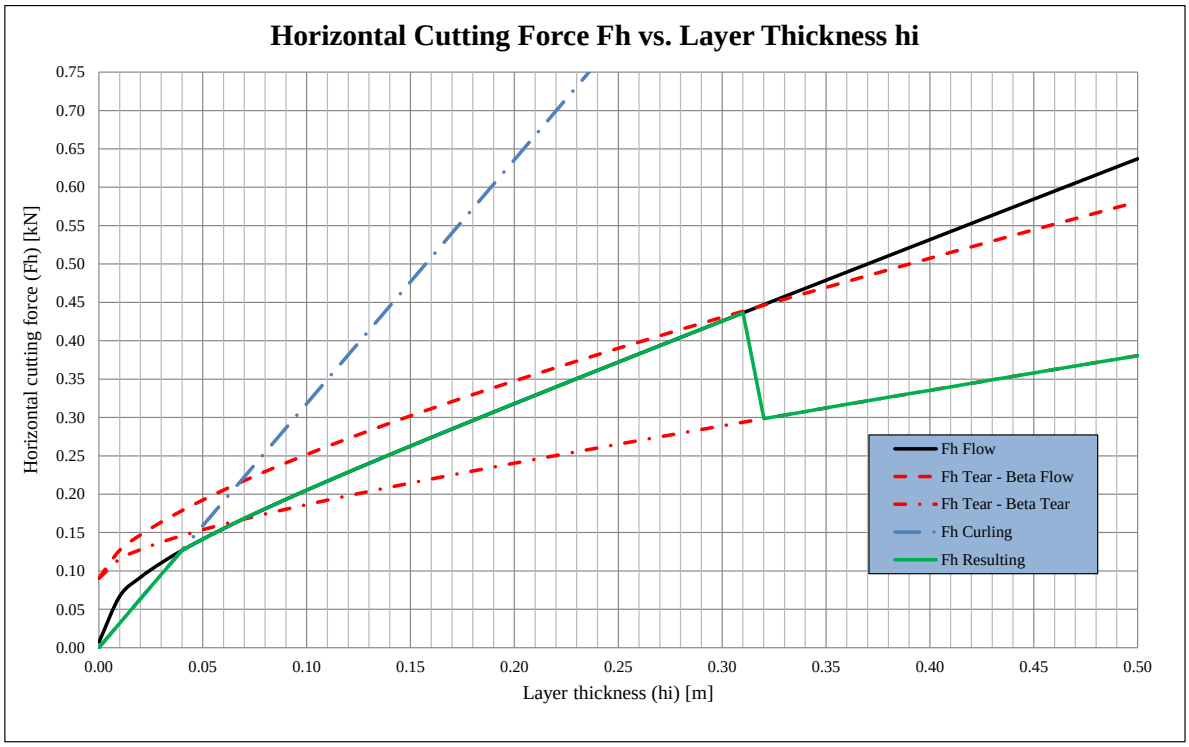

Figure 2.32 – Clay failure type dependent on layer thickness with horizontal cutting force (Miedema, 2014)

The horizontal cutting force starts of will the curling type when the thickness is smaller than 0.04 m. For the region 0.04 up to 0.31 m the flow type is the failure type curing the clay cutting process. When the tension is the mobilized clay region in the failure plane is stronger than the tensile failure, because of the thickness of the cut clay layer. There is a jump from 0.44 kN to 0.30 kN, because the tear type will occur during cutting. If the layer thickness goes from 0.35 m back to 0.20 m the failure is a continuous process so if clay fails tear type it will not jump back to flow type. Somewhere between the tear and curling type the switch is made back to flow type.

For the vertical cutting force have the same regions of failure type, but during the curling type the blade gets pushed upwards for a clay layer thickness smaller than 0.10 m.

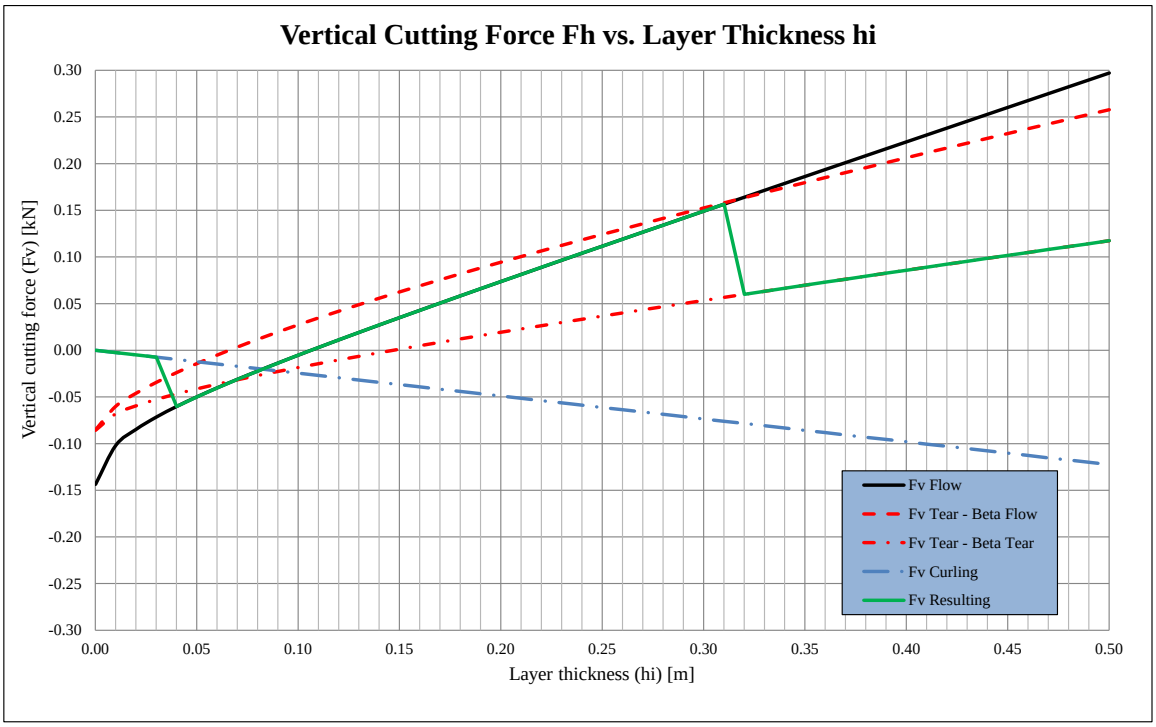

Figure 2.33 - Clay failure type dependent on layer thickness with vertical cutting force (Miedema, 2014)

The conditions that determine the different types of failure are based on the relation between adhesion and cohesion as well as internal and external friction. To avoid confusion between the four values, some additional information is necessary.

2.6.5. Mohr Coulomb

The internal friction and cohesion are derived from the Mohr circle. The stress state of a point can be described by two principal stresses that act on that point under a certain angle. These stresses are perpendicular to each other.

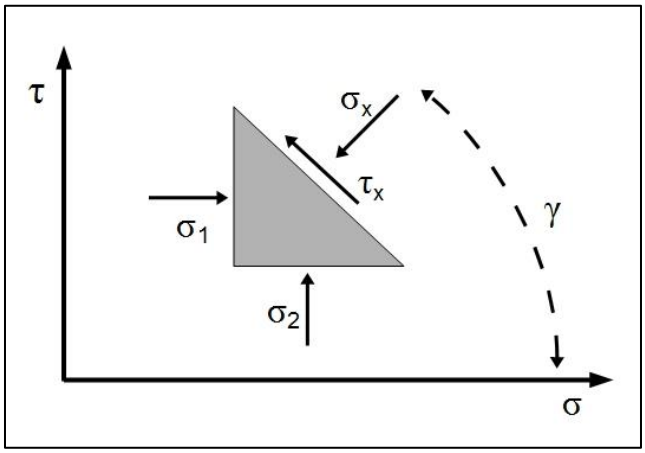

Figure 2.34 - Stresses on a soil element

The force equilibrium in horizontal and vertical direction of the stresses shown in Figure 2.34 leads to a description of the principal stresses:

$$\sigma_1 = \sigma_x \cdot \cos(\gamma) + \tau \cdot \sin(\gamma) \quad \text{2.6.15}$$

$$\sigma_2 = \sigma_x \cdot \sin(\gamma) - \tau \cdot \cos(\gamma) \quad \text{2.6.16}$$

Here σ_1 is the major principal stress [Pa] and σ_2 is the minor principal stress [Pa]. σ_x is the inclined stress [Pa], γ is the orientation of the shear plane and τ is the shear stress [Pa]. Rewriting these equations 2.6.15 and 2.6.16 for the shear stress τ and the normal stress σ results in:

$$\sigma = \left(\frac{\sigma_1 + \sigma_2}{2}\right) + \left(\frac{\sigma_1 - \sigma_2}{2}\right) \cdot cos(2\gamma) \quad \text{2.6.17}$$

$$\tau = \left(\frac{\sigma_1 - \sigma_2}{2}\right) \cdot sin(2\gamma) \quad \text{2.6.18}$$

Squaring equation 2.6.17 and 2.6.18 results in a formula for a circle that describes the stress state of a soil at any angle for a given principal stress. This circle is called the Mohr circle and can be used to graphically describe stress states. In Figure 2.35 a visual display including cohesion, shear strength and tensile strength.

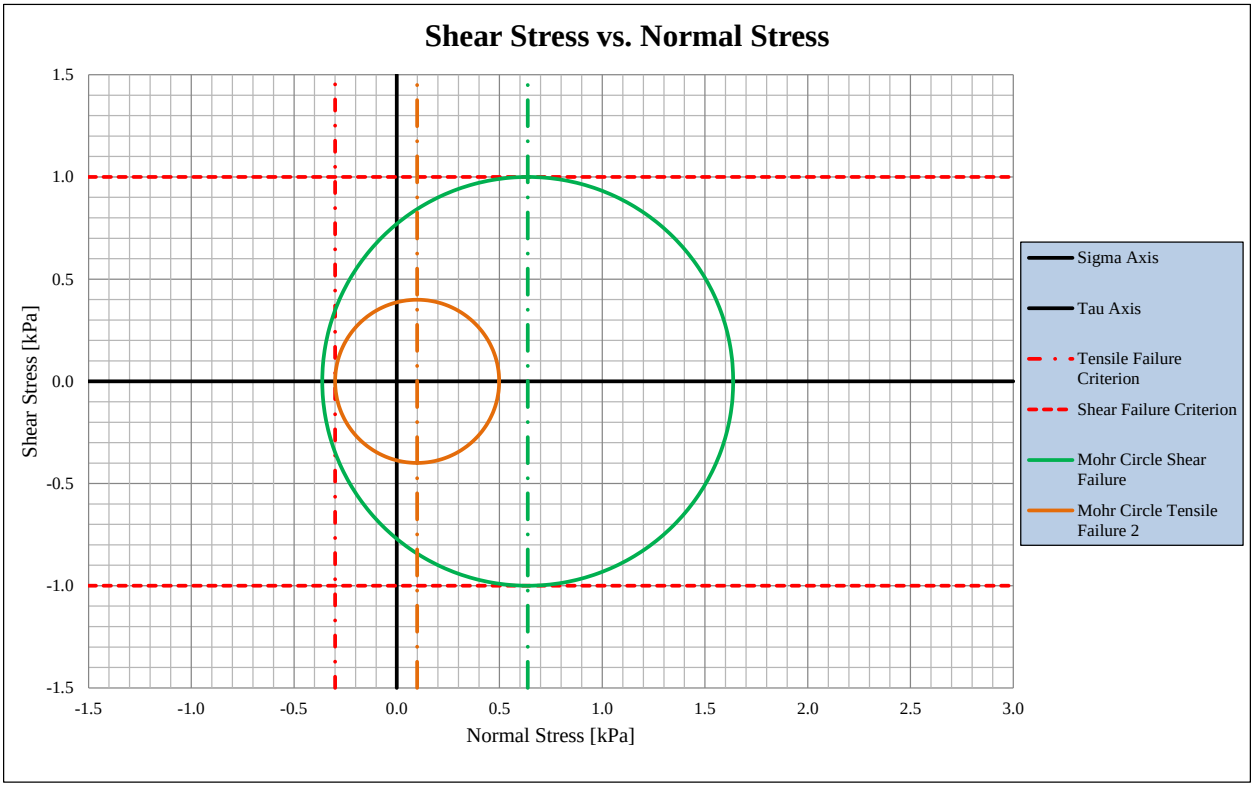

Figure 2.35 - Mohr circle with cohesion, intern friction angle, tensile strength and stress state (Miedema, 2014)

The two circles in Figure 2.35 represent two different states the clay is and could be. The orange circle is the tensile failure circle and the failure envelop with tensile strength being the boundary on the left (red line). The green circle is the current stress state of the clay. If the current stress state intersects with the stress axis or x axis with a higher value than the tensile strength, the clay will fail by tensile.

Adding up and rewriting equation 2.6.17 and 2.6.18 leads to the Mohr Coulomb failure criterion. This criterion describes the shear strength of soil based on its cohesion, stress state and internal friction angle. The cutting theory of Miedema is based on this criterion in equation 2.6.19.

$$\tau = c + \sigma \cdot \tan(\varphi) \qquad 2.6.19$$

Here σ is the effective stress [Pa], φ is the internal friction angle [degree] and c is the internal shear strength [Pa] or coshesion.

2.7. φ = 0 concept

Cohesion and adhesion are dominant in clay cutting with the φ = 0 concept. The internal and external friction angles are assumed zero as are the gravity, inertial forces and pore pressures. This is an result of the values being so small that they maybe neglegted. This simplifies the cutting equations. Clay however is subject to strengthening, which means that the internal and external shear strength increase with an increasing strain rate.

When clay is under undrained conditions, which means that the water in the pores is unable to flow out with increasing stress, there are no internal and external frictions with the φ = 0 concept. With a high strain rate the water cannot flow out the pores resulting in additional pressure. If the grain stresses do not change, the shear stresses do not change and effectively the friction does not change, according to Coulomb. So there is no relation between the additional pressure and the shear stress, therefore φ = 0 (Miedema, 2014). The internal friction and cohesion are calculated with the Mohr circle from Mohr Coulomb (1900).

2.8. Cohesion vs. Adhesion

The adhesive strength of clay is assumed to be a percentage of the cohesive strength. The estimated percentage runs between 60-100%. The assumptions made in the CCS32 software are on the safe side to ensure the payloads of the buckets are not too high during estimating. For soft clay, the percentage is up to 100% gradually decreasing to 52% for hard clay, see Table 2.5 and paragraph 2.9 for the CCS32 software. The software clay data input is based on the American Petrolium Institue norms that state at least 50% of the cohesive strength can be used for the adhesive strength (API, 1993).

Table 2.5 - CCS32 cohesion and adhesion values

Clay	Cohesion [kPa]	Adhesion [kPa]	Adhesion/Cohesion [%]
Very soft	12	12	100
Soft	24	24	100
Medium	48	40	83
Stiff	96	70	73
Very Stiff	192	120	63
Hard	388	200	52

The currently used adhesive strengths of the clay are not completely known and are assumed. The development from very soft to medium must decrease to 60% and further to 10%-0% for the very stiff to hard clay, see Table 2.7 and Figure 2.36. This is based on handling different clays and from previous research done by Sangry 1972, Littleton 1972, Kooistra et al. 1998 and van der Wielen 2014, see Table 2.6. An educated hypothesis is when for example the transition zone between rock and clay with a strength of 400 kPa has no adhesion and an internal friction angle of approximately 20 degrees. The clay's adhesive strength must decrease with increasing cohesive strength. The experiments supporting the prediction will be discussed later in chapter 3.

Table 2.6 - Previous clay studies on cohesion and adhesion relation

Clay type	Study	Cohesion [kPa]	Adhesion [kPa]	Adhesions/Cohesion [%]
Illite	Littleton (1979)	19	16	84
Mattagami	Sangrey (1972)	23.3	14	60
River clay	Van der Wielen (2014)	26.9	15.6	58
K112	Kooistra et al. (1998)	28	18.5	66
Leda	Sangrey (1972)	55.9	2.8	5
Ladrador	Sangrey (1972)	69.1	3.5	5
Eem #72	Kooistra et al. (1998)	75	5.1	7
Eem #50	Kooistra et al. (1998)	149	0	0
Eem #59	Kooistra et al. (1998)	238	0	0

Table 2.7 - Prediction cohesion and adhesion values

Clay	Cohesion [kPa]	Adhesion [kPa]	Adhesions/Cohesion [%]
Very soft	12	12.0	100
Soft	24	19.2	80
Medium	48	28.8	60
Stiff	96	38.4	40
Very Stiff	192	19.4	10
Hard	388	0	0

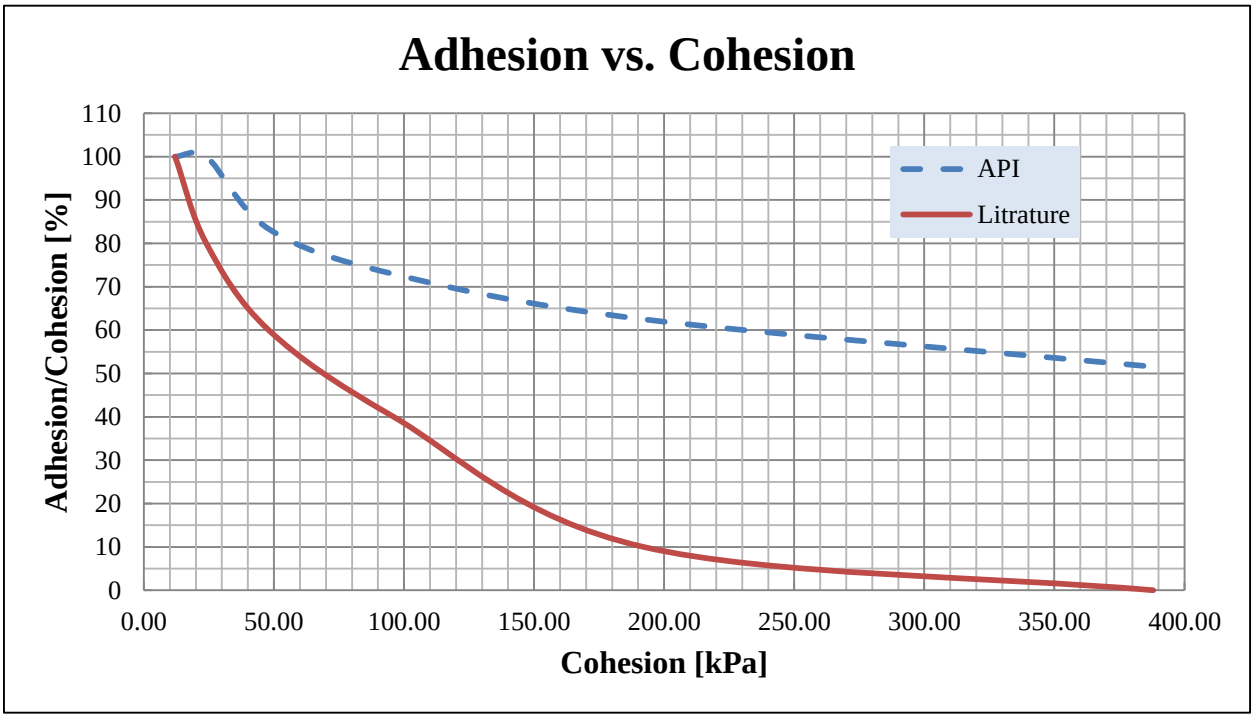

Figure 2.36- Clay cohesion and adhesion prediction

The strength of clays with decreasing internal shear strength or adhesive strength must have an explanation. For increasing clay strength and assuming a decreasing adhesive strength the clay strength during cutting must come from increasing internal and external friction angle. With the clay cutting theory the $\varphi = 0$ concept is assumed, but this would mean the sand cutting theory must be applied for clays with a decreasing adhesive strength. All this information on clamshell buckets, soil mechanics and cutting theory is implemented in a software tool CCS32.

2.9. Clamshell Closing Simulation 32 software

The information on bucket geometry, bucket kinematics, clay properties and clay cutting has been put in a Clamshell Closing Simulations software (CCS32). The CCS32 software was used to simulate a clamshell bucket closing in sand or clay. It was created by S.A. Miedema in 1989 for GLDD with the main purpose to be able to make better production estimates. Using the software is very simple. The first step is to select a bucket and the second step is to select a soil. After this the simulation can be started. The software has several outputs on the right-hand side of the software window, see Figure 2.37.

- Situ production or clamshell payload in the bucket
- Time of closing clamshell
- Vertical position of the bucket lip (Y-lip)
- Winch power needed to close bucket
- Specific energy of one bucket closing cycle
- Total sticky effect from one bucket closing cycle
- Rope force needed to close bucket.
- Force in the arms of the bucket

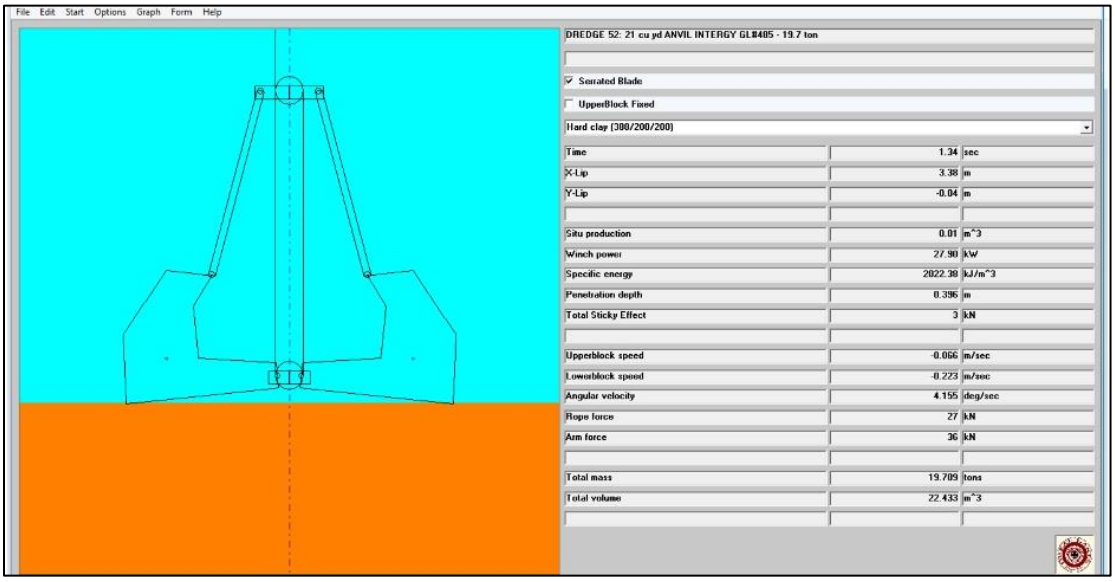

Figure 2.37 – CCCS 32 software home screen (Miedema, 1989)

The CCS32 software has an option to display a set of graphs with the following over time or bucket span:

- Bucket bite profile over bucket span
- Power and production graphs
- Horizontal forces graphs
- Vertical forces graphs
- Velocities and forces graphs

2.9.1. Clamshell simulation phases

As previously discussed, the CCS32 software also works in closing phases. After making the bucket and soil selection, the simulation was started and the clamshell closing phase 1 starts. There are three different phases with closing the clamshell bucket:

- Phase 1: soil penetration

- Phase 2: bucket closing
- Phase 3: Lifting the bucket

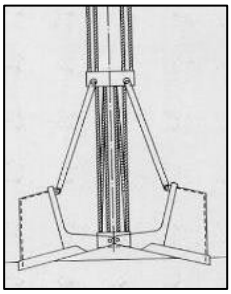

Figure 2.38 - Phase 1 soil penetration with the bucket

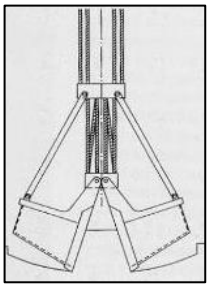

Figure 2.39 - Phase 2 closing of the bucket

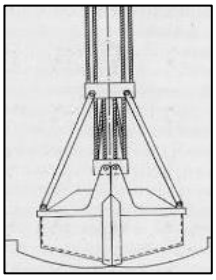

Figure 2.40 - Phase 3 bucket closed continued with lifting

Figure 2.41 displays a closer view of the clamshell bucket without teeth. Teeth can be mounted on the bucket lips depending on the soil type. For medium to hard clay teeth should have no effect on the production.

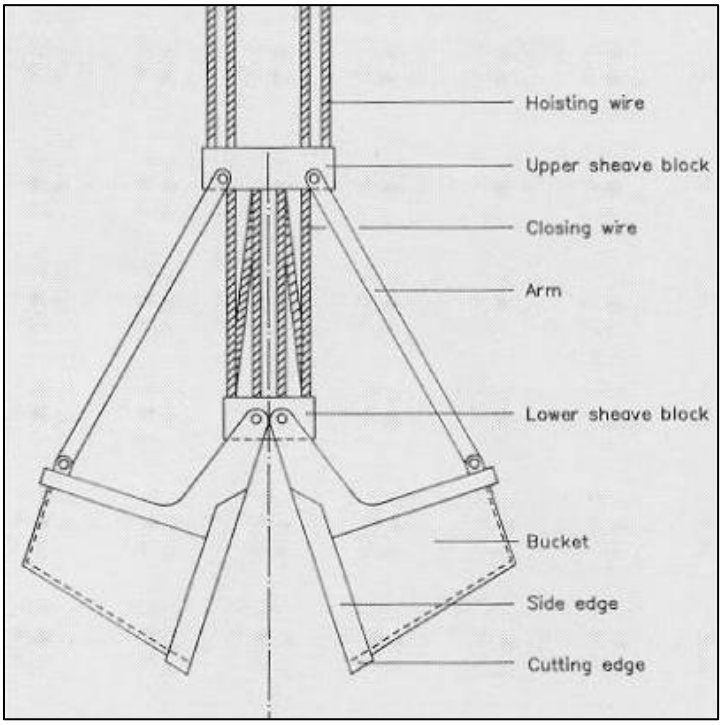

Figure 2.41 - Clamshell bucket global sketch of side view (Miedema & Vlasblom, 2006)

2.9.2. Clamshell bucket parameters adjustable in CCS32

The CCS32 has several parameters that can be adjusted to design various existing and concept buckets. The clamshell bucket, sand and clay properties can be modified to create the desired input. The adjustable inputs of the clamshell are the following:

- Bucket arm
- Bucket parameter
    - Adhesive factors

    - Inner width
    - Lip thickness
    - Mass
    - Opening angle
    - Cutting angle
    - Adhesive cutting length
- Bucket coordinates
    - Centre point of gravity (COG)
- Lower sheave block mass
- Upper sheave block mass
- Rope/sheave layout
    - Rope speed
    - Speed ratio
    - Maximum rope force
    - Maximum winch force
- Adhesion, width and serrated blade factor

The adjustable inputs for the clay properties are listed below:

- Clay ball distribution, shape factor and density
- Cohesion
- Adhesion
- Tensile strength
- Wall friction
- Bulked concentration
- Internal and external friction

2.9.3. Clamshell bucket parameters influencing the production

The simulations were conducted to understand and determine the sensitivity of the bucket's normative parameters that increase the payload and reduce the forces needed to close the clamshell bucket. The influence of each parameter was examined with CCS32 data output. The parameters which had notable influence and were not an adjustable factor in the software were labelled to be normative. With these normative parameters the sensitivity analysis was done and results will be discussed in chapter 5. The bucket opening angle is set at 87 degree and is a given condition. The normative parameters are:

- Cutting angle of bucket bowl lips
- Centre point of gravity (COG)
    - X-coordinates
    - Y-coordinates
    - Combinations of X and Y coordinates
- Adhesive cutting length of the bucket bowl
- Total weight of the bucket
- Total span of the bucket
- Total width of the bucket

2.9.3.1. Cutting angle of bucket bowl lips

The cutting angle of the bucket bowl lips is the angle that the steel makes after the start of the tip on the inside of the bowl, see Figure 2.8. This must not be confused with opening angle of the bucket (paragraph 2.2.2), this is the bucket's angle when opened. The cutting angle has an effect on the amount of force generated. This is similar to the blade angle and explained in paragraph 2.6.2.

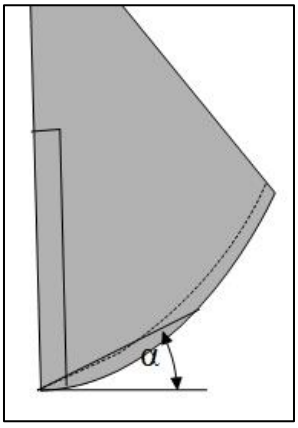

Figure 2.42 – Cutting angle of clamshell bucket

2.9.3.2. Adhesive cutting length

The adhesive cutting length is the part of the bucket bowl that contributes to the total sticky effect. By varying the cutting length, the contribution to the total sticky effect and situ production can be influenced. The contribution to the total sticky effect is the steel surface that is in contact with the clay. The red triangle in Figure 2.43 is the contact area. The cutting length is the distance between X9 and X7A/X8 depending on the bucket, see Figure 2.43.

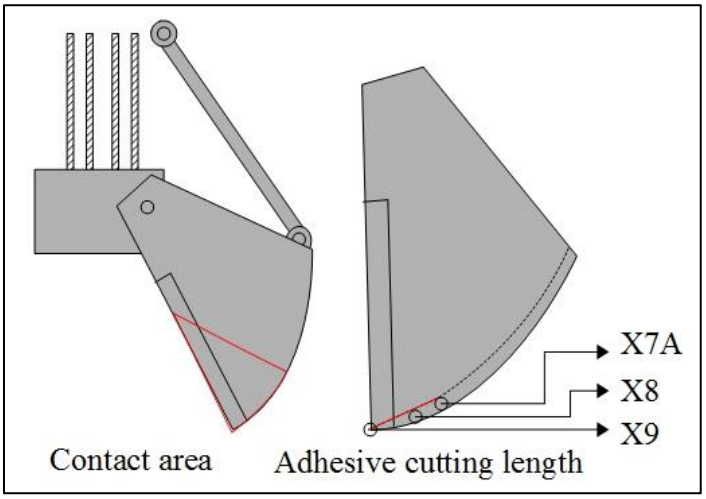

Figure 2.43 - Adhesive length and contact area

2.9.3.3. Centre point of gravity

The centre point of gravity (COG) is the point of the bucket where the earth's gravitational force acts. The two bucket half are similar, but only the two bucket halves combined will give an evenly balanced bucket. The assumption was that if the COG was moved more to the edge of the bucket, this would generate larger momentum for better clay penetration. A better clay penetration will result in a higher production of clay. In the CCS32 software, this meant adjusting the range of X-direction and Y-direction values of the COG to create a larger arm. The combinations of X and Y coordinates to see the total effect are shown in Figure 2.44, which is an example of possible X and Y-direction locations.

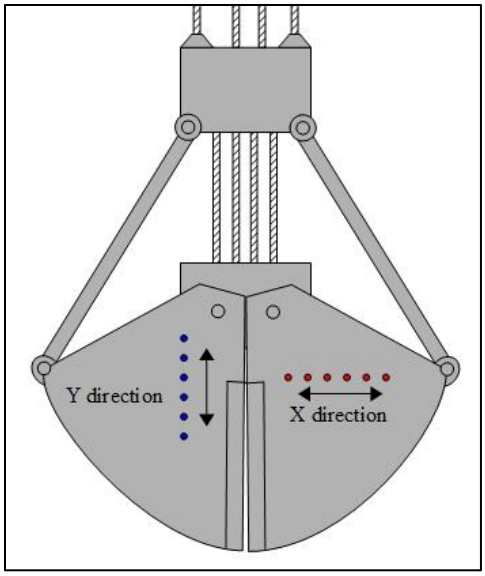

Figure 2.44 - COG sensitivity analysis possible locations

2.9.3.4. Total weight of the bucket

The total weight of the bucket is determined by the upper and lower sheave blocks, bucket arms and bucket bowl. It can be varied and may have effect on the penetration phase of the grab closing cycle.

2.9.3.5. Total span of the bucket

Varying the span of the bucket is possible but will have effect on the forces on the bucket. it will also vary the footprint of the bucket, see Figure 2.45.

2.9.3.6. Total width of the bucket

Varying the width of the bucket will have effect on the foot print of the grab. Increasing the footprint may result in a larger payload each cycle. The width is the side of the bucket, see Figure 2.45.

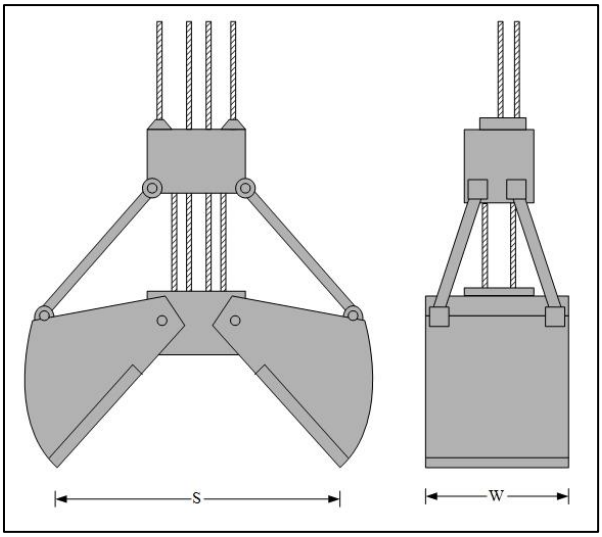

Figure 2.45 – Span and with of the bucket

3. Adhesive natural field clay experiments

The provided information on the clamshell bucket, soil mechanics and cutting theory in chapter 2 has given the proper tools to fully understand this study on the clamshell bucket production optimization. The following chapter covers an important part of the study, the relation of the adhesive strength with clay for increasing cohesive strength which is needed to be able to predict productions. To overcome this hurdle a test set-up must be designed, constructed and used to measure adhesive strength of natural field clays. The adhesive test set-up (ATS) had as main goal to measure the adhesion of clay and to examine the increasing clay strength or cohesion and adhesion possible decrease to zero. A couple of criteria arose during the brainstorming phase of different test set-up designs. An adhesive test set-up should be

- able to measure the adhesion of the clay.
- able to reproduce each test, because a test must be repeated to see if the measurement is in proper range and therefore valid for these circumstances.
- able to eliminate traces of other materials, like sand that will influence the measurement because of its internal and external friction angle. The resistance created by the friction angles will give a higher value than present in the clay.
- able to generate sufficient force to move a steel surface over a clay surface.
- able to use with natural field clay samples
- able to eliminate other forces

3.1. Comparable adhesive research

A similar research was done with an experimental study of the adhesion between clay and steel (Littleton, 1976). The research was a complete set of parameters for the shearing resistance between two different clays, illite and kaolinite, and a smooth steel surface. The test set-up was a standard 60 mm square shear box modified by replacing the bottom half of the box by a solid steel block. The strain rate of the tests were done at 0.01 mm/s. The quick-undrained tests were initially consolidated to a vertical pressure of 0.1 N/mm^2.

The most noticeable difference in behaviour between the two clays was shown by the quick undrained tests. The peak and residual stresses for illite, shown in Figure 3.1, are indicative for overconsolidation throughout the stress range. Failure envelopes for illite, shown in Figure 3.2, were drawn for clay-to-clay peak stresses and clay-to-steel residual stresses. The normal and overconsolidated characteristics for tests on kaolinite, Figure 3.3 and Figure 3.4, depend on whether the specimen is sheared above or below the consolidation pressure. The kaolinite-to-steel failure envelope, shown in Figure 3.5, was drawn using the shear stress for 1 mm specimen displacement.

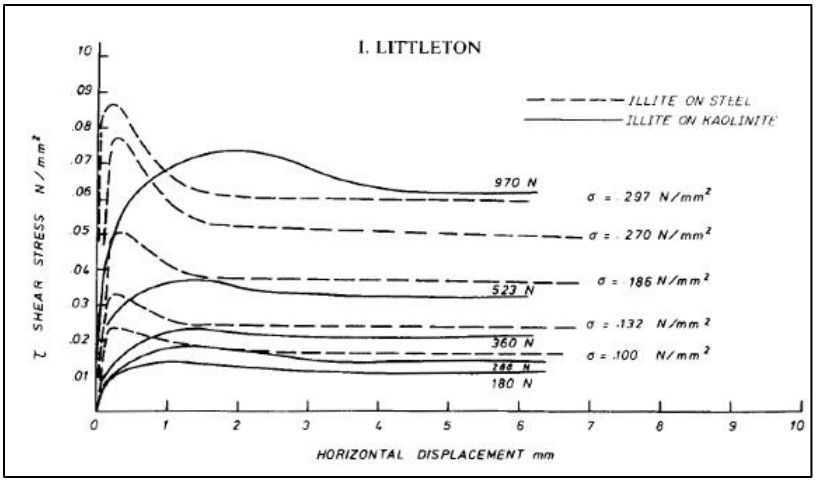

Figure 3.1 - Stress displacement curves for consolidated undrained shear box tests on illite

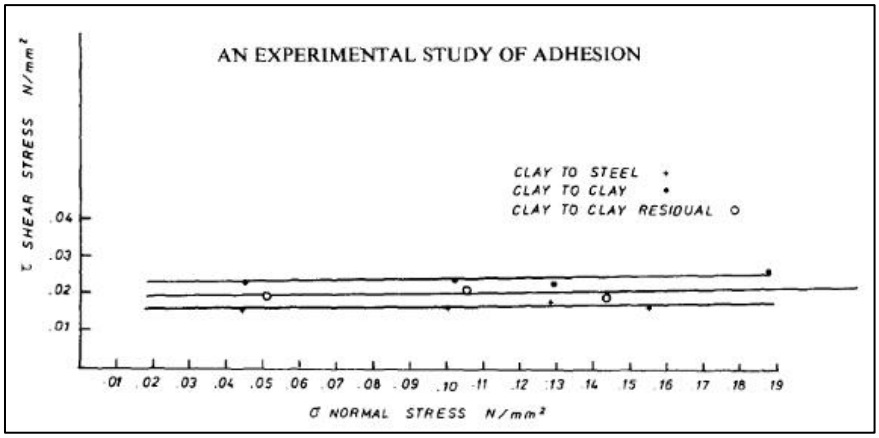

Figure 3.2 - Failure envelop for quick undrained shear box tests for illite

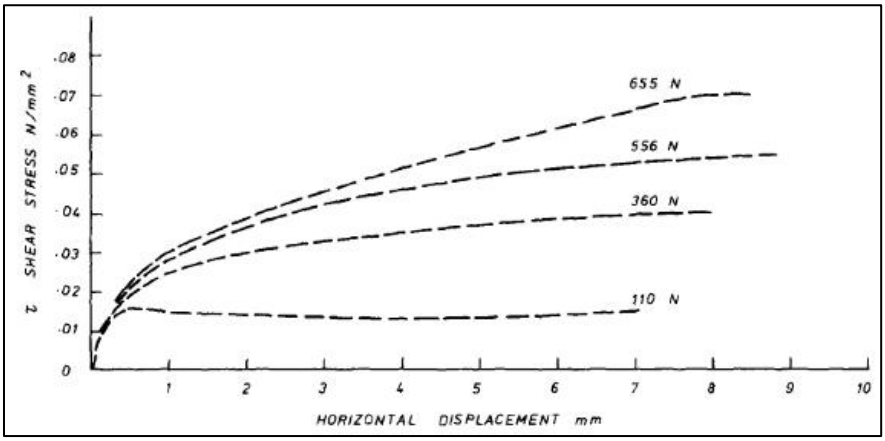

Figure 3.3 - Stress displacement curves for quick undrained shear box tests kaolinite-kaolinite

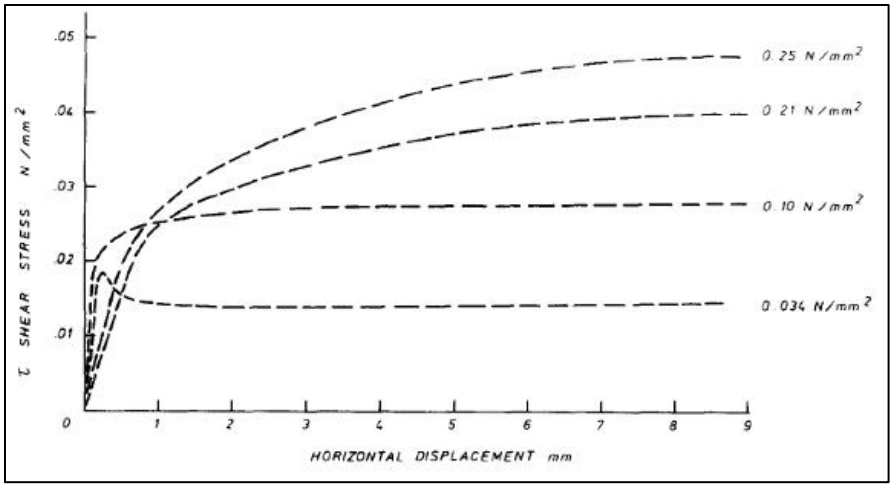

Figure 3.4 - Stress displacement curves for quick undrained shear box tests kaolinite on steel

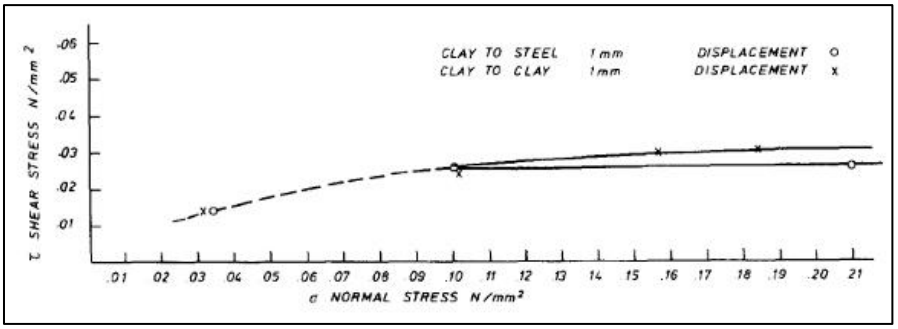

Figure 3.5 - Results for quick undrained shear box test for kaolinite

The peak stresses with illite-to-steel occur at small displacements. Littleton thought it was possible to compare residual stresses to determine the adhesive factor by using the equation 3.1.1.

$$Adhesion\ factor = \frac{Shear\ strength\ mobilised\ in\ skin\ friction}{undisturbed\ shear\ strength} \qquad 3.1.1$$

Littleton tentatively suggested that the adhesion factor between the peak shear stress for clay-to-steel and clay-to-clay is about 1.3 [-] at small displacements such as 0.25 mm with over consolidated clay. This value drops progressively to a value of between 0.7-0.8 by approximately 2 mm-3 mm displacement and is nearly constant thereafter. Adhesion factors of approximately 1.4 [-] were observed at small displacements with normally consolidated clay. As the specimen deformation increases, the adhesion factor drops progressively to below 0.6 by 10 mm.

Summarizing the main observations, it appears that in all cases examined the clay-to-steel tests initially have a higher strength than the clay-to-clay tests at comparable small displacements. With the clay on steel, failure at the interface is fairly sudden and further deformation occurs for little change in shear stress.

The results that Littleton suggested were that for clay-to-steel experiments the most uniform adhesion factors are obtained using the residual shear stress of an over-consolidated clay for displacements >3 mm. Values of 0.75 are typical for fast loading cases but this reduces to about 0.6 for long term tests. Littleton's study on clay-to-steel

adhesion factors indicates a high resistance in the beginning of the shear box movement and decreases shortly after 2-3 mm and becomes constant. The overconsolidation of the clay increases its resistance, but nevertheless the adhesive factor is calculated from the experiments and used in his conclusion. With this current study, the vertical force on the samples is much lower and therefore also reducing the normal stresses. As a result of this there will be no overconsolidation, but it will have two possible downsides, see paragraph 3.7. In Littleton's study the clay samples consist of illite or kaolinite clay, the natural field clays will have inevitable traces of other types of soils and therefore possible clay properties. This may also have an effect on the adhesive property and comparability with Littleton's work.

3.2. Adhesive test set-up design

The adhesive test set-up design evolved on the drawing board, taking the test set-up criteria into account. The test set-up had different concepts with as starting point pushing a thin wall steel cylinder into the clay, see Figure 3.6 concept 1. The diameter of the cylinder would be increased to have a repeatable test on the same clay sample. The adhesion measured would be the force needed divided by the cylinder surface in contact with the clay. This was not the best option, because this was more cutting the clay than measuring the “stickiness” or adhesion of the clay.

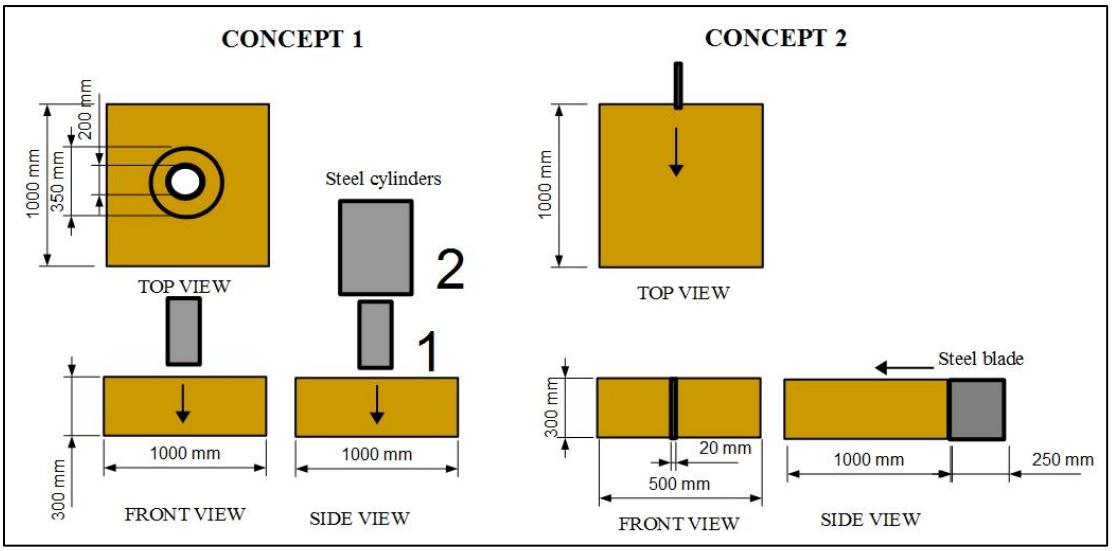

Figure 3.6 – First and second concepts of the adhesive test set-up

Concept 2 had the same problem, but seemed more applicable considering the cutting theory. Pushing a steel blade through or along clay may result in additional forces by pushing or cutting the clay in front of the steel surface. By making sketches and discussing its feasibility and usability, the final design of the adhesive test set-up resulted in Figure 3.7. This was a top and bottom plate filled with clay, though which a steel blade would be pulled. This made it repeatable if the surface layer of clay was taken off. The AutoCAD drawing can be found in Appendix A.

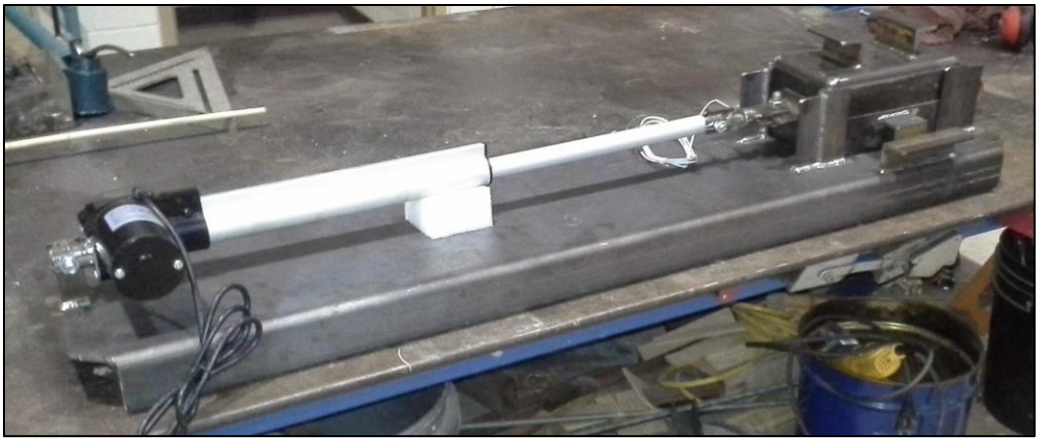

Figure 3.7 – Final design of the adhesive test set-up

With the design done on paper, a local contractor near College Station, Texas helped out on constructing the adhesive test set-up. The steel plate base on which to place the electric actuator, top and bottom plate holders and handles was the contractor's idea to increase usability and ease.

3.3. Layout adhesive test Set-up

The adhesive test set-up's final design was used to record the force needed to pull a steel blade between two layers of clay. The adhesive testing of the natural field clays were cut into a proper size and slightly remoulded to fit in the top and bottom plate. The set-up consists of the following:

- **Top plate** to hold clay
- **Bottom plate** to hold clay
- **Steel Blade** to pull through the top and bottom plate
- **Electrical actuator** (3500 N) for pulling the blade
- **Speed controller** with direction switch
- **Load cell** (1kN) to record the force needed
- **Support wheel** to make sure the blade and actuator stayed horizontally inline during the test
- **Ruler with indicator** (+2 magnets to keep rule in place) to measure the speed by distance travelled and recorded time needed
- **Steel base** to keep all parts in place and easy moving around
- **Video cameras** to record the test and use to determine blade speed during test
- **Spirit level** to ensure that the blade is horizontal

The white screen surrounding half of the test set-up was to create a clear background for the video recordings, see Figure 3.8. Two cameras were used to record the each measurement of the natural field clays. One camera was focused on the ruler and indicator with a small part on the top and bottom plate. The other camera was focused on the entire test set-up to make sure each test could be reviewed if there were strange fluctuations in the recordings. For the general layout of the test set-up with measurement equipment and recording software, see Figure 3.9.

Figure 3.8 - Adhesion test set-up

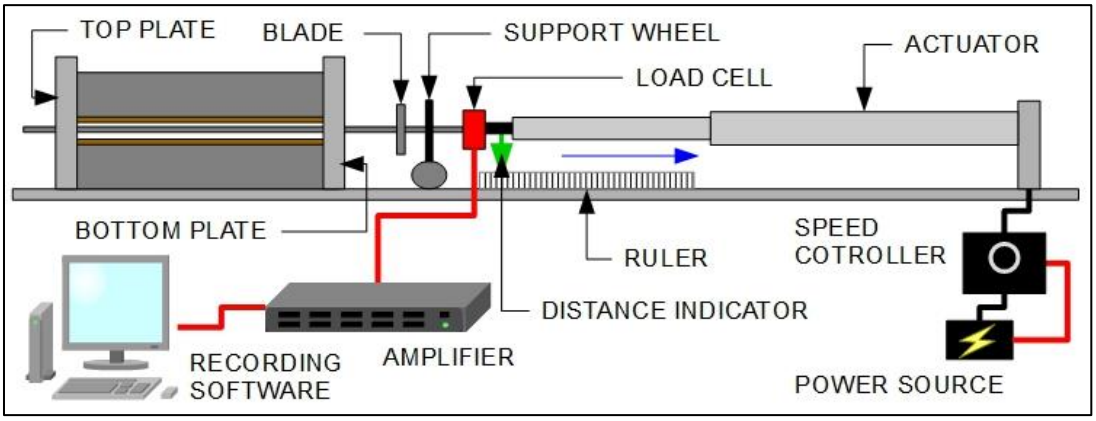

Figure 3.9 - Adhesion test set-up layout

3.3.1. Actuator speed controller

After the final design was constructed an additional interest arose: could the cutting speed have influence on the clay adhesive strength? The electric actuator can push and pull the blade at a predetermined speed. By adding a speed controller to the test set-up the speed of the blade pulling could be varied between 8 mm/s down to 0.4 mm/s. This was done to measure the effect of speed on the clay's resistance force. If a blade is pulled with a high speed it is possible that some kind of vacuum effect occurs, creating an additional resistance force when pulling the blade. For specifications on the electric actuator, load cell and speed controller, see Appendix B. For the layout and connection between actuator and speed controller, see Figure 3.10.

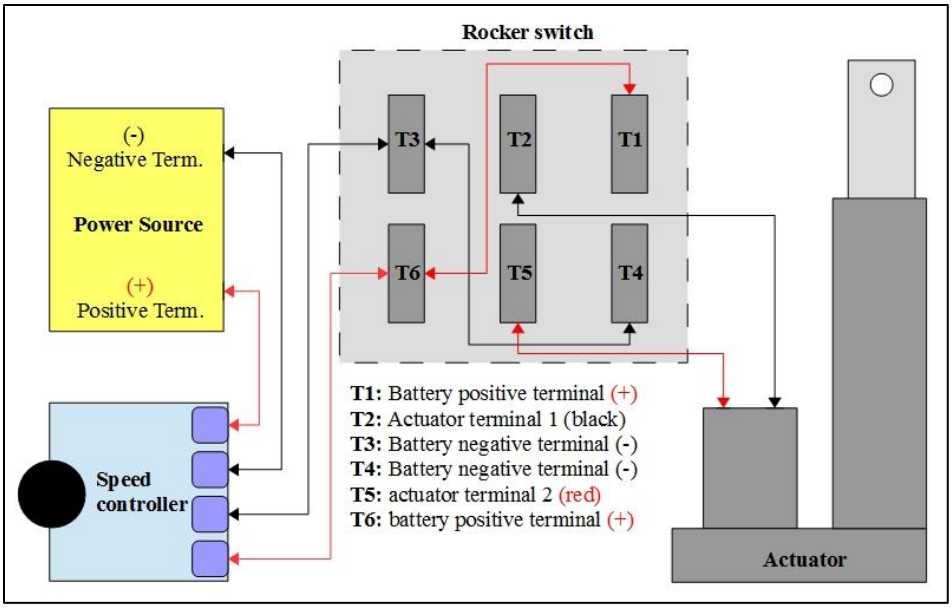

Figure 3.10 – Speed controller connection layout

3.4. Blade pulling force recording system

The recording system is needed to record the pulling force needed to pull the steel blade out from between the two layers of clay. The recording system consists of the load cell, an amplifier and computer with software. The load cell was able to measure up to 1000 Newton of force. The assumption was the pulling force would not exceed 800 Newton, therefore a 1 kN load cell was deemed sufficient with a safety factor included. The amplifier is to increase the signal strength of the load cell to ensure the computer with software would be able to read the signal.

3.4.1. Load cell calibration

The load cell was calibrated to make sure the force recorded is correct. This is done by increasing the load on the load cell and recording the voltage output. This will create a linear line between force and voltage and is needed to ensure the software was able to record the proper pulling force. A wooden pallet was hooked onto the load cell that was connected to the forklift providing an area to stack weights. Each weight was approximately 2.3-2.7 kg increasing the weight to 25 kg in total. For each weight added on to the pallet a voltage output was recorded until approximately 25 kg was on the pallet. With the known weights and voltage outputs a calibration file was created to make sure the load cell output could be correctly read by the software.

3.4.2. Recording software Helios

The recording software, Helios, was developed by E. Sonne at Texas A&M University in 2012 and was available for usage for all the adhesive testing. The software provided the option to set the recording length in seconds, the frequency or recordings per second in Hertz. Before starting a recording the initiation must be done and gauges must be zeroed out. After initiation the acquisition had to be prepared with selecting sampling rate [Hz], sampling time [seconds], calibration file and raw and calibrated data output files, see Figure 3.11.

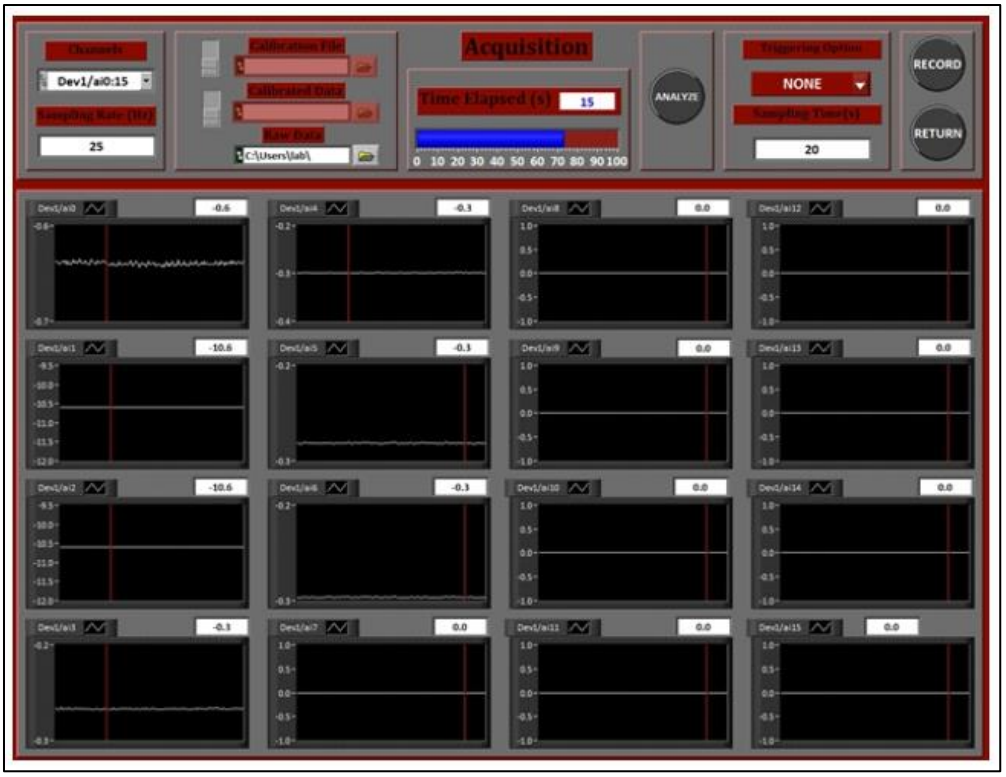

Figure 3.11 – Recording software Helios

3.5. Adhesive strength calculation from test set-up

The design of the adhesion test set-up makes it possible to determine the adhesive strength of clay. The pulling force recorded by the load cell divided by the blade surface in contact with the clay will give the adhesive stress in [N/mm^2], see Figure 3.12. The adhesive stress can be translated into an adhesive strength by multiplying the value with 1000. The forces on the blade during a measurement are the normal force, pulling force and adhesive force. The shear force (F_{shear}) only occurs if there is an external friction angle and therefore an internal friction angle. The normal force (F_{normal}) is from the weight of the top plate, clay and blade. The normal force was increased with one and two weights (5.3 and 4.7 kg) during different tests to if there was internal friction in the clay. The pulling force (F_{pull}) is recorded by the load cell connected to recording software. In the opposite direction of the pulling force is the measured adhesive force ($F_{adhesion}$) with a possible internal friction force (F_{shear}), see Figure 3.12.

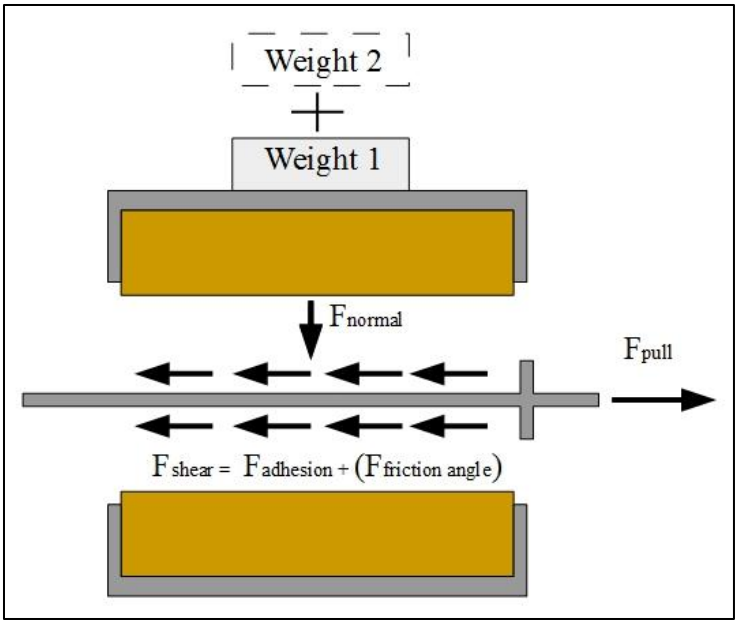

Figure 3.12 – Cross section of adhesive test set-up with forces

3.6. Adhesive testing procedure

The tests that have been carried out to measure the adhesive strength of the natural field clays were done following a specific procedure. This procedure was followed for all of the 54 tests done on the clays. The following steps were taken to conduct each measurement:

1. Weigh filled top plate, bottom plate and blade
2. Place bottom plate in set-up and connect blade to line-up
3. Connect blade to load cell and back up blade to starting position
4. Place top plate and if needed place additional weights
5. Set up software with calibration file and zero out load cell
6. Select file to record to and frequency
7. Turn on cameras and start recording
8. Flip switch to start pulling blade
9. Turn off cameras after blade is fully retracted
10. Remove top plate and possible weights
11. Unbolt blade and clean blade
12. End of one test

3.7. Tested natural field clays

The three natural field clays were acquired from different project locations of GLDD throughout the US... :

- Delaware river clay, 1840 kg/m^3
    - A soft, silty clay retrieved from the Delaware River near Philadelphia, Pennsylvania at a depth of 40 feet from a clamshell bucket after being placed on the bow of the scow. The clay sample shipping was done by wrapping the samples in several layers of cellophane and aluminium foil. Shipping was done in a box with wall protection filled up with bubble wrap. This was a safe way of keeping the water content and clay properties intact as much as possible.
- Freeport grey clay, 1950 kg/m^3

- Retrieved from Freeport, Texas at a depth of 44 feet of a hopper drag head when idle on deck. The firm grey clay from Freeport, Texas was collected by me personally at the job site. The hopper crew had loaded big chunks of clay in a bucket after wrapping it in cellophane and aluminium foil. The Freeport clay sample was loaded in the back of the truck and driven back to the Texas A&M lab in College Station, Texas.

- Freeport red clay, 2160 kg/m^3
  - Retrieved from Freeport, Texas at a depth of 44 feet of a hopper drag head when idle on deck. This firm red clay was collected and shipped in the same way as the Freeport grey clay. The red clay had similar transport procedure as the grey clay from Freeport.

3.8. Adhesive test set-up boundary conditions

The adhesive test set-up has limitations. During the clay sample preparation, the sample has to be cut to the proper size of for the top and bottom plate and the blade has to be in contact with the clay surface during the test. Two problems arise from these procedures. Firstly, the clay surface in contact with the blade is cut and may have a different effect on the blade compared to its original state. Secondly, the blade contact with the clay surface may vary if the blade and plates are not properly stacked or are moved if the blade pulling is not horizontal enough creating an additional force ($F_{additional}$) during blade pulling, see Figure 3.13.

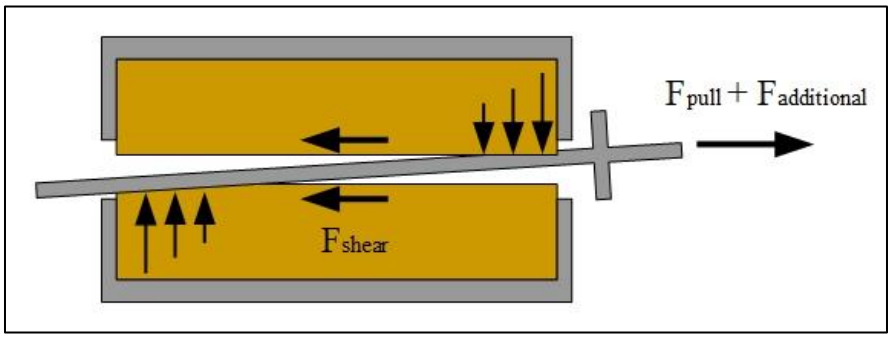

Figure 3.13 – Additional pulling force if blade is not horizontal

After a test is done the clay sample may have moved more in the corners of the top and bottom plate and may remould the sample and its properties. This effect could also occur when adding weights on top of the top plate. After each test the contact surface needs to be flattened and prepared for the next test to keep the full contact with the blade during a test. The remoulding may have an influence on the adhesive properties of the clay sample.

The contact area between the blade and the clay was not always the full surface of the blade. This means that the stress measured could be lower and could be solved by reducing the blade surface used in the calculations. The possibility for water particles to escape over time before, during and after the measurements was minimized as much as possible. But it is inevitable that with increasing vertical forces the clay had a history that influences the clay strength and contact area with the blade.

3.9. Additional testing on natural field clays

The natural field clays were also be tested to create a good profile of the tested clay samples. The additional information on clay properties will create a clear and full spectrum study on the adhesive testing of the natural field clay samples. Moreover, if the measurements have an unexpected result, it is possible to find a reason for the effect with one of the additional clay property tests on the clay sample. The additional clay property tests that will be conducted are:

- Atterberg limits, measuring the plastic and liquid limits (PL, LL)
- UU-traxial test, measuring the undrained shear strength (S_u)
- Mineralogy with x-ray diffraction (external company), recording the kaolinite, illite, etc. present in the clay sample

The data acquired will be presented in the next chapter.

4. Results of adhesive experiments and additional tests

The previous chapter covered the configuration and usage of the design and the construction of an adhesive test set-up for natural field clays. The adhesive force can be measured with this test set-up and with the additional testing explained we can go on to determine the clay properties of the three natural field clays from US soil.

This chapter consists of the acquired data and an explanation of the determination of adhesive strength. This is done with different approaches, because traces of other materials can interfere with the $\varphi = 0$ concept, see paragraph 2.7. The additional testing, Atterberg limits, UU-traxial test and Mineralogy were done simultaneously with the adhesive experiments of the natural field clays. The results of that are presented in this chapter has led to a paper that has been submitted to the WEDA expo & summit in Houston, 2015. The paper can be found in Appendix F.

4.1. Additional testing results

The three natural field clays that were tested are very different clays and this is visible in the variation of the Atterberg limits, the UU-traxial tests and from the mineralogy report.

4.1.1. Natural field clays Atterberg limits results

During the Atterberg limits tests the Delaware River clay has a lower tolerance with water particle tolerance or low redundancy. Both the Freeport grey and red clay have a similar liquid limit (LL) and almost equal plastic limit (PL). The similar value is something that was not expected, because the clay samples are retrieved from the same region and had different colours; this does not imply that the properties have to be similar. With the residue of the tests, a block of 5x5x5 cm was cut from the three natural field clay to measure the weights. By using the volume and weight the specific gravity was calculated. All the three clays have a very high specific gravity, considering the fact that clays are normally between 1500-1800 kg/m^3.

Table 4.1 - Atterberg limits natural field clays

Clay	Liquid Limit [%]	Plastic Limit [%]	Specific gravity [kg/m^3]
Delaware, Philadelphia	30.5	19.1	1837
Freeport Grey, Texas	61.5	23.6	1952
Freeport Red, Texas	60.5	18.2	2160

4.1.2. Natural field clays undrained shear strengths results

The undrained shear strengths of the natural field clays were tested under three different circumstances (5, 100 and 170% / hour), because during the blade pulling experiments the clay may is also tested with two different pulling speeds. This is done by increasing the load ram speed of the UU-traxial test. For all values of the field clays of the three different UU-traxial speeds and the additional Torvane test, see Table 4.2.

The Delaware River clay from Philadelphia, Pennsylvania has a strength of 12 kPa and is therefore a very soft clay. The Delaware sample's undrained shear strength decreases with increasing speed of the load ram, which is normal because the clay "resistance" is very low with very soft clay and therefore it will easily deform.

Table 4.2 - Undrained shear strength of natural field clays

Clay	Standard UU-Traxial (5%/hour) [kPa]	Fast UU-Traxial (100%/hour) [kPa]	Very Fast UU-Traxial (170%/hour) [kPa]	Torvane[1] [kPa]
Delaware, Philadelphia	12	11	10	34
Freeport Grey, Texas	22	17	14	45
Freeport Red, Texas	90	83	89	-

4.1.3. Natural field clay mineralogy's

The mineralogy tests are done with x-ray diffraction that identifies different types of atomic and molecular structures by recording the deflection. Each atomic and molecular structure has its own deflection angle and in this way the clay mineralogy is determined. The results of the x-ray diffraction testing on the clay specimens are summarized in this paragraph. The highly silty nature of the Delaware sample is observed and reflected in the high quartz content i.e. the silt is finely ground up quartz sand. The Texas clays are mostly illite with some kaolinite and the Delaware clay is roughly equal amounts of both.

4.1.3.1. Delaware, Philadelphia

The Delaware River clay retrieved from Philadelphia, Pennsylvania has a highly silty nature. This is observed from the high presence of quartz, i.e. the silt is finely ground up quartz sand. Just over a quarter of the sample consists of kaolinite and this is a very common ingredient to be present in clay samples. This is similar for the presence of illite in the clay sample, but it is a fifth of the total sample.

Table 4.3 - Delaware, Philadelphia mineralogy

Phase	Composition	Concentration Estimated [%]
Quartz	SiO_2	52
Kaolinite	$Al_2Si_2O_5(OH)_4$	27
Rutile	TiO_2	<1
Mica/Illite	$KAl_2(Si_3Al)O_{10}(OH)_2$	20
Hematite	Fe_2O_3	<1

4.1.3.2. Freeport Grey, Texas

The grey clay retrieved from Freeport, Texas has a very high presence of illite (59%). With a substantial amount of quartz present in the clay sample there is a good possibility this sample has some internal friction. With the internal friction present there is also an external friction angle present. These angles may have had some influence on the blade pulling force during the adhesive strength experiments.

[1] The Torvane test was conducted after all the adhesive testing was done. This created a stronger clay than initially was measured with the UU-traxial tests.

Table 4.4 - Freeport Grey, Texas mineralogy

Phase	Composition	Concentration Estimated [%]
Quartz	SiO_2	31
Kaolinite	$Al_2Si_2O_5(OH)_4$	2
Rutile	TiO_2	<1
Mica/Illite	$KAl_2(Si_3Al)O_{10}(OH)_2$	59
Feldspar	$(K,Na)AlSi_3O_8$	7

4.1.3.3. Freeport Red, Texas

The red clay from Freeport, Texas has also a very high presence of illite (60%), making it useful in comparison with the similar research done by Littleton (1976). Quartz is also present giving the sample some internal friction and therefore some external friction angle, which may have resulted in a higher blade pulling force. The other phases present are hardly noticeable.

Table 4.5 – Freeport Red, Texas mineralogy

Phase	Composition	Concentration Estimated [%]
Quartz	SiO_2	19
Calcite	$CaCO_3$	11
Rutile	TiO_2	<1
Anatase	TiO_2	<1
Dolomite	$CaMg(C0_3)_2$	<1
Mica/Illite	$KAl_2(Si_3Al)O_{10}(OH)_2$	60
Kaolinite	$Al_2Si_2O_5(OH)_4$	9
Montmorillonite	$(Na,Ca)_{0.3}(Al,Mg)_2Si_4O_{10}(OH)_2 \cdot nH_2O$	trace

4.2. Natural field clays adhesive strengths

The determination of the adhesive strength of the natural field clays is done via different approaches. The first approach is extrapolating the fitting curve to the y-axis to extract the adhesive strength of the different field clays. The second is to evaluate the data sets as indivuals and then drawing a linear line through the points. The final one is the φ=0 approach. Here the φ=0 concept is taken into account, averaging all values and resulting in an average adhesive stress with an average normal stress. All graphs of the different approaches can be found in Appendix I.

All the recordings gave a raw data set that was copied into Excel to create a graph used to examine the experiments. Each experiment was recorded at a frequency of 50 Hz, meaning every second five data points were recorded. The clay sample length was 230 mm in length and the blade was 280 mm in length. The full contact between the total blade surface and the clay was therefore 50 mm. The blade pulling speeds were 8 mm/s or 0.4 mm/s meaning that a recording has approximately 6 or 125 seconds during a full contact between full blade length and clay sample. Figure 4.1 and Figure 4.2, with the orange area highlighted, show the time windows that the average pulling force is determined during full contact between steel and clay.

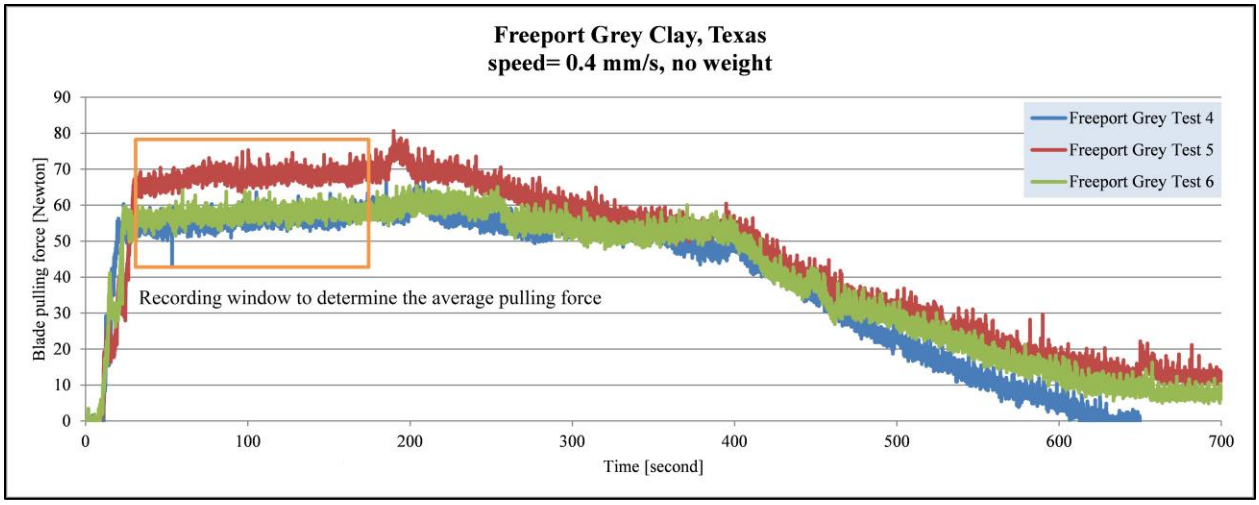

Figure 4.1 – Pulling force determination from raw data graph at low speed

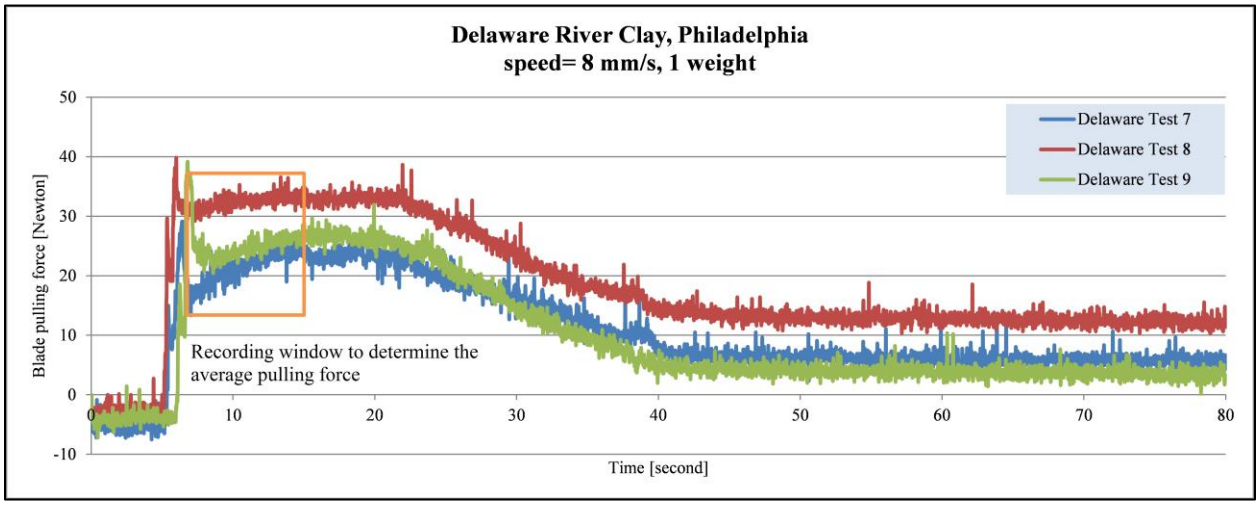

Figure 4.2 – Pulling force determination from raw data graph at high speed

4.2.1. Adhesive data points

The data retrieved from all 54 test on natural field clays are evaluated on possible measured adhesion. The different approaches will be discussed in the following paragraphs. The data points of the different tested clays show different scatter and patterns, see Figure 4.3.

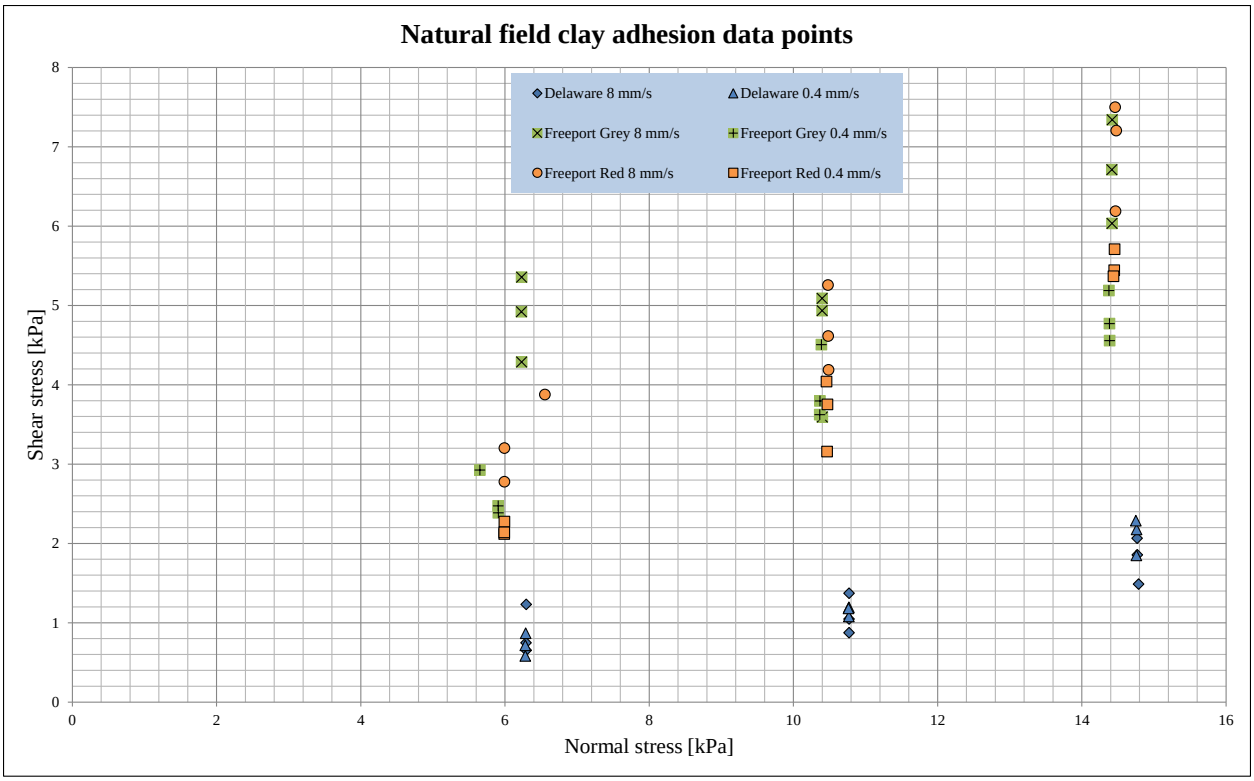

Figure 4.3 – Data points of adhesive experiments

The normal stress was adjusted by adding weights on the top plate and weighed with a scale before each adhesive test, see Figure 3.12. There were three vertical forces on the clay sample and blade: firstly, its own weight; secondly, its own weight and one extra weight and finally, its own weight with two extra weights. These three vertical forces increased the normal stress on the clay and the steel blade. The normal stresses were calculated by using equation 4.2.1.

$$\sigma_n = \frac{F_{v,blade}}{A_{blade}} \qquad 4.2.1$$

σ_n is the normal stress in [N/mm^2] with $F_{v,blade}$ and A_{blade} being the vertical force [N] and blade surface in [mm^2]. The shear stress is calculated in a similar way, only the vertical force ($F_{v,blade}$) is replaced by the average pulling force (F_{pull}) in the recorded time window (paragraph 4.2), see equation 4.2.2.

$$\tau_b = \frac{F_{pull}}{A_{blade}} \qquad 4.2.2$$

4.2.2. Extrapolation approach towards adhesive clay properties

The first approach is the extrapolation approach by using fitted trend lines. The trend lines are selected according to the best fit. With the equations the intersection with the y-axis is determined. The instersection with the y-axis or shear stress is used to determine the adhesion present in the natural field clay. The equations and intersection (x=0 or normal stress = 0) are presented in Table 4.6.

Table 4.6 - Extrapolations approach trendline equations

Clay	Pulling speed [mm/s]	Trend line equation	Shear stress / X=0 [N/mm^2]
Delaware, Philadelphia	0.4	$y = 0.0168x^2 - 0.1909x + 1.2546$	1.25 / 0.71
	8	$y = 0.0149x^2 - 0.2042x + 1.2546$	1.25 / 0.87
Freeport Grey, Texas	0.4	$y = 0.0747x^2 - 1.3183x + 10.167$	10.17 / 4.37
	8	$y = 1.7389e^{0.0733x}$	1.74
Freeport Red, Texas	0.4	$y = 0.0162x^2 - 0.0619x + 1.224$	1.22
	8	$y = 0.0527x^2 - 0.0844x + 2.7898$	2.79

These data points with trend lines are displayed in a graph with adhesive stress [N/mm^2] over normal stress [N/mm^2] on the axis; see Figure 4.4.

If the line would be horizontal, it may be concluded that there is no external friction angle and therefore no internal friction angle present. With increasing normal force, the clay strength may not increase if there is no internal friction angle. The trendline should be horizontal with increasing normal stress to measure pure adhesion. This is supported by a study of Littleton (1976) with illite and koalinte clay, see paragraph 3.1.

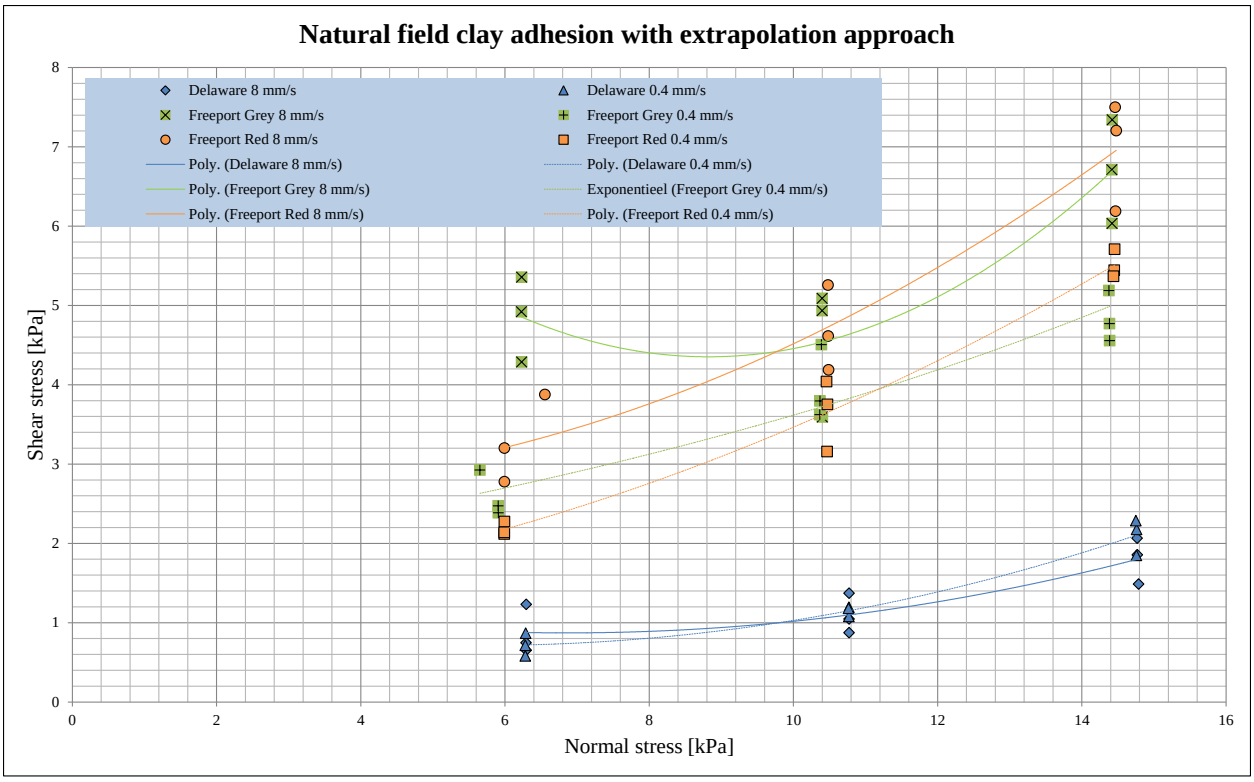

Figure 4.4 – Extrapolation approach shear stress over normal stress

The trend lines of Delaware river caly 8 , 0.4 mm/s and Freeport grey clay 0.4 mm/s have increasing shear stress with lower normal stresses. This is not possible and makes this approach unreliable. A boundary condition to this approach is the minimum value of the trend line is used for intersection with the y-axis if the trend line increases with lower normal stresses. This shear stress values with the clay strengths can be found in Table 4.7.

Table 4.7 – Extrapolation approach results

Clay	Pulling speed [mm/s]	Cohesion (UU-traxial) [kPa]	Adhesion [kPa]	Adhesion/Cohesion [%]
Delaware, Philadelphia	0.4	11.5	0.71	6.2
	8	10.1	0.87	8.6
Freeport Grey, Texas	0.4	25.9	4.37	16.9
	8	17.3	1.74	10.1
Freeport Red, Texas	0.4	102.1	1.22	1.2
	8	89.0	2.79	3.1

The cohesive values of the natural field clays are from the undrained, unconsolidated traxial tests. These UU-traxial test have as condition that the clays are assumed to have no internal friction angle (φ=0).

4.2.3. Linear approach towards adhesive data

For each of the natural field clays a linear line trend line is added to evaluate the shear stress. Similar to the exprapolation approach the intersection of the trend line with the y-axis is the possible adhesive stress. In Table 4.8 the equations of the linear trend lines can be found. The Delaware river clay 0.4 mm/s and Freeport red clay 0.4 mm/s have negative values when intersecting the vertical axis. This is not possible and will be assumed to be zero.

Table 4.8 - Linear approach trend line equations

Clay	Pulling speed [mm/s]	Trend line equation	Shear stress / X=0 [N/mm^2]
Delaware, Philadelphia	0.4	$y = 0.1619 - 0.3919$	-0.39 / 0
	8	$y = 0.1079x + 0.1136$	0.11
Freeport Grey, Texas	0.4	$y = 0.2622x + 1.1296$	1.13
	8	$y = 0.223x + 3.0547$	3.05
Freeport Red, Texas	0.4	$y = 0.3922x - 0.2632$	-0.26 / 0
	8	$y = 0.4445x + 0.3648$	0.36

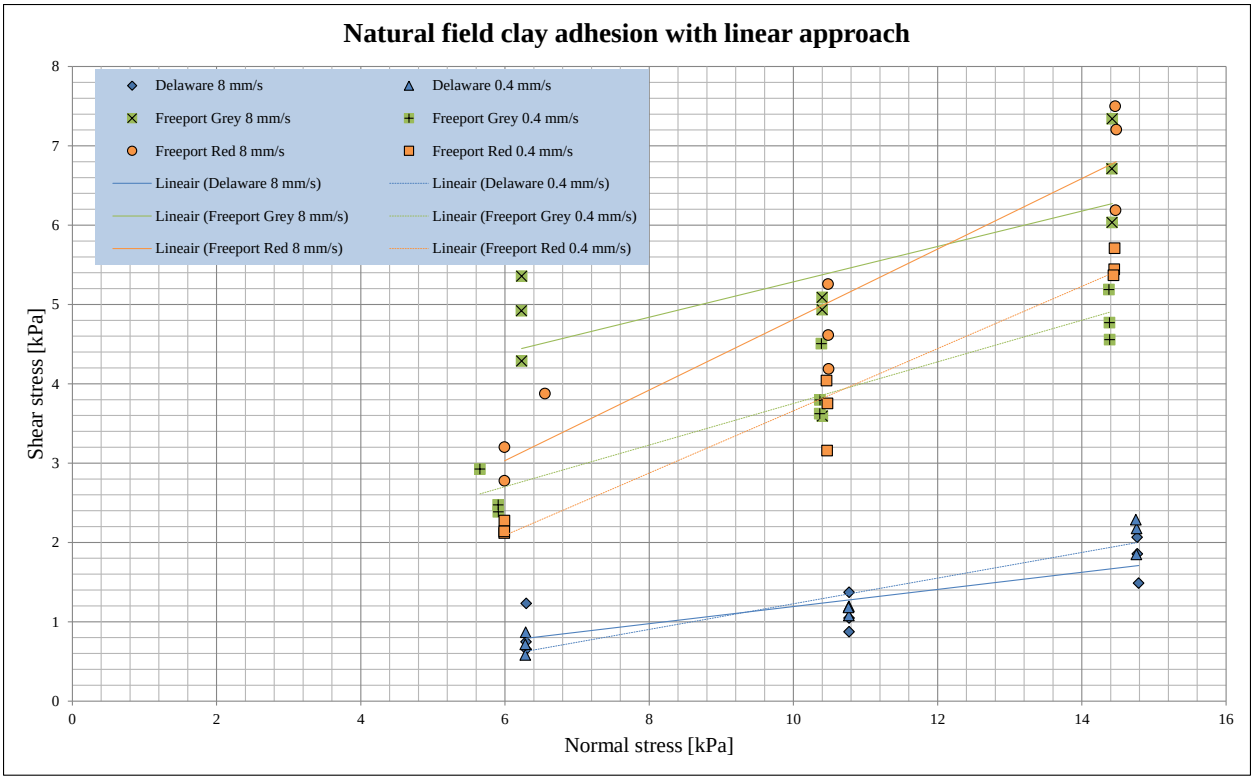

Figure 4.5 – Linear approach shear stress over average normal stress

The trend lines intersection below or on zero of the shear stress can be conluded that there was no adhesion measured. The results of the cohesion (φ=0), adhesion and A/C percentage see Table 4.9.

Table 4.9 – Linear approach results

Clay	Pulling speed [mm/s]	Cohesion (UU-traxial) [kPa]	Adhesion [kPa]	Adhesion/Cohesion [%]
Delaware, Philadelphia	0.4	11.5	0	0
	8	10.1	0.11	1.1
Freeport Grey, Texas	0.4	25.9	1.13	4.4
	8	17.3	3.05	17.6
Freeport Red, Texas	0.4	102.1	0	0
	8	89.0	0.36	0.4

With no adhesion present only friction force was measured. There is an angle of internal friction present, because an external friction angle was measured.

If the line would be horizontal intersecting a set of data points, it may be concluded that there is no external friction angle and therefore no internal friction angle present. With an adhesive value a calculation is made to determine the possible angle of external friction for every natural field clay (3 test for every 3 normals stresses), see equation 4.2.3. The average of all the solutions are usded to calculate the internal friction angle, see equation 4.2.4.

$$\delta = \left(\frac{\tau_b - \sigma_n}{\tau_{b,n=0}}\right) \cdot 180\pi \qquad 4.2.3$$

$$\varphi = \frac{3}{2}\delta \qquad 4.2.4$$

φ and δ are the internal and external friction angle in degrees. The τ_b, σ_n and $\tau_{b,n=0}$ are the shear stress, normal stress and shear stress or adhesion all in kPa. The red dotted line in Figure 4.6 is used to determine the cohesive strength without an internal friction angle. However, due of the difference between a measured cohesion of the UU-traxial test and determined internal friction angle the cohesive strength is lower, see Figure 4.7. The recalculated cohesive strengths of the clay can be found in Table 4.10.

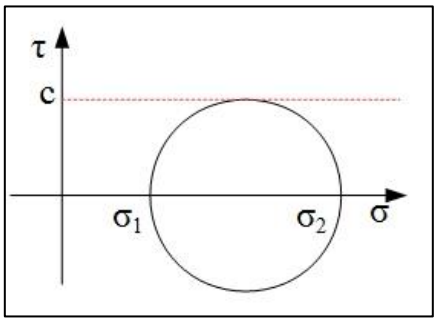

Figure 4.6 – Mohr circle with phi=0

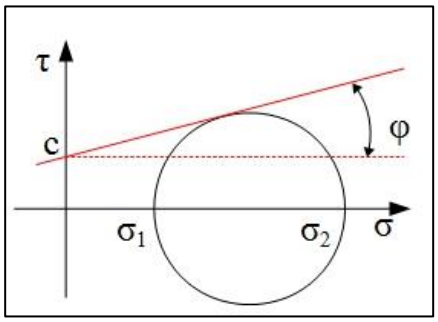

Figure 4.7 – Mohr circle with phi>0

$$\tau = c + \sigma \cdot \tan(\varphi) \qquad 4.2.5$$

With τ for the shear stress [kPa], *c* for cohesion [kPa], σ for the effective stress [kPa], φ and δ are the internal and external friction angle in degree. σ

Table 4.10 – Linear approach recalculated results

Clay	Pulling speed [mm/s]	Internal friction angle [degree]	Recalculated Cohesion [kPa]	Adhesion [kPa]	Recalcutalted Adhesions/Cohesion [%]
Delaware, Philadelphia	0.4	10.4	9.4	0	0
	8	10.3	8.5	0.11	1.3
Freeport Grey, Texas	0.4	16.3	18.3	1.13	6.2
	8	19.2	11.3	3.05	27.0
Freeport Red, Texas	0.4	30.0	43.1	0	0
	8	36.0	24.3	0.36	1.5

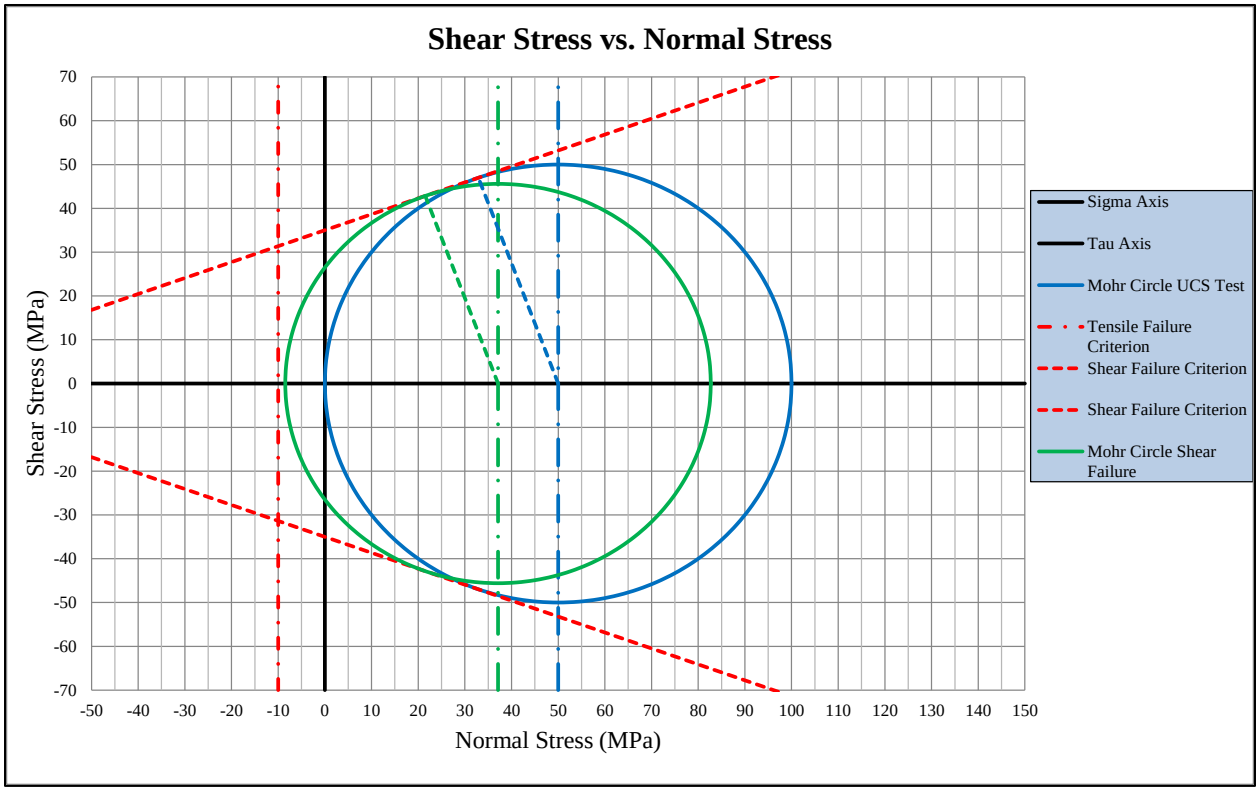

Figure 4.8 - Mohr circle with cohesion, intern friction angle, tensile strength and stress state

The two circles in Figure 4.8 represent two different states; what the clay is and what it could be. The blue circle is the measured UCS and is used to determine the failure envelop, with tensile strength being the boundary on the left. The green circle is the current stress state of the clay. If the current stress state intersects with the stress axis or x-axis with a higher value than the tensile strength, the clay will fail by tensile.

4.2.4. φ = 0 approach towards adhesive clay properties

Referring to the φ=0 principle explained in paragraph 2.7, the approach of φ=0 is done to evaluate the possibility of no internal/external friction angle being present in the tested clays. With this approach, all data from every test was averaged leaving two data points of each natural field clay, the pulling speed of 8 and 0.4 mm/s.

To acquire the adhesive stress [N/mm^2] from these data points, a horizontal line is drawn to the y-axis, or adhesive stress axis. In Figure 4.6 the horizontal red line represents the angle of internal friction. With the φ = 0 approach, the line is horizontal and therefore it is also horizontal in Figure 4.9. In Table 4.11, the results of the φ = 0 approach are presented. An important remark on this approach is that the average adhesive stress is not dependent on the average normal stress, because the stresses are averages.

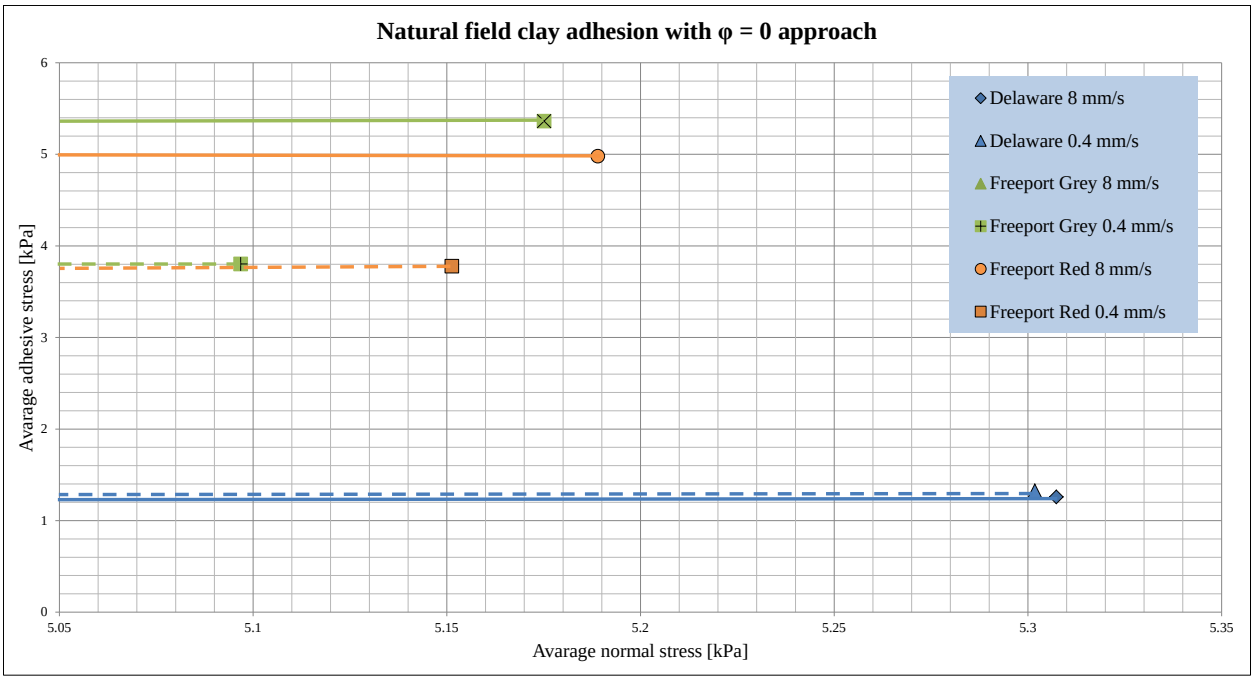

Figure 4.9 – Φ =0 approach average shear stress over average normal stress

Table 4.11 – Φ = 0 approach results

Clay	Pulling speed [mm/s]	Cohesion (UU-traxial) [kPa]	Adhesion [kPa]	Adhesions/ Cohesion [%]	Internal friction angle [degree]
Delaware, Philadelphia	0.4	11.5	1.32	11.5	0
	8	10.1	1.26	13.5	0
Freeport Grey, Texas	0.4	25.9	3.80	14.7	0
	8	17.3	5.36	31.0	0
Freeport Red, Texas	0.4	102.1	3.78	3.7	0
	8	89	4.98	5.6	0

For the Freeport red clay both the data points are either equal or lower compared to the Freeport grey clay. This means that with increasing strength there is a decrease of adhesion. However, the Delaware River clay implies there is an increase of the adhesion from very soft to soft clay. The blade pulling speed has no effect on the Delaware river clay. However, with a lower speed the Freeport red and grey clay have a lower adhesive strength. This could mean that water flow out the pores has more time, or a lower "vacuum" occurs, resulting in a lower pulling force or adhesive stress, when divided by the blade surface.

4.2.5. Average approach towards adhesive clay properties

With the average approach the following is done: the data points of the three tests done at the three normal stresses (+/-6, +/-10.5 and +/-14.5 N/mm^2) are averaged for each of the natural field clays. In other words, test 1, 2 an3 become one data point just like test 4, 5 and 6 and so on. Between these average data points a line is drawn to see the development between the different normal stresses. The line between the first (+/- 6 N/mm2) and second (+/-10.5 N/mm2) data point was used to intersect with the shear stress axis, see The average approach is not possible for the Freeport grey 8 mm/s, because the average of the first data point is higher than the second average data point. It is not possible to have an increasing shear stress with a decreasing normal stress. The solution for the Freeport grey 8

mm/s a line is to draw the line (red line, Figure 4.10) from data point 3 (14.4 N/mm normal stress) towards the average value of datapoints 1 and 2, letting it eventually intersect with the shear stress axis.

Table 4.12 for results.

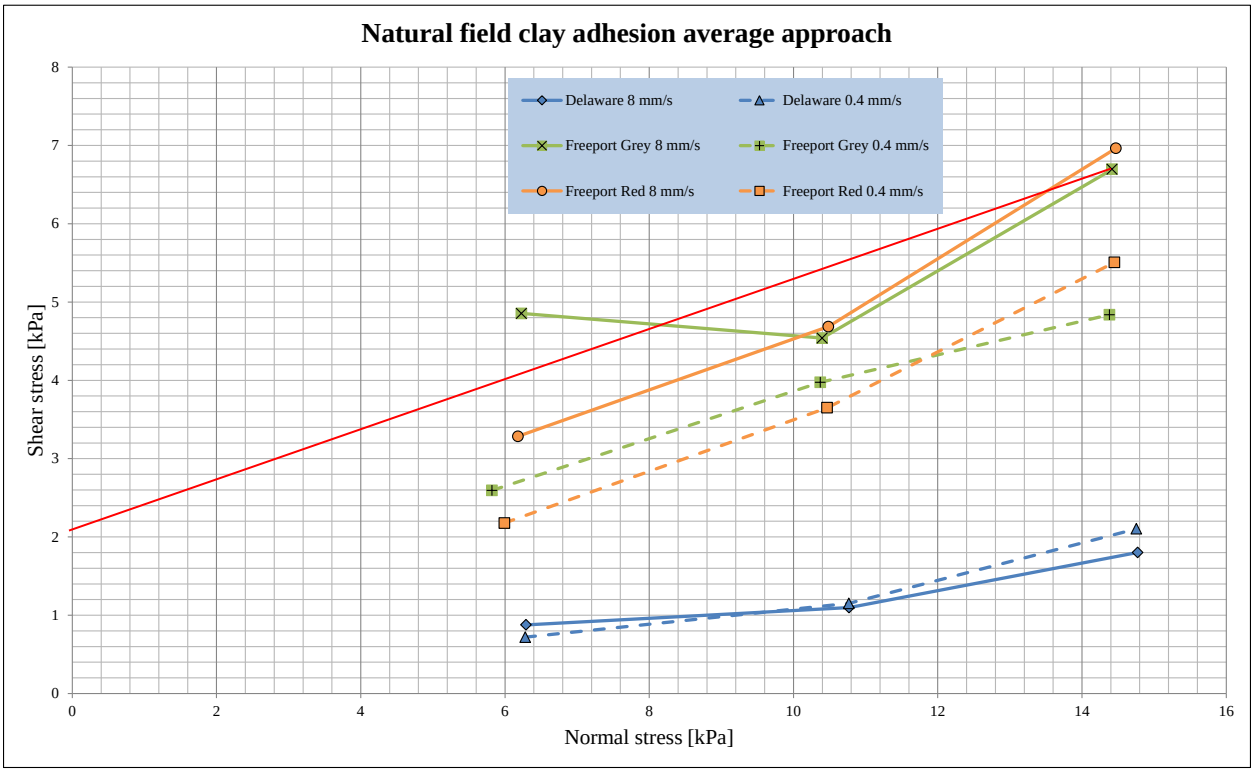

Figure 4.10 – Average approach of adhesive experiments

The average approach is not possible for the Freeport grey 8 mm/s, because the average of the first data point is higher than the second average data point. It is not possible to have an increasing shear stress with a decreasing normal stress. The solution for the Freeport grey 8 mm/s a line is to draw the line (red line, Figure 4.10) from data point 3 (14.4 N/mm normal stress) towards the average value of datapoints 1 and 2, letting it eventually intersect with the shear stress axis.

Table 4.12 – Average approach results

Clay	Pulling speed [mm/s]	Cohesion (UU-traxial) [kPa]	Adhesion [kPa]	Adhesion/Cohesion [%]
Delaware, Philadelphia	0.4	11.5	0.18	1.6
	8	10.1	0.62	6.1
Freeport Grey, Texas	0.4	25.9	0.83	3.2
	8	17.3	2.05	11.8
Freeport Red, Texas	0.4	102.1	0.23	0.2
	8	89.0	1.25	1.4

Similar to the linear approaches the cohesion must be recalculated with the measured internal friction angle, see Table 4.13.

Table 4.13 – Average approach recalculated results

Clay	Pulling speed [mm/s]	Internal friction angle [degree]	Recalculated Cohesion [kPa]	Adhesion [kPa]	Recalcutalted Adhesions/Cohesion [%]
Delaware, Philadelphia	0.4	4.7	10.6	0.18	1.7
	8	8.7	8.6	0.62	7.2
Freeport Grey, Texas	0.4	24.6	14.0	0.83	5.9
	8	27.7	8.2	2.05	25
Freeport Red, Texas	0.4	28.1	47.6	0.23	0.5
	8	28.9	40.0	1.25	3.1

4.3. Adhesive experiments conclusion

The adhesive test set-up with the approaches to the experimental adhesive data has led to confirming the prediction of adhesive strength development with increasing cohesive strength. The softer Delaware river clays and the Freeport red clay (0.4 mm/s) show a linear relation between normal stress and shear stress, meaning there is no adhesion measured. With an increasing cohesive strength of the clay there is a decrease of the adhesive strength. In addition to the decreasing adhesion, there is an increase in the internal friction angle (φ). This can be concluded from the data of the Freeport grey clay (8 mm/s) and the stiffer Freeport red clay (8 mm/s). The internal friction angle for the Freeport red clay is +/- 30 degrees, however the internal friction angle will have a limit.
With the presence of quartz and other materials with an internal friction angle (mineralogy results, see paragraph 4.1.3) a friction angle was reassured. The Freeport grey clay has a relative low adhesion/cohesion percentage for a cohesive strength of 17 kPa. The stiffer Freeport red clay with a cohesive strength of 87 kPa has an even lower adhesion/cohesion percentage. This implies that with increasing clay strength, the adhesion decreases to zero.

Table 4.14 - Cohesion and adhesion conclusion for 8 mm/s from linear approach

Clay	Cohesion [kPa]	Adhesion [kPa]	Adhesion/ Cohesion [%]	Internal friction [degree]	External friction [degree]
Delaware, Philadelphia	8.5	0.11	1.3	10.3	6.9
Freeport Grey, Texas	11.3	1.13	10	19.2	12.8
Freeport Red, Texas	24.3	0.36	1.5	36.0	24.0

The two different pulling speeds, 8 and 0.4 mm/s, have shown that with a higher pulling speed a higher pulling force is required. This effect can be explained by the low permeability of the clay. By pulling the blade at a low speed the water in the pores have time to flow out, decreasing the “suction” effect.

The prediction for soft clays having an adhesion/cohesion percentage of almost 100% is not known. This is a rather harsh statement, because only one soft natural field clay has been tested in this study. This also may be concluded for the Freeport grey and red clay, these clays do not have the a/c percentage that was predicted, see Figure 4.11.

The Delaware River clay contains a high quantity of quartz confirmed by the x-ray diffraction and therefore results in a recorded external friction. The Delaware River clay, due to the fact that the internal and external friction of the clay is very small, results in an unnoticeable extra force. The difference between the two blade pulling speeds is even smaller and therefore the internal friction may be neglected for soft clays.

For the Freeport grey clay, there is a balance between quartz and illite. This causes the Freeport grey clay to also have an external friction angle, however the strength of the Freeport grey clay is larger than the Delaware River clay

resulting in a higher external and internal friction angle. For the Freeport red clay, a decrease of the internal friction had occurred because of a smaller steel-to-clay contact area.

This makes the Freeport red clay very interesting, because it has a high strength, but a very low measured adhesion. The increase of the normal stresses with the adhesive testing showed an increase of the pulling force of the blade and therefore an increase in the adhesive stresses. It may be concluded that there is an internal friction angle, because there is 19% quartz present in de Freeport red clay sample. However, the cohesive strength of the red clay must have a larger internal friction angle, more than that of 19% quartz present. The strength of the red clay sample is 89 kPa and this is too low for an adhesive force to create a relatively low blade pulling force.

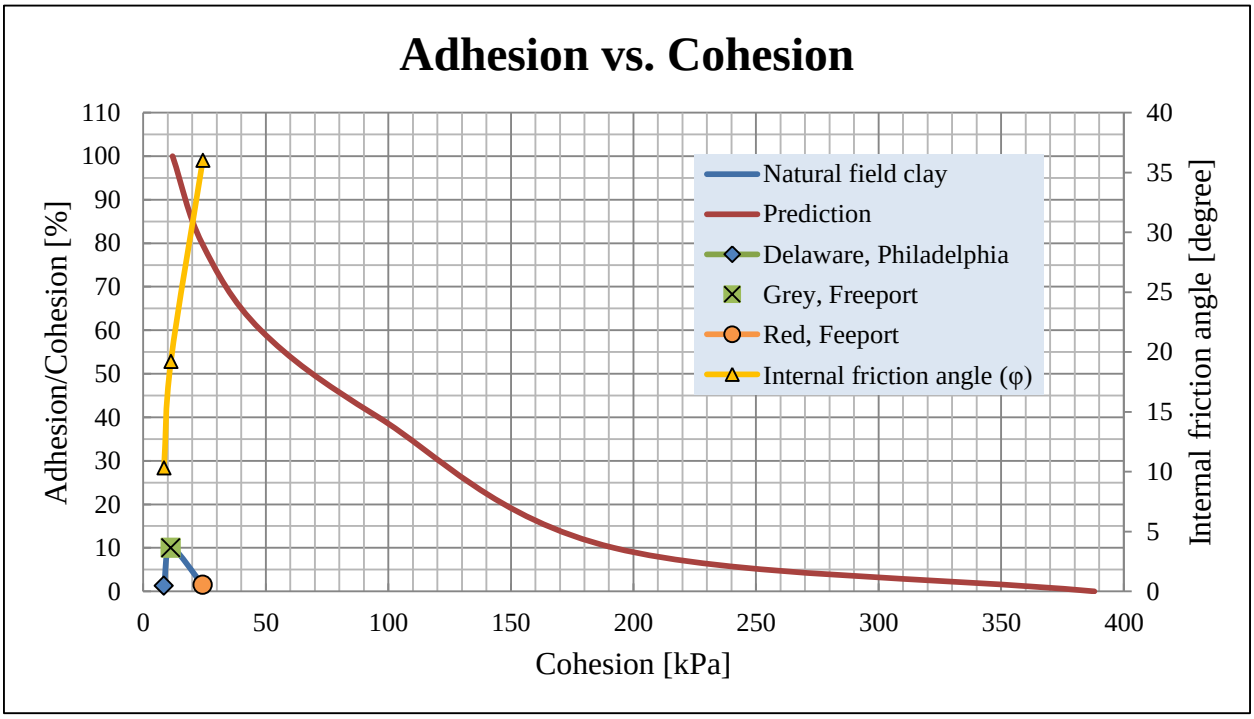

Figure 4.11 – Prediction and natural field clays relation of adhesion, cohesion and internal friction angle

5. Clamshell bucket sensitivity analysis

In the previous chapter all adhesive test and additional tests results are presented. The data is also analysed to determine the possible correlation between cohesion/adhesion and new insights in clay adhesive properties.

The Clamshell cable bucket has different aspects such as shape or mechanics that have been accepted and remained unchanged for the past decades. The clamshell bucket sensitivity analysis will be conducted with the software Clamshell Closing (CCS32) as tool. The grab will be varied on several parts that may have influence on the increasing the production [m^3] for one clamshell closing cycle.

The GL485 and GL484 are a 16 m^3 and a 9 m^3 size bucket used for firm to hard clays. To maximize the usage of the sensitivity analysis these two buckets will be used and evaluated. The effects of variations in the following bucket dimension are listed below:

1. The bucket's cutting angle
2. The bucket's adhesive cutting length
3. The bucket's centre point of gravity
4. The bucket's total weight
5. The bucket's total span
6. The bucket's total width

The GL485 and GL484 are subjected to the sensitivity analysis for stiff clay. This chapter will highlight the most interesting and notable effects of the modifications to the normative parameters. All other values can be found in Appendix C.

5.1. GL485 and GL484 clamshell properties

Great Lakes Dredge & Dock owns a large variation of buckets from different producers for different applications. GLDD uses smaller and heavier buckets for excavation of the stiffer clays. GLLD owns a certain amount of buckets for this clay region and two were selected, the GL485 and GL484. The general bucket properties and software iputs forf these buckets can be found in Table 5.1 The available drawings of the grabs can be found in Appendix D. A list of common used buckets and general information on the clamshell dredges of GLDD can be found in Appendix E.

Table 5.1 - GL484 and GL485 bucket properties

Properties	**GL484**	**GL485**
Size [m^3]	9	16
Weight [ton]	29.5	24.5
Footprint [m^2]	13	19
Producer [-]	Hawco	Intergy
Software properties	**GL484**	**GL485**
Cutting angle (CA) [degree]	3.95	3.5
Adhesive cutting length (ACL) [m]	0.55	0.95
Centre point of gravity (COG) [m]	(0.35; 1.55)	(0.55; 2.29)
Total bucket weight[2] (TBW) [ton]	22.443	24.607
Total bucket span (TBS) [m]	5.90	6.80
Total bucket width (BW) [m]	2.25	2.85

[2] Total bucket weight consists: bucket bowls, bucket arms, upper and lower sheaves

5.2. GL485 sensitivity analysis

The simulation for the GL485 16 m^3 and 24.61 tons (weight in software) clamshell bucket will be subjected to the sensitivity analysis to examine the effect of the normative parameters on the production. To highlight the importance of the adhesive property of clay in the clay cutting process, the stiff clay adhesive and tensile strength properties are varied to examine the effect on the production [m^3]. The stiff clay has a cohesive strength of 90 kPa, adhesive strength of 70 kPa and a tensile strength of 70 kPa, see Figure 5.1 and Table 5.2. This will also be done with the GL484 bucket in paragraph 5.3.

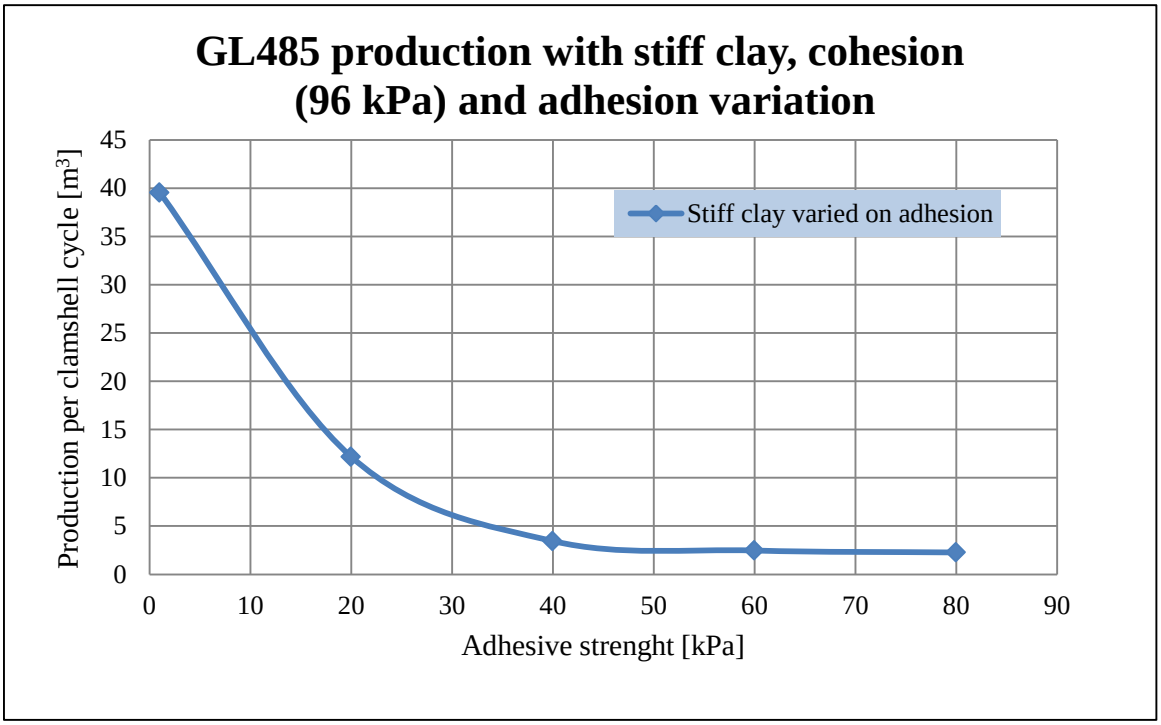

Figure 5.1 - GL485 production for adhesion variation of stiff clay

Table 5.2 - GL485 production for adhesion variation of default stiff clay

Adhesion [kPa]	Production [m^3]	Compared to original [%]
70 (original)	2.36	0
1	39.56	+1576
20	12.18	+416
40	3.45	+46
60	2.47	+4.7
80	2.27	-3.8

The GL485 grab has a starting point to which all data acquired in every simulation needs to be compared. These are the original output values of the GL485 without any modifications. The data output of the original output values are in Table 5.3.

Table 5.3 - GL485 default output values from CCS32 software

GL485 sensitivity analysis original output values	
Time [s]	20.24
X-lip [m]	0
Y-lip [m]	-0.21
Situ production [m^3]	2.36
Winch power [kW]	104.74
Specific energy [kJ/m^3]	502.19
Penetration depth [m]	0.007
Total sticky effect [kN] (Adhesive force)	27
Upper block speed [m/s]	0.284
Lower block speed [m/s]	0.066
Angular velocity [degree/s]	7.792
Rope force [kN]	103
Arm force [kN]	145
Total mass [ton]	19.709
Total volume [m^3]	22.433

5.2.1. GL485 bucket cutting angle

The GL485 has sharp bucket lips and already a relatively small cutting angle compared to other 16 m^3 grabs. This will give a different aspect to the sensitivity analysis, but nevertheless its influence on production and forces are examined and results can be found in Figure 5.2 and Table 5.4. The angles in Figure 5.2 are not the real angle, but a representation of the angles.

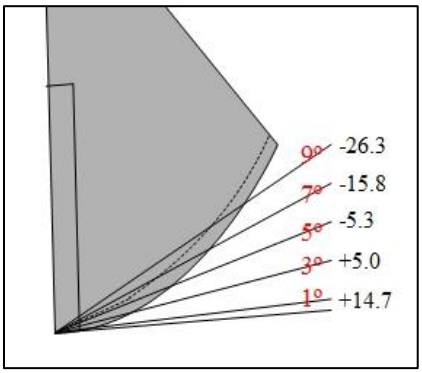

Figure 5.2 - GL485 CA payload percentage difference with default stiff clay

Table 5.4 - GL485 CA production percentage difference with original stiff clay

Cutting angles [degree]	Production [m^3]	Compared to original [%]
3.5 (original)	2.36	0
1	2.55	+14.7
3	2.39	+5.0
5	2.25	-5.3
7	2.12	-15.8
9	2.00	-26.3

Decreasing the cutting angle has a positive effect on the production. However, decreasing the cutting angle will have a negative effect on the strength of the grab. With a relatively long thin bucket, the lip will deform quicker and the level of wear and tear will be higher.

5.2.2. GL485 adhesive cutting length analysis

The original adhesive cutting length (ACL) is 0.95 m and a production for stiff clay of 2.36 m^3. In Figure 5.3 and Table 5.5 I have listed the percentages compared to the production of stiff clay without any adjustments.

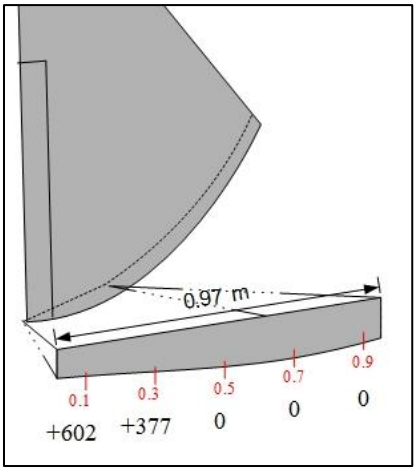

Figure 5.3 - GL485 ACL payload percentage difference with default stiff clay

Table 5.5 – GL485 ACL production difference with default stiff clay

Adhesive cutting length [m]	Production [m^3]	Compared to original [%]
0.97 (original)	2.36	0
0.1	16.37	+602
0.3	11.26	+377
0.5	2.36	0
0.7	2.36	0
0.9	2.36	0

The adhesive cutting length is the contact surface between the grab's steel and the clay. By reducing the cutting length or contact surface, a significant increase could be realized in the production. This making the reduction of the adhesive cutting length one of the most effective ways of increasing the production, but is hard to realize.

5.2.3. GL485 centre point of gravity analysis

For the centre point of gravity of the bucket GL485, Figure 5.4, Table 5.6 and Table 5.7 are the summaries of the stiff clay sensitivity analysis. These parameter adjustments can be realized by adding weight to the grab on strategic locations. The original COG coordinates are (0.59; 2.29) and the production for stiff clay is 2.36 m^3.

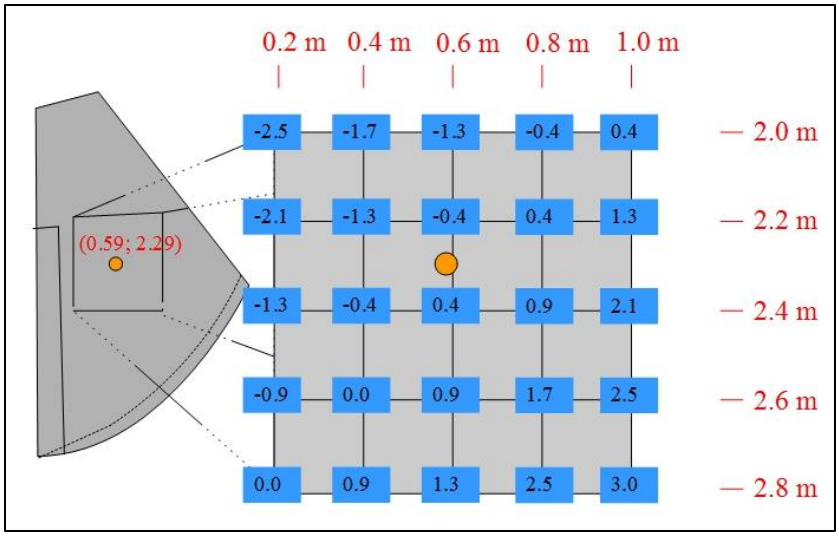

Figure 5.4 - GL485 COG payload percentage difference with default stiff clay

Table 5.6 - GL485 COG payload production with default stiff clay

Production [m^3]	X=0.2 m	X=0.4 m	X=0.6 m	X=0.8 m	X=1.0 m
Y=2.0 m	2.30	2.32	2.33	2.35	2.37
Y=2.2 m	2.31	2.33	2.35	2.37	2.39
Y=2.4 m	2.33	2.35	2.37	2.38	2.41
Y=2.6 m	2.34	2.36	2.38	2.40	2.42
Y=2.8 m	2.36	2.38	2.39	2.42	2.43

Table 5.7 - GL485 COG payload percentage difference with default stiff clay

Percentage [%]	X=0.2 m	X=0.4 m	X=0.6 m	X=0.8 m	X=1.0 m
Y=2.0 m	-2.5	-1.7	-1.3	-0.4	+0.4
Y=2.2 m	-2.1	-1.3	-0.4	+0.4	+1.3
Y=2.4 m	-1.3	-0.4	+0.4	+0.9	+2.1
Y=2.6 m	-0.9	0.0	+0.9	+1.7	+2.5
Y=2.8 m	0.0	+0.9	+1.3	+2.5	+3.0

The effect on the production by moving the centre point of gravity in horizontal direction (X) is larger than in vertical direction (Y). The total effect of adjusting the COG is small, but it is very applicable to increase the production.

5.2.4. GL485 bucket total weight

The total bucket weight can be varied by adding weight to the existing bucket. The GL485 has a weight of 19.709 ton in the software and this is higher in reality. The weight increase has a very positive effect on the production and is very feasible, Table 5.8. There is a limitation to adding weight and that is the hoisting capacity of the cranes on the dredges.

Table 5.8 – GL485 TBW production difference with default stiff clay

Total bucket weight [ton]	Production [m^3]	Compared to original [%]
19.709 (original)	2.36	0
21.709	2.61	+10.6
23.709	2.85	+20.8
25.709	3.1	+31.4
27.709	3.35	+42.0
29.709	3.62	+53.4

5.2.5. GL485 bucket total span

The clamshell bucket can be varied in two directions to increase the footprint. It can be done by increasing the bucket span (Figure 5.5) or bucket width (Figure 5.6). The original span of the GL485 bucket is 6.8 m and this is varied by increasing and decreasing the span to measure the total effect on the production, see Table 5.9.

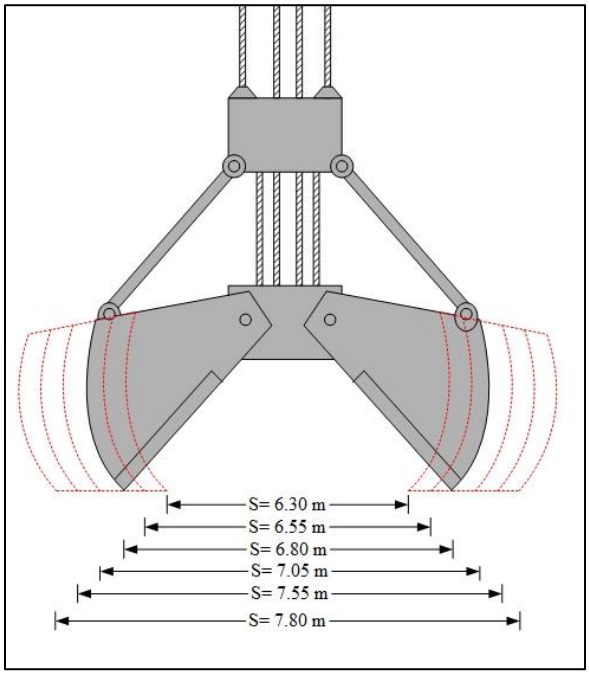

Figure 5.5 - GL484 total bucket span variation with default stiff clay

Table 5.9 – GL485 TBS production difference with default stiff clay

Total bucket span [m]	Production [m^3]	Compared to original [%]
6.80 (original)	2.36	0
6.30	2.15	-8.9
6.55	2.25	-4.7
7.05	2.44	+3.4
7.3	2.53	+7.2
7.55	2.60	+10.2
7.8	2.68	+13.6

The increase of the bucket span is a good option to increase the production. We have to take into account that if the clay is stiffer or stronger, a kind of scraping of the top clay layer is done. By increasing the scraping distance the

total production will be increased. The downside is that the penetration decreases with increasing bucket span. The increasing distance of the bucket lip and sheave blocks results in a lower penetration of the clay.

5.2.6. GL485 bucket total width

A second option to increase the foot print of the grab, is to vary the width of the bucket. The original width is 2.82 m with a production of 2.36 m^3. Results and location variation can be found in Table 5.10 and Figure 5.6. The COG adjustment can be done with existing buckets, but the total grab weight must be considered. The cranes on the clamshell dredges have a maximum hoisting capacity and this is a limitation for the bucket weight.

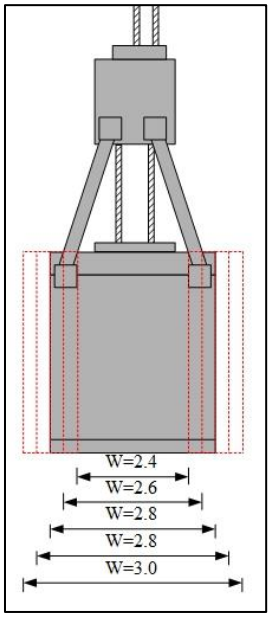

Figure 5.6 - GL484 total bucket width variation with default stiff clay

Table 5.10 – GL485 BW production difference with default stiff clay

Total bucket width [m]	Production [m^3]	Compared to original [%]
2.82 (original)	2.36	0
2.40	2.31	-2.1
2.60	2.34	-0.9
2.80	2.36	0.0
3.00	2.38	+0.9
3.20	2.40	+1.7

The variation of the bucket width has little effect on the production. The effect is similar to the COG variation, but it only feasible when constructing a new bucket.

5.3. GL484 sensitivity analysis

The GL484 bucket is mainly used by GLDD when running into very stiff or rock material during dredging. The greater weight reflects the stronger construction of the bucket hand this also helps the penetration. The sensitivity analysis with stiff clay is used to make it comparable with the GL485. The starting point of the GL484 clamshell bucket and its outputs are listed in Table 5.11. With these values, all adjustments are expressed in an increase or decrease with percentages.

Table 5.11 - GL484 original output values from CCS32 software

GL484 sensitivity analysis original output values	
Time [s]	20.87
X-lip [m]	0
Y-lip [m]	-0.91
Situ production [m^3]	4.76
Winch power [kW]	231.92
Specific energy [kJ/m^3]	322.28
Penetration depth [m]	0
Total sticky effect [kN] (Adhesive force)	183
Upper block speed [m/s]	0.282
Lower block speed [m/s]	0.119
Angular velocity [degree/s]	7.645
Rope force [kN]	228
Arm force [kN]	431
Total mass [ton]	25.612
Total volume [m^3]	10.228

Confirming the importance of adhesion during clay cutting and therefore the influence on the production, Figure 5.7 displays the relation between adhesion and production of the GL484, $9m^3$ bucket. The variation is done with the adhesive and tensile strength of the clay.

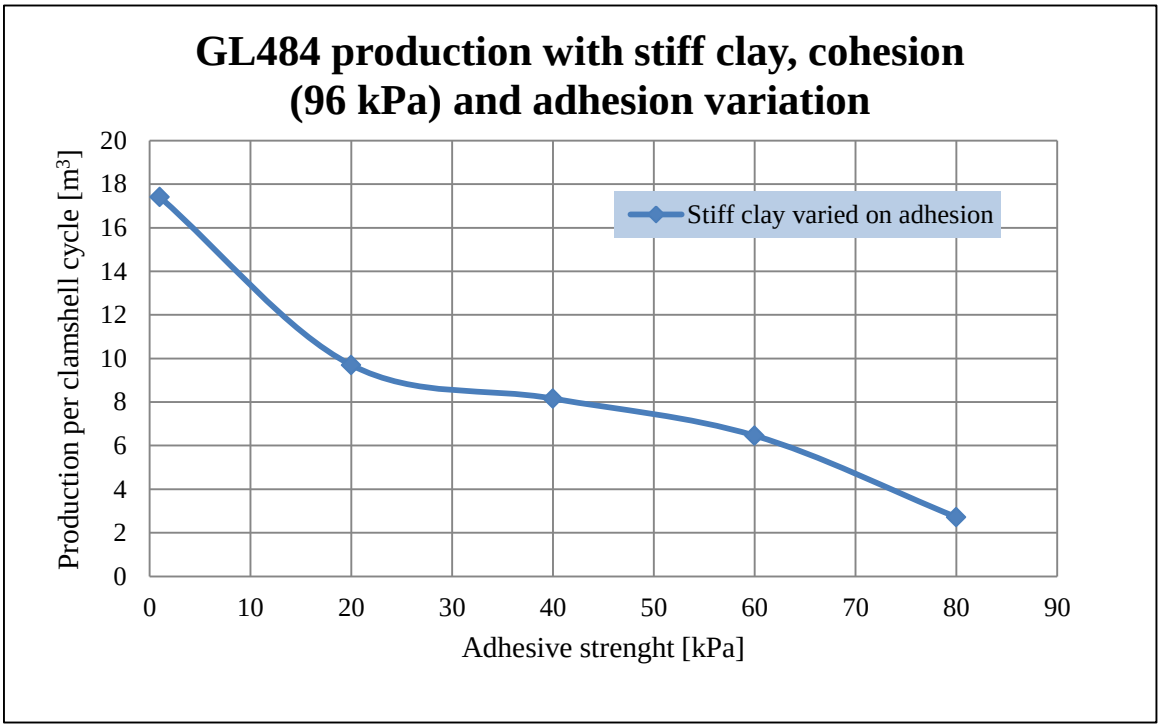

Figure 5.7 - GL484 production for adhesion variation of stiff clay

Table 5.12 - GL484 production for adhesion variation of default stiff clay

Adhesion [kPa]	Production [m^3]	Compared to original [%]
70 (original)	4.76	0
1	17.41	+266
20	9.70	+104
40	8.16	+71
60	6.46	+36
80	2.72	-43

5.3.1. GL484 bucket cutting angle

The original cutting angle of the GL484 is 3.98 degree and this is a normal cutting angle for heavy duty buckets.

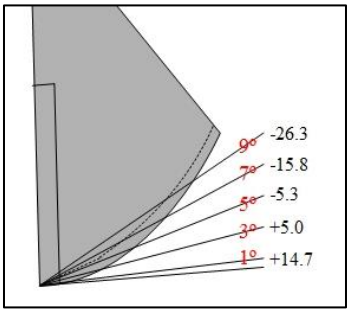

Figure 5.8 - GL484 CA payload percentage difference with default stiff clay

Table 5.13 - GL484 CA production percentage difference with default stiff clay

Cutting angles [degree]	Production [m^3]	Compared to original [%]
3.98 (original)	4.76	0
1	5.46	+14.7
3	5.00	+5.0
5	4.51	-5.3
7	4.01	-15.8
9	3.51	-26.3

Noticeable for the cutting angle is that for both GL485 and GL484 the cutting angle has the same effect on the production. Making this parameter uniform, but still having the limitation of not decreasing the angle too much to prevent a too thin bucket lip. The minimum lip thickness required to withstand the wear and tear is 12.7 cm.

5.3.2. GL484 adhesive cutting length analysis

The adhesive cutting length of the GL484 is much shorter compared to the GL485. A minor 0.55 m of the bucket bowl contributes to the clay cutting process. Figure 5.9 and Table 5.14 display and summarize the effects of reducing the ACL.

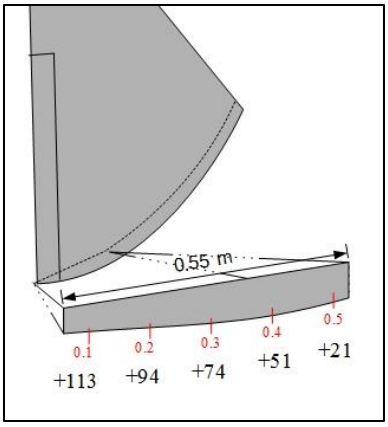

Figure 5.9 - GL484 ACL payload percentage difference with default stiff clay

Table 5.14 – GL484 ACL production difference with default stiff clay

Adhesive cutting length [m]	Production [m^3]	Compared to original [%]
0.55 (original)	4.76	0
0.1	10.14	+113
0.2	9.25	+94
0.3	8.30	+74
0.4	7.21	+51
0.5	5.77	+21

The effect on the production with stiff clay by reducing the adhesive cutting length is very large. Reducing the contact between the steel and clay by 5 cm will already increase the production with 21%. If possible, the reduction of the ACL is a good option for finding the optimum clamshell bucket design.

5.3.3. GL484 centre point of gravity analysis

The original centre point of gravity coordinates of the GL484 are (0.34; 1.55). In Figure 5.10, an overview is given of the variation grid for the X and Y directions. The production quantities and percentage differences with the original production can be found in Table 5.15 and Table 5.16.

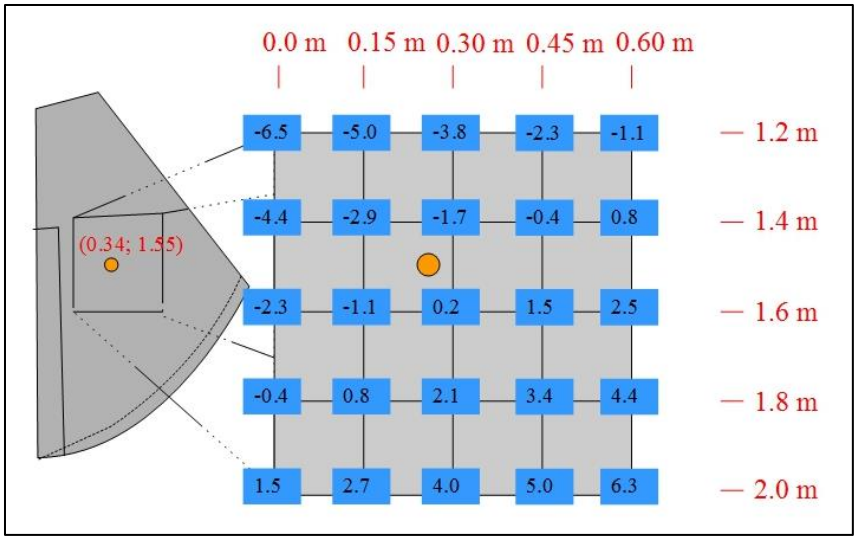

Figure 5.10 - GL484 COG payload percentage difference with original stiff clay

Table 5.15 - GL484 COG payload production with default stiff clay

Production [m^3]	X=0.0 m	X=0.15 m	X=0.30 m	X=0.45 m	X=0.60 m
Y=1.2 m	4.45	4.52	4.58	4.65	4.71
Y=1.4 m	4.55	4.62	4.68	4.74	4.80
Y=1.6 m	4.65	4.71	4.77	4.83	4.88
Y=1.8 m	4.74	4.80	4.86	4.92	4.97
Y=2.0 m	4.83	4.89	4.95	5.00	5.06

Table 5.16 - GL484 COG payload percentage difference with default stiff clay

Percentage [%]	X=0.0 m	X=0.15 m	X=0.30 m	X=0.45 m	X=0.60 m
Y=1.2 m	-6.5	-5.0	-3.8	-2.3	-1.1
Y=1.4 m	-4.4	-2.9	-1.7	-0.4	+0.8
Y=1.6 m	-2.3	-1.1	+0.2	+1.5	+2.5
Y=1.8 m	-0.4	+0.8	+2.1	+3.4	+4.4
Y=2.0 m	+1.5	+2.7	+4.0	+5.0	+6.3

The production of the GL484 is influenced by moving the centre point of gravity lower and outward when closed. Lowering (y-direction) the COG has a greater positive influence on the production than moving it outwards (x-direction).

5.3.4. GL484 bucket total weight

The GL484 has a weight of 25.612 ton in the software. The total weight increase has a very positive effect on the production and it is very feasible, see Table 5.17. Similar to the GL485, there is a limitation to adding weight and it is the hoisting capacity of the cranes on the dredges. For the Dredge 54 this is 61 ton, but the effect of adding weight to the bucket was increased to examine the effect.

Table 5.17 – GL484 TBW production difference with default stiff clay

Total bucket weight [ton]	Production [m^3]	Compared to original [%]
25.612 (original)	4.76	0
27.612	5.78	+21.4
29.612	6.54	+37.4
31.612	7.15	+50.2
33.612	7.68	+61.3
35.612	8.14	+71.0

5.3.5. GL484 bucket total span

The variation of the bucket span around 5.90 m has a positive effect on the production. The positive effect on the production is noticeable for all spans above 5.90 m and in our first measurable case 6.15 m, see Figure 5.11 and Table 5.18.

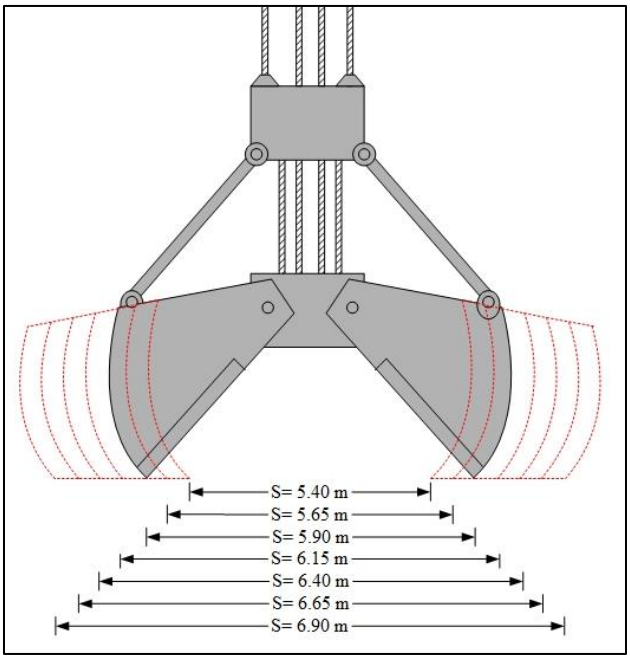

Figure 5.11 - GL484 total bucket span variation with original stiff clay

Table 5.18 – GL484 TBS production difference with default stiff clay

Total bucket span [m]	Production [m^3]	Compared to original [%]
5.90 (original)	4.76	0
5.40	4.15	-12.8
5.65	4.63	-2.7
6.15	5.49	+15.3
6.40	5.85	+22.9
6.65	6.19	+30.0
6.90	6.48	+36.1

The increase of the span will give a larger footprint and results in an increasing production, however it also gives the bucket less stability. The stability is challenged by the currents and conditions underwater when the bucket is on the

sea bed. One can imagine a relative narrow and long bucket will be easier to tip over when placing in on an angled sea bed with a current.

5.3.6. GL484 bucket total width

The width of the GL484 is constructed at 2.21 m and is varied around this value to measure the effects on the production. Increasing the width will also increase stability when placing the bucket on the soil bed. The variations and effects on the production are interesting, because when the width of the bucket is reduced a positive effect is measured, see Figure 5.12 and Table 5.19.

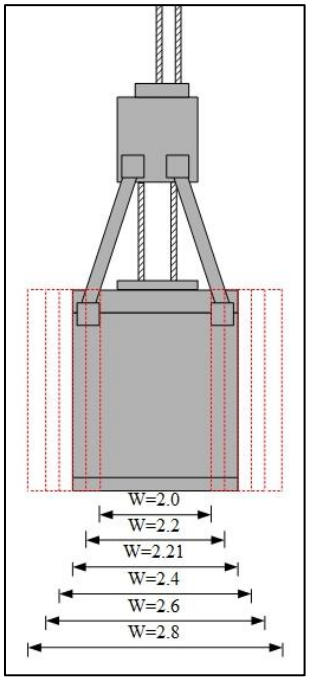

Figure 5.12 - GL484 total bucket width variation with original stiff clay

Table 5.19 – GL485 BW production difference with original stiff clay

Total bucket width [m]	Production [m^3]	Compared to original [%]
2.21 (original)	4.76	0
2.00	5.07	+6.5
2.20	5.07	+6.5
2.40	4.79	+0.6
2.60	4.06	-14.7
2.80	3.31	-36.3

The width reduction may have the effect of increasing the force on the bucket lips and creating more momentum that will result in a scoop of clay or larger production.

5.4. Clamshell bucket sensitivity analysis conclusion

For both grabs GL485 and GL484 the five normative parameters have similar and slightly different effects on the production. The GL485 has the largest increase of the production with ACL reduction and least with increasing BW. For the GL484 reducing ACL is most effective for increasing the production and repositioning the COG the least. Taking the feasibility and amount of reduction or increase needed of each parameter a reorganised of the effects are made in Table 5.20.

Table 5.20 - GL485 and GL484 conclusion parameter effects on production

Positive effect on the production	GL485	GL484
1	Increase total bucket weight	Reduce adhesive cutting length
2	Lower and outwards COG	Increase total bucket weight
3	Reduce adhesive cutting length	Increase bucket span
4	Increase bucket width	Decrease cutting angle
5	Reduce cutting angle	Decrease bucket width

For the GL485, the 16 m^3 and 24.5 ton grab, the effects of the normative parameters are listed from very little to very large effects on the production in m^3: total bucket width (BW), centre point of gravity (COG), total bucket span (TBS), cutting angle (CA), total bucket width (TBW) and adhesive cutting length (ACL). These modifications have to be taken into perspective. The ACL has an increase of 377% of m^3 by reducing the clay-to-steel by 70%. This is somewhat unrealistic, because clay still has to be cut to excavate the clay. The CA must have an angle of 1 degree (original 3.5 degree) and then the increase is 14.7%. This small angle is unrealistic and is already at its minimum considering the bucket bowl is a curved shape. Therefore we need to reconsider the normative parameters and their variations for the productions the following sequence of the GL485 grab:

1. Increasing bucket weight
2. Lowering and outwards moving centre point of gravity
3. Reducing adhesive cutting length
4. Increasing total bucket width
5. Reducing cutting angle

The GL484, 9 m^3 and 29.5 ton grab has been subjected to the sensitivity analysis with similar normative parameters. Ranging from the least effect on the production to having the most effect: COG, BW, CA, TBS, TBW and the most effect on the production is achieved by altering the ACL. With this grab the ACL needs to be reduced with 50 mm and the increase of production is 21%. This is plausible and therefore making it the number one adjustment for smaller and heavier clamshell buckets. The cutting angle reduction has a limitation similar to the GL485 and is ranked too high. For the total bucket width variation only width reduction will increase production. Taking clamshell optimization into account a relative small footprint is not most effective when large areas must be cleared of clay. With this said, a GL484 list is slightly changed taking all factors into account with number 1 being the most effective and feasible parameter for increasing production :

1. Reducing adhesive cutting length
2. Increasing total bucket weight
3. Increasing total bucket span
4. Lowering and outwards moving centre point of gravity
5. Reduction cutting angle
6. Decreasing total bucket width

6. Clamshell bucket concepts

Chapter 4 had all the results of the adhesive experiments and the additional tests: the Atterberg limits, the UU-traxial and the mineralogy. The data acquired from the adhesive experiments were approached in different ways to evaluate the correlation between normal stresses and adhesive stresses. Finally, the relation between the cohesion and adhesion of the tested natural field clays are evaluated.

With the clamshell bucket sensitivity analysis done in chapter 5 and the test results from chapter 4, I can now present different concepts of possible clamshell bucket improvements on for optimization of the production [m^3/s]. Each bucket concept may have one or various adjustments. All the buckets will be subjected to a multi criteria analysis in paragraph 6.5 to determine which the best bucket is and which concept should be further developed. The concepts are created in the CCS 32 software with GL485 as base bucket design.

6.1. Great Lakes bucket X

The clamshell bucket concept GLX's main feature to improve production is to increase bucket shell thickness; see Figure 6.1 (red dotted line). This modification has direct influence on the total bucket weight (TBW), centre point of gravity (COG) and possible the cutting angle (CA). By increasing the weight of the bucket in both bucket sensitivity analyses of the GL485 and GL484, the conclusions were a positive effect on the productions, see paragraphs 5.2.4 and 5.3.4. One must consider that the maximum hoisting capacity of the cranes on the dredges is the limitation for all bucket concepts that have an increased bucket weight.

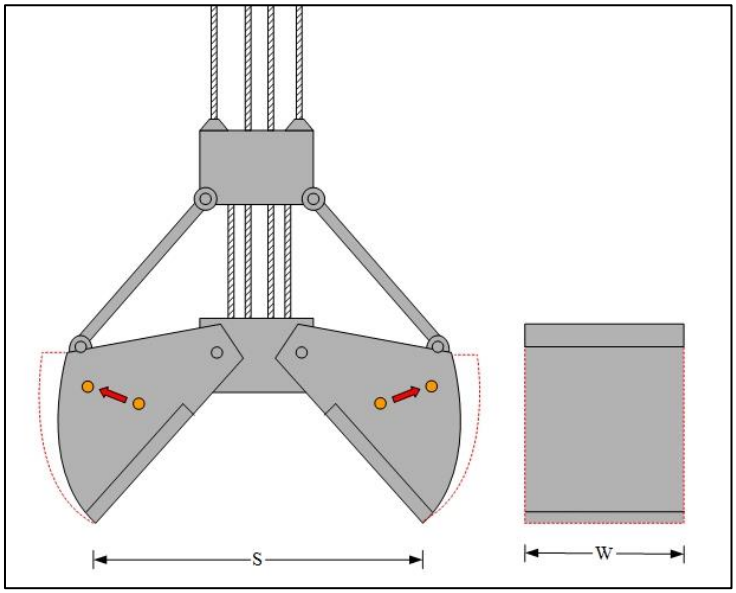

Figure 6.1 – Bucket concept GLX

By adding the weight, that is greater near the connection with the bucket arm, the centre point of gravity is moved outwards and raised, see Figure 6.1. This also has a positive effect on the production for the GL485 and GL484, see paragraph 5.2.3 and 5.3.3. By repositioning the COG, the contribution of the TBW will increase the penetrating force and will extended the TBW contribution during the closing phase. The weight of the bucket creates a momentum during penetration and closing phase and will have a positive effect clay penetration force, see Figure 6.2.

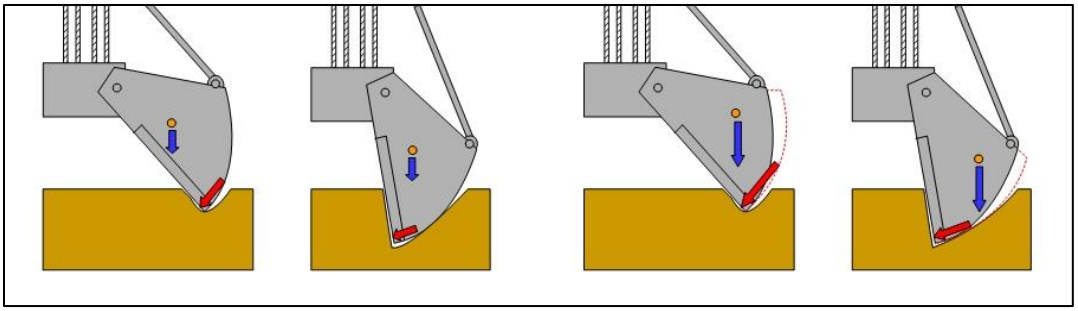

Figure 6.2 – Bucket concept GLX additional momentum

Modifying the bucket bowl by adding steel will have effect on the thickness of the bucket bowl and therefore the cutting angle. The weight added on to the grab will be more near the bucket arm and will have no influence on the cutting angle. The total percentage effect on the closing time, production and stick effect, see Table 6.1. The sticky effect is the total generated adhesive force between the clay and grab. All the output of the CCS 32 software can be found in Appendix K.

Table 6.1 - Relative change compared to default output of clamshell bucket concept GLX

Parameters						
BW [ton]	19.71	21.69	23.69	25.69	27.69	29.69
COG [m]	(0.59;2.29)	(0.62;1.67)	(0.65;1.81)	(0.67;2.26)	(0.71;2.51)	(0.74;2.76)
Percentages						
Closing time	20.33 s	0.0	0.0	0.0	0.1	0.1
Production	2.35 m^3	10.2	20.0	30.6	40.9	52.3
Sticky effect	27 kN	14.8	25.9	40.7	51.9	66.7

6.2. Great Lakes bucket Y

The GLY clamshell bucket concept takes a conventional bucket footprint and increases this and keeping the bucket weight constant. This is done by increasing the total bucket span (TBS) and total bucket width (BW). The sensitivity analyses of the TBS and BW have both shown different effects depending on the bucket. For increasing the TBS both buckets, GL485 and GL484, have an increase of the production of stiff clay. The production increase has a larger effect for the GL484 than for the GL485. Increasing the TBS with 0.25 m, the GL484 production is increased by 15.6% and the GL485 production only 5.4% see paragraph 5.2.5 and 5.3.5.

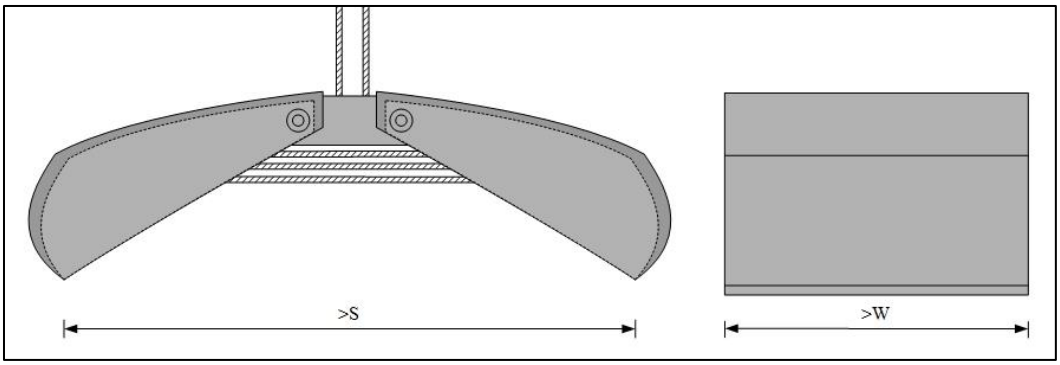

Figure 6.3 – Bucket concept GLY

For the GL485, the BW has a positive effect on the production if the width is increased above the original value, see paragraph 5.2.6. By increasing the width of GL485 the footprint is increased, with a larger footprint the clay can be scrapped and will result in more clay ending up in the bucket. The heavier and smaller bucket GL484 has an increase of clay production only when the BW is decreased. This bucket is more dependent on the penetration depth to create a higher production. By reducing the bucket width the bucket lips will have the same amount of force on a smaller clay-to-steel contact area resulting in a larger clay penetration depth, see paragraph 5.3.6. The total percentage effect on the closing time, production and stick effect, see Table 6.2. All the output of the CCS 32 software can be found in Appendix K.

Table 6.2 - - Relative change compared to default utput of clamshell bucket concept GLY

Parameters							
TBW[m]	2.82	2.4	2.6	2.8	3.0	3.2	3.4
TBS [m]	6.8	6.30	6.55	7.05	7.30	7.55	7.80
Percentages							
Closing time	20.33 s	-2.4	-1.2	1.1	2.3	3.4	4.5
Production	2.35 m^3	-10.2	-5.1	3.8	8.5	12.3	16.2
Sticky effect	27 kN	25.9	14.8	-.37	-14.8	-25.9	-33.3

6.3. Great Lakes bucket Z

The main feature of the GLZ bucket concept is reducing the clay-to-steel contact surface to have influence on the production in a positive way. The sensitivity analysis of the adhesive cutting length (ACL) and the cutting angle (CA) results are applicable on GLZ concept. As mentioned at concept GLX, the cutting angle increase has a negative effect on the clay production. This effect is similar for GL485 and GL484 and a decrease in production will occur with this concept, see Figure 6.4.

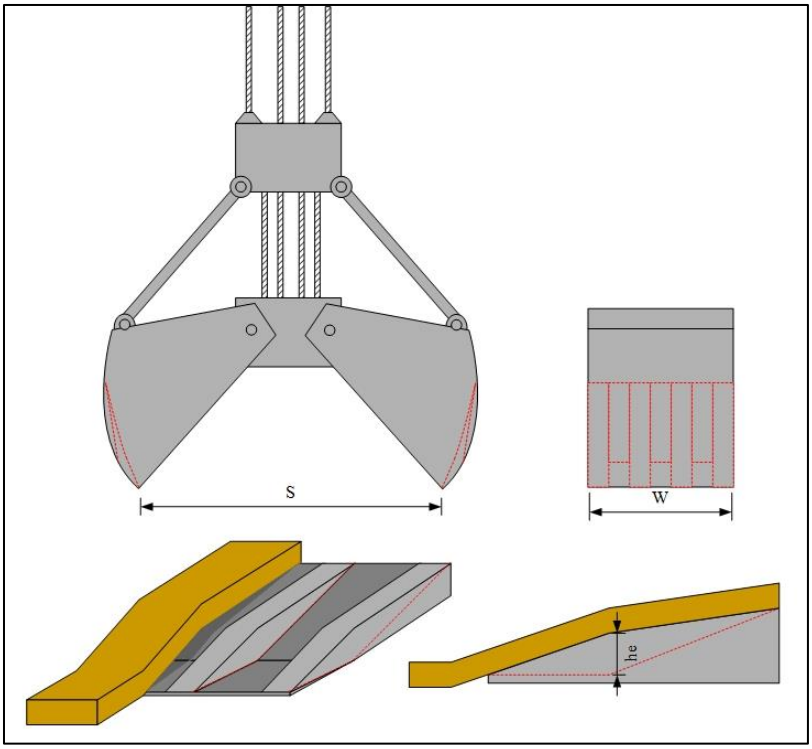

Figure 6.4 – Bucket concept GLZ

The GLZ concept has a design that will reduce the contact surface between clay-to-steel, but it will not decrease the force needed to penetrate or cut the clay. The clay is lifted away from the bucket bowl by means of an elevated teeth profile. The reduction of the ACL has a major effect on increasing the production for both GL485 and GL484. The GL484 has an increase of production by decreasing the ACL a little. However, for the GL485 the ACL must be reduced over 70% which results in a major effect, see paragraph 5.2.2. This makes the concept harder to implement and adjust for future bucket design, moreover the clay has to stick together to be "lifted" from the bucket bowl. The total percentage effect on the closing time, production and stick effect, see Table 6.3. All the output of the CCS 32 software can be found in Appendix K.

Table 6.3 - - Relative change compared to default output of clamshell bucket concept GLZ

Parameters						
ACL [%]	100	90	80	70	60	50
CA [°]	3.5	7	7	7	7	7
Percentages						
Closing time	20.33 s	0	-0.1	-0.2	-0.3	-0.4
Production	2.35 m^3	-1.3	9.8	23.8	41.7	66.0
Sticky effect	27 kN	-7.4	7.4	25.9	48.2	77.8

6.4. Great Lakes bucket XYZ

The GLXY concepts is a combination of all three previous clamshell bucket. This is increasing the total weight by adding weight to the bucket bowl (GLX), increasing the width and span of the bucket (GLY) and reducing the contact between steel-to-clay (GLZ).

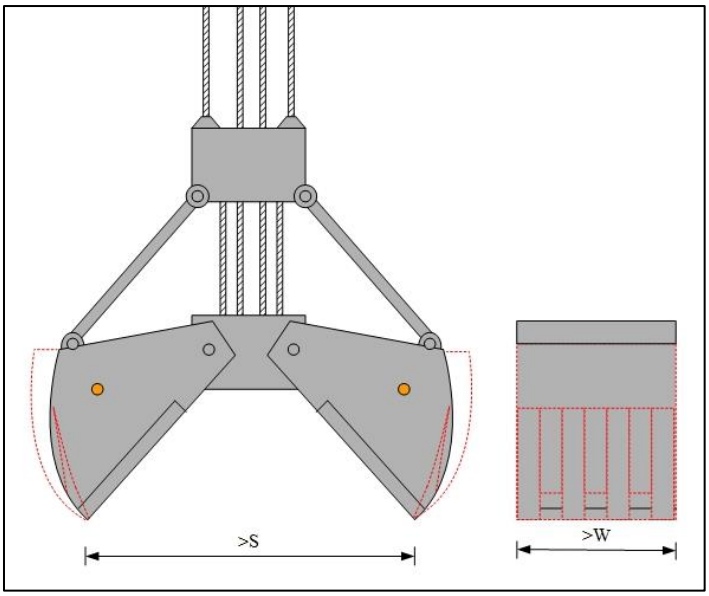

Figure 6.5 – Bucket concept GLZ

The total percentage effect on the closing time, production and stick effect, see Table 6.4. All the output of the CCS 32 software can be found in Appendix K.

Table 6.4 - - Relative change compared to default output of clamshell bucket concept GLXYZ

Parameters							
ACL [%]	100	90	80	70	60	50	50
TBW[m]	2.82	2.4	2.6	2.8	3.0	3.2	3.4
TBS [m]	6.8	6.30	6.55	7.05	7.30	7.55	7.80
BW [ton]	19.71	21.69	23.69	25.69	27.69	29.69	29.69
COG [m]	(0.59;2.29)	(0.62;1.67)	(0.65;1.81)	(0.67;2.26)	(0.71;2.51)	(0.74;2.76)	(0.74;3.01)
CA [°]	3.5	7	7	7	7	7	7
Percentages							
Closing time	20.33 s	-2.1	-1.0	1.3	2.4	3.4	4.6
Production	2.35 m^3	-2.6	28.1	68.5	119.6	194.0	204.7
Sticky effect	27 kN	33.3	51.9	66.7	96.3	137.0	118.5

6.5. Multi criteria analysis of clamshell bucket concepts

The multi criteria analysis (MCA) of clamshell bucket concepts has a purpose to evaluate the best possible option in new design or modifications to exciting clamshell buckets. Each of the four concepts are graded form 1 to 5 for different criteria with 5 being the highest score and 1 the lowest.

Table 6.5 - Multi criteria analysis scores and factors of the clamshell bucket concepts

Criteria	GLX	GLY	GLZ	GLXYZ	Factor
Production	4	3	4	5	2
Sticky effect	3	5	2	1	0.5
Hoisting cap.	2	2	4	3	2
Footprint	3	5	3	5	1.5
Closing time	5	3	5	2	2
Feasibility	5	4	3	2	1
Wear and tear	5	4	4	4	1
Total score	38	**36**	**36.5**	**34**	-

Each criteria has a particular impact on the total score and may need a short discerption to fully understand the criteria.

- Production: production is the cubic meters of soil, in our case clay, that is in the grab after the closing simulation. The concept bucket with the highest production will get a score of a 5. If there is no increase of production the score is a 2. With a decrease of production the score is a 1.
- Sticky effect: the sticky effect is the total generated adhesive force between the clay and grab. The lowest sticky effect will get a score of 5.
- Hoisting capacity: this is the limitation that the crane can handle on the clamshell dredges. When concepts exceed the hoisting capacity of all dredges to have an increase in production a score of 1 was given.
- Footprint: this is the increase of the bucket span in combination with the bucket width. The concept with a largest footprint will get a score of a 5.
- Closing time: the closing time is the time needed to completely close the grab. The bucket concepts with the lowest closing time will be graded with a 5.
- Feasibility: this is the state or degree of being easily or conveniently done. The bucket concept with the most feasible solution was graded with a 5.
- Wear and tear: during the usage of the bucket wear and tear will occur. The concept that will with stand the wear and tear the longest in time is grade a 5.
- Total score: this is all the scores multiplied with the factor and added up. The concept with the overall highest score is best choice considering the options of clamshell bucket concepts.

6.6. Clamshell bucket concepts conclusion

The conclusion is mainly based on the results of the MCA and therefore the GLX is the best solution to increasing production in cubic meters per second, see Table 6.6. The GLX bucket concept is adding weight to the bucket to increasing the total weight of the bucket and moving the centre point of gravity (COG) outwards, see Figure 6.6. The MCA is based on the following criteria: production, sticky effect (adhesive force), hoisting capacity dredge crane, bucket footprint, closing time, feasibility and wear and tear. With production, hoisting capacity and closing time having the highest factor contributing to the total score.

Table 6.6 - Multi criteria analysis of the clamshell bucket concepts conclusion

Criteria	GLX	GLY	GLZ	GLXYZ	Factor
Production	4	3	4	5	2
Sticky effect	3	5	2	1	0.5
Hoisting cap.	2	2	4	3	2
Footprint	3	5	3	5	1.5
Closing time	5	3	5	2	2
Feasibility	5	4	3	2	1
Wear and tear	5	2	4	4	1
Total score	38	**34**	**36.5**	**34**	-

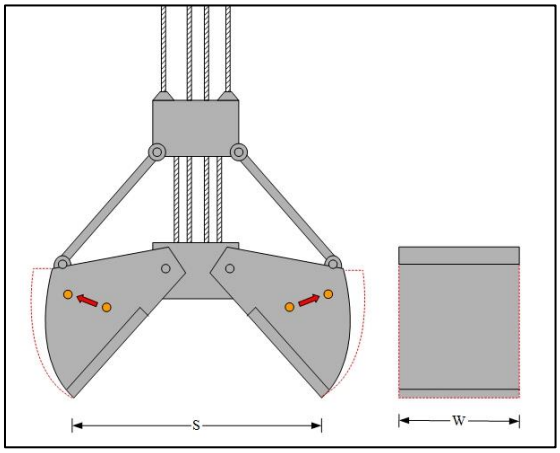

Figure 6.6 – Bucket concept solution GLX

The effect of increasing the bucket weight and repositioning the COG is that: first there is an larger initial penetration into the clay and secondly a larger momentum is created during the closing phase, making it easy to cut stiffer clays and finally increasing the production of clay, see Figure 6.7.

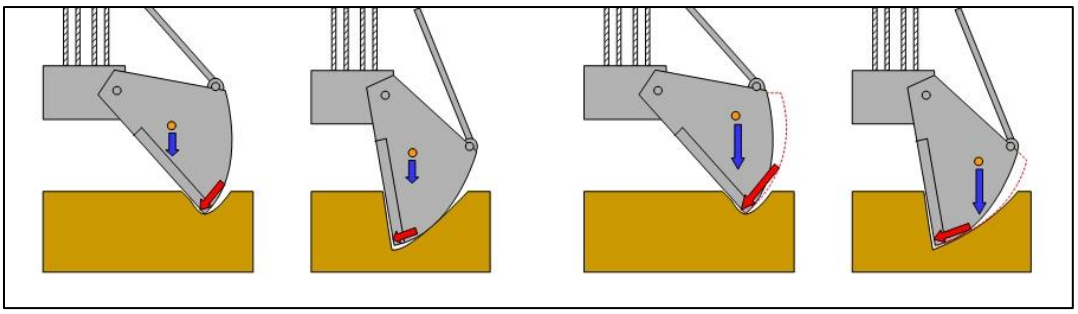

Figure 6.7 – Bucket concept GLX additional momentum

7. Conclusion

This study was on the optimization of the clamshell bucket's (or grab) cubic meter [m^3] production per cycle [s] for stiffer clays and has evolved in more than the optimization. The various parts of this study (being the cohesion/adhesion relationship of clay, the clamshell bucket sensitivity analysis and the clamshell buckets concepts) have given an interesting result and the following conclusions were drawn.

7.1. Conclusion concerning the relation between cohesion and adhesion

The adhesive test set-up with the approaches to the experimental adhesive data has led to confirming the prediction of adhesive strength development with increasing cohesive strength. The softer Delaware river clays and the Freeport red clay (0.4 mm/s) show a linear relation between normal stress and shear stress, meaning there is no adhesion measured. With an increasing cohesive strength of the clay there is a decrease of the adhesive strength. In addition to the decreasing adhesion, there is an increase in the internal friction angle (φ). This can be concluded from the data of the Freeport grey clay (8 mm/s) and the stiffer Freeport red clay (8 mm/s). The internal friction angle for the Freeport red clay is +/- 30 degrees, however the internal friction angle will have a limit. This has a major influence on the productions [m^3/s] and production estimates of stiffer clays with clamshell dredges or any other dredging equipment.

The two different pulling speeds, 8 and 0.4 mm/s, have shown that with a higher pulling speed a higher pulling force is required. This effect can be explained by the low permeability of the clay. By pulling the blade at a low speed the water in the pores have time to flow out, decreasing the "suction" effect.

7.2. Conclusion bucket sensitivity analysis

The clamshell bucket sensitivity analysis has created an insight into the effect of adjusting particular grab parameters to increase the production or payload [m^3] per grab closing cycle [s]. The used buckets, GL485 and GL484, have different effects on the normative parameters.

For both grabs GL485 and GL484 the five normative parameters have similar and slightly different effects on the production. The GL485 has the largest increase of the production with ACL reduction and least with increasing BW. For the GL484 reducing ACL is most effective for increasing the production and repositioning the COG the least. Taking the feasibility and amount of reduction or increase needed of each parameter a reorganised of the effects are made in Table 5.20.

Table 7.1 - GL485 and GL484 conclusion parameter effects on production

Positive effect on the production	GL485	GL484
1	Increase total bucket weight	Reduce adhesive cutting length
2	Lower and outwards COG	Increase total bucket weight
3	Reduce adhesive cutting length	Increase bucket span
4	Increase bucket width	Decrease cutting angle
5	Reduce cutting angle	Decrease bucket width

7.3. Conclusion concerning the clamshell bucket concepts

The clamshell bucket sensitivity (Chapter 5) and the clamshell bucket concepts (Chapter 6) are a combination of data and creativity that has resulted in new opportunities for clamshell bucket design. The conclusion is mainly based on the results of the MCA and therefore the GLX is the best solution to increasing production in cubic meters per second, see Table 6.6. The GLX bucket concept is adding weight to the bucket to increasing the total weight of

the bucket and moving the centre point of gravity (COG) outwards, see Figure 6.6. The MCA is based on the following criteria: production, sticky effect, hoisting capacity dredge crane, bucket footprint, closing time, feasibility and wear and tear. With production, hoisting capacity and closing time having the highest factor contributing to the total score.

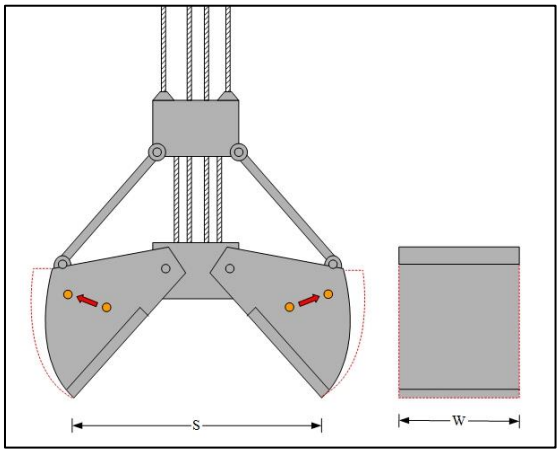

Figure 7.1 – Bucket concept solution GLX

7.4. Recommendation

My recommendation are focused on the adhesive test set-up and possible future opportunities.

7.4.1. Test set-up

One has to consider that when designing, constructing and using a test set-up there is a budget and a time window to do the experiments. Every researcher will agree with me there is never too much data and there is always a time constraint to get it done. Therefore each test set-up has its pros and cons.

For future use of the test set-up make sure the vertical load or normal stress can be increased drastically at least up to 200 N/mm^2. This will help in the determination of adhesive stress and possible internal friction angle. The will be also the ultimate test for the designed adhesive test set-up to verify if it records what it was made for.

Make sure you have several top and bottom plates that can be filled with natural field clays. This will save you time and you can over fill the box without having it to clean between clay tests.

7.4.2. Future research

There are different opportunities for future research from the conclusions of this study. The first is to acquire additional data on the development of the correlation between cohesion, adhesion and friction angles. This includes determining what the limit is for internal friction angle of clay.

The opportunities are also in constructing and testing scale models of the clamshell bucket concepts. The clamshell closing simulations gave insight in the adjustments, but theory and practice are not comparable. Additional aspects like, cycle time, footprint layout and wear and tear could be taken into account to complete the clamshell bucket optimization for production.

Nomenclature

A	Adhesive force	[N]
A_{blade}	Pulling blade surface	[m^2]
A_0	Bucket footprint / grab area	[m^2]
a	External undrained shear strength / adhesive strength	[Pa]
C	Cohesive force	[N]
c	Internal undrained shear strength / cohesive strength	[Pa]
c_m	Pseudo cohesion	[Pa]
E_{sp}	Specific cutting energy	[Pa]
F_H / F_h	Horizontal cutting force	[N]
$F_{additional}$	Additional pulling force	[N]
$F_{adhesion}$	Adhesive force	[N]
F_{pull}	Blade pulling force	[N]
F_{shear}	Shear force	[N]
F_V / F_v	Vertical cutting force	[N]
F_{res}	Resulting cutting force	[N]
G	Gravitation force from cut soil	[N]
g	Gravitation (9.81)	[m/s^2]
h_b	Height cutting blade	[m]
h_i	Thickness soil layer cut	[m]
I	Inertia force from cut soil	[Nm]
K_1	Resulting force between cut soil shear plane and stationary soil	[N]
K_2	Resulting force between cutting blade and shear plane	[N]
LL	Liquid limit	[%]
LI	Plastic index	[-]
M	Mass of bucket parts	[kg]
m_f	Payload	[kg]
m_g	Dead weight	[kg]
N_1	Normal force from stationary soil	[N]
N_2	Normal force from cutting blade	[N]
N_c	The cohesion and friction of a weightless material	[-]
N_q	the friction of a matrial possessing weight	[-]
N_γ	The friction of a weightless material upon addition of a surcharge q on the ground surface	[-]
PI	Plastic index	[-]
PL	Plastic limit	[%]
S	Bucket span	[m]
SL	Shrinkage limit	[%]
S_1	Shear force on stationary soil	[N]
S_2	Shear force on cutting blade	[N]
S_u	Undrained shear strength	[Pa]
UCS	Unconfined compressive strength	[Pa]
V_c	Velocity cutting blade	[m/s]
W	Bucket width	[m]
W_1	Water pressure force on stationary soil	[N]
W_2	Water pressure force on the cutting tool	[N]
w	Width of cutting blade	[m]
z	Number of sheaves on bucket	[-]

Greek symbols

α	Blade angle	[degree]
β	Shear angle	[degree]
γ	Orientation of the shear plane	[degree]
γ_t	Unit weight	[$kg \cdot m^2/s^2$]

δ	External friction angle	[degree]
λ	Bucket opening angle	[degree]
ρ	Density	[kg/m^3]
σ	Normal stress	[Pa]
σ’	Effective stress	[Pa]
σ_1	Major principal stress	[Pa]
σ_3	Minor principal stress	[Pa]
σ_x	Inclined stress	[Pa]
τ	Shear stress	[Pa]
τ_b	Shear stress on pulling blade	[Pa]
φ	Internal friction angle	[degree]

Subscript

c	Curling type	[-]
E	Bucket side in contact with soil	[-]
f	Flow type	[-]
h	Horizontal	[-]
l	Lower sheave block	[-]
s	Shear type	[-]
t	Tear type	[-]
u	Upper sheave block	[-]
v	Vertical	[-]
1	Lower sheave block	[-]
2	Upper sheave block	[-]
3	Bucket shell	[-]

8. Nomenclature fold-out

A	Adhesive force	[N]
A_{blade}	Pulling blade surface	[m^2]
A_0	Bucket footprint / grab area	[m^2]
a	External undrained shear strength	[Pa]
C	Cohesive force	[N]
c	Internal undrained shear strength	[Pa]
F_H / F_h	Horizontal cutting force	[N]
$F_{additional}$	Additional pulling force	[N]
$F_{adhesion}$	Adhesive force	[N]
F_{pull}	Blade pulling force	[N]
F_{shear}	Shear force	[N]
F_V / F_v	Vertical cutting force	[N]
F_{res}	Resulting cutting force	[N]
G	Gravitation force from cut soil	[N]
h_i	Thickness soil layer cut	[m]
I	Inertia force from cut soil	[Nm]
K_1	Resulting force between cut soil shear plane and stationary soil	[N]
K_2	Resulting force between cutting blade and shear plane	[N]
N_1	Normal force from stationary soil	[N]
N_2	Normal force from cutting blade	[N]
S	Bucket span	[m]
S_1	Shear force on stationary soil	[N]
S_2	Shear force on cutting blade	[N]
S_u	Undrained shear strength	[Pa]
UCS	Unconfined compressive strength	[Pa]
V_c	Velocity cutting blade	[m/s]
W	Bucket width	[m]
W_1	Water pressure force on stationary soil	[N]
W_2	Water pressure force on the cutting tool	[N]
w	Width of cutting blade	[m]
z	Number of sheaves on bucket	[-]

Greek symbols

α	Blade angle	[degree]
β	Shear angle	[degree]
δ	External friction angle	[degree]
λ	Bucket opening angle	[degree]
ρ	Density	[kg/m^3]
σ	Normal stress	[Pa]
σ'	Effective stress	[Pa]
σ_1	Major principal stress	[Pa]
σ_3	Minor principal stress	[Pa]
τ	Shear stress	[Pa]
τ_b	Shear stress from pulling blade	[Pa]
φ	Internal friction angle	[degree]

Subscript

a	Bucket arm	[-]
h	Horizontal	[-]
l	Lower sheave block	[-]
u	Upper sheave block	[-]
v	Vertical	[-]
1	Lower sheave block	[-]
2	Upper sheave block	[-]
3	Bucket shell	[-]

List of figures

List of tables

9. References

API. (1993). *American petroleum institute soil properties.* Houston.

Bauerschlag, D. (1979). *Untersuchungen zum Fullverhalten von Motorgreifgern.* Hannover: University Hannover.

de Jong, P., Becker, S., Wittekoek, S., & Miedema, S. (1992). *The Closing Process of Clamshell Dredges in Water-Saturated Sand.* Bombay: Technical University Delft.

Gebhardt, R. (1972). Eindringwiederstande korniger haufwerke. *Hebezeuge und fordermittel 12*, pg. 241-247.

Graham, J., Crooks, J. H., & Bell, L. (1983). Time effects on the stress-strain behaviour of natural soft clays. *Gotechnique, Vol. 3*, pg. 327-340.

Great Lakes Dredge & Dock. (2008). *Soil properties American and International standards.* Oak Brook.

Hatamura, Y., & Chijiiwa, K. (1975). Analysis of the Mechanism of Soil Cutting: 1st report, cutting patterns of soil. *Bulletin of the JSM, Vol. 18, No. 120*, pg. 619-626.

Hatamura, Y., & Chijiiwa, K. (1976a). Analysis of the mechanism of soil cutting: 2nd report, Deformation and internal stress o soil in cutting. *Bulletin of the JSM, Vol. 19, No. 131*, pg. 555-563.

Hatamura, Y., & Chijiiwa, K. (1977a). Analysis of teh mechanism of soil cutting: 4th rport, Properties of soils related cutting. *Bulletin of JSME, Vol. 20, No. 139*, pg. 130-137.

Hatamura, Y., & Chijiiwa, K. (1977b). Analysis of teh mechanism of soil cutting: 5th report, Cutting theories of soils. *Bulletin of JSME, Vol. 20, No. 141*, 388-395.

Hatamurat, Y., & Chijiiwa, K. (1976b). Analysis of the mechanism of soil cutting: 3rd report, Distribution of stresses on cutting blade and cuttin force. *Bullentin of JSME, Vol. 19, No. 137*, 1376-1384.

Hupe, W., & Schuszter, W. (1965). Verbesserte Motorgreifer als Beitrag zur allgemeinen Verbesserung des Greiferumschlages. *Hebezeuge und Fordermittel*, pg. 6-9.

Kooistra, A., Verhoef, P., Broere, W., Ngan-Tillard, D., & van Tol, A. (1998). Appraisal of stickness of natural clays from laboratory tests. In R. Hack, R. Azzam, & R. Charlier, *Engineering Geology and Infrustructure*, pg. 101-113.

Lambe, T.W. & Whitman, R.V. (1979), *Soil Mechanics*. John Wiley & Sons, New York

Littleton, I. (1976). An experimental study of the adhesion between clay and steel. *Journal of Terramechanics*, 141-152.

Manufacturing, M. Clamshell bucket. *2 & 3 line buckets.* Theodore.

Miedema, S. A. (1987). *Berekening van de snijkrachten bij het snijden van volledig met water verzadigdd zand.* Delft: Ph. D. thesis, Delft University of Technology.

Miedema, S. A. (1989). Clamshell Closing Simulation software 32 (CCS32). Delft, Zuid-Holland, The Netherlands.

Miedema, S. A. (2009). *New Developments of cutting theories with respect to dredging, the cutting of clay & rock.* Phoenix: WEDA XXlX.

Miedema, S. A. (2010). *The influence of the strain rate on cutting processes.* Beijing, China: ISOPE.

Miedema, S. A. (2014). *The Delft sand, clay & rock cutting model.*

Miedema, S. A., & Vlasblom, W. J. (2006). *The closing process of Clamshell Dredges in water-saturated sand.* Delft.

Mitchell, J. K., & Soga, K. (2005). *Fundamentals of Soil Behavior.* New Jersey: John Wiley & Sons, Inc.

Niemann, G. (1935). Neue erkentniss im Greiferbou. *VDI 79*, pg. 325-328.

Ninnelt, A. (1924). *Uber Kraft- und Arbeitsverteiling an Greifern- besonderes an Motorgreifern.* Wittenberg.

Pfahl, G. (1912). Kraftverteilung und greifen bei selbst greifern. *VDI*, pg. 1-4.

Potyondy, J. G. (1961). Skin friction between various soils and construction material. In J. G. Potyondy, *Geotechnique 2*, pg. 339-353.

Rao, S. (2011). *Mechanical Vibrations 5th edition in si units*, pg. 577-581.Singapore: Pearson Eduaction South Asia Pte Ltd.

Sangrey, D. (1972). Naturally cemented sentive soils. In D. Sangrey, *Geotechnique*, pg. 139-152.

Scheffler, M. (1972). Neue Erkenntnisse uber die Auslegung von Zweischalen- Schuttgutgreifern. *Hebezeuge und fordermittel 12*.

Schleffler, M., Pajer, G., & Kurth, F. (1976). *Grundlagen der Fordertechnik.* Berlin.

Sonne, E. (2012). Helios Data Acquisition Program. College station, Texas, US.

Tauber, B. (1958). The effect of the design of a calbe grab on its scooping capacity. *Coll. of sientific works of MLTI 8*, pg. 30-34.

Torke, H. (1962). Untersuchungen uber den fullvorgang bei Versuchen im Sand. *Deutsche Hebe und Fordertechnik*.

van der Wielen, V. (2014). *Physical modelling of soft clay cutting for plane strain conditions, Master Thesis.* Delft.

Van Oord. (2015, Mei 5). *Deep sea dredging solution.* Retrieved Mei 15, 2015, from www.vanoord.com: http://www.vanoord.com/news/2015-van-oord-develops-deep-dredging-solution

Wikipedia. (2015, 3 4). *Minerals*. Retrieved 3 4, 2015, from Wikipedia: http://en.wikipedia.org/wiki/Montmorillonite

Wikipedia. (2015, 03 20). *X-ray diffraction*. Retrieved 03 20, 2015, from Wikipedia: http://en.wikipedia.org/wiki/X-ray_crystallography

Wilkinson, H. N. (1963). Research in the design of grabs by tests on models. *Proceedings of Institution of mechanical engineering 178*, pg. 831-846.

Wittekoek, S. (1991a). *The determination of the closing process of clamshell dreges in water saturated sand.* Delft: Vakgroept Transporttechnologie.

Wittekoek, S. (1991c). *The validation of a calculation method fo the simulation of the colosing process of clamshell grabs for dredding purposes.* Delft: Vakgroep Transporttechnologie.

Witterkoek, S. (1991b). *The development of an improved clamshell.* Delft: Vakgroep Transporttechnologie.

10. Appendix

10.1. Appendix A

10.1.1. AutoCAD drawing adhesive test set-up

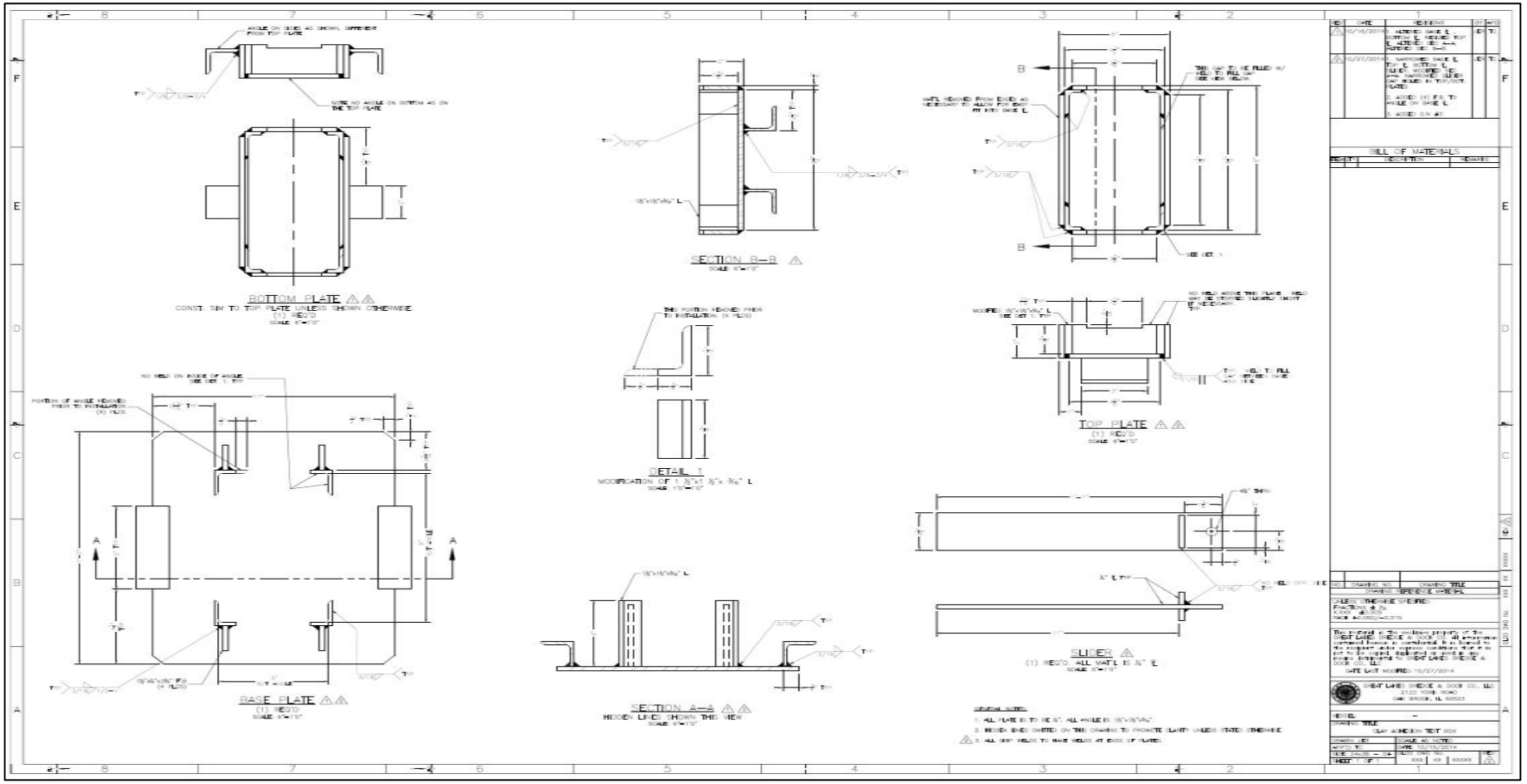

10.2. Appendix B

10.2.1. Electric actuator

- Force: 1000 lbs
- Stroke: 12 inch
- Built in limit: switches, not movable
- Input: 12VDC
- Speed: approximately 1/5” per sec (loaded)

The **10'' Stroke 1000lb Force Linear Actuator** features 1000 lbs force with aluminium shaft, and a tough plastic case. It also features two wire configuration for ease of use, 12vdc operation, fixed limit switches and is very quiet. Use MB3 mounting brackets for these style actuators.

Model	FA-1000-L-12-XX
Dynamic Force	1000 lbs
Static force	1000 lbs
Speed at Full load	1/5 “/s
Duty cycle	20%
IP Rating	43
Input	12v DC
Max Draw	5 A
Limit Switch	-26°C/65°C (-15°F/150°F)
Safety Certification	CE
Bracket(s)	**$\underline{MB_3}$ or $\underline{MB_3U}$**
Stroke	12”
Retracted Length	18.88”
Extended Length	30.88”
Weight	5.9 lbs

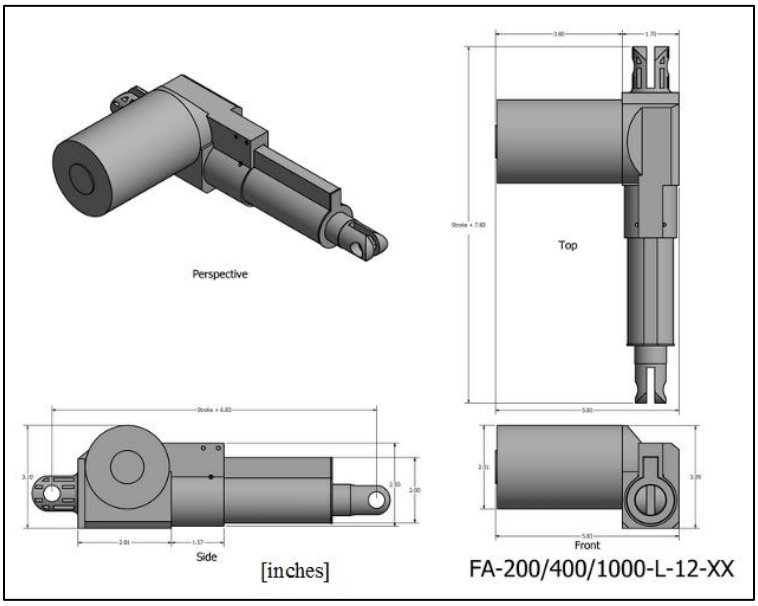

All information and pictures is from Firgelli Automations website

10.2.2. Speed controller specifications

The Firgelli Automations Speed Controller allows you to control the speed of our FA-RMS, FA-PO-35, FA-PO-150, FA-35-S, FA-RA, FA-150, FA-240, FA-04, FA-05, FA-200-L, FA-400-L, FA-1000-L, FA-TR-35, FA-200-TR, FA-450-TR and all our gear motor products.

Designed using a motor controller and high frequency Pulse Width Modulation (PWM) you are able to control the speed of your Actuator/Motor in either direction with minimal impact on the force output. The speed controller will allow you to slow the actuator down, but not increase the speed beyond the speed at which it runs with no controller.

The FA-SC24 is intended to control the speed of one Linear actuator or motor, Do not connect two actuators/motors to the same FA-SC24. The slowest the actuator/motor will run is about 10% of the full speed. Reducing the speed can affect the maximum load the actuator can move.

The FA-SC24 does not have a case, this is to allow heat to dissipate from the heat sinks.

- 12V-40V operation
- Handles up to 10A (400W)
- 10% to 80% speed range
- Quiet due to higher PWM frequency

All information and pictures is from Firgelli Automations website

10.2.3. Load cell specifications

Small in size and capable of providing highly accurate readings, the LCFD Series miniature load cells are precision sub miniature load cells for industrial applications requiring a small size and high accuracy. They are all stainless steel, measure both tension and compression loads and have male thread studs for load attachment. The exclusive internal design provides superior long term stability and minimizes the effects of small off-axis loads. Compatible Meters: DP41-W, DP41-S, DP25-S

The LCFD is also available in metric configurations, with ranges from 0-10 to 0-5,000 N and metric threads. Please see the LCMFD for complete details, or contact our Pressure department for more information..

SPECIFICATIONS

Excitation:

≤10 lb/50 N: 5 Vdc

≥25 lb/100 N: 10 Vdc

Output:

2.2 lb/10 N: 1.5 mV/V (nom)

≥5 lb/20 N: 2 mV/V (nom)

Accuracy (Linearity and Hysteresis Combined):

≤100 lb/500 N: ±0.15% FSO

≥250 lb/1000 N: ±0.20% FSO

Repeatability:

≤2.2 lb: ± 0.15% FSO

≥5 lb/10 N: 0.20% FSO

5-Point Calibration (in Tension): 0%, 50%, 100%, 50%, 0%

Zero Balance: ±2% FSO

Operating Temp Range: -54 to 121°C (-65 to 250°F)

Compensated Temp Range: 16 to 71°C (60 to 160°F)

Thermal Effects:

Span: ±0.009% FSO/°C

Zero: ±0.009% FSO/°C

Safe Overload: 150% of capacity

Ultimate Overload: 300% of capacity

Bridge Resistance: 350 Ω minimum

Construction: Stainless steel

Electrical Connection: 1.5 m (5') 4-conductor, shielded cable

≤10 lb/50 N: SS over braided PTFE with temperature compensation board

Protection Class: IP65

All information and pictures are from omega EU website

10.3. Appendix C

10.3.1. GL485 Sensitivity analysis data

10.3.1.1. CA

Original value		**CA=3,5**	**CA =1**	**CA=3**	**CA=5**	**CA=7**	**CA=9**
TIME	s	20,24	20,3	20,32	20,33	20,35	20,36
X-LIP	m	0	0	0	0	0	0
Y-LIP	m	-0,21	-0,23	-0,21	-0,2	-0,18	-0,17
SITU PRODUCTION	m^3	2,36	2,55	2,39	2,25	2,12	2
WINCH POWER	kW	104,74	101,56	104,67	103,26	101,53	99,23
SPECIFIC ENGERGY	kJ/m^3	502,19	486,45	502,34	517,67	533,05	548,84
PENETRATION DEPTH	m	0,007	0,007	0,007	0,007	0,007	0,007
TOTAL STICKY EFFECT	kN	27	32	28	25	23	20
UPPERBLOCK SPEED	m/sec	0,284	0,306	0,287	0,274	0,263	0,255
LOWERBLOCK SPEED	m/sec	0,066	0,085	0,069	0,058	0,049	0,042
ANGULAR VELOCITY	deg/sec	7,792	7,901	7,785	7,706	7,641	7,594
ROPE FORCE	kN	103	100	103	102	100	98
ARM FORCE	kN	145	142	146	144	142	138
TOTAL MASS	tons	19,709	19,709	19,709	19,709	19,709	19,709
TOTAL VOLUME	m^3	22,433	22,433	22,433	22,433	22,433	22,433

Percentages		**CA=3,5**	**CA =1**	**CA=3**	**CA=5**	**CA=7**	**CA=9**
TIME	s	0	0,3	0,4	0,44	0,54	0,59
X-LIP	m						
Y-LIP	m	0	9,52	0	-4,76	-14,29	-19,05
SITU PRODUCTION	m^3	0	8,05	1,27	-4,66	-10,17	-15,25
WINCH POWER	kW	0	-3,04	-0,07	-1,41	-3,06	-5,26
SPECIFIC ENGERGY	kJ/m^3	0	-3,13	0,03	3,08	6,15	9,29
PENETRATION DEPTH	m	0	0	0	0	0	0
TOTAL STICKY EFFECT	kN	0	18,52	3,7	-7,41	-14,81	-25,93
UPPERBLOCK SPEED	m/sec	0	7,75	1,06	-3,52	-7,39	-10,21
LOWERBLOCK SPEED	m/sec	0	28,79	4,55	-12,12	-25,76	-36,36
ANGULAR VELOCITY	deg/sec	0	1,4	-0,09	-1,1	-1,94	-2,54
ROPE FORCE	kN	0	-2,91	0	-0,97	-2,91	-4,85
ARM FORCE	kN	0	-2,07	0,69	-0,69	-2,07	-4,83
TOTAL MASS	tons	0	0	0	0	0	0
TOTAL VOLUME	m^3	0	0	0	0	0	0

10.3.1.2. ACL

Original value	m	ACL=0,97	0,1 m	0,3 m	0,5 m	0,7 m	0,9 m
TIME	s	20,24	19,04	19,33	20,32	20,32	20,32
X-LIP	m	0	0	0	0	0	0
Y-LIP	m	-0,21	-1,51	-1,22	-0,21	-0,21	-0,21
SITU PRODUCTION	m^3	2,36	16,57	11,26	2,36	2,36	2,36
WINCH POWER	kW	104,74	339,34	356,95	103,75	103,75	103,75
SPECIFIC ENGERGY	kJ/m^3	502,19	163,95	199,87	506,08	506,25	506,25
PENETRATION DEPTH	m	0,007	0,007	0,007	0,007	0,007	0,007
TOTAL STICKY EFFECT	kN	27	433	329	27	27	27
UPPERBLOCK SPEED	m/sec	0,284	0,261	0,303	0,283	0,283	0,283
LOWERBLOCK SPEED	m/sec	0,066	0,047	0,082	0,066	0,066	0,066
ANGULAR VELOCITY	deg/sec	7,792	7,631	7,88	7,762	7,762	7,762
ROPE FORCE	kN	103	334	351	102	102	102
ARM FORCE	kN	145	473	498	145	145	145
TOTAL MASS	tons	19,709	19,709	19,709	19,709	19,709	19,709
TOTAL VOLUME	m^3	22,433	22,433	22,433	22,433	22,433	22,433

Percentages	m	ACL=0,97	0,1 m	0,3 m	0,5 m	0,7 m	0,9 m
TIME	s	0	-5,93	-4,5	0,4	0,4	0,4
X-LIP	m						
Y-LIP	m	0	619,05	480,95	0	0	0
SITU PRODUCTION	m^3	0	602,12	377,12	0	0	0
WINCH POWER	kW	0	223,98	240,8	-0,95	-0,95	-0,95
SPECIFIC ENGERGY	kJ/m^3	0	-67,35	-60,2	0,77	0,81	0,81
PENETRATION DEPTH	m	0	0	0	0	0	0
TOTAL STICKY EFFECT	kN	0	1503,7	1118,52	0	0	0
UPPERBLOCK SPEED	m/sec	0	-8,1	6,69	-0,35	-0,35	-0,35
LOWERBLOCK SPEED	m/sec	0	-28,79	24,24	0	0	0
ANGULAR VELOCITY	deg/sec	0	-2,07	1,13	-0,39	-0,39	-0,39
ROPE FORCE	kN	0	224,27	240,78	-0,97	-0,97	-0,97
ARM FORCE	kN	0	226,21	243,45	0	0	0
TOTAL MASS	tons	0	0	0	0	0	0
TOTAL VOLUME	m^3	0	0	0	0	0	0

10.3.1.3. COG

Original value	x	X=0,59	X=0,2	X=0,4	X=0,6	X=0,8	X=1,0
TIME	s	20,24	20,32	20,32	20,32	20,32	20,32
X-LIP	m	0	0	0	0	0	0
Y-LIP	m	-0,21	-0,21	-0,21	-0,21	-0,21	-0,21
SITU PRODUCTION	m^3	2,36	2,32	2,34	2,36	2,38	2,4
WINCH POWER	kW	104,74	106,89	105,85	104,04	103,33	101,88
SPECIFIC ENGERGY	kJ/m^3	502,19	523,93	515,25	506,32	497,64	488,13
PENETRATION DEPTH	m	0,007	0,007	0,007	0,007	0,007	0,007
TOTAL STICKY EFFECT	kN	27	26	27	27	28	28
UPPERBLOCK SPEED	m/sec	0,284	0,281	0,282	0,283	0,284	0,286
LOWERBLOCK SPEED	m/sec	0,066	0,064	0,065	0,006	0,067	0,068
ANGULAR VELOCITY	deg/sec	7,792	7,75	7,757	7,763	7,77	7,777
ROPE FORCE	kN	103	105	104	102	102	100
ARM FORCE	kN	145	149	148	145	144	142
TOTAL MASS	tons	19,709	19,709	19,709	19,709	19,709	19,709
TOTAL VOLUME	m^3	22,433	22,433	22,433	22,433	22,433	22,433

percentages	x	Y=2,29	Y=2,0	Y=2,2	Y=2,4	Y=2,6	Y=2,8
TIME	s	0	0,4	0,4	0,4	0,4	0,4
X-LIP	m						
Y-LIP	m	0	0	0	0	0	0
SITU PRODUCTION	m^3	0	-1,69	-0,85	0	0,85	1,69
WINCH POWER	kW	0	2,05	1,06	-0,67	-1,35	-2,73
SPECIFIC ENGERGY	kJ/m^3	0	4,33	-1,73	-1,78	-1,73	-1,89
PENETRATION DEPTH	m	0	0	0	0	0	0
TOTAL STICKY EFFECT	kN	0	-3,7	0	0	3,7	3,7
UPPERBLOCK SPEED	m/sec	0	-1,06	-0,7	-0,35	0	0,7
LOWERBLOCK SPEED	m/sec	0	-3,03	-1,52	-90,91	1,52	3,03
ANGULAR VELOCITY	deg/sec	0	-0,54	-0,45	-0,37	-0,28	-0,19
ROPE FORCE	kN	0	1,94	0,97	-0,97	-0,97	-2,91
ARM FORCE	kN	0	2,76	2,07	0	-0,69	-2,07
TOTAL MASS	tons	0	0	0	0	0	0
TOTAL VOLUME	m^3	0	0	0	0	0	0

Original value	**y**	**Y=2,29**	**Y=2,0**	**Y=2,2**	**Y=2,4**	**Y=2,6**	**Y=2,8**
TIME	s	20,24	20,32	20,32	20,32	20,33	20,33
X-LIP	m	0	0	0	0	0	0
Y-LIP	m	-0,21	-0,21	-0,21	-0,21	-0,21	-0,21
SITU PRODUCTION	m^3	2,36	2,33	2,35	2,37	2,38	2,4
WINCH POWER	kW	104,74	104,06	104,61	104,46	104,27	105,03
SPECIFIC ENGERGY	kJ/m^3	502,19	516,78	509,53	503,36	496,04	490,47
PENETRATION DEPTH	m	0,007	0,007	0,007	0,007	0,007	0,007
TOTAL STICKY EFFECT	kN	27	27	27	27	27	27
UPPERBLOCK SPEED	m/sec	0,284	0,284	2,83	0,283	2,83	0,283
LOWERBLOCK SPEED	m/sec	0,066	0,066	0,006	0,066	0,065	0,065
ANGULAR VELOCITY	deg/sec	7,792	7,765	7,765	7,763	7,76	7,76
ROPE FORCE	kN	103	102	103	103	103	103
ARM FORCE	kN	145	145	146	146	145	146
TOTAL MASS	tons	19,709	19,709	19,709	19,709	19,709	19,709
TOTAL VOLUME	m^3	22,433	22,433	22,433	22,433	22,433	22,433

percentages	**y**	**Y=2,29**	**Y=2,0**	**Y=2,2**	**Y=2,4**	**Y=2,6**	**Y=2,8**
TIME	s	0	0,4	0,4	0,4	0,44	0,44
X-LIP	m						
Y-LIP	m	0	0	0	0	0	0
SITU PRODUCTION	m^3	0	-1,27	-0,42	0,42	0,85	1,69
WINCH POWER	kW	0	-0,65	-0,12	-0,27	-0,45	0,28
SPECIFIC ENGERGY	kJ/m^3	0	2,91	1,46	0,23	-1,22	-2,33
PENETRATION DEPTH	m	0	0	0	0	0	0
TOTAL STICKY EFFECT	kN	0	0	0	0	0	0
UPPERBLOCK SPEED	m/sec	0	0	896,48	-0,35	896,48	-0,35
LOWERBLOCK SPEED	m/sec	0	0	-90,91	0	-1,52	-1,52
ANGULAR VELOCITY	deg/sec	0	-0,35	-0,35	-0,37	-0,41	-0,41
ROPE FORCE	kN	0	-0,97	0	0	0	0
ARM FORCE	kN	0	0	0,69	0,69	0	0,69
TOTAL MASS	tons	0	0	0	0	0	0
TOTAL VOLUME	m^3	0	0	0	0	0	0

Original value	**x=0,2**	**Y=2,29**	**Y=2,0**	**Y=2,2**	**Y=2,4**	**Y=2,6**	**Y=2,8**
TIME	s	20,24	20,32	20,32	20,33	20,33	20,33
X-LIP	m	0	0	0	0	0	0
Y-LIP	m	-0,21	-0,21	-0,21	-0,21	-0,21	-0,21
SITU PRODUCTION	m^3	2,36	2,3	2,31	2,33	2,34	2,36
WINCH POWER	kW	104,74	106,69	107,31	107,02	107,24	107,7
SPECIFIC ENGERGY	kJ/m^3	502,19	535,07	528,22	520,29	513,36	506,88
PENETRATION DEPTH	m	0,007	0,007	0,007	0,007	0,007	0,007
TOTAL STICKY EFFECT	kN	27	26	26	26	27	27
UPPERBLOCK SPEED	m/sec	0,284	0,282	0,281	0,281	0,281	0,281
LOWERBLOCK SPEED	m/sec	0,066	0,064	0,064	0,064	0,064	0,063
ANGULAR VELOCITY	deg/sec	7,792	7,753	7,752	7,749	7,748	7,747
ROPE FORCE	kN	103	105	106	105	106	106
ARM FORCE	kN	145	149	150	149	149	150
TOTAL MASS	tons	19,709	19,709	19,709	19,709	19,709	19,709
TOTAL VOLUME	m^3	22,433	22,433	22,433	22,433	22,433	22,433

percentages	**x=0,2**	**Y=2,29**	**Y=2,0**	**Y=2,2**	**Y=2,4**	**Y=2,6**	**Y=2,8**
TIME	s	0	0,4	0,4	0,44	0,44	0,44
X-LIP	m						
Y-LIP	m	0	0	0	0	0	0
SITU PRODUCTION	m^3	0	-2,54	-2,12	-1,27	-0,85	0
WINCH POWER	kW	0	1,86	2,45	2,18	2,39	2,83
SPECIFIC ENGERGY	kJ/m^3	0	6,55	5,18	3,6	2,22	0,93
PENETRATION DEPTH	m	0	0	0	0	0	0
TOTAL STICKY EFFECT	kN	0	-3,7	-3,7	-3,7	0	0
UPPERBLOCK SPEED	m/sec	0	-0,7	-1,06	-1,06	-1,06	-1,06
LOWERBLOCK SPEED	m/sec	0	-3,03	-3,03	-3,03	-3,03	-4,55
ANGULAR VELOCITY	deg/sec	0	-0,5	-0,51	-0,55	-0,56	-0,58
ROPE FORCE	kN	0	1,94	2,91	1,94	2,91	2,91
ARM FORCE	kN	0	2,76	3,45	2,76	2,76	3,45
TOTAL MASS	tons	0	0	0	0	0	0
TOTAL VOLUME	m^3	0	0	0	0	0	0

Original value	**x=0,4**	**Y=2,29**	**Y=2,0**	**Y=2,2**	**Y=2,4**	**Y=2,6**	**Y=2,8**
TIME	s	20,24	20,32	20,32	20,32	20,33	20,34
X-LIP	m	0	0	0	0	0	0
Y-LIP	m	-0,21	-0,21	-0,21	-0,21	-0,21	-0,21
SITU PRODUCTION	m^3	2,36	2,32	2,33	2,35	2,36	2,38
WINCH POWER	kW	104,74	105,57	105,36	106	106,06	106,32
SPECIFIC ENGERGY	kJ/m^3	502,19	525,63	518,14	511,19	504,23	497,35
PENETRATION DEPTH	m	0,007	0,007	0,007	0,007	0,007	0,007
TOTAL STICKY EFFECT	kN	27	27	27	27	27	27
UPPERBLOCK SPEED	m/sec	0,284	0,283	0,282	0,282	0,282	0,282
LOWERBLOCK SPEED	m/sec	0,066	0,065	0,065	0,065	0,065	0,064
ANGULAR VELOCITY	deg/sec	7,792	7,759	7,757	7,756	7,755	7,753
ROPE FORCE	kN	103	104	104	104	104	105
ARM FORCE	kN	145	147	147	148	148	148
TOTAL MASS	tons	19,709	19,709	19,709	19,709	19,709	19,709
TOTAL VOLUME	m^3	22,433	22,433	22,433	22,433	22,433	22,433

percentages	**x=0,4**	**Y=2,29**	**Y=2,0**	**Y=2,2**	**Y=2,4**	**Y=2,6**	**Y=2,8**
TIME	s	0	0,4	0,4	0,4	0,44	0,49
X-LIP	m						
Y-LIP	m	0	0	0	0	0	0
SITU PRODUCTION	m^3	0	-1,69	-1,27	-0,42	0	0,85
WINCH POWER	kW	0	0,79	0,59	1,2	1,26	1,51
SPECIFIC ENGERGY	kJ/m^3	0	4,67	3,18	1,79	0,41	-0,96
PENETRATION DEPTH	m	0	0	0	0	0	0
TOTAL STICKY EFFECT	kN	0	0	0	0	0	0
UPPERBLOCK SPEED	m/sec	0	-0,35	-0,7	-0,7	-0,7	-0,7
LOWERBLOCK SPEED	m/sec	0	-1,52	-1,52	-1,52	-1,52	-3,03
ANGULAR VELOCITY	deg/sec	0	-0,42	-0,45	-0,46	-0,47	-0,5
ROPE FORCE	kN	0	0,97	0,97	0,97	0,97	1,94
ARM FORCE	kN	0	1,38	1,38	2,07	2,07	2,07
TOTAL MASS	tons	0	0	0	0	0	0
TOTAL VOLUME	m^3	0	0	0	0	0	0

Original value	**x=0,6**	**Y=2,29**	**Y=2,0**	**Y=2,2**	**Y=2,4**	**Y=2,6**	**Y=2,8**
TIME	s	20,24	20,32	20,32	20,32	20,32	20,26
X-LIP	m	0	0	0	0	0	0
Y-LIP	m	-0,21	-0,21	-0,21	-0,21	-0,21	-0,21
SITU PRODUCTION	m^3	2,36	2,33	2,35	2,37	2,38	2,39
WINCH POWER	kW	104,74	103,9	104,07	104,43	104,92	105,32
SPECIFIC ENGERGY	kJ/m^3	502,19	515,69	508,85	502	495,7	488,14
PENETRATION DEPTH	m	0,007	0,007	0,007	0,007	0,007	0,007
TOTAL STICKY EFFECT	kN	27	27	27	27	27	27
UPPERBLOCK SPEED	m/sec	0,284	0,284	0,283	0,283	0,283	0,284
LOWERBLOCK SPEED	m/sec	0,066	0,066	0,066	0,066	0,066	0,065
ANGULAR VELOCITY	deg/sec	7,792	7,765	7,763	7,764	7,762	7,79
ROPE FORCE	kN	103	102	102	103	103	103
ARM FORCE	kN	145	145	145	146	146	146
TOTAL MASS	tons	19,709	19,709	19,709	19,709	19,709	19,709
TOTAL VOLUME	m^3	22,433	22,433	22,433	22,433	22,433	22,433

percentages	**x=0,6**	**Y=2,29**	**Y=2,0**	**Y=2,2**	**Y=2,4**	**Y=2,6**	**Y=2,8**
TIME	s	0	0,4	0,4	0,4	0,4	0,1
X-LIP	m						
Y-LIP	m	0	0	0	0	0	0
SITU PRODUCTION	m^3	0	-1,27	-0,42	0,42	0,85	1,27
WINCH POWER	kW	0	-0,8	-0,64	-0,3	0,17	0,55
SPECIFIC ENGERGY	kJ/m^3	0	2,69	1,33	-0,04	-1,29	-2,8
PENETRATION DEPTH	m	0	0	0	0	0	0
TOTAL STICKY EFFECT	kN	0	0	0	0	0	0
UPPERBLOCK SPEED	m/sec	0	0	-0,35	-0,35	-0,35	0
LOWERBLOCK SPEED	m/sec	0	0	0	0	0	-1,52
ANGULAR VELOCITY	deg/sec	0	-0,35	-0,37	-0,36	-0,39	-0,03
ROPE FORCE	kN	0	-0,97	-0,97	0	0	0
ARM FORCE	kN	0	0	0	0,69	0,69	0,69
TOTAL MASS	tons	0	0	0	0	0	0
TOTAL VOLUME	m^3	0	0	0	0	0	0

Original value	**x=0,8**	**Y=2,29**	**Y=2,0**	**Y=2,2**	**Y=2,4**	**Y=2,6**	**Y=2,8**
TIME	s	20,24	20,24	20,24	20,24	20,25	20,26
X-LIP	m	0	0	0	0	0	0
Y-LIP	m	-0,21	-0,21	-0,21	-0,21	-0,21	-0,21
SITU PRODUCTION	m^3	2,36	2,35	2,37	2,38	2,4	2,42
WINCH POWER	kW	104,74	103	103,76	103,8	103,45	103,67
SPECIFIC ENGERGY	kJ/m^3	502,19	507,41	500,13	492,99	487,56	480,5
PENETRATION DEPTH	m	0,007	0,007	0,007	0,007	0,007	0,007
TOTAL STICKY EFFECT	kN	27	28	28	28	28	28
UPPERBLOCK SPEED	m/sec	0,284	0,286	0,285	0,285	0,285	0,285
LOWERBLOCK SPEED	m/sec	0,066	0,067	0,067	0,067	0,066	0,066
ANGULAR VELOCITY	deg/sec	7,792	7,801	7,8	7,799	7,798	7,796
ROPE FORCE	kN	103	101	102	102	101	102
ARM FORCE	kN	145	143	144	144	144	144
TOTAL MASS	tons	19,709	19,709	19,709	19,709	19,709	19,709
TOTAL VOLUME	m^3	22,433	22,433	22,433	22,433	22,433	22,433

percentages	**x=0,8**	**Y=2,29**	**Y=2,0**	**Y=2,2**	**Y=2,4**	**Y=2,6**	**Y=2,8**
TIME	s	0	0	0	0	0,05	0,1
X-LIP	m						
Y-LIP	m	0	0	0	0	0	0
SITU PRODUCTION	m^3	0	-0,42	0,42	0,85	1,69	2,54
WINCH POWER	kW	0	-1,66	-0,94	-0,9	-1,23	-1,02
SPECIFIC ENGERGY	kJ/m^3	0	1,04	-0,41	-1,83	-2,91	-4,32
PENETRATION DEPTH	m	0	0	0	0	0	0
TOTAL STICKY EFFECT	kN	0	3,7	3,7	3,7	3,7	3,7
UPPERBLOCK SPEED	m/sec	0	0,7	0,35	0,35	0,35	0,35
LOWERBLOCK SPEED	m/sec	0	1,52	1,52	1,52	0	0
ANGULAR VELOCITY	deg/sec	0	0,12	0,1	0,09	0,08	0,05
ROPE FORCE	kN	0	-1,94	-0,97	-0,97	-1,94	-0,97
ARM FORCE	kN	0	-1,38	-0,69	-0,69	-0,69	-0,69
TOTAL MASS	tons	0	0	0	0	0	0
TOTAL VOLUME	m^3	0	0	0	0	0	0

Original value	**x=1,0**	**Y=2,29**	**Y=2,0**	**Y=2,2**	**Y=2,4**	**Y=2,6**	**Y=2,8**
TIME	s	20,24	20,24	20,24	20,24	20,25	20,25
X-LIP	m	0	0	0	0	0	0
Y-LIP	m	-0,21	-0,21	-0,21	-0,21	-0,22	-0,22
SITU PRODUCTION	m^3	2,36	2,37	2,39	2,41	2,42	2,43
WINCH POWER	kW	104,74	101,65	101,77	102,08	102,31	102,14
SPECIFIC ENGERGY	kJ/m^3	502,19	497,72	490,93	485,35	479,45	471,41
PENETRATION DEPTH	m	0,007	0,007	0,007	0,007	0,007	0,007
TOTAL STICKY EFFECT	kN	27	28	28	28	28	28
UPPERBLOCK SPEED	m/sec	0,284	0,287	0,287	0,286	0,286	0,286
LOWERBLOCK SPEED	m/sec	0,066	0,068	0,068	0,067	0,067	0,067
ANGULAR VELOCITY	deg/sec	7,792	7,808	7,807	7,805	7,804	7,802
ROPE FORCE	kN	103	100	100	100	100	100
ARM FORCE	kN	145	141	141	142	142	142
TOTAL MASS	tons	19,709	19,709	19,709	19,709	19,709	19,709
TOTAL VOLUME	m^3	22,433	22,433	22,433	22,433	22,433	22,433

percentages	**x=1,0**	**Y=2,29**	**Y=2,0**	**Y=2,2**	**Y=2,4**	**Y=2,6**	**Y=2,8**
TIME	s	0	0	0	0	0,05	0,05
X-LIP	m						
Y-LIP	m	0	0	0	0	4,76	4,76
SITU PRODUCTION	m^3	0	0,42	1,27	2,12	2,54	2,97
WINCH POWER	kW	0	-2,95	-2,84	-2,54	-2,32	-2,48
SPECIFIC ENGERGY	kJ/m^3	0	-0,89	-2,24	-3,35	-4,53	-6,13
PENETRATION DEPTH	m	0	0	0	0	0	0
TOTAL STICKY EFFECT	kN	0	3,7	3,7	3,7	3,7	3,7
UPPERBLOCK SPEED	m/sec	0	1,06	-76,06	0,7	0,7	0,7
LOWERBLOCK SPEED	m/sec	0	3,03	3,03	1,52	1,52	1,52
ANGULAR VELOCITY	deg/sec	0	0,21	0,19	0,17	0,15	0,13
ROPE FORCE	kN	0	-2,91	-2,91	-2,91	-2,91	-2,91
ARM FORCE	kN	0	-2,76	-2,76	-2,07	-2,07	-2,07
TOTAL MASS	tons	0	0	0	0	0	0
TOTAL VOLUME	m^3	0	0	0	0	0	0

10.3.1.4. TBW

Original value	**ton**	**6,57**	**2**	**4**	**6**	**8**	**10**
TIME	s	20,24	20,25	20,25	20,26	20,26	20,27
X-LIP	m	0	0	0	0	0	0
Y-LIP	m	-0,21	-0,23	-0,24	-0,26	-0,28	-0,29
SITU PRODUCTION	m^3	2,36	2,61	2,85	3,1	3,35	3,62
WINCH POWER	kW	104,74	114,62	124,51	133,42	142,2	150,88
SPECIFIC ENGERGY	kJ/m^3	502,19	504,47	504,08	504,64	504,88	505,03
PENETRATION DEPTH	m	0,007	0,016	0,025	0,033	0,042	0,05
TOTAL STICKY EFFECT	kN	27	31	34	37	41	44
UPPERBLOCK SPEED	m/sec	0,284	0,289	0,295	0,3	0,305	0,31
LOWERBLOCK SPEED	m/sec	0,066	0,07	0,075	0,079	0,083	0,088
ANGULAR VELOCITY	deg/sec	7,792	7,823	7,856	7,888	7,918	79,48
ROPE FORCE	kN	103	112	122	131	139	148
ARM FORCE	kN	145	159	173	185	197	210
TOTAL MASS	tons	19,709	21,709	23,709	25,709	27,709	29,709
TOTAL VOLUME	m^3	22,433	22,433	22,433	22,433	22,433	22,433

percentages	**ton**	**6,57**	**2**	**4**	**6**	**8**	**10**
TIME	s	0	0,05	0,05	0,1	0,1	0,15
X-LIP	m						
Y-LIP	m	0	9,52	14,29	23,81	33,33	38,1
SITU PRODUCTION	m^3	0	10,59	20,76	31,36	41,95	53,39
WINCH POWER	kW	0	9,43	18,88	27,38	35,76	44,05
SPECIFIC ENGERGY	kJ/m^3	0	0,45	0,38	0,49	0,54	0,57
PENETRATION DEPTH	m	0	128,57	257,14	371,43	500	614,29
TOTAL STICKY EFFECT	kN	0	14,81	25,93	37,04	51,85	62,96
UPPERBLOCK SPEED	m/sec	0	1,76	3,87	5,63	7,39	9,15
LOWERBLOCK SPEED	m/sec	0	6,06	13,64	19,7	25,76	33,33
ANGULAR VELOCITY	deg/sec	0	0,4	0,82	1,23	1,62	920,02
ROPE FORCE	kN	0	8,74	18,45	27,18	34,95	43,69
ARM FORCE	kN	0	9,66	19,31	27,59	35,86	44,83
TOTAL MASS	tons	0	10,15	20,3	30,44	40,59	50,74
TOTAL VOLUME	m^3	0	0	0	0	0	0

10.3.1.5. TBS

Original value	m	s=0=6,80	s= -0,5	s= -0,25	s= 0,25	s=0,5	s=0,75	s=1,0
TIME	s	20,24	19,88	20,1	20,55	20,77	21	21,23
X-LIP	m	0	0	0	0	0	0	0
Y-LIP	m	-0,21	-0,23	-0,22	-0,2	-0,19	-0,18	-0,17
SITU PRODUCTION	m^3	2,36	2,15	2,25	2,44	2,53	2,6	2,68
WINCH POWER	kW	104,74	93,02	97,79	108,64	114,02	115,1	117,4
SPECIFIC ENGERGY	kJ/m^3	502,19	480,85	493,86	518,86	531,93	541,16	554,61
PENETRATION DEPTH	m	0,007	0,006	0,006	0,006	0,006	0,006	0,006
TOTAL STICKY EFFECT	kN	27	29	28	26	25	24	22
UPPERBLOCK SPEED	m/sec	0,284	0,304	0,293	0,275	0,269	0,264	0,26
LOWERBLOCK SPEED	m/sec	0,066	0,083	0,074	0,059	0,054	0,05	0,046
ANGULAR VELOCITY	deg/sec	7,792	7,889	7,823	7,717	7,678	7,648	7,629
ROPE FORCE	kN	103	92	96	107	112	113	116
ARM FORCE	kN	145	130	136	152	159	161	164
TOTAL MASS	tons	19,709	19,7	19,7	19,7	19,7	19,7	19,7
TOTAL VOLUME	m^3	22,433	16,495	19,423	25,492	28,62	31,819	35,097

percentages	m	s=0=6,80	s= -0,5	s= -0,25	s= 0,25	s=0,5	s=0,75	s=1,0
TIME	s	0	-1,78	-0,69	1,53	2,62	3,75	4,89
X-LIP	m							
Y-LIP	m	0	9,52	4,76	-4,76	-9,52	-14,29	-19,05
SITU PRODUCTION	m^3	0	-8,9	-4,66	3,39	7,2	10,17	13,56
WINCH POWER	kW	0	-11,19	-6,64	3,72	8,86	9,89	12,09
SPECIFIC ENGERGY	kJ/m^3	0	-4,25	-1,66	3,32	5,92	7,76	10,44
PENETRATION DEPTH	m	0	-14,29	-14,29	-14,29	-14,29	-14,29	-14,29
TOTAL STICKY EFFECT	kN	0	7,41	3,7	-3,7	-7,41	-11,11	-18,52
UPPERBLOCK SPEED	m/sec	0	7,04	3,17	-3,17	-5,28	-7,04	-8,45
LOWERBLOCK SPEED	m/sec	0	25,76	12,12	-10,61	-18,18	-24,24	-30,3
ANGULAR VELOCITY	deg/sec	0	1,24	0,4	-0,96	-1,46	-1,85	-2,09
ROPE FORCE	kN	0	-10,68	-6,8	3,88	8,74	9,71	12,62
ARM FORCE	kN	0	-10,34	-6,21	4,83	9,66	11,03	13,1
TOTAL MASS	tons	0	-0,05	-0,05	-0,05	-0,05	-0,05	-0,05

TOTAL VOLUME	m^3	0	-26,47	-13,42	13,64	27,58	41,84	56,45

10.3.1.6. BW

Original value	**m**	**w=2,82**	**w=2,4**	**w=2,6**	**w=2,8**	**w=3,0**	**w=3,2**
TIME	s	20,24	20,22	20,23	20,24	20,26	20,27
X-LIP	m	0	0	0	0	0	0
Y-LIP	m	-0,21	-0,24	-0,22	-0,21	-0,2	-0,19
SITU PRODUCTION	m^3	2,36	2,31	2,34	2,36	2,38	2,4
WINCH POWER	kW	104,74	104,54	104,59	105,23	104,94	105,02
SPECIFIC ENGERGY	kJ/m^3	502,19	510,27	506,14	503,68	501,65	499,09
PENETRATION DEPTH	m	0,007	0,02	0,014	0,008	0,002	0
TOTAL STICKY EFFECT	kN	27	32	30	27	26	24
UPPERBLOCK SPEED	m/sec	0,284	0,291	0,287	0,284	0,282	0,279
LOWERBLOCK SPEED	m/sec	0,066	0,071	0,068	0,066	0,064	0,062
ANGULAR VELOCITY	deg/sec	7,792	7,832	7,812	7,794	7,778	7,72
ROPE FORCE	kN	103	102	103	103	103	103
ARM FORCE	kN	145	145	145	146	146	146
TOTAL MASS	tons	19,709	19,709	19,709	19,709	19,709	19,709
TOTAL VOLUME	m^3	22,433	19,092	20,683	22,274	23,865	25,456

percentages	**m**	**w=2,82**	**w=2,4**	**w=2,6**	**w=2,8**	**w=3,0**	**w=3,2**
TIME	s	0	-0,1	-0,05	0	0,1	0,15
X-LIP	m						
Y-LIP	m	0	14,29	4,76	0	-4,76	-9,52
SITU PRODUCTION	m^3	0	-2,12	-0,85	0	0,85	1,69
WINCH POWER	kW	0	-0,19	-0,14	0,47	0,19	0,27
SPECIFIC ENGERGY	kJ/m^3	0	1,61	0,79	0,3	-0,11	-0,62
PENETRATION DEPTH	m	0	185,71	100	14,29	-71,43	-100
TOTAL STICKY EFFECT	kN	0	18,52	11,11	0	-3,7	-11,11
UPPERBLOCK SPEED	m/sec	0	2,46	1,06	0	-0,7	-1,76
LOWERBLOCK SPEED	m/sec	0	7,58	3,03	0	-3,03	-6,06
ANGULAR VELOCITY	deg/sec	0	0,51	0,26	0,03	-0,18	-0,92
ROPE FORCE	kN	0	-0,97	0	0	0	0
ARM FORCE	kN	0	0	0	0,69	0,69	0,69
TOTAL MASS	tons	0	0	0	0	0	0
TOTAL VOLUME	m^3	0	-14,89	-7,8	-0,71	6,38	13,48

10.3.2. GL484 Sensitivity analysis data

10.3.2.1. CA

Original value	degree	CA=3,98	CA =1	CA=3	CA=5	CA=7	CA=9
TIME	s	20,87	20,79	20,85	20,91	20,99	21,07
X-LIP	m	0	0	0	0	0	0
Y-LIP	m	-0,91	-0,99	-0,94	-0,87	-0,8	-0,71
SITU PRODUCTION	m^3	4,76	5,46	5	4,51	4,01	3,51
WINCH POWER	kW	231,92	236,85	233,54	224,6	214,71	200,83
SPECIFIC ENGERGY	kJ/m^3	322,28	299,17	314,01	331,84	353,6	380,5
PENETRATION DEPTH	m	0	0	0	0	0	0
TOTAL STICKY EFFECT	kN	183	205	191	174	154	133
UPPERBLOCK SPEED	m/sec	0,282	0,266	0,279	0,283	0,282	0,281
LOWERBLOCK SPEED	m/sec	0,119	0,105	0,117	0,12	0,119	0,118
ANGULAR VELOCITY	deg/sec	7,645	7,55	7,633	7,651	7,647	7,645
ROPE FORCE	kN	228	233	230	221	211	198
ARM FORCE	kN	431	440	434	418	399	374
TOTAL MASS	tons	25,612	25,612	25,612	25,612	25,612	25,612
TOTAL VOLUME	m^3	10,228	10,228	10,228	10,228	10,228	10,228

percentages	degree	CA=3,98	CA =1	CA=3	CA=5	CA=7	CA=9
TIME	s	0	-0,38	-0,1	0,19	0,57	0,96
X-LIP	m						
Y-LIP	m	0	8,79	3,3	-4,4	-12,09	-21,98
SITU PRODUCTION	m^3	0	14,71	5,04	-5,25	-15,76	-26,26
WINCH POWER	kW	0	2,13	0,7	-3,16	-7,42	-13,41
SPECIFIC ENGERGY	kJ/m^3	0	-7,17	-2,57	2,97	9,72	18,07
PENETRATION DEPTH	m	0	0	0	0	0	0
TOTAL STICKY EFFECT	kN	0	12,02	4,37	-4,92	-15,85	-27,32
UPPERBLOCK SPEED	m/sec	0	-5,67	-1,06	0,35	0	-0,35
LOWERBLOCK SPEED	m/sec	0	-11,76	-1,68	0,84	0	-0,84
ANGULAR VELOCITY	deg/sec	0	-1,24	-0,16	0,08	0,03	0
ROPE FORCE	kN	0	2,19	0,88	-3,07	-7,46	-13,16
ARM FORCE	kN	0	2,09	0,7	-3,02	-7,42	-13,23
TOTAL MASS	tons	0	0	0	0	0	0
TOTAL VOLUME	m^3	0	0	0	0	0	0

10.3.2.2. ACL

Original value	m	ACL=0,55	0.1 m	0.2 m	0.3 m	0.4 m	0.5 m
TIME	s	20,87	20,48	20,52	20,58	20,67	20,81
X-LIP	m	0	0	0	0	0	0
Y-LIP	m	-0,91	-1,37	-1,34	-1,27	-1,18	-1,03
SITU PRODUCTION	m^3	4,76	10,14	9,25	8,3	7,21	5,77
WINCH POWER	kW	231,92	196,74	215,98	238,32	250,11	248,98
SPECIFIC ENGERGY	kJ/m^3	322,28	194,95	211,99	231,62	255,55	290,57
PENETRATION DEPTH	m	0	0	0	0	0	0
TOTAL STICKY EFFECT	kN	183	303	294	278	252	216
UPPERBLOCK SPEED	m/sec	0,282	0,145	0,167	0,281	0,297	0,301
LOWERBLOCK SPEED	m/sec	0,119	-0,001	0,018	0,118	0,132	0,136
ANGULAR VELOCITY	deg/sec	7,645	6,829	6,96	7,635	7,727	7,756
ROPE FORCE	kN	228	194	213	235	246	245
ARM FORCE	kN	431	366	402	443	465	463
TOTAL MASS	tons	25,612	25,612	25,612	25,612	25,612	25,612
TOTAL VOLUME	m^3	10,228	10,228	10,228	10,228	10,228	10,228

percentages		ACL=0,55	0.1 m	0.2 m	0.3 m	0.4 m	0.5 m
TIME	s	0	-1,87	-1,68	-1,39	-0,96	-0,29
X-LIP	m						
Y-LIP	m	0	50,55	47,25	39,56	29,67	13,19
SITU PRODUCTION	m^3	0	113,03	94,33	74,37	51,47	21,22
WINCH POWER	kW	0	-15,17	-6,87	2,76	7,84	7,36
SPECIFIC ENGERGY	kJ/m^3	0	-39,51	-34,22	-28,13	-20,71	-9,84
PENETRATION DEPTH	m	0	0	0	0	0	0
TOTAL STICKY EFFECT	kN	0	65,57	60,66	51,91	37,7	18,03
UPPERBLOCK SPEED	m/sec	0	-48,58	-40,78	-0,35	5,32	6,74
LOWERBLOCK SPEED	m/sec	0	-100,84	-84,87	-0,84	10,92	14,29
ANGULAR VELOCITY	deg/sec	0	-10,67	-8,96	-0,13	1,07	1,45
ROPE FORCE	kN	0	-14,91	-6,58	3,07	7,89	7,46
ARM FORCE	kN	0	-15,08	-6,73	2,78	7,89	7,42
TOTAL MASS	tons	0	0	0	0	0	0
TOTAL VOLUME	m^3	0	0	0	0	0	0

10.3.2.3. COG

Original value	x	x=0,34	x=0	x=0,15	x=0,3	x=0,45	x=0,6
TIME	s	20,87	20,9	20,9	20,88	20,88	20,87
X-LIP	m	0	0	0	0	0	0
Y-LIP	m	-0,91	-0,88	-0,89	-0,9	-0,91	-0,91
SITU PRODUCTION	m^3	4,76	4,54	4,61	4,67	4,73	4,79
WINCH POWER	kW	231,92	231,19	229,64	231,73	227,25	229,64
SPECIFIC ENGERGY	kJ/m^3	322,28	339,72	333,16	326,67	320,6	314,6
PENETRATION DEPTH	m	0	0	0	0	0	0
TOTAL STICKY EFFECT	kN	183	174	177	179	182	184
UPPERBLOCK SPEED	m/sec	0,282	0,227	0,258	0,281	0,282	0,284
LOWERBLOCK SPEED	m/sec	0,119	0,115	0,116	0,118	0,119	0,121
ANGULAR VELOCITY	deg/sec	7,645	7,619	7,632	7,646	7,648	7,666
ROPE FORCE	kN	228	228	226	228	224	226
ARM FORCE	kN	431	430	427	431	423	427
TOTAL MASS	tons	25,612	25,612	25,612	25,612	25,612	25,612
TOTAL VOLUME	m^3	10,228	10,228	10,228	10,228	10,228	10,228

percentages	x	x=0,34	x=0	x=0,15	x=0,3	x=0,45	x=0,6
TIME	s	0	0,14	0,14	0,05	0,05	0
X-LIP	m						
Y-LIP	m	0	-3,3	-2,2	-1,1	0	0
SITU PRODUCTION	m^3	0	-4,62	-3,15	-1,89	-0,63	0,63
WINCH POWER	kW	0	-0,31	-0,98	-0,08	-2,01	-0,98
SPECIFIC ENGERGY	kJ/m^3	0	5,41	-2,04	-2,01	-1,88	-1,86
PENETRATION DEPTH	m	0	0	0	0	0	0
TOTAL STICKY EFFECT	kN	0	-4,92	-3,28	-2,19	-0,55	0,55
UPPERBLOCK SPEED	m/sec	0	-19,5	-8,51	-0,35	0	0,71
LOWERBLOCK SPEED	m/sec	0	-3,36	-2,52	-0,84	0	1,68
ANGULAR VELOCITY	deg/sec	0	-0,34	-0,17	0,01	0,04	0,27
ROPE FORCE	kN	0	0	-0,88	0	-1,75	-0,88
ARM FORCE	kN	0	-0,23	-0,93	0	-1,86	-0,93
TOTAL MASS	tons	0	0	0	0	0	0
TOTAL VOLUME	m^3	0	0	0	0	0	0

Original value	**y**	**Y=1,55**	**Y=1,2**	**Y=1,4**	**Y=1,6**	**Y=1,8**	**Y=2,0**
TIME	s	20,87	20,89	20,89	20,87	20,87	20,87
X-LIP	m	0	0	0	0	0	0
Y-LIP	m	-0,91	-0,88	-0,89	-0,91	-0,92	-0,93
SITU PRODUCTION	m^3	4,76	4,52	4,61	4,79	4,88	4,96
WINCH POWER	kW	231,92	224,88	229,75	231,15	233,58	233,72
SPECIFIC ENGERGY	kJ/m^3	322,28	339,19	330,96	320,44	313,23	306,39
PENETRATION DEPTH	m	0	0	0	0	0	0
TOTAL STICKY EFFECT	kN	183	175	178	183	186	189
UPPERBLOCK SPEED	m/sec	0,282	0,281	0,282	0,282	0,282	0,282
LOWERBLOCK SPEED	m/sec	0,119	0,118	0,118	0,119	0,119	0,119
ANGULAR VELOCITY	deg/sec	7,645	7,644	7,65	7,648	7,651	7,644
ROPE FORCE	kN	228	221	226	228	230	230
ARM FORCE	kN	431	418	427	430	434	435
TOTAL MASS	tons	25,612	25,612	25,612	25,612	25,612	25,612
TOTAL VOLUME	m^3	10,228	10,228	10,228	10,228	10,228	10,228

percentages	**y**	**Y=1,55**	**Y=1,2**	**Y=1,4**	**Y=1,6**	**Y=1,8**	**Y=2,0**
TIME	s	0	0,1	0,1	0	0	0
X-LIP	m						
Y-LIP	m	0	-3,3	-2,2	0	1,1	2,2
SITU PRODUCTION	m^3	0	-5,04	-3,15	0,63	2,52	4,2
WINCH POWER	kW	0	-3,04	-0,94	-0,33	0,72	0,78
SPECIFIC ENGERGY	kJ/m^3	0	5,25	2,69	-0,57	-2,81	-4,93
PENETRATION DEPTH	m	0	0	0	0	0	0
TOTAL STICKY EFFECT	kN	0	-4,37	-2,73	0	1,64	3,28
UPPERBLOCK SPEED	m/sec	0	-0,35	0	0	0	0
LOWERBLOCK SPEED	m/sec	0	-0,84	-0,84	0	0	0
ANGULAR VELOCITY	deg/sec	0	-0,01	0,07	0,04	0,08	-0,01
ROPE FORCE	kN	0	-3,07	-0,88	0	0,88	0,88
ARM FORCE	kN	0	-3,02	-0,93	-0,23	0,7	0,93
TOTAL MASS	tons	0	0	0	0	0	0
TOTAL VOLUME	m^3	0	0	0	0	0	0

Original value	x=0	Y=1,55	Y=1,2	Y=1,4	Y=1,6	Y=1,8	Y=2,0
TIME	s	20,87	20,9	20,9	20,9	20,89	20,88
X-LIP	m	0	0	0	0	0	0
Y-LIP	m	-0,91	-0,87	-0,88	-0,89	-0,9	-0,91
SITU PRODUCTION	m^3	4,76	4,45	4,55	4,65	4,74	4,83
WINCH POWER	kW	231,92	227,95	229,22	231,98	235,99	237,83
SPECIFIC ENGERGY	kJ/m^3	322,28	351,56	342,77	334,51	326,75	319,3
PENETRATION DEPTH	m	0	0	0	0	0	0
TOTAL STICKY EFFECT	kN	183	171	175	178	185	183
UPPERBLOCK SPEED	m/sec	0,282	0,278	0,278	0,278	0,278	0,278
LOWERBLOCK SPEED	m/sec	0,119	0,115	0,115	0,115	0,116	0,116
ANGULAR VELOCITY	deg/sec	7,645	7,624	7,62	7,619	7,63	7,627
ROPE FORCE	kN	228	224	226	228	232	234
ARM FORCE	kN	431	424	426	431	439	442
TOTAL MASS	tons	25,612	25,612	25,612	25,612	25,612	25,612
TOTAL VOLUME	m^3	10,228	10,228	10,228	10,228	10,228	10,228

percentages	x=0	Y=1,55	Y=1,2	Y=1,4	Y=1,6	Y=1,8	Y=2,0
TIME	s	0	0,14	0,14	0,14	0,1	0,05
X-LIP	m						
Y-LIP	m	0	-4,4	-3,3	-2,2	-1,1	0
SITU PRODUCTION	m^3	0	-6,51	-4,41	-2,31	-0,42	1,47
WINCH POWER	kW	0	-1,71	-1,16	0,03	1,75	2,55
SPECIFIC ENGERGY	kJ/m^3	0	9,09	6,36	3,79	1,39	-0,92
PENETRATION DEPTH	m	0	0	0	0	0	0
TOTAL STICKY EFFECT	kN	0	-6,56	-4,37	-2,73	1,09	0
UPPERBLOCK SPEED	m/sec	0	-1,42	-1,42	-1,42	-1,42	-1,42
LOWERBLOCK SPEED	m/sec	0	-3,36	-3,36	-3,36	-2,52	-2,52
ANGULAR VELOCITY	deg/sec	0	-0,27	-0,33	-0,34	-0,2	-0,24
ROPE FORCE	kN	0	-1,75	-0,88	0	1,75	2,63
ARM FORCE	kN	0	-1,62	-1,16	0	1,86	2,55
TOTAL MASS	tons	0	0	0	0	0	0
TOTAL VOLUME	m^3	0	0	0	0	0	0

Original value	**x=0,15**	**Y=1,55**	**Y=1,2**	**Y=1,4**	**Y=1,6**	**Y=1,8**	**Y=2,0**
TIME	s	20,87	20,89	20,89	20,89	20,88	20,88
X-LIP	m	0	0	0	0	0	0
Y-LIP	m	-0,91	-0,88	-0,89	-0,9	-0,91	-0,92
SITU PRODUCTION	m^3	4,76	4,52	4,62	4,71	4,8	4,89
WINCH POWER	kW	231,92	229,04	230,34	233,09	232,04	237,29
SPECIFIC ENGERGY	kJ/m^3	322,28	344,5	336,15	328,19	320,69	313,49
PENETRATION DEPTH	m	0	0	0	0	0	0
TOTAL STICKY EFFECT	kN	183	174	177	180	183	186
UPPERBLOCK SPEED	m/sec	0,282	0,28	0,28	0,28	0,28	0,28
LOWERBLOCK SPEED	m/sec	0,119	0,117	0,117	0,117	0,117	0,117
ANGULAR VELOCITY	deg/sec	7,645	7,636	7,633	7,636	7,632	7,636
ROPE FORCE	kN	228	225	227	229	228	234
ARM FORCE	kN	431	426	428	434	432	441
TOTAL MASS	tons	25,612	25,612	25,612	25,612	25,612	25,612
TOTAL VOLUME	m^3	10,228	10,228	10,228	10,228	10,228	10,228

percentages	**x=0,15**	**Y=1,55**	**Y=1,2**	**Y=1,4**	**Y=1,6**	**Y=1,8**	**Y=2,0**
TIME	s	0	0,1	0,1	0,1	0,05	0,05
X-LIP	m						
Y-LIP	m	0	-3,3	-2,2	-1,1	0	1,1
SITU PRODUCTION	m^3	0	-5,04	-2,94	-1,05	0,84	2,73
WINCH POWER	kW	0	-1,24	-0,68	0,5	0,05	2,32
SPECIFIC ENGERGY	kJ/m^3	0	6,89	4,3	1,83	-0,49	-2,73
PENETRATION DEPTH	m	0	0	0	0	0	0
TOTAL STICKY EFFECT	kN	0	-4,92	-3,28	-1,64	0	1,64
UPPERBLOCK SPEED	m/sec	0	-0,71	-0,71	-0,71	-0,71	-0,71
LOWERBLOCK SPEED	m/sec	0	-1,68	-1,68	-1,68	-1,68	-1,68
ANGULAR VELOCITY	deg/sec	0	-0,12	-0,16	-0,12	-0,17	-0,12
ROPE FORCE	kN	0	-1,32	-0,44	0,44	0	2,63
ARM FORCE	kN	0	-1,16	-0,7	0,7	0,23	2,32
TOTAL MASS	tons	0	0	0	0	0	0
TOTAL VOLUME	m^3	0	0	0	0	0	0

Original value	**x=0,3**	**Y=1,55**	**Y=1,2**	**Y=1,4**	**Y=1,6**	**Y=1,8**	**Y=2,0**
TIME	s	20,87	20,89	20,88	20,88	20,87	20,87
X-LIP	m	0	0	0	0	0	0
Y-LIP	m	-0,91	-0,89	-0,9	-0,91	-0,92	-0,93
SITU PRODUCTION	m^3	4,76	4,58	4,68	4,77	4,86	4,95
WINCH POWER	kW	231,92	229,17	228,8	231,74	231,76	237,14
SPECIFIC ENGERGY	kJ/m^3	322,28	337,73	329,67	322,07	314,81	307,89
PENETRATION DEPTH	m	0	0	0	0	0	0
TOTAL STICKY EFFECT	kN	183	177	180	183	185	188
UPPERBLOCK SPEED	m/sec	0,282	0,282	0,281	0,282	0,281	0,282
LOWERBLOCK SPEED	m/sec	0,119	0,118	0,118	0,118	0,118	0,119
ANGULAR VELOCITY	deg/sec	7,645	7,65	7,643	7,646	7,642	7,649
ROPE FORCE	kN	228	226	225	228	228	233
ARM FORCE	kN	431	426	426	431	431	441
TOTAL MASS	tons	25,612	25,61	25,61	25,61	25,61	25,61
TOTAL VOLUME	m^3	10,228	10,246	10,246	10,246	10,246	10,246

percentages	**x=0,3**	**Y=1,55**	**Y=1,2**	**Y=1,4**	**Y=1,6**	**Y=1,8**	**Y=2,0**
TIME	s	0	0,1	0,05	0,05	0	0
X-LIP	m						
Y-LIP	m	0	-2,2	-1,1	0	1,1	2,2
SITU PRODUCTION	m^3	0	-3,78	-1,68	0,21	2,1	3,99
WINCH POWER	kW	0	-1,19	-1,35	-0,08	-0,07	2,25
SPECIFIC ENGERGY	kJ/m^3	0	4,79	2,29	-0,07	-2,32	-4,47
PENETRATION DEPTH	m	0	0	0	0	0	0
TOTAL STICKY EFFECT	kN	0	-3,28	-1,64	0	1,09	2,73
UPPERBLOCK SPEED	m/sec	0	0	-0,35	0	-0,35	0
LOWERBLOCK SPEED	m/sec	0	-0,84	-0,84	-0,84	-0,84	0
ANGULAR VELOCITY	deg/sec	0	0,07	-0,03	0,01	-0,04	0,05
ROPE FORCE	kN	0	-0,88	-1,32	0	0	2,19
ARM FORCE	kN	0	-1,16	-1,16	0	0	2,32
TOTAL MASS	tons	0	-0,01	-0,01	-0,01	-0,01	-0,01
TOTAL VOLUME	m^3	0	0,18	0,18	0,18	0,18	0,18

Original value	**x=0,45**	**Y=1,55**	**Y=1,2**	**Y=1,4**	**Y=1,6**	**Y=1,8**	**Y=2,0**
TIME	s	20,87	20,88	20,87	20,87	20,86	20,86
X-LIP	m	0	0	0	0	0	0
Y-LIP	m	-0,91	-0,9	-0,91	-0,92	-0,93	-0,94
SITU PRODUCTION	m^3	4,76	4,65	4,74	4,83	4,92	5
WINCH POWER	kW	231,92	225,73	230,66	23059	230,16	235,09
SPECIFIC ENGERGY	kJ/m^3	322,28	331,21	323,42	316,06	309,11	302,4
PENETRATION DEPTH	m	0	0	0	0	0	0
TOTAL STICKY EFFECT	kN	183	180	182	185	188	190
UPPERBLOCK SPEED	m/sec	0,282	0,283	0,283	0,283	0,283	0,283
LOWERBLOCK SPEED	m/sec	0,119	0,12	0,12	0,12	0,12	0,12
ANGULAR VELOCITY	deg/sec	7,645	7,652	7,654	7,652	7,649	7,654
ROPE FORCE	kN	228	222	227	227	227	231
ARM FORCE	kN	431	420	429	429	428	437
TOTAL MASS	tons	25,612	25,612	25,612	25,612	25,612	25,612
TOTAL VOLUME	m^3	10,228	10,228	10,228	10,228	10,228	10,228

percentages	**x=0,45**	**Y=1,55**	**Y=1,2**	**Y=1,4**	**Y=1,6**	**Y=1,8**	**Y=2,0**
TIME	s	0	0,05	0	0	-0,05	-0,05
X-LIP	m						
Y-LIP	m	0	-1,1	0	1,1	2,2	3,3
SITU PRODUCTION	m^3	0	-2,31	-0,42	1,47	3,36	5,04
WINCH POWER	kW	0	-2,67	-0,54	9842,65	-0,76	1,37
SPECIFIC ENGERGY	kJ/m^3	0	2,77	0,35	-1,93	-4,09	-6,17
PENETRATION DEPTH	m	0	0	0	0	0	0
TOTAL STICKY EFFECT	kN	0	-1,64	-0,55	1,09	2,73	3,83
UPPERBLOCK SPEED	m/sec	0	0,35	0,35	0,35	0,35	0,35
LOWERBLOCK SPEED	m/sec	0	0,84	0,84	0,84	0,84	0,84
ANGULAR VELOCITY	deg/sec	0	0,09	0,12	0,09	0,05	0,12
ROPE FORCE	kN	0	-2,63	-0,44	-0,44	-0,44	1,32
ARM FORCE	kN	0	-2,55	-0,46	-0,46	-0,7	1,39
TOTAL MASS	tons	0	0	0	0	0	0
TOTAL VOLUME	m^3	0	0	0	0	0	0

Original value	x=0,6	Y=1,55	Y=1,2	Y=1,4	Y=1,6	Y=1,8	Y=2,0
TIME	s	20,87	20,87	20,86	20,86	20,86	20,85
X-LIP	m	0	0	0	0	0	0
Y-LIP	m	-0,91	-0,91	-0,92	-0,93	-0,94	-0,95
SITU PRODUCTION	m^3	4,76	4,71	4,8	4,88	4,97	5,06
WINCH POWER	kW	231,92	227,02	227,74	229,28	231,17	235,6
SPECIFIC ENGERGY	kJ/m^3	322,28	324,91	317,4	310,36	303,57	297,07
PENETRATION DEPTH	m	0	0	0	0	0	0
TOTAL STICKY EFFECT	kN	183	182	185	187	190	192
UPPERBLOCK SPEED	m/sec	0,282	0,285	0,284	0,285	0,285	0,285
LOWERBLOCK SPEED	m/sec	0,119	0,121	0,121	0,121	0,121	0,122
ANGULAR VELOCITY	deg/sec	7,645	7,66	7,662	7,662	7,665	7,669
ROPE FORCE	kN	228	223	224	226	228	232
ARM FORCE	kN	431	422	424	426	430	438
TOTAL MASS	tons	25,612	25,612	25,612	25,612	25,612	25,612
TOTAL VOLUME	m^3	10,228	10,228	10,228	10,228	10,228	10,228

percentages	x=0,6	Y=1,55	Y=1,2	Y=1,4	Y=1,6	Y=1,8	Y=2,0
TIME	s	0	0	-0,05	-0,05	-0,05	-0,1
X-LIP	m						
Y-LIP	m	0	0	1,1	2,2	3,3	4,4
SITU PRODUCTION	m^3	0	-1,05	0,84	2,52	4,41	6,3
WINCH POWER	kW	0	-2,11	-1,8	-1,14	-0,32	1,59
SPECIFIC ENGERGY	kJ/m^3	0	0,82	-1,51	-3,7	-5,81	-7,82
PENETRATION DEPTH	m	0	0	0	0	0	0
TOTAL STICKY EFFECT	kN	0	-0,55	1,09	2,19	3,83	4,92
UPPERBLOCK SPEED	m/sec	0	1,06	-57,09	1,06	1,06	1,06
LOWERBLOCK SPEED	m/sec	0	1,68	1,68	1,68	1,68	2,52
ANGULAR VELOCITY	deg/sec	0	0,2	0,22	0,22	0,26	0,31
ROPE FORCE	kN	0	-2,19	-1,75	-0,88	0	1,75
ARM FORCE	kN	0	-2,09	-1,62	-1,16	-0,23	1,62
TOTAL MASS	tons	0	0	0	0	0	0
TOTAL VOLUME	m^3	0	0	0	0	0	0

10.3.2.4. TBW

Original value	ton	8.54	2	4	6	8	10
TIME	s	20.87	20.78	20.72	20.67	20.62	20.58
X-LIP	m	0	0	0	0	0	0
Y-LIP	m	-0.91	-1.03	-1.11	-1.18	-1.24	-1.29
SITU PRODUCTION	m^3	4.76	5.78	6.54	7.15	7.68	8.14
WINCH POWER	kW	231.92	252.42	267.91	27628	288.43	294.1
SPECIFIC ENGERGY	kJ/m^3	322.28	301.84	291.19	284.24	279.01	274.79
PENETRATION DEPTH	m	0	0	0.004	0.011	0.018	0.025
TOTAL STICKY EFFECT	kN	183	214	237	254	269	282
UPPERBLOCK SPEED	m/sec	0.282	0.293	0.304	0.313	0.322	0.327
LOWERBLOCK SPEED	m/sec	0.119	0.129	0.138	0.146	0.154	0.158
ANGULAR VELOCITY	deg/sec	7.645	7.714	7.775	7.83	7.889	7.909
ROPE FORCE	kN	228	248	264	272	284	289
ARM FORCE	kN	431	469	498	514	536	541
TOTAL MASS	tons	25.612	27.612	29.612	31.612	33.612	35.612
TOTAL VOLUME	m^3	10.228	10.228	10.228	10.228	10.228	10.228

Percentages	ton	8.54	2	4	6	8	10
TIME	s	0	-0.43	-0.72	-0.96	-1.2	-1.39
X-LIP	m						
Y-LIP	m	0	13.19	21.98	29.67	36.26	41.76
SITU PRODUCTION	m^3	0	21.43	37.39	50.21	61.34	71.01
WINCH POWER	kW	0	8.84	15.52	11812.73	24.37	26.81
SPECIFIC ENGERGY	kJ/m^3	0	-6.34	-9.65	-11.8	-13.43	-14.74
PENETRATION DEPTH	m	0	0	0.4	1.1	1.8	2.5
TOTAL STICKY EFFECT	kN	0	16.94	29.51	38.8	46.99	54.1
UPPERBLOCK SPEED	m/sec	0	3.9	7.8	10.99	14.18	15.96
LOWERBLOCK SPEED	m/sec	0	8.4	15.97	22.69	29.41	32.77
ANGULAR VELOCITY	deg/sec	0	0.9	1.7	2.42	3.19	3.45
ROPE FORCE	kN	0	8.77	15.79	19.3	24.56	26.75
ARM FORCE	kN	0	8.82	15.55	19.26	24.36	25.52
TOTAL MASS	tons	0	7.81	15.62	23.43	31.24	39.04
TOTAL VOLUME	m^3	0	0	0	0	0	0

10.3.2.5. TBS

Original value	m=5.9m	s=0	s= -0,5	s= -0,25	s= 0,25	s=0,5	s=0,75	s=1,0
TIME	s	20.87	20.32	20.53	20.96	21.18	21.41	21.64
X-LIP	m	0	0	0	0	0	0	0
Y-LIP	m	-0.91	-1.02	-1.04	-1.03	-1.02	-1.01	-0.99
SITU PRODUCTION	m^3	4.76	4.15	4.63	5.49	5.85	6.19	6.48
WINCH POWER	kW	231.92	162.33	169.9	263.11	295.4	326.57	355.2
SPECIFIC ENGERGY	kJ/m^3	322.28	303.91	311.59	326.2	333.49	340.96	348.71
PENETRATION DEPTH	m	0	0.009	0.009	0.009	0.009	0.009	0.009
TOTAL STICKY EFFECT	kN	183	187	203	228	236	243	246
UPPERBLOCK SPEED	m/sec	0.282	0.292	0.284	0.262	0.249	0.235	0.22
LOWERBLOCK SPEED	m/sec	0.119	0.128	0.121	0.102	0.09	0.078	0.064
ANGULAR VELOCITY	deg/sec	7.645	7.706	7.659	7.531	7.455	7.371	7.28
ROPE FORCE	kN	228	160	194	259	291	321	350
ARM FORCE	kN	431	302	366	489	549	607	661
TOTAL MASS	tons	25.612	25.612	25.612	25.612	25.612	25.612	25.612
TOTAL VOLUME	m^3	10.228	5.599	6.952	9.743	11.197	12.699	14.254

Percentages	m=5.9m	s=0	s= -0,5	s= -0,25	s= 0,25	s=0,5	s=0,75	s=1,0
TIME	s	0	-2.64	-1.63	0.43	1.49	2.59	3.69
X-LIP	m							
Y-LIP	m	0	12.09	14.29	13.19	12.09	10.99	8.79
SITU PRODUCTION	m^3	0	-12.82	-2.73	15.34	22.9	30.04	36.13
WINCH POWER	kW	0	-30.01	-26.74	13.45	27.37	40.81	53.16
SPECIFIC ENGERGY	kJ/m^3	0	-5.7	-3.32	1.22	3.48	5.8	8.2
PENETRATION DEPTH	m	0	0.9	0.9	0.9	0.9	0.9	0.9
TOTAL STICKY EFFECT	kN	0	2.19	10.93	24.59	28.96	32.79	34.43
UPPERBLOCK SPEED	m/sec	0	3.55	0.71	-7.09	-11.7	-16.67	-21.99
LOWERBLOCK SPEED	m/sec	0	7.56	1.68	-14.29	-24.37	-34.45	-46.22
ANGULAR VELOCITY	deg/sec	0	0.8	0.18	-1.49	-2.49	-3.58	-4.77
ROPE FORCE	kN	0	-29.82	-14.91	13.6	27.63	40.79	53.51
ARM FORCE	kN	0	-29.93	-15.08	13.46	27.38	40.84	53.36
TOTAL MASS	tons	0	0	0	0	0	0	0

TOTAL VOLUME	m^3	0	-45.26	-32.03	-4.74	9.47	24.16	39.36

10.3.2.6. BW

Original value	**m**	**w=2,21**	**w=2.0**	**w=2.0**	**w=2.2**	**w=2.4**	**w=2.6**
TIME	s	20.87	20.74	20.79	20.87	21.01	21.19
X-LIP	m	0	0	0	0	0	0
Y-LIP	m	-0.91	-1.04	-0.99	-0.91	-0.77	-0.58
SITU PRODUCTION	m^3	4.76	5.07	5.07	4.79	4.06	3.31
WINCH POWER	kW	231.92	299.92	232.7	231.87	214.99	187.35
SPECIFIC ENGERGY	kJ/m^3	322.28	318.94	315.34	321.55	350.49	402.08
PENETRATION DEPTH	m	0	0.009	0	0	0	0
TOTAL STICKY EFFECT	kN	183	217	204	184	146	101
UPPERBLOCK SPEED	m/sec	0.282	0.274	0.279	0.282	0.279	0.264
LOWERBLOCK SPEED	m/sec	0.119	0.112	0.116	0.119	0.116	0.103
ANGULAR VELOCITY	deg/sec	7.645	7.6	7.627	7.65	7.633	7.541
ROPE FORCE	kN	228	226	229	228	212	184
ARM FORCE	kN	431	428	433	431	400	348
TOTAL MASS	tons	25.612	25.612	25.612	25.612	25.612	25.612
TOTAL VOLUME	m^3	10.228	8.331	9.256	10.182	11.108	12.033

Percentages	**m**	**w=2,21**	**w=2.0**	**w=2.2**	**w=2.4**	**w=2.6**	**w=2.8**
TIME	s	0	-0.62	-0.38	0	0.67	1.53
X-LIP	m						
Y-LIP	m	0	14.29	8.79	0	-15.38	-36.26
SITU PRODUCTION	m^3	0	6.51	6.51	0.63	-14.71	-30.46
WINCH POWER	kW	0	29.32	0.34	-0.02	-7.3	-19.22
SPECIFIC ENGERGY	kJ/m^3	0	-1.04	-2.15	-0.23	8.75	24.76
PENETRATION DEPTH	m	0	0.9	0	0	0	0
TOTAL STICKY EFFECT	kN	0	18.58	11.48	0.55	-20.22	-44.81
UPPERBLOCK SPEED	m/sec	0	-2.84	-1.06	0	-1.06	-6.38
LOWERBLOCK SPEED	m/sec	0	-5.88	-2.52	0	-2.52	-13.45
ANGULAR VELOCITY	deg/sec	0	-0.59	-0.24	0.07	-0.16	-1.36
ROPE FORCE	kN	0	-0.88	0.44	0	-7.02	-19.3
ARM FORCE	kN	0	-0.7	0.46	0	-7.19	-19.26
TOTAL MASS	tons	0	0	0	0	0	0
TOTAL VOLUME	m^3	0	-18.55	-9.5	-0.45	8.6	17.65

10.4. Appendix D

10.4.1. Available drawing GL485

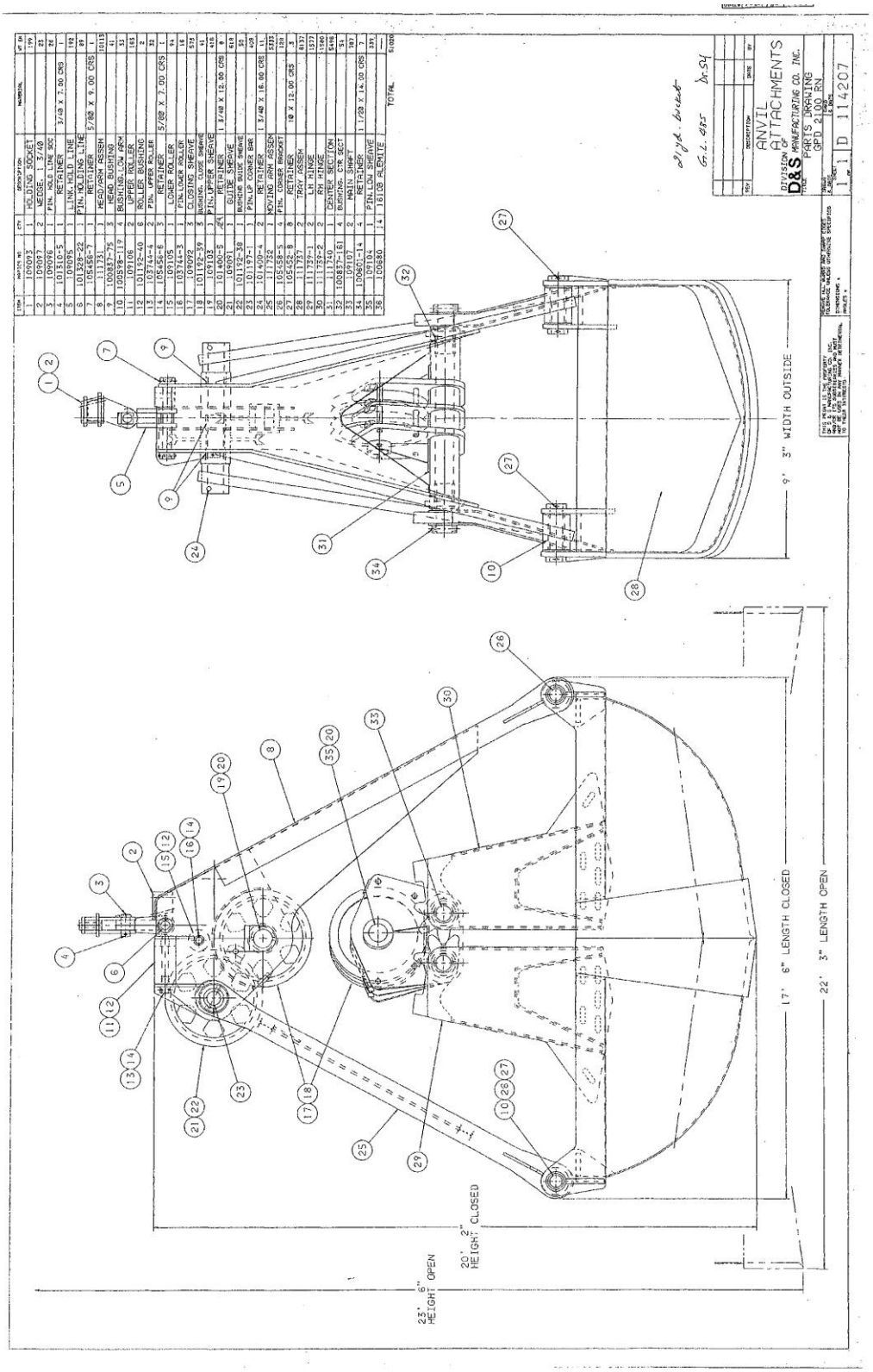

10.4.2. Drawing GL484

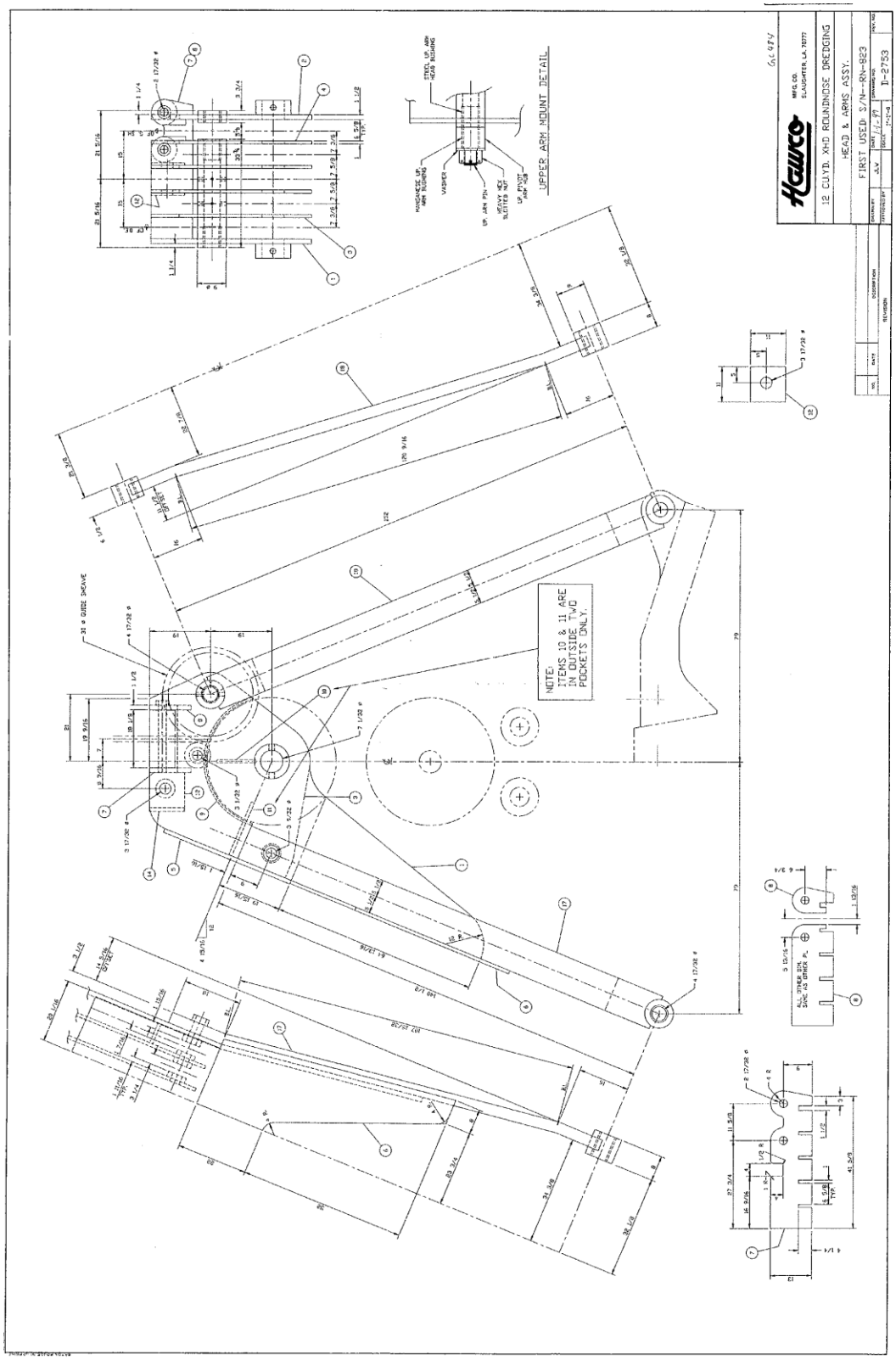

10.5. Appendix E

The clamshell is a dredge tool that is used for deepening waterways and harbours as well as environmental clean-up. The advantages of a clamshell compared to other dredging tools are:

- Working in limited space on site
- Can work on environmental spills
- Environmental regulation, no hydraulic fluid driven systems
- Can work on harder soils with boulders
- Can work in shallow water
- Shallow floating
- Blasted rock excavation
- Long disposal distance and cost efficiency with scows
- Relativly low power/operational costs

The clamshell is mounted on a barge with three spuds. Spuds are used to keep the barge with clamshell in place. The rear spud can tilt to allow the clamshell barge move forward or backwards. Another option is working with wires to keep position. This is only done if the spud length is insufficient to reach the bottom. The advantage of this feature is that certain clamshell can work up to 46 meter (150 ft.). On the other hand, the clamshell is less accurate during lowering and placing the bucket on the designated area.

The clamshell consists of a crane and a clam bucket. The bucket and the clamshell are connected via two steel wires. One wire is for hoisting and lowering the bucket and the other is for closing the bucket. Figure 10.1 and Figure 10.2shows a global sketch of the clamshell dredge and bucket. For production a secondary barge must be present to store the excavated soils. The secondary barge will transport the soils to the designated area or dock.

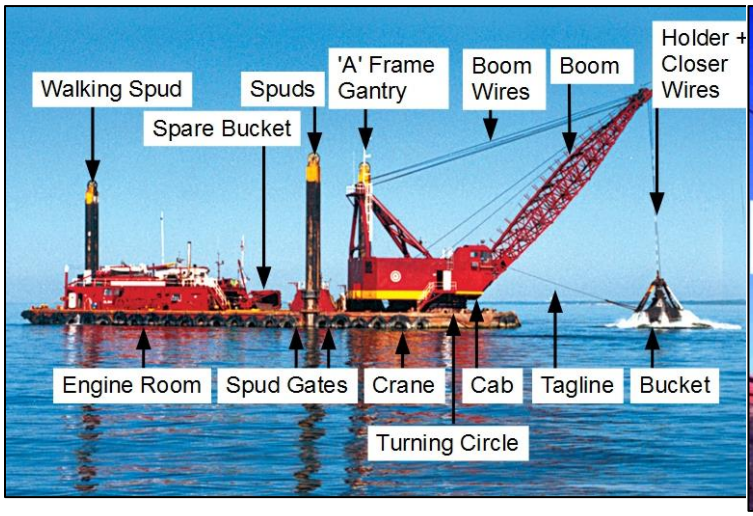

Figure 10.1 - Clamshell dredge

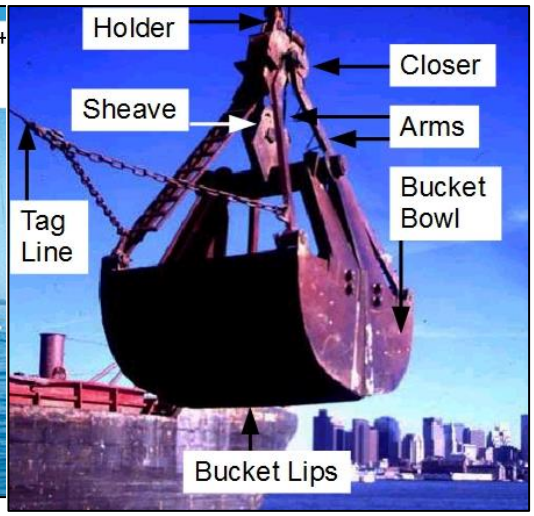

Figure 10.2 - Clamshell Bucket

10.5.1. GLDD Clamshell Dredgers

Great Lakes Dredge & Dock Company has four Clamshell dredgers at this moment: the 51, 53, 54, and 55. Each clamshell differs in size and hoisting capacity. Table 10.1 is an overview of the GLDD-owned clamshell dredgers.

Table 10.1 - GLDD clamshell dredge overview

Clamshell Dredger	HULL				Digging Depth		Hoisting Capacity [ton]
	Length [m]	Width [m]	Depth [m]	Draft [m]	Spud [m]	Wire [m]	
51	46.7	13.4	2.7	2.1	17.7	36.6	36.3
53	50.3	18.3	3.1	1.8	18.3	-	45.9
54	56.4	18.3	3.4	1.9	22.6	45.7	59.0
55	50.3	15.2	3.2	2.2	19.8	45.7	47.6

10.5.2. Clamshell Buckets

There are different dredging buckets, each with its own advantages for a certain job or soil.

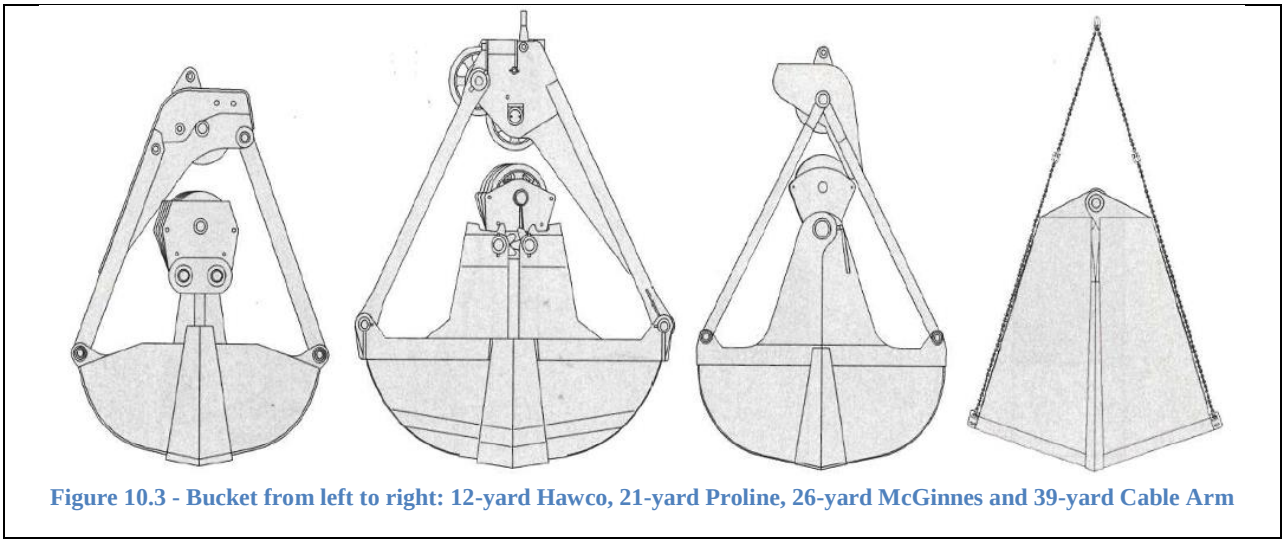

Figure 10.3 - Bucket from left to right: 12-yard Hawco, 21-yard Proline, 26-yard McGinnes and 39-yard Cable Arm

Each bucket has its own purpose the smaller heavier buckets are mainly used for stiffer and harder materials. The bigger Cable Arm buckets are for soft and silt materials. The strength of the soil determines which bucket is suitable for the job. GLDD owns different buckets from different suppliers. Table 10.2 gives an overview of the most commonly used buckets by the clamshell dredgers of GLDD.

Table 10.2 - GLDD bucket overview most used clamshell buckets

Clamshell dredge	Bucket ID	Capacity		Weight		Producer
		US $[CY]$	INT. $[m^3]$	US $[lbs]$	INT. $[tons]$	
51	GL#518	20	15.29	33,000	14.87	Cable Arm
	GL#492	18	13.76	32,000	14.15	Hawco
	GL#459	18	13.76	28,900	13.11	McGinnes
	GL#491	14	10.70	31,000	14.06	Hawco
	GL#421	9	6.88	32,000	14.51	Esco
53	GL#511	26	19.88	35,000	15.88	Cable Arm
	GL#493	26	19.88	38,000	17.24	Hawco
	GL#471	26	19.88	34,700	15.74	McGinnes
	GL#508	18	13.76	47,500	21.55	Anvil
	GL#487	10	7.65	53,000	24.04	Pro Line/Anvil

54	GL#515	50	38.23	37,500	17.01	Cable Arm
	GL#494	26	19.88	33,000	14.97	Atlas
	GL#509	21	16.06	55,000	24.95	Anvil
	GL#485	21	16.06	55,000	24.95	Anvil-Owen
	GL#485	***21***	***16.06***	***49,000***	***22.23***	***Intergy***
	GL#484	***12***	***9.17***	***65,000***	***29.48***	***Hawco***
55	GL#516	30	22.94	39,650	17.98	Cable Arm
	GL#498	40	30.58	34,900	15.83	Cable Arm
	GL#468	26	19.88	37,200	16.87	McGinnes
	GL#519	18	13.76	46,000	20.87	Anvil
	GL#510	18	13.76	45,000	20.41	Steel Processors
	GL#480	12	9.17	65,000	29.48	Hawco

10.6. Appendix F

10.6.1. WEDA summit & expo 2015 paper

THE INFLUENCE OF ADHESION ON CUTTING PROCESSES IN DREDGING

T. A. A. Combe[3] and S. A. Miedema[4]

ABSTRACT

In the US the clamshell dredge is a widely used dredging tool. The clamshell dredge is often used for excavation of clay, both soft and hard. The production of stiffer clays needs to be increased and there is room for improvement. During the cutting of clay the cohesion and adhesion or internal and external friction angle are the dominant factors. With the created interest on the adhesive and cohesive clay, behavior during cutting study is conducted. This paper's hypothesis is that with increasing clay strength (cohesion) the adhesion decreases to zero. To be able to measure the adhesive property of clay, a test set-up was designed and constructed. The adhesive test set-up was designed, constructed and used in the Haynes Coastal Engineering Laboratory at the Texas A&M University in College Station, Texas and financially supported by Great Lakes Dredge & Dock. The adhesion validation was done with natural field clays from Delaware River in Philadelphia and from Freeport, Texas (Grey and Red clay). The testing clays acquired from the field had some additional testing done with UU-Traxial and Atterberg limits to determine its properties. The final test was the x-ray diffraction to determine the mineralogy. The adhesive tests were carried out at a dedicated experimental facility. The results of the adhesive experiments show a decrease of adhesion and increasing internal friction angle with increasing cohesive strength from the Freeport grey clay (17 kPa) to Freeport red clay (89 kPa). This may have great implications for production estimations of clamshells and other equipment.

Keywords: dredging, clamshell bucket, cutting processes, clay, clay cutting, clay properties, adhesion, internal friction angle

INTRODUCTION

The dredging industry has different tools to do the job. For the shallow drift, shallow water, confined space or the very deep dredging the clamshell (grab) dredge is the best option. In the United States of America the leading dredging company Great Lakes Dredge & Dock (GLDD) owns four clamshell dredges. The clamshell has been a widely used tool for loading and offloading ships in the docks. The clamshell's main purpose was to scope and move dry material on and off ships in the docks. The bucket design has hardly changed over the past decades; moreover, the bucket design was not developed for other excavated material like clay. The clamshell dredge has two main closing mechanisms, a cable or hydraulic closing system (Figure 4). The cable or mechanical grab is operated by manipulation of the closing and hoisting wires, making it the most dependable type. The digging process consists of releasing the holding wire and rolling up the closing wire. As the grab needs its own weight to penetrate the soil, closing the grab by means of a closing wire could be seen as a disadvantage: the forces in the closing rope tend to lift up the grab, thus decreasing the cutting forces and therefore the production.

[3] Student, Great Lakes Dredge & Dock, 2122 York Road, Oakbrook, Illinois 60523, USA, T: 630-574-3000, Email: t.a.a.combe@gmail.com

[4] Scientist, Delft University of Technology, Faculty 3mE, The Netherlands, T: +31-15-2788359, Email: s.a.miedema@3me.tudelft.nl

Figure 4. Hydraulic (left) and cable (right) clamshell bucket (grab) (Mack Manufacturing)

During the closing phase of the grab, the clay cutting processes commence until the grab is closed. The forces created by the cutting process have influence on the bucket design and maybe on any modification. The cutting theory for sand and clay was developed in 1987 by Miedema. The clay cutting process is a simplification of the sand cutting equation. The sand cutting theory contains the pore pressure and friction that contribute for calculating the vertical and horizontal forces. In addition to the pore pressure and gravity, the gravity and inertia also have influence on the total horizontal and vertical forces. The clay cutting theory is simplified with the $\varphi = 0$ concept or the internal friction (φ) is zero. In clay there is no internal friction and internal friction angle. With this concept, the dominant factors in clay cutting are the cohesion or internal shear strength and adhesion or external shear strength. The relationship between cohesion and adhesion is that the adhesion is expressed by a percentage of the cohesion. This varies between from 100 % for soft clays to 60 % for hard clays, but these percentages are not completely known. The current prediction is that for stiffer clays the adhesion is almost zero for stiff clays and beyond. The relationship between cohesion and adhesion will be investigated to see if the assumption is correct. To emphasize the influence of adhesion in the production, simulations were done with clamshell closing software by varying the adhesive and tensile strength properties of stiff clay. In Figure 5 the production over the adhesive property is displayed presenting the magnificent influence of the adhesive strength. The proper adhesive strength input is of essence in production of clay. This may have great implications for production estimations of clamshells and other equipment.

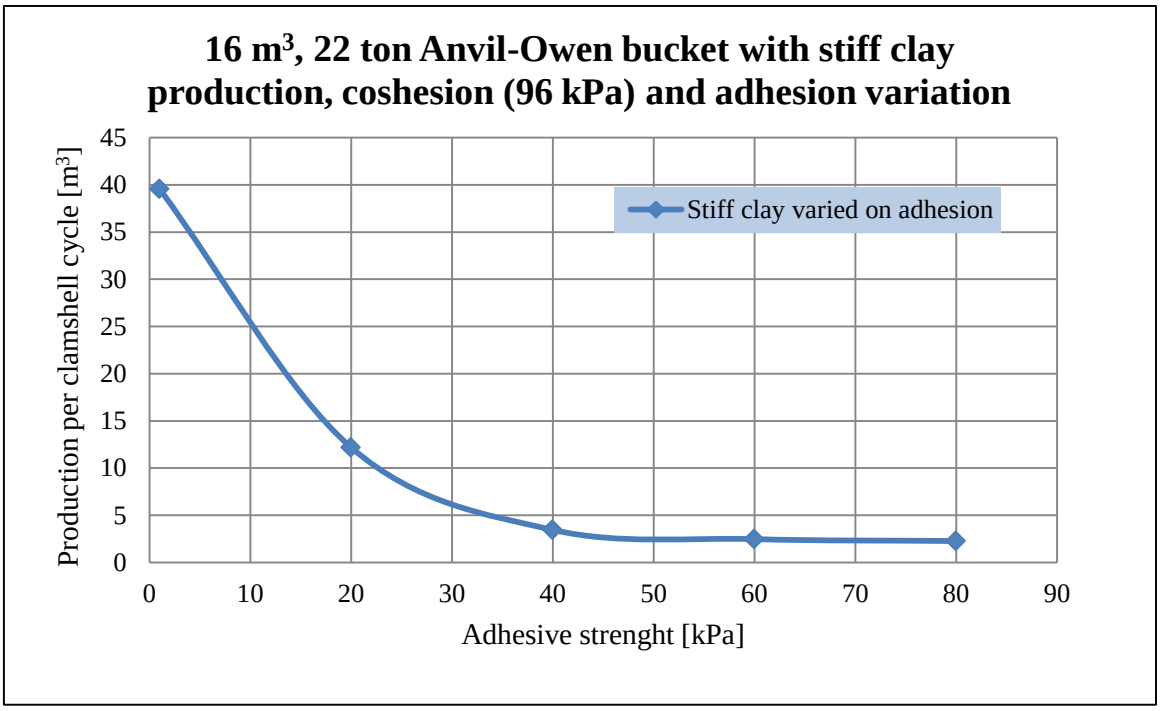

Figure 5. Production sensitivity analysis by varying adhesive strength of stiff clay

ADHESIVE NATURAL FIELD CLAY EXPERIMENTS

The relation of the adhesive strength with clay for increasing cohesive strength needs to be able to predict productions. To overcome this hurdle a test set-up was designed, constructed and used to measure adhesive strength of natural field clays. The adhesive test set-up (ATS) had as main goal to measure the adhesion of clay and to prove that with increasing clay strength or cohesion, adhesion decreases to zero. A couple of criteria arose during the brainstorming phase of different test set-up designs. An adhesive test set-up should be

- able to measure the adhesion of the clay.
- able to reproduce each test, because a test must be repeated to see if the measurement is in proper range and therefore valid for these circumstances.
- able to eliminate traces of other materials, like sand that will influence the measurement because of its internal and external friction angle. The resistance created by the friction angles will give a higher value than present in the clay.
- able to generate sufficient force to move s steel surface over s clay surface.

Adhesive test set-up design

The ATS design evolved on the drawing board, taking the test set-up criteria into account. The test set-up had different concepts with as starting point pushing a thin wall steel cylinder into the clay, see Figure 6 concept 1. The diameter of this cylinder would be increased to have a repeatable test on the same clay sample. The adhesion measured would be the force needed divided by the cylinder surface in contact with the clay. This was not the best option, because this was more cutting the clay than measuring the “stickiness” or adhesion of the clay.

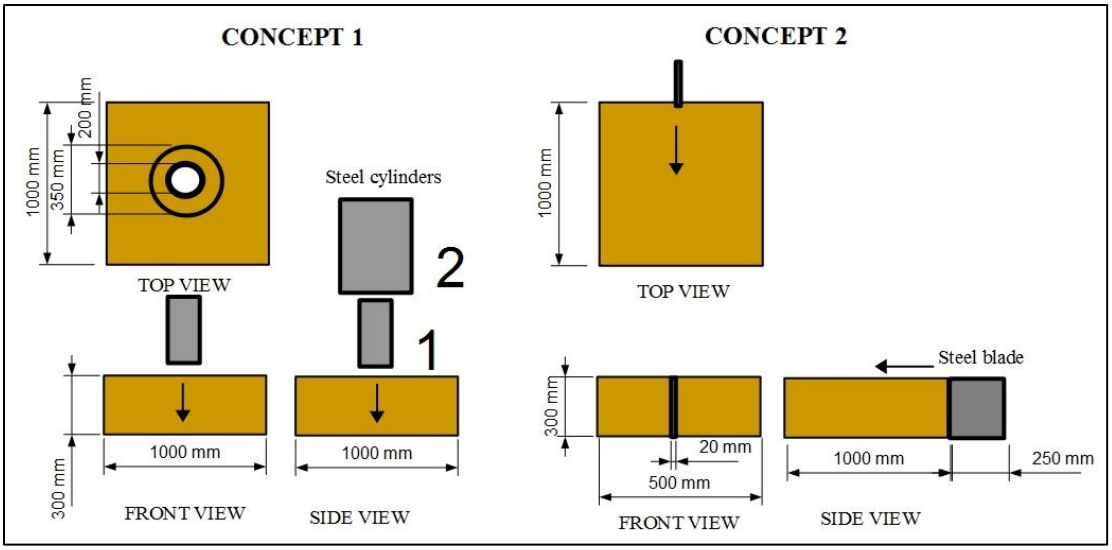

Figure 6. First and second concepts of the adhesive test set-up

Concept 2 had the same problem, but seemed more applicable considering the cutting theory. Pushing a steel blade through or along clay may result in additional forces by pushing or cutting the clay in front of the steel surface. By making sketches and discussing its feasibility and usability the final design of the ATS resulted in Figure 7. This was a top and bottom plate filled with clay, through which a steel blade would be pulled.

Figure 7. Final design of the adhesive test set-up

With the design on paper, a local contractor near College Station, Texas helped out on constructing the ATS. The steel plate base on which to place the electric actuator, top and bottom plate holders and handles was the contractor's idea to increase usability and ease.

Layout adhesive test set-up

The adhesive test set-up's final design was used to record the force needed to pull a steel blade between two layers of clay. The adhesive testing of the natural field clays were cut into a proper size and slightly remolded to fit in the top and bottom plate. The set-up consists of the following:

- Top plate to hold clay
- Bottom plate to hold clay
- Steel Blade to pull through the top and bottom plate
- Electrical actuator (3500 N) for pulling the blade
- Speed controller with direction switch
- Load cell (1 kN) to record the force needed
- Support wheel to make sure the blade and actuator stayed horizontally inline during the test

- Ruler with indicator (+2 magnets to keep rule in place) to measure the speed by distance travelled and recorded time needed
- Steel base to keep all parts in place and easy moving around
- Video cameras to record the test and use to determine blade speed during test

The white screen surrounding half of the test set-up was to create a clear background for the video recordings, see Figure 8.Two cameras were used to record the each measurement of the natural field clays. One camera was focused on the ruler and indicator with a small part on the top and bottom plate. The other camera was focused on the entire test set-up to make sure each test could be reviewed if there were strange fluctuations in the recordings. For the general layout of the test set-up with measurement equipment and recording software, see Figure 9.

Figure 8. Adhesion test set-up during experiments

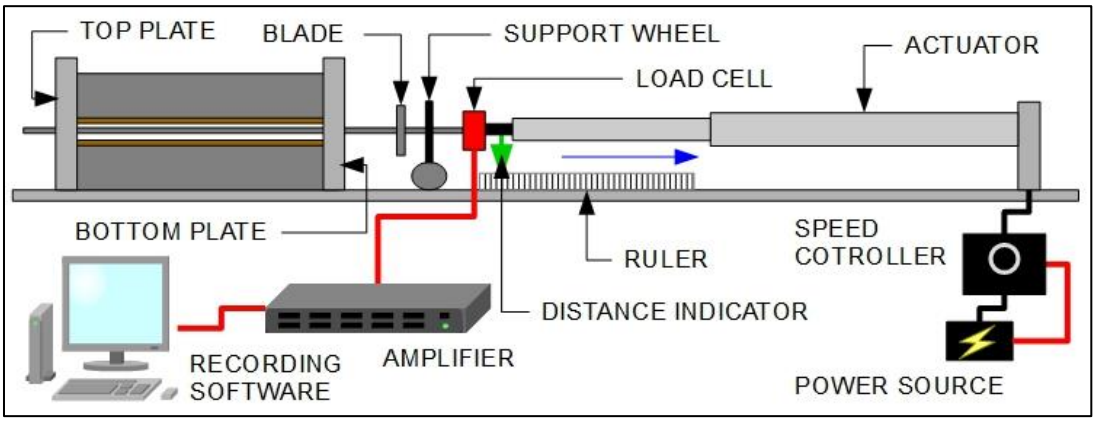

Figure 9. Adhesion test set-up layout

Actuator speed controller

After the final design was constructed, an additional interest arose: could the adhesive strength have influence on the clay cutting speed? The electric actuator can push and pull the blade at a predetermined speed. By adding a speed controller to the test set-up the speed of the blade pulling could be varied between 8.0 mm/s down to 0.4 mm/s. This was done to measure the effect of speed on the clay's resistance force. If a blade is pulled with a high speed, it is possible that some kind of vacuum effect occurs, creating an additional resistance force when pulling the blade. For the layout and connection between actuator and speed controller, see Figure 10.

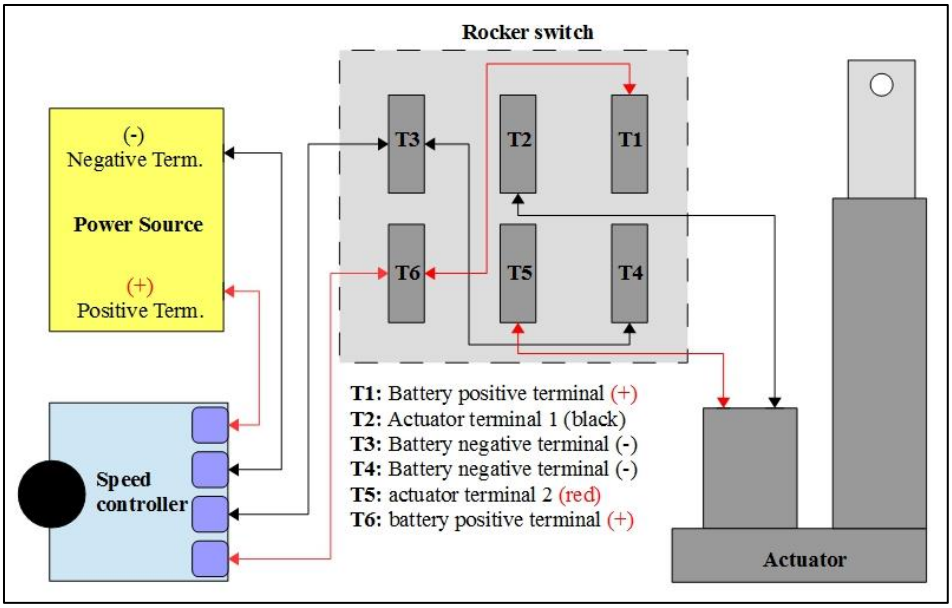

Figure 10. Speed controller connection layout

Blade pulling force recoding system

The recording system was needed to record the pulling force needed to pull the steel blade out from between the two layers clay. The recording system consisted of the load cell, an amplifier and a computer with software. The load cell was able to measure up to 1000 Newton of force. The assumption was the pulling force would not exceed 800 Newton and therefore taking 1 kN load cell was deemed sufficient to have a safety factor included. The amplifier was to increase the signal strength of the load cell to ensure the computer with software would be able to read the signal.

Load cell calibration

The load cell was calibrated to make sure the force recorded was correct. This is done by increasing the load on the load cell and recording the voltage output. This created a linear line between force and voltage and was needed to ensure the software was able to record the proper pulling force. A wooden pallet was hooked onto the load cell that was connected to the forklift providing an area to stack weights. Each weight was approximately 2.3-2.7 kg increasing the weight to 25 kg in total. For each weight added on to the pallet a voltage output was recorded until approximately 25 kg was on the pallet. With the known weights and voltage outputs a calibration file was created to make sure the load cell output could be correctly read by the software.

Recording software Helios

The recording software, Helios, was developed by Sonne at the University Texas A&M in 2012 and was available for usage for all the adhesive testing. The software provided the option to set the recording length in seconds, the frequency or recordings per second in Hertz. Before starting a recording, the initiation must be done and gauges must be zeroed out. After initiation the acquisition had to be prepared with selecting sampling rate [Hz], sampling time [seconds], calibration file and raw and calibrated data output files, see Figure 11.

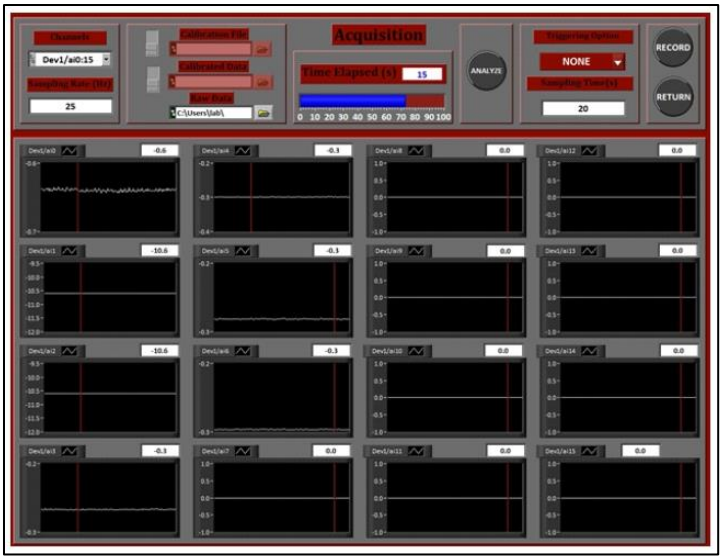

Figure 11. Recording software Helios

Adhesive strength calculation from test set-up

The design of the adhesion test set-up made it possible to determine the adhesive strength of clay. The pulling force recorded by the load cell divided by the blade surface in contact with the clay gave the adhesive stress in [N/mm^2], see Figure 12. The adhesive stress can be translated into an adhesive strength by multiplying the value with 1000. The forces on the blade during a measurement are the normal force, pulling force and adhesive force. The shear force (F_{shear}) only occurs if there is an external friction angle and therefore an internal friction angle. The normal force (F_{normal}) is from the weight of the top plate, clay and blade. The normal force was increased with one and two weights during different tests to determine the adhesive stress and possible internal friction in the clay. The pulling force (F_{pull}) was recorded by the load cell connected to recording software. In the opposite direction of the pulling force is the measured adhesive force ($F_{adhesion}$) with a possible internal friction force (F_{shear}), see Figure 12.

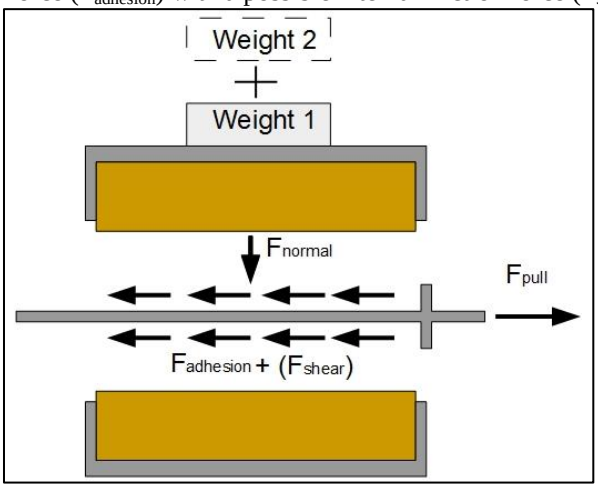

Figure 12. Cross section of adhesive test set-up with forces

Adhesive testing procedure

The tests that have been carried out by recording the adhesive strength of the natural field clays were done following a specific procedure. This procedure was followed for all of the 54 tests done on the clays. The following steps were taken to conduct each measurement:

13. Weigh filled top plate, bottom plate and blade
14. Place bottom plate in set-up and connect blade to line-up
15. Connect blade to load cell and back up blade to starting position
16. Place top plate and if needed place additional weights

17. Set up software with calibration file and zero out load cell
18. Select file to record to and frequency
19. Turn on cameras and start recording
20. Flip switch to start pulling blade
21. Turn off cameras after blade is fully retracted
22. Remove top plate and possible weights
23. Unbolt blade and clean blade
24. End of one test

Tested natural field clays

The natural field clays were acquired from different project locations of GLDD throughout the US. A soft, but silt Delaware river clay was acquired from a job site in Philadelphia, Pennsylvania. The clay sample shipping was done by wrapping the samples in several layers of cellophane and aluminum foil. Shipping was done in a box with wall protection filled up with bubble wrap. This was a safe way of keeping the water content and clay properties intact as much as possible. The firm grey and stiff red clay from Freeport, Texas was collected by me personally at the job site. The hopper crew had loaded big chunks of clay in a bucket after wrapping it in cellophane and aluminum foil. The Freeport clay samples were loaded in the back of the truck and driven back to the Texas A&M lab in College Station, Texas. There were three natural field clays available for testing:

- Delaware river clay, 1840 kg/m^3
  - Retrieved from Philadelphia, Pennsylvania a depth of 40 feet from a clamshell bucket after being placed on the bow of the scow.
- Freeport grey clay, 1950 kg/m^3
  - Retrieved from Freeport, Texas at a depth of 44 feet of a hopper drag head when idle on deck
- Freeport red clay, 2160 kg/m^3
  - Retrieved from Freeport, Texas at a depth of 44 feet of a hopper drag head when idle on deck

Adhesive test set-up boundary conditions

The ATV has limitations in testing the adhesive strength of the clay and possible testing method. During the clay sample preparation, the sample has to be cut to the proper size of for the top and bottom plate and the blade has to be in contact with the clay surface during the test. Two problems arise from these procedures. Firstly, the clay surface in contact with the blade is cut and may have a different effect on the blade compared to its original state. Secondly, the blade contact with the clay surface may vary if the blade and plates are not properly stacked or are moved if the blade pulling is not horizontal enough creating an additional force ($F_{additional}$) during blade pulling, see Figure 13.

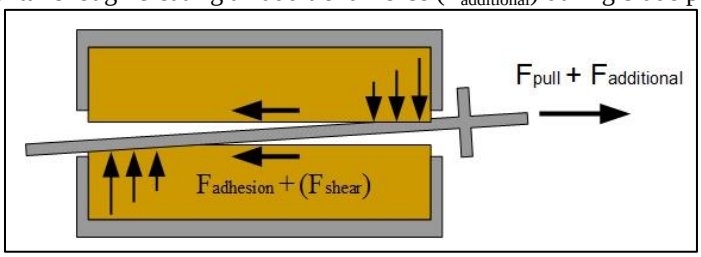

Figure 13. Additional pulling force if blade is not horizontal

After a test is done the clay sample may have moved more in the corners of the top and bottom plate and may remold the sample and its properties. This effect could also occur when adding weights on top of the top plate. After each test the contact surface needs to be flattened and prepared for the next test to keep the full contact with the blade during a test. The remolding may have an influence on the adhesive properties of the clay sample.

The contact area between the blade and the clay was not always the full surface of the blade. This means that the stress measured could be higher by reducing the blade surface used in the calculations. The possibility for water particles to escape over time before, during and after the measurements was minimized as much as possible. But it is inevitable that with increasing vertical forces the clay had a history that influences the clay strength and contact area with the blade.

Additional testing on natural field clays

The natural field clays were also tested to create a good profile of the tested clay samples. The additional information on clay properties created a clear and full spectrum study on the adhesive testing of the natural field clay samples. Moreover, if the measurements had an unexpected result, it would have been possible to find a reason for

the effect with one of the additional clay property tests on the clay sample. The additional clay property tests that were conducted are:

- Atterberg Limits, measuring the Plastic and Liquid limits (PL, LL)
- UU-traxial test, measuring the undrained shear strength (S_u)
- Mineralogy with x-ray diffraction (external company), recording the kaolinite, illite, etc. present in the clay sample

RESULTS OF ADHESIVE EXPERIMENTS AND ADDITIONAL TESTS

All the tests and experiments explained in the above part are completed and will be presented in this part. It contains the acquired data and explanation of the determination of adhesive strength with different approaches, because traces of other materials can interfere with the $\varphi = 0$ concept. The additional testing, Atterberg limits, UU-traxial test and Mineralogy were done simultaneously with the adhesive experiments of the natural field clays.

Additional testing results

The three natural field clays that were tested are very different clays, because of the variation of Atterberg limits, UU-traxial tests and mineralogy report.

Natural field clays Atterberg limit results

During the Atterberg limits tests, the Delaware river clay had a lower tolerance absorbing water particle. Both the Freeport Grey and Red clay had a similar liquid limit (LL) and an almost equal plastic limit (PL). This was something that was not expected, because the clay samples were retrieved from the same region. However, this does not imply that the properties have to be similar. With the residue of the tests a block of 5x5x5 cm was cut from the three natural field clays to measure its weight. By using the volume and weight, the specific gravity was calculated. All the three clays have a very high specific gravity, considering the fact that clays are normally between 1500-1800 kg/m^3.

Table 1. Atterberg limits natural field clays

Clay	Liquid Limit [%]	Plastic Limit [%]	Specific gravity [kg/m^3]
Delaware, Philadelphia	30.5	19.1	1837
Freeport Grey, Texas	61.5	23.6	1952
Freeport Red, Texas	60.5	18.2	2160

Natural field clays undrained shear strength

The natural field clays were tested under three different circumstances (5, 100 and 170 %/hour), because during the blade pulling the "vacuum" of the clay may also result from increasing strength by increasing the load ram speed of the UU-traxial test. For all values of the field clays of the three different UU-traxial speeds and the additional Torvane test, see Table 2. The Delaware river clay from Philadelphia, Pennsylvania has a strength of 12 kPa and is therefore a very soft clay. The Delaware sample's undrained shear strength decreases with increasing speed of the load ram, which is normal because the clay "resistance" is very low with very soft clay and therefore it will easily deform.

Table 2. Undrained shear strength of natural field clays

Clay	Standard UU-Traxial (5%/hour) [kPa]	Fast UU-Traxial (100%/hour) [kPa]	Very Fast UU-Traxial (170%/hour) [kPa]
Delaware, Philadelphia	12	11	10
Freeport Grey, Texas	22	17	14
Freeport Red, Texas	90	83	89

Natural field clay mineralogy's

The mineralogy tests were done with x-ray diffraction that identifies different types of atomic and molecular structures by recording the deflection. Each atomic and molecular structure has its own deflection angle and in this way the clay mineralogy was determined. The results of the x-ray diffraction testing on the clay specimens are summarized in this paragraph. The highly silt nature of the Delaware sample that was observed is reflected in the high quartz content – i.e. the silt is finely ground up quartz sand. The Texas clays are mostly illite with some kaolinite and the Delaware clay is roughly equal amounts of both.

Delaware, Philadelphia clay

The Delaware river clay retrieved from Philadelphia, Pennsylvania had a highly silt nature. This was observed from the high presence of quartz – i.e. the silt is finely ground up quartz sand. Just over a quarter of the sample consisted of kaolinite and it is a very common ingredient to be present in clay samples. This is similar for the presence of illite in the clay sample, but it was a fifth of the total sample.

Table 3. Delaware, Philadelphia clay mineralogy

Phase	Composition	Concentration Estimated [%]
Quartz	SiO_2	52
Kaolinite	$Al_2Si_2O_5(OH)_4$	27
Rutile	TiO_2	<1
Mica/Illite	$KAl_2(Si_3Al)O_{10}(OH)_2$	20
Hematite	Fe_2O_3	<1

Freeport grey, Texas clay

The grey clay retrieved from Freeport, Texas had a very high presence of illite (59%). With a substantial amount of quartz present in the clay sample there is a good possibility this sample has some internal friction. With the internal friction present there is also an external friction angle present. These angles may have had some influence on the blade pulling force during the adhesive strength experiments.

Table 4. Freeport grey, Texas clay mineralogy

Phase	Composition	Concentration Estimated [%]
Quartz	SiO_2	31
Kaolinite	$Al_2Si_2O_5(OH)_4$	2
Rutile	TiO_2	<1
Mica/Illite	$KAl_2(Si_3Al)O_{10}(OH)_2$	59
Feldspar	$(K,Na)AlSi_3O_8$	7

Freeport red, Texas clay

The red clay from Freeport, Texas also had a very high presence of illite (60%). Quartz was also present giving the sample some internal friction and therefore some external friction angle, which may have resulted in a higher blade pulling force. The other phases present were hardly noticeable.

Table 5. Freeport red, Texas clay

Phase	Composition	Concentration Estimated [%]
Quartz	SiO_2	19
Calcite	$CaCO_3$	11
Rutile	TiO_2	<1
Anatase	TiO_2	<1
Dolomite	$CaMg(C0_3)_2$	<1
Mica/Illite	$KAl_2(Si_3Al)O_{10}(OH)_2$	60
Kaolinite	$Al_2Si_2O_5(OH)_4$	9
Montmorillonite	$(Na,Ca)_{0.3}(Al,Mg)_2Si_4O_{10}(OH)_2 \cdot nH_2O$	trace

Natural field clays adhesives strengths

The determination of the adhesive strength of the natural field clays was done with different approaches. The first approach was extrapolating the data with a fitting curve to the intersection with y-axis to determine the adhesive strength of the different field clays. Another approach was the φ=0 approach. This approach takes the φ=0 concept into account averaging all values and having an average adhesive stress with an average normal stress.

All the recordings gave a raw data set that was copied into Excel to create a graph used to examine the experiments. All the experiments were recorded at a frequency of 50 Hz, meaning every second, five data points were recorded.

The clay sample length was 230 mm in length and the blade was 280 mm in length. The full contact between the total blade surface and the clay was therefore 50 mm. The blade pulling speeds were 8 mm/s or 0.4 mm/s meaning that a recording has 6 or 125 seconds during a full contact between full blade length and clay sample. Figure 14 and Figure 15 with the orange area highlighted show the time windows that the average pulling force is determined during full contact between steel and clay.

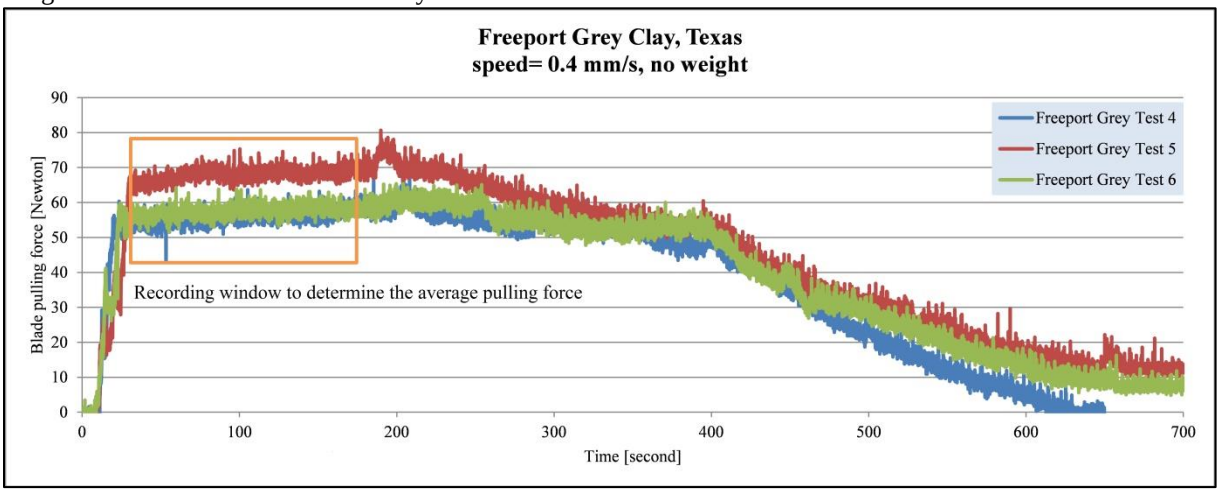

Figure 14. Pulling force determination from recorded data graph at low speed (0.4 mm/s)

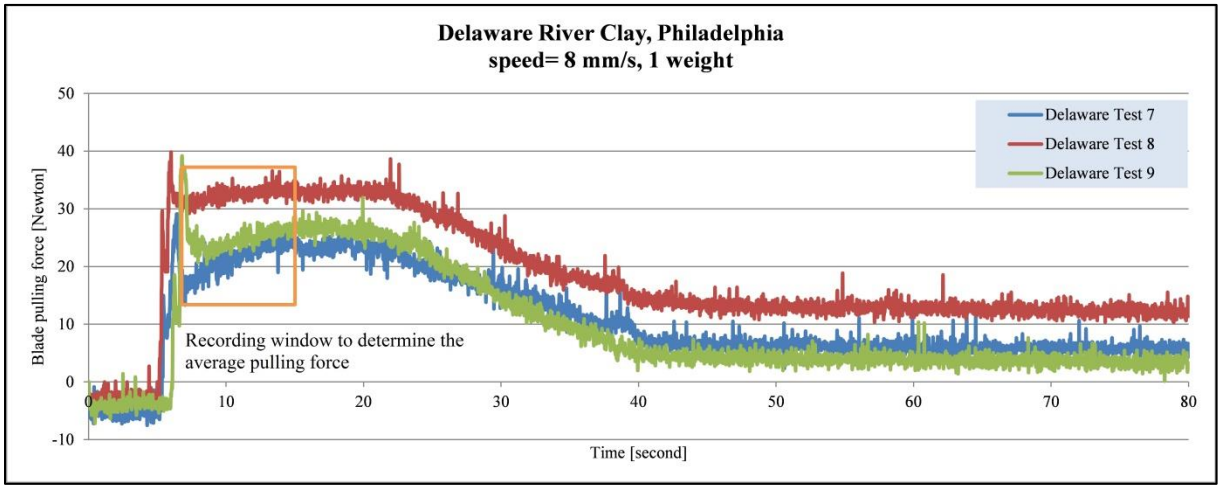

Figure 15. Pulling force determination from recorded data graph at high speed (8.0 mm/s)

Extrapolation approach towards adhesive clay properties

By using the data acquired from the adhesive experiments of the three natural field clays, the data is approached by extrapolation of the data points. This extrapolation added a trend line that was fitted to each data set acquired. This trend line intersected with the vertical adhesive stress axis. The intersection with the vertical axis is the adhesive stress [N/mm2] for clay at 8 or 0.4 mm/s. The data points of the three natural field clays are the average of the three tests at a particular speed and vertical force. These data points with trend lines are displayed in a graph with adhesive stress [N/mm2] over normal stress [N/mm2] on the axis; see Figure 16 and Table 6.

The normal stress was adjusted by adding weights on the top plate and weighed with a scale before each adhesive test, see Figure 12. There were three vertical forces on the clay sample and blade: firstly its own weight; secondly its own weight and one extra weight and finally its own weight with two extra weights. These three vertical forces increased the normal stress on the clay and the steel blade. The normal stress was calculated by using equation 1.

$$\sigma_n = \frac{F_{normal}}{A_{blade}} \quad (1)$$

σ_n is the normal stress in [n/mm2] with F_{normal} and A_{blade} being the vertical force [N] and blade surface in [mm2]. The shear stress was calculated in a similar way, only the vertical force (F_{normal}) was replaced by the average pulling force (F_{pull}) in the recorded time window, see equation 2.

$$\sigma_s = \frac{F_{pull}}{A_{blade}} \quad (2)$$

If the line would be horizontal, it may be concluded that there is no external friction angle and therefore no internal friction angle present. With increasing normal force the clay strength may not increase if there is no internal friction angle. The trend line should be horizontal with increasing normal stress. The recorded pulling force (F_{pull}) by the load cell divided by the blade surface area (A_{blade}) results in the shear stress at a given normal stress. The trend line of each data set from the tests intersects the vertical axis at a particular adhesive stress.

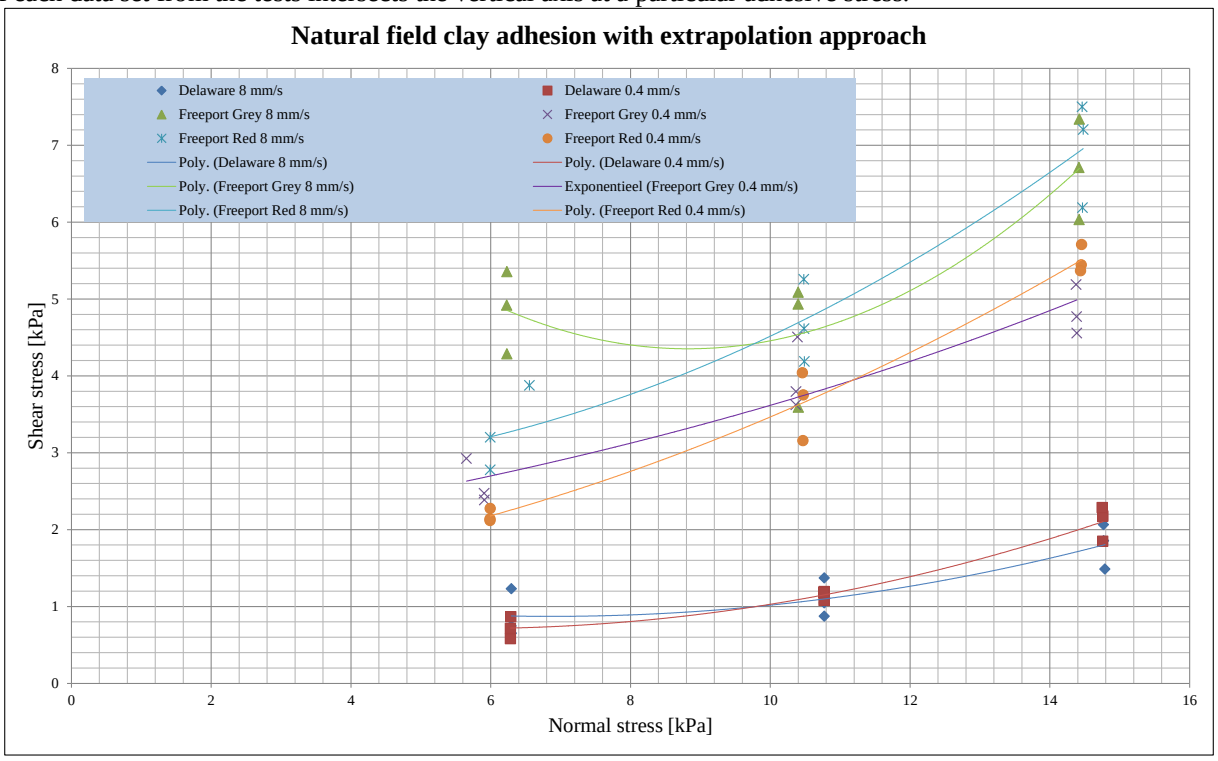

Figure 16. Extrapolation approach shear stress over normal stress

All the trend lines are inclined, which means that there is an external/internal friction angle present in the natural field clays. After calculation of the cohesion of the clays, each clay must be corrected for the external/internal friction recorded.

An increasing trend line left of the data points is not realistic and it can be noticed that this occurs with the Freeport grey clay 8 mm/s. A minimum value was determined and that is the lowest point in the curve of the trend line. Both the trend lines for the Freeport red clay have the same angle, but the adhesive stress is higher for the 8 mm/s experiments. For the Delaware River clay both the adhesive stress and the internal friction can be considered to be constant. The difference is the possible recording error and this is inevitable. But with an external and internal friction angle the cohesive strength of clay must be recalculated with the circle of Mohr, see Figure 17.

Table 6. Extrapolation approach results

Clay	Pulling speed [mm/s]	Cohesion (UU-traxial) [kPa]	Adhesion [kPa]	Adhesions/ Cohesion [%]	Internal friction angle [degree]	Recalculated Cohesion [kPa]
Delaware, Philadelphia	0.4	11.5	0.70	6.1	4.00	10.8
	8	10.1	0.90	8.9	2.17	9.8
Freeport Grey, Texas	0.4	25.9	1.74	6.7	16.34	19.6
	8	17.3	5.00	29.0	1.42	16.9
Freeport Red,	0.4	102.1	1.22	1.2	4.75	94.5

Texas	8	89.0	2.79	3.1	15.35	86.6

The inclined black line in Figure 17 is used to determine the correct cohesive strength, because of the difference between a measured external and calculated internal friction angle, see equations 3 and 4. The recalculated cohesive or real cohesive strengths of the clay can be found in Table 6.

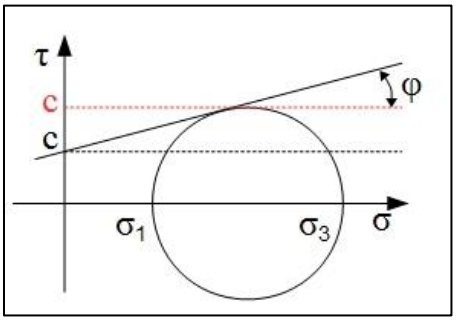

Figure 17. Mohr circle extrapolation and phi=0 approach

$$\tau = c + \sigma \cdot \tan(\varphi) \quad (3)$$

$$\varphi = \frac{3}{2}\delta \quad (4)$$

With τ for the shear stress [kPa], c for cohesion [kPa], σ for the effective stress [kPa], φ and δ are the internal and external friction angle in degree. The red line in Figure 17 is used with φ=0 approach, but more on this approach in the next paragraph.

φ = 0 approach towards adhesive clay properties

The φ=0 principle is in effect with this approach. The approach of φ=0 was used to evaluate the possibility of an internal/external friction angle being present in the tested clays. With this approach all data was averaged of every test leaving of each natural field clay two data point, the pulling speed of 8 and 0.4 mm/s. A total of six data points is the result of this approach. To acquire the adhesive stress [N/mm2] from these data points, a horizontal line was drawn to the y-axis, or adhesive stress axis. This was because with the circle of Mohr the intersection between the line and circle is at the top of the circle of Mohr. In Figure 17, the horizontal red line represents the angel of internal friction. With the φ = 0 approach the line is horizontal and therefore also horizontal in Figure 18. In Table 7, the results of the φ = 0 approach are presented. An important remark on this approach is that the average adhesive stress is not dependent on the average normal stress, because the stresses are averages.

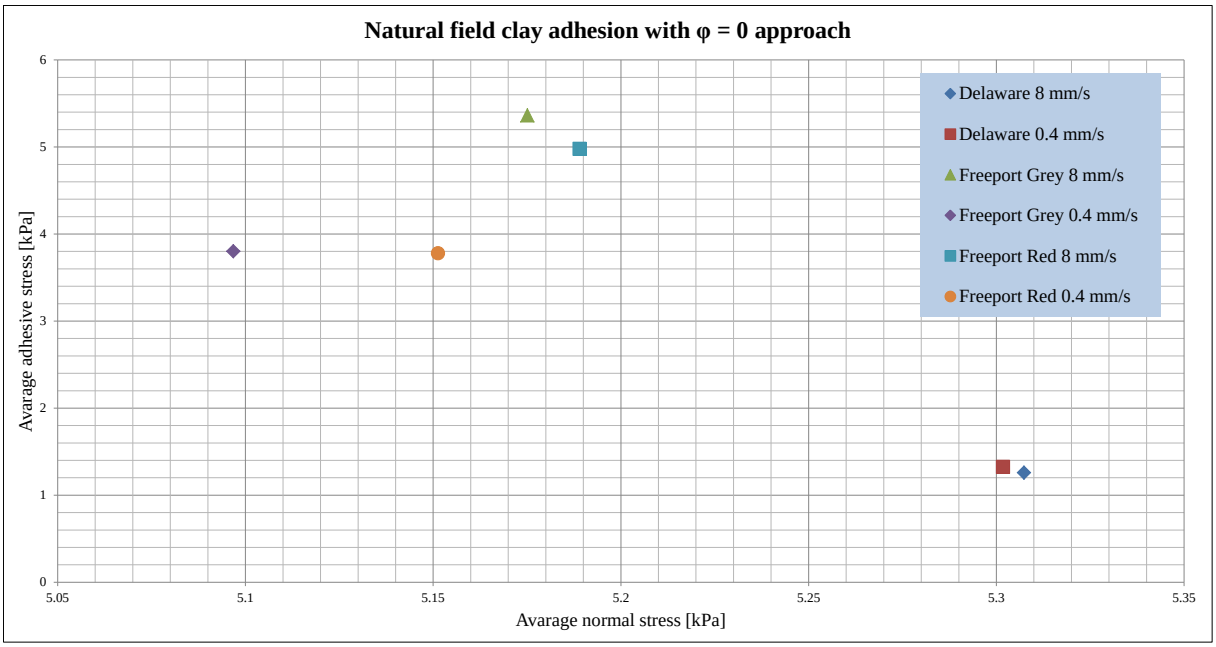

Figure 18. Φ =0 approach average adhesive stress over average normal stress

Table 7. Φ = 0 approach results

Clay	Pulling speed [mm/s]	Cohesion (UU-traxial) [kPa]	Adhesion [kPa]	Adhesions/ Cohesion [%]	Internal friction [degree]
Delaware, Philadelphia	0.4	11.5	1.32	11.5	0
	8	10.1	1.36	13.5	0
Freeport Grey, Texas	0.4	25.9	3.80	14.7	0
	8	17.3	5.36	31.0	0
Freeport Red, Texas	0.4	102.1	3.78	3.7	0
	8	89	4.98	5.6	0

For the Freeport red clay both the data points are equal or lower compared to the Freeport grey clay, which means that with increasing strength there is a decrease of adhesion. However, the Delaware River clay implies there is an increase of the adhesion from very soft to soft clay. The blade pulling speed has no effect on the Delaware River clay. However, with a lower speed, the Freeport red and grey clay have a lower adhesive strength. This could mean that water flow out the pores has more time or lower "vacuum" occurs, resulting in a lower pulling force or adhesive stress when divided by the blade surface.

CONCLUSION

With an increasing cohesive strength of the clay there is a decrease to zero for the adhesive strength. In addition to the decreasing adhesion there is an increase in the internal friction angle (φ). This can be concluded from the data of the Freeport grey clay of 17 kPa cohesive strength with 5.4 kPa adhesion and the stiffer Freeport red clay with a cohesive strength of 89 kPa with a minor 5 kPa adhesive strength. The internal friction angle for the Freeport red clay is 15 degrees, however the internal friction angle will have a limit between 15-20 degrees considering rock has an internal friction angle of approximately 20 degrees. This has a major influence on the productions [m^3] and production estimates of stiffer clays with clamshell dredges or any other dredging equipment.

LIST OF SYMBOLS

A_{blade}	Pulling blade surface	[m^2]
a	External undrained shear strength/ adhesive strength	[Pa]
c	Internal undrained shear strength/ cohesive strength	[Pa]
$F_{additional}$	Additional pulling force	[N]
$F_{adhesion}$	Adhesive force	[N]
F_{normal}	Vertical force on pulling blade	[N]
F_{pull}	Blade pulling force	[N]
F_{shear}	Shear force	[N]
LL	Liquid limit	[%]
PL	Plastic limit	[%]
S_u	Undrained shear strength	[Pa]
δ	External friction angle	[degree]
λ	Bucket opening angle	[degree]
ρ	Density/ Specific gravity	[kg/m3]
σ	Normal stress	[Pa]
σ_s	Shear stress	[N/mm2]
σ_a	Adhesive stress	[N/mm2]
σ_1	Major principal stress	[Pa]
σ_3	Minor principal stress	[Pa]
τ	Shear stress	[Pa]
φ	Internal friction angle	[degree]

REFERENCES

API. (1993). *American petroleum institute.* Houston.

Bauerschlag, D. (1979). *Untersuchungen zum Fullverhalten von Motorgreifgern.* Hannover: University Hannover.

de Jong, P., Becker, S., Wittekoek, S., & Miedema, S. (1992). *The Closing Process of Clamshell Dredges in Water-Saturated Sand.* Bombay: Technical University Delft.

Gebhardt, R. (1972). Eindringwiederstande korniger haufwerke. *Hebezeuge und fordermittel 12*, pp. 241-247.

Graham, J., Crooks, J. H., & Bell, L. (1983). Time effects on the stress-strain behaviour of natural soft clays. *Gotechnique, Vol. 3*, 327-340.

Great Lakes Dredge & Dock. (2008). *Soil properties American and International standards.* Oak Brook.

Hatamura, Y., & Chijiiwa, K. (1975). Analysis of the Mechanism of Soil Cutting: 1st report, cutting patterns of soil. *Bulletin of the JSM, Vol. 18, No. 120*, 619-626.

Hatamura, Y., & Chijiiwa, K. (1976a). Analysis of the mechanism of soil cutting: 2nd report, Deformation and internal stress o soil in cutting. *Bulletin of the JSM, Vol. 19, No. 131*, 555-563.

Hatamura, Y., & Chijiiwa, K. (1977a). Analysis of teh mechanism of soil cutting: 4th rport, Properties of soils related cutting. *Bulletin of JSME, Vol. 20, No. 139*, 130-137.

Hatamura, Y., & Chijiiwa, K. (1977b). Analysis of teh mechanism of soil cutting: 5th report, Cutting theories of soils. *Bulletin of JSME, Vol. 20, No. 141*, 388-395.

Hatamurat, Y., & Chijiiwa, K. (1976b). Analysis of the mechanism of soil cutting: 3rd report, Distribution of stresses on cutting blade and cuttin force. *Bullentin of JSME, Vol. 19, No. 137*, 1376-1384.

Hupe, W., & Schuszter, W. (1965). Verbesserte Motorgreifer als Beitrag zur allgemeinen Verbesserung des Greiferumschlages. *Hebezeuge und Fordermittel*, pp. 6-9.

Kooistra, A., Verhoef, P., Broere, W., Ngan-Tillard, D., & van Tol, A. (1998). Appraisal of stickness of natural clays from laboratory tests. In R. Hack, R. Azzam, & R. Charlier, *Engineering Geology and Infrustructure* (pp. 101-113).

Littleton, I. (1976). An experimental study of the adhesion between clay and steel. *Journal of Terramechanics*, 141-152.

Manufacturing, M. Clamshell bucket. *2 & 3 line buckets.* Theodore.

Miedema, S. A. (1987). *Berekening van de snijkrachten bij het snijden van volledig met water verzadigdd zand.* Delft: Delft University of Technology.

Miedema, S. A. (1989). Clamshell Closing Simulation software 32 (CCS32). Delft, Zuid-Holland, The Netherlands.

Miedema, S. A. (2009). *New Developments of cutting theories with respect to dredging, the cutting of clay & rock.* Phoenix: WEDA XXlX.

Miedema, S. A. (2010). *The influence of the strain rate on cutting processes.* Beijing, China: ISOPE.

Miedema, S. A. (2014). *The Delft sand, clay & rock cutting model.*

Miedema, S. A., & Vlasblom, W. J. (2006). *The closing process of Clamshell Dredges in water-saturated sand.* Delft.

Mitchell, J. K., & Soga, K. (2005). *Fundamentals of Soil Behavior.* New Jersey: John Wiley & Sons, Inc.

Niemann, G. (1935). Neue erkentniss im Greiferbou. *VDI 79*, pp. 325-328.

Ninnelt, A. (1924). *Uber Kraft- und Arbeitsverteiling an Greifern- besonderes an Motorgreifern.* Wittenberg.

Pfahl, G. (1912). Kraftverteilung und greifen bei selbst greifern. *VDI*, pp. Teil 1-4.

Potyondy, J. G. (1961). Skin friction between various soils and construction material. In J. G. Potyondy, *Geotechnique 2* (pp. 339-353).

Rao, S. (2011). *Mechanical Vibrations 5th edition in si units, pg. 577-581.* Singapore: Pearson Eduaction South Asia Pte Ltd.

Sangrey, D. (1972). Naturally cemented sentive soils. In D. Sangrey, *Geotechnique* (pp. 139-152).

Scheffler, M. (1972). Neue Erkenntnisse uber die Auslegung von Zweischalen- Schuttgutgreifern. *Hebezeuge und fordermittel 12*.

Schleffler, M., Pajer, G., & Kurth, F. (1976). *Grundlagen der Fordertechnik.* Berlin.

Sonne, E. (2012). Helios Data Acquisition Program. College station, Texas, US.

Tauber, B. (1958). The effect of the design of a calbe grab on its scooping capacity. *Coll. of sientific works of MLTI 8*, pp. 30-34.

Torke, H. (1962). Untersuchungen uber den fullvorgang bei Versuchen im Sand. *Deutsche Hebe und Fordertechnik*.

van der Wielen, V. (2014). *Physical modelling of soft clay cutting for plane strain conditions, Master Thesis.* Delft.

Van Oord. (2015, Mei 5). *Deep sea dredging solution.* Retrieved Mei 15, 2015, from www.vanoord.com: http://www.vanoord.com/news/2015-van-oord-develops-deep-dredging-solution

Wikipedia. (2015, 3 4). *Minerals*. Retrieved 3 4, 2015, from Wikipedia: http://en.wikipedia.org/wiki/Montmorillonite

Wikipedia. (2015, 03 20). *X-ray diffraction*. Retrieved 03 20, 2015, from Wikipedia: http://en.wikipedia.org/wiki/X-ray_crystallography

Wilkinson, H. N. (1963). Research in the design of grabs by tests on models. *Proceedings of Institution of mechanical engineering 178*, 831-846.

Wittekoek, S. (1991a). *The determination of the closing process of clamshell dreges in water saturated sand.* Delft: Vakgroept Transporttechnologie.

Wittekoek, S. (1991c). *The validation of a calculation method fo the simulation of the colosing process of clamshell grabs for dredding purposes.* Delft: Vakgroep Transporttechnologie.

Witterkoek, S. (1991b). *The development of an improved clamshell.* Delft: Vakgroep Transporttechnologie.

CITATION

Combe, T. A.A. and Miedema, S. A. "The influence of adhesion on cutting processes in dredging," *Proceedings of the Western Dredging Association and Texas A&M University Center for Dredging Studies' "Dredging Summit and Expo 2015"*, Houston, Texas, USA, June 22-25, 2015.

10.7. Appendix G

10.7.1. Liquid limit Delaware River clay

Atterberg Limits Determination

Sample No. Dela_Phil_1 Project GLDD
Boring No. Dela-Phil_1 Location Delaware river, Philadelphia
Depth 44 ft.
Description of sample
Date 11-21-2014 Tested by Thomas combe

Liquid Limit Determination

Can No.	Dela-4	Dela-5	Dela-6	Dela-7
Mass of can (g)	1.5	1.5	1.5	1.5
Mass of wet soil + can (g)	7.37	7.56	9.27	9.17
Mass of dry soil + can (g)	6.11	6.21	7.49	7.32
Mass of dry soil (g)				
Mass of water (g)				
Water content, (%)				
No. of drops	42	35	26	20

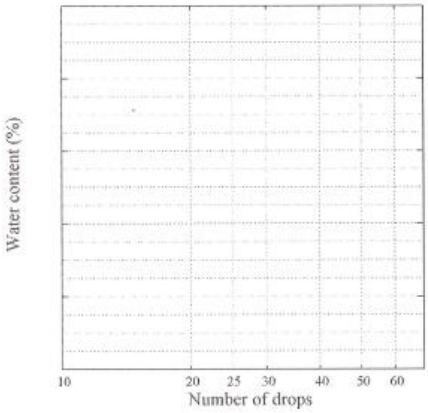

LIQUID LIMIT =
PLASTIC LIMIT =
PLASTICITY INDEX =

Plastic Limit Determination

Can No.	Dela-1	Dela-2	Dela-3	
Mass of can (g)	1.5	1.5	1.5	
Mass of wet soil + can (g)	9.56	9.13	9.02	
Mass of dry soil + can (g)	8.17	7.90	7.91	
Mass of dry soil (g)				
Mass of water (g)				
Water content, (%)				

G. Biscontin Civil Engineering Department

10.7.2. Liquid limit Freeport Grey clay

Atterberg Limits Determination

Sample No. FP_Grey-1 Project GLDD
Boring No. FP-Grey-1 Location Freeport, Texas
Depth 40 ft.
Description of sample Grey clay
Date 11-21-2014 Tested by Thomas Combe

Liquid Limit Determination

Can No.	FR-GR-4	FR-GR-5	FR-GR-6	FR-GR-7
Mass of can (g)	1.5	1.5	1.5	1.5
Mass of wet soil + can (g)	9.13	8.21	12.37	9.46
Mass of dry soil + can (g)	6.53	5.87	8.40	6.42
Mass of dry soil (g)				
Mass of water (g)				
Water content, (%)				
No. of drops	51	47	33	21

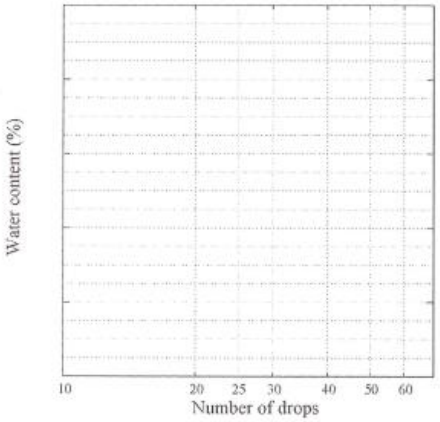

LIQUID LIMIT =
PLASTIC LIMIT =
PLASTICITY INDEX =

Plastic Limit Determination (7.47)

Can No.	FP-GR-1	FP-GR-2	FP-GR-3	
Mass of can (g)	1.5	1.5	1.5	
Mass of wet soil + can (g)	9.18	8.46	8.13	
Mass of dry soil + can (g)	7.54	6.96	6.20	
Mass of dry soil (g)				
Mass of water (g)				
Water content, (%)				

G. Biscontin Civil Engineering Department

10.7.3. Liquid limit Freeport Red clay

Atterberg Limits Determination

Sample No. FR-Red-1 Project GLDD
Boring No. FR-Red-1 Location Freeport, Texas
Depth 40 ft.
Description of sample RED CLAY
Date 11-21-2014 Tested by Thomas Combe

Liquid Limit Determination

Can No.	FR-RD-4	FR-RD-5	FR-RD-6	
Mass of can (g)	1.5	1.5	1.5	
Mass of wet soil + can (g)	8.22	9.59	10.56	
Mass of dry soil + can (g)	5.68	6.50	7.08	
Mass of dry soil (g)				
Mass of water (g)				
Water content, (%)				
No. of drops	28	23	20	

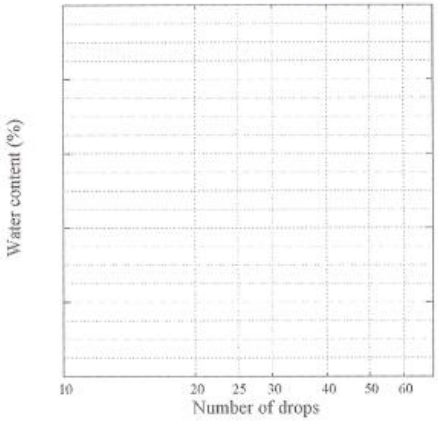

LIQUID LIMIT =
PLASTIC LIMIT =
PLASTICITY INDEX =

Plastic Limit Determination

Can No.	FP-RED-1	FP-RED-2	FP-RED-3	
Mass of can (g)	1.5	1.5	1.5	
Mass of wet soil + can (g)	9.17	8.64	8.32	
Mass of dry soil + can (g)	7.67	7.28	7.86	
Mass of dry soil (g)				
Mass of water (g)				
Water content, (%)				

G. Biscontin Civil Engineering Department

10.8. Appendix H

10.8.1. Mineralogy report

RJ LEE GROUP
DELIVERING SCIENTIFIC RESOLUTION

LABORATORY REPORT

Great Lakes Dredge & Dock Company		Report Date:	January 16, 2015
2122 York Road		Samples Received:	December 4, 2014
Oak Brook, IL 60523		RJ Lee Group Job No.:	CUH1034689-0, -1
ATTENTION:	Gregory Sraders	Client Job No.:	N/A
Telephone:	630-574-2969	Purchase Order No.:	658357

ANALYSIS: Qualitative Phase Identification of Clay Minerals
METHOD: X-ray diffraction (XRD) of an Oriented Slide

Each specimen was mixed with DI water and hydrated for 24 hours. Each specimen was then sonicated and then pipetted onto a glass slide and allowed to air dry into an oriented mount. The specimens were run on a PANalytical X'Pert Pro diffractometer using copper radiation. Next, the oriented specimens were treated with ethylene glycol and scanned again by XRD. The slides then underwent two heat treatments; the first at 400°C for an hour and the second at 550°C for an hour. The specimens were scanned following each heat treatment. The resulting diffraction patterns were overlain, analyzed with the X'Pert HighScore program using the ICDD PDF4+ database and the USGS Clay Identification Flow Diagram. Results are presented in Figures 1, 4 and 7.

ANALYSIS: Phase Identification and Quantification of Crystalline Phases
METHOD: Rietveld Method

Each sample was ground to a fine powder and then placed into a back-loaded sample holder for analysis. The specimens were analyzed utilizing a PANalytical X'Pert Pro diffractometer using Cu Kα radiation from 5-90° 2Θ with a step size of 0.017° 2Θ for 120.015 seconds/step.

The resulting diffraction patterns were then analyzed using X'Pert HighScore Plus search-match software utilizing the ICDD PDF4+ database to identify the phases present. The diffraction patterns, and the corresponding legends illustrating peak matching results are shown in Figures 2, 5 and 8.

HighScore Plus was also utilized to attempt to quantify the phases present in each sample by Rietveld refinement. Rietveld refinement is a full-pattern fitting method, the goal of which is to use structural data from the PDF4+ database to construct a calculated profile that is as similar as possible to the measured profile of the sample, as obtained by XRD. By refining the model, the

differences between the two profiles is minimized and each phase can be quantified. The Rietveld models produced, along with their corresponding difference plots are shown in Figures 3, 6 and 9.

Tables 1-3 below contain phase identification and quantification results for samples: "*Freeport Red sample 1*," "*Freeport Grey sample 1*," and "*Delaware sample 1*," corresponding to RJ Lee Group sample numbers: 10304976,10304977 and 10304978, respectively. Sample 10304976 (*Freeport Red sample 1)* contained quartz, calcite, kaolinite, mica, and very low levels of rutile, anatase, dolomite and montmorillonite. The montmorillonite that was identified during the clay analysis was not overly apparent in the Rietveld XRD scan, and was therefore left out of the Rietveld model. Sample 10304977 (*Freeport Grey sample 1)* was found to contain quartz, mica, kaolinite, feldspar and a small amount of rutile. Sample 10304978 (*Delaware sample 1)* contained mostly quartz, kaolinite and mica, with small amounts of rutile and hematite. In all three samples, the clay minerals mica and kaolinite were modeled with some difficulty due to the preferred orientation their crystal structures exhibit. The preferred orientation was taken into account during modeling, however, it is possible that these phase percentages are overestimated.

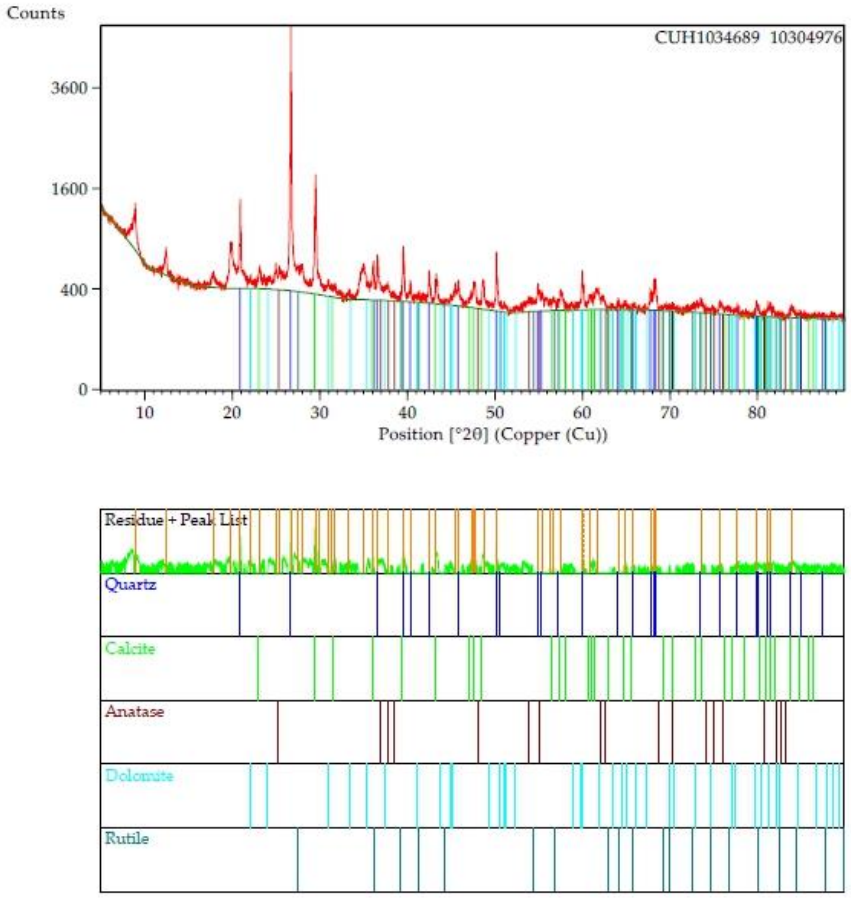

Figure 2 –X-ray diffraction pattern of as-received specimen *"Freeport Red sample 1"*, with position (degrees 2θ) along the x-axis and intensity (counts) along the y-axis (top). Corresponding legend denoting phase matches (bottom).

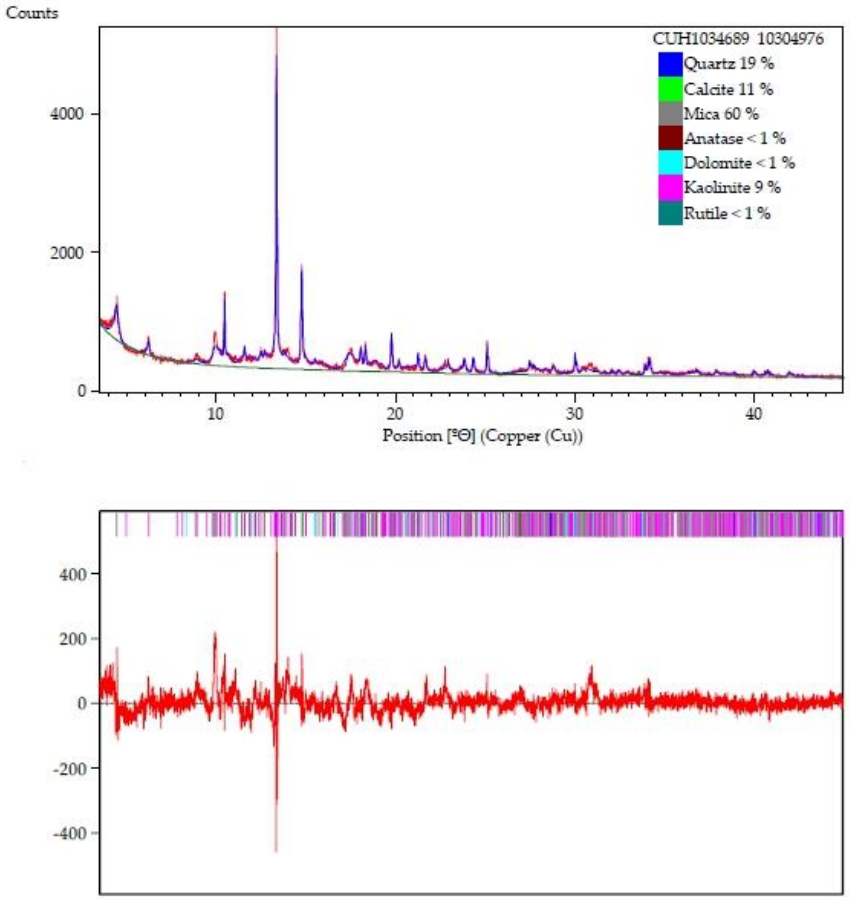

Figure 3 – X-ray diffraction pattern of sample *"Freeport Red sample 1,"* (RJ Lee Group 10304976), with degrees 2θ along the x-axis and intensity (counts) along the y-axis (red) overlain with the calculated pattern derived from Rietveld Refinement (blue) (top). Corresponding difference plot showing the difference between the experimental and calculated patterns (bottom).

Client Sample No.: Freeport Grey sample 1
RJ Lee Group Sample No.: 10304977

Phase	Composition	Concentration Estimated
Quartz	SiO_2	31
Kaolinite	$Al_2Si_2O_5(OH)_4$	2
Rutile	TiO_2	< 1
Mica/Illite	$KAl_2(Si_3Al)O_{10}(OH)_2$	59
Feldspar	$(K,Na)AlSi_3O_8$	7
Unknown(s)	-	Trace

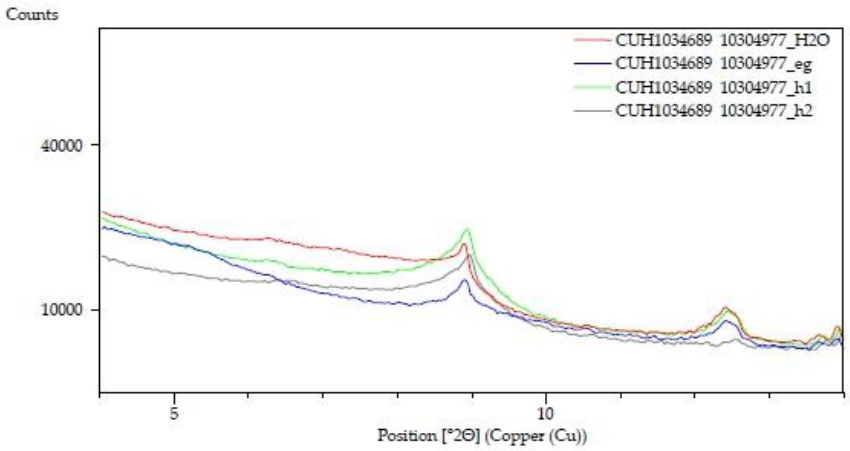

Figure 4 – Overlay of x-ray diffraction patterns for specimens: "*Freeport Grey sample 1*_air dried," (in red), "*Freeport Grey sample 1*_eg," (in blue), "*Freeport Grey sample 1_ht1*," (in green) and "*Freeport Grey sample 1_ht2*" (in grey), with position (degrees 2θ) along the x-axis and intensity (counts) along the y-axis. The patterns have been zoomed to the region between 4-14°2θ to show detail. The 8.8 ° 2Θ reflection did not change, and therefore represents mica/illite. There was a lessening of intensity of the 12.5° 2Θ reflection after the second heat treatment, which is indicative of kaolinite.

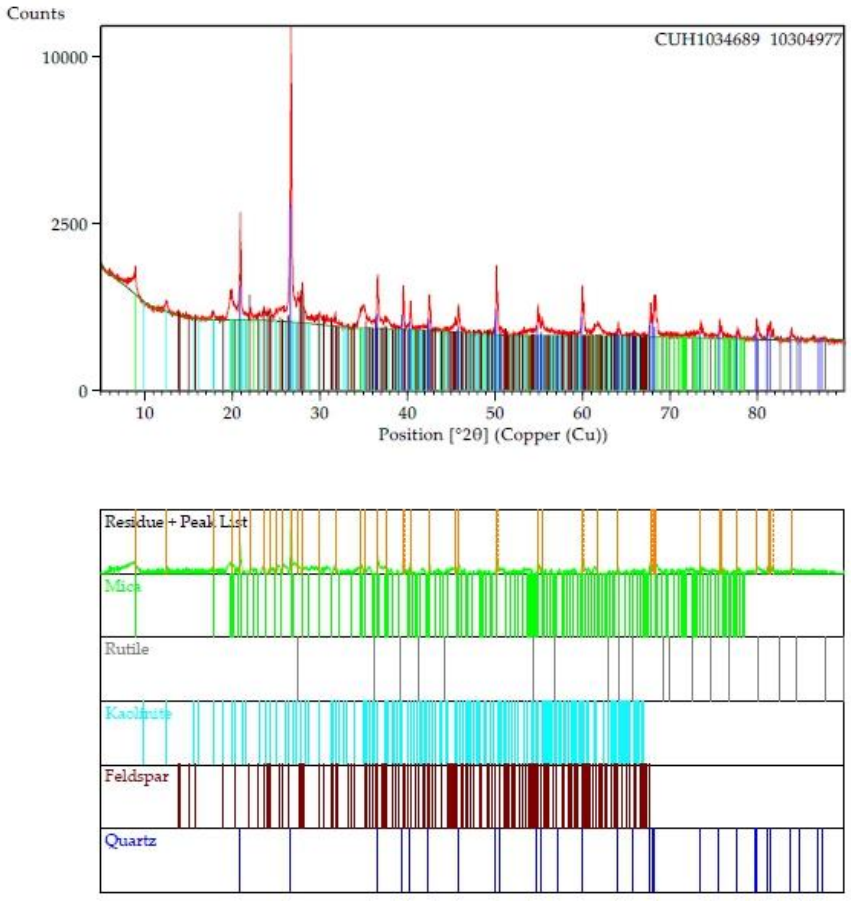

Figure 5 –X-ray diffraction pattern of as-received specimen *"Freeport Grey sample 1"*, with position (degrees 2θ) along the x-axis and intensity (counts) along the y-axis (top). Corresponding legend denoting phase matches (bottom).

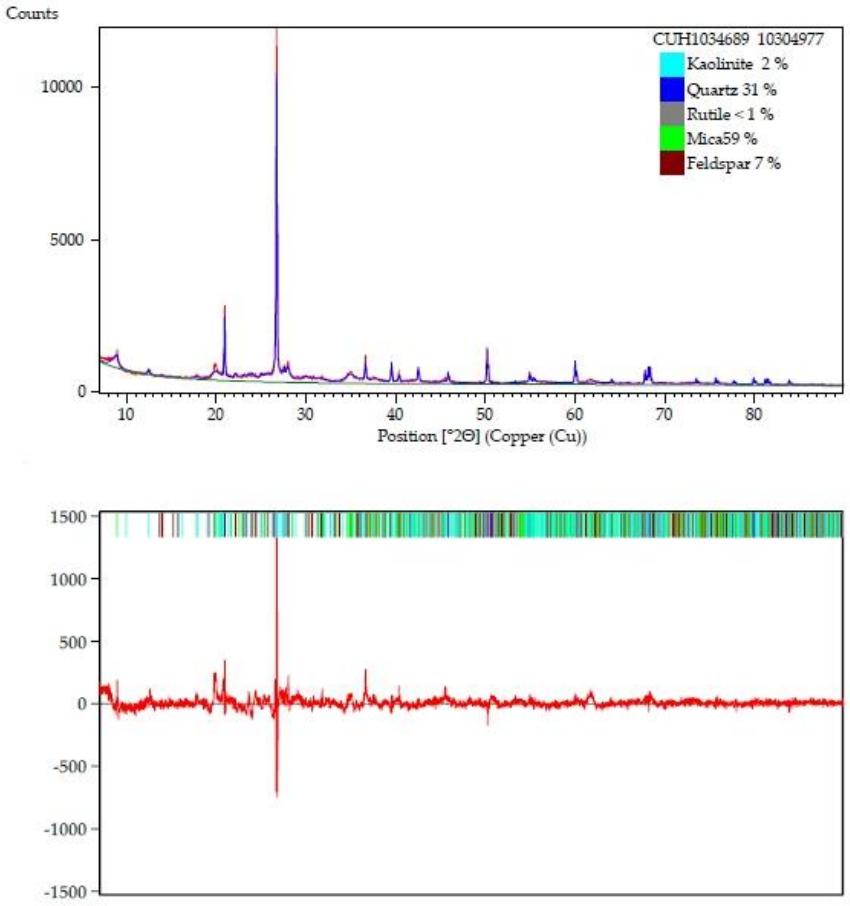

Figure 6 – X-ray diffraction pattern of sample *"Freeport Grey sample 1,"* (RJ Lee Group 10304977), with degrees 2θ along the x-axis and intensity (counts) along the y-axis (red) overlain with the calculated pattern derived from Rietveld Refinement (blue) (top). Corresponding difference plot showing the difference between the experimental and calculated patterns (bottom).

Client Sample No.: Delaware sample 1
RJ Lee Group Sample No.: 10304978

Phase	Composition	Concentration Estimated
Quartz	SiO_2	52
Kaolinite	$Al_2Si_2O_5(OH)_4$	27
Rutile	TiO_2	< 1
Mica/Illite	$KAl_2(Si_3Al)O_{10}(OH)_2$	20
Hematite	Fe_2O_3	< 1
Unknown(s)	-	Trace

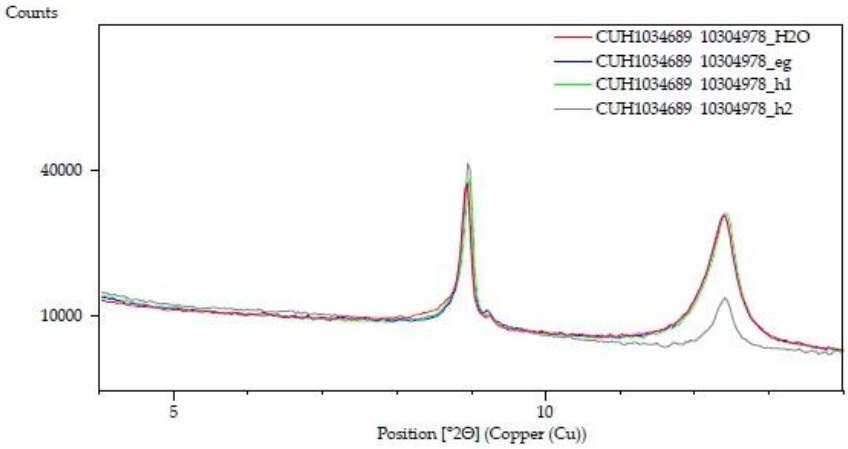

Figure 7 – Overlay of x-ray diffraction patterns for specimens: *"Delaware sample 1*_air dried," (in red), *"Delaware sample 1*_eg," (in blue), *"Delaware sample 1_ht1,"* (in green) and *"Delaware sample 1_ht2"* (in grey), with position (degrees 2θ) along the x-axis and intensity (counts) along the y-axis. The patterns have been zoomed to the region between 4-14°2θ to show detail. The only change that occurred in the pattern was a lessening of intensity of the 12.5° 2Θ reflection after the second heat treatment, indicating that this reflection is most likely kaolinite. The 8.8 ° 2Θ reflection did not change, and is therefore mica/illite.

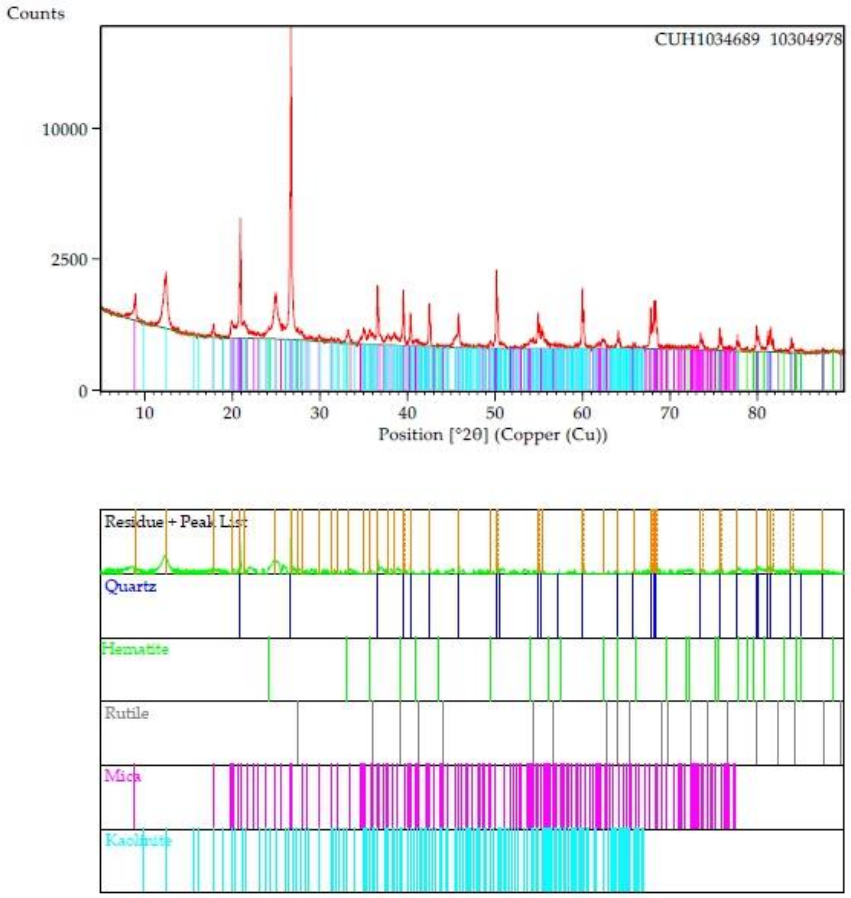

Figure 8 –X-ray diffraction pattern of as-received specimen *"Delaware sample 1"*, with position (degrees 2θ) along the x-axis and intensity (counts) along the y-axis (top). Corresponding legend denoting phase matches (bottom).

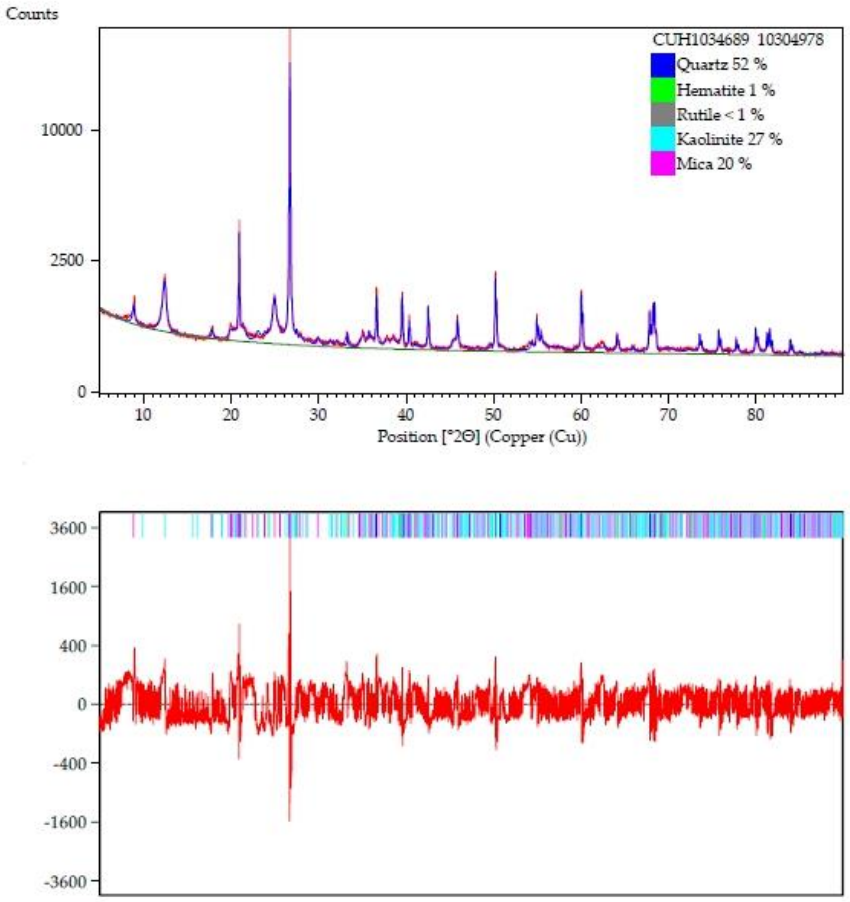

Figure 9 – X-ray diffraction pattern of sample *"Delaware sample 1,"* (RJ Lee Group 10304978), with degrees 2θ along the x-axis and intensity (counts) along the y-axis (red) overlain with the calculated pattern derived from Rietveld Refinement (blue) (top). Corresponding difference plot showing the difference between the experimental and calculated patterns (bottom).

Authorized Signature _____ Date 01/16/15

Shannon Arlauckas
Scientist, X-ray Diffraction Group

This laboratory operates in accord with ISO 17025:2005 guidelines, and holds a limited scope of accreditations under different accrediting agencies; refer to http://www.rjlg.com/about-us/accreditations/ for more information and current status.

10.9. Appendix I

10.9.1. Extrapolation approach graph

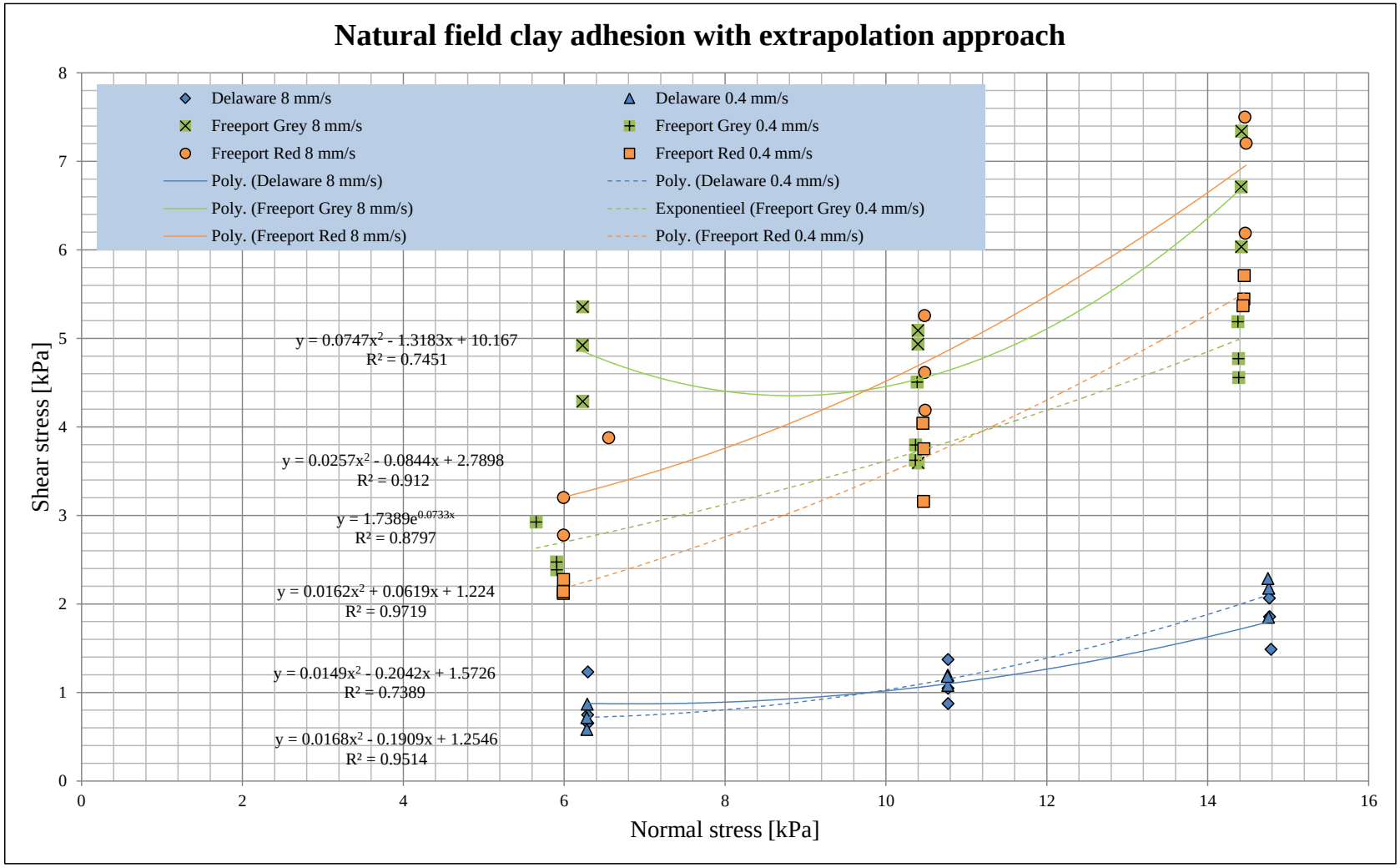

10.9.2. Linear approach graph

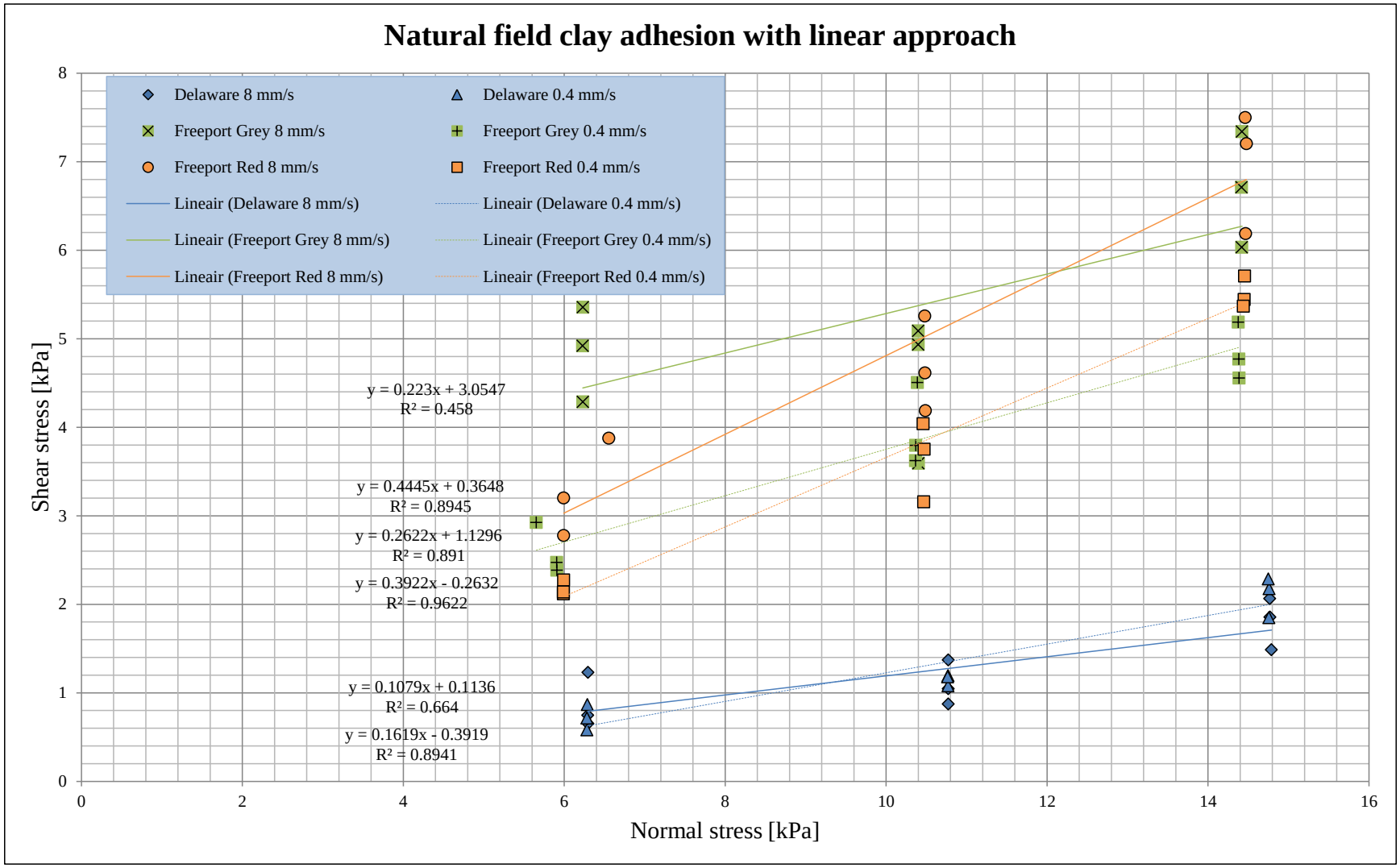

10.9.3. Φ = 0 approach graph

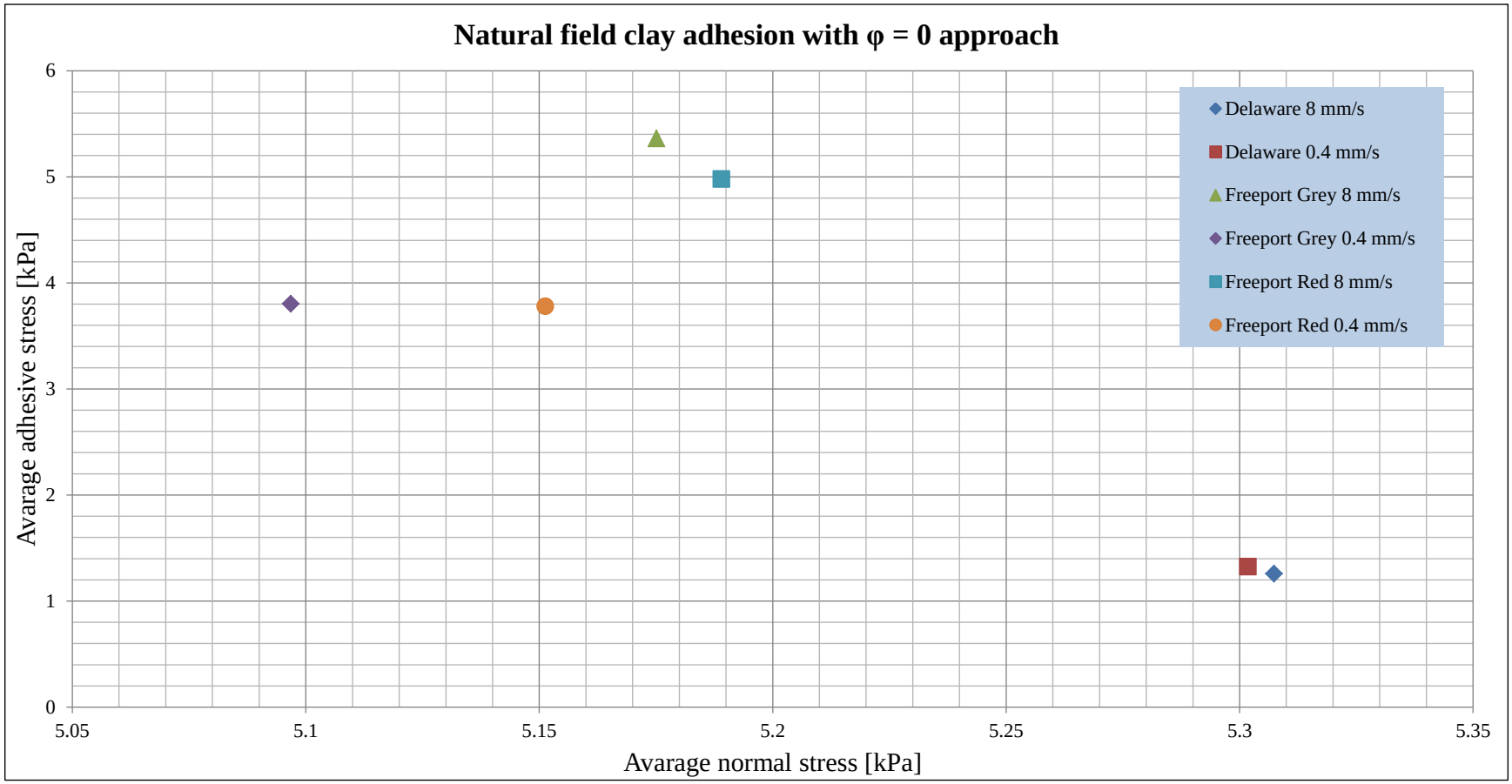

10.9.4. Average approach graph

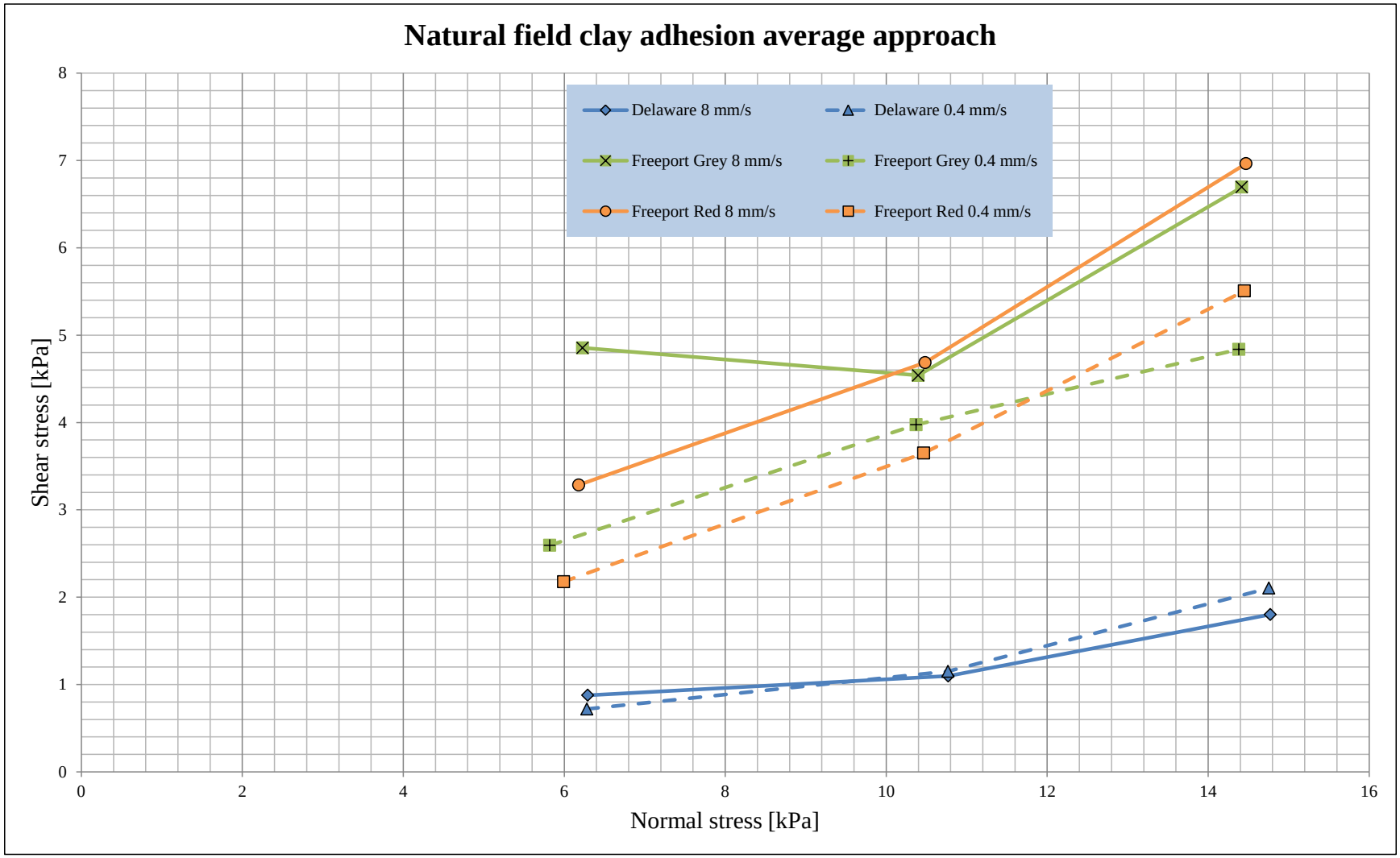

10.10. Appendix J

10.10.1. Delaware river clay adhesive test set-up graphs

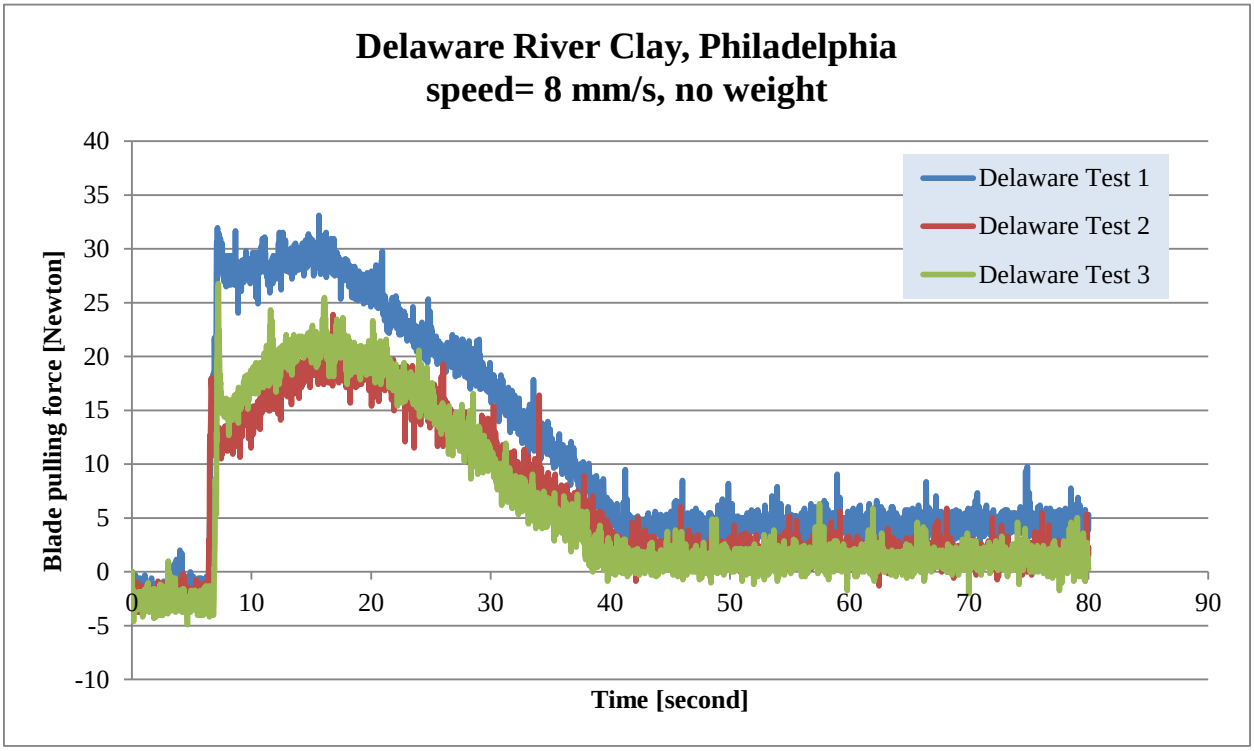

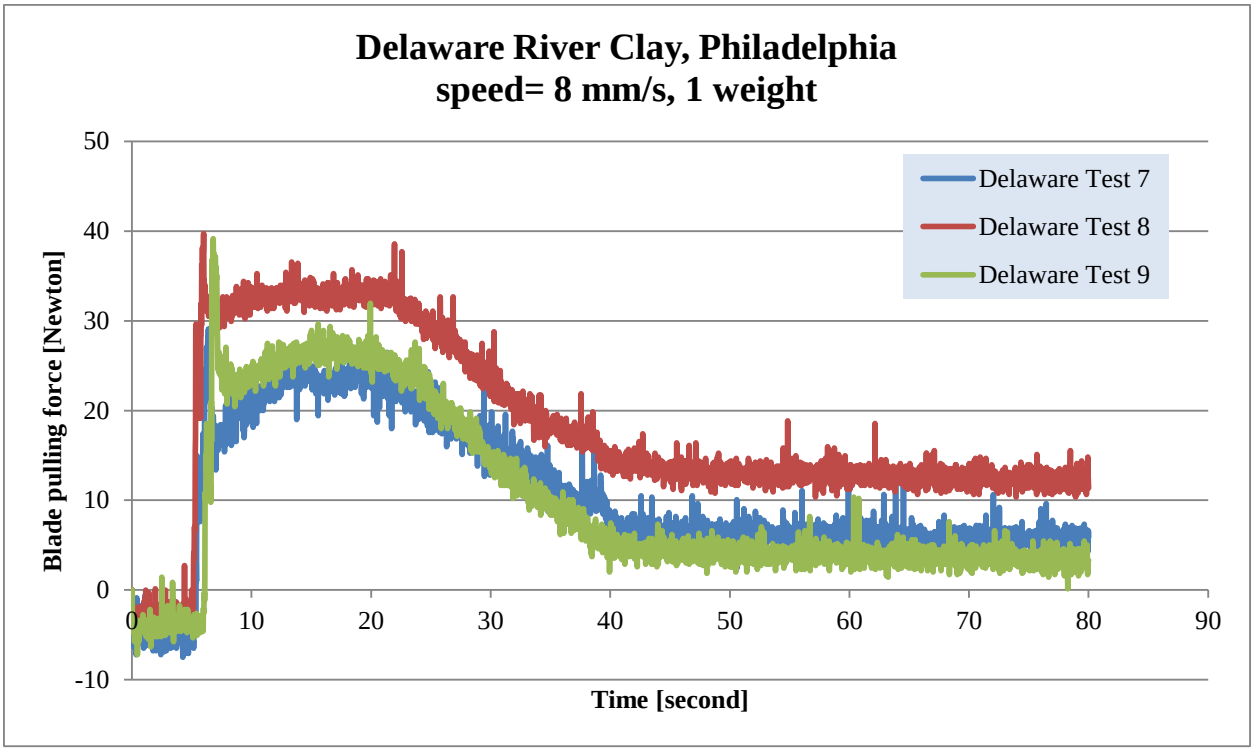

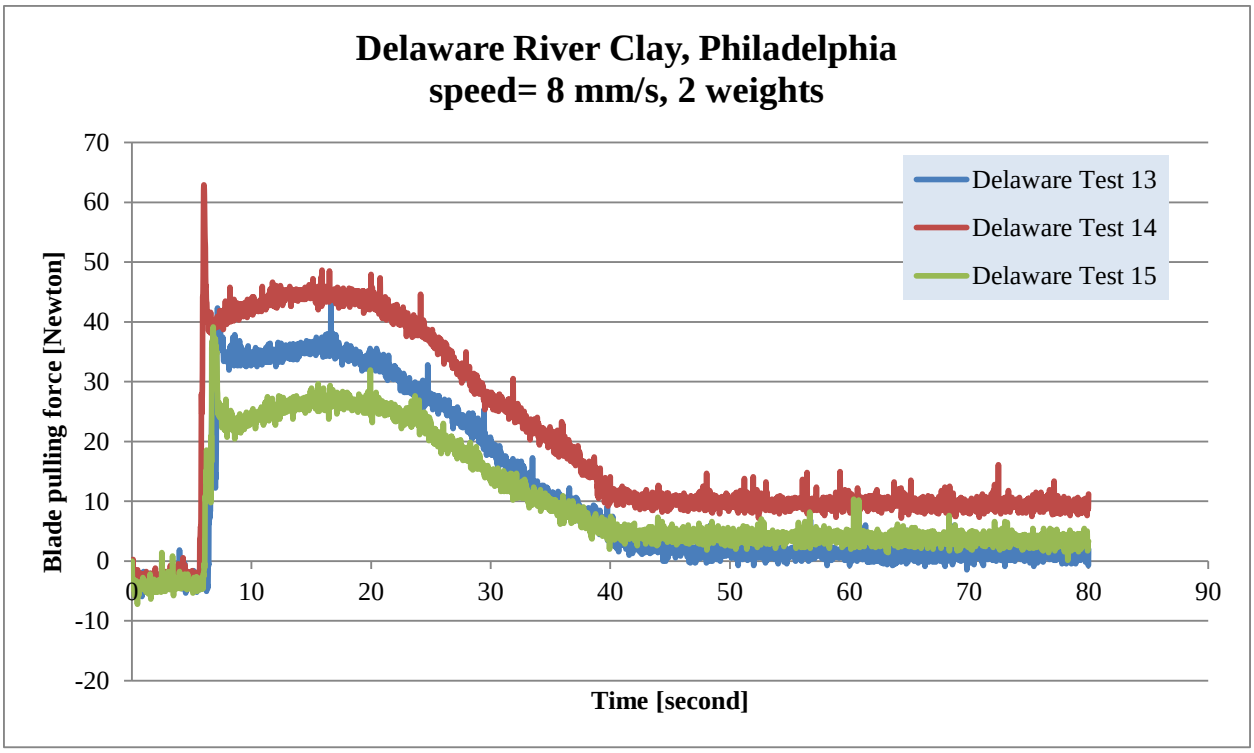
Delaware River Clay, Philadelphia
speed= 8 mm/s, 2 weights
Blade pulling force [Newton]
70
60
50
40
30
20
10
0
-10
-20
0
10
20
30
40
50
60
70
80
90
Time [second]
Delaware Test 13
Delaware Test 14
Delaware Test 15

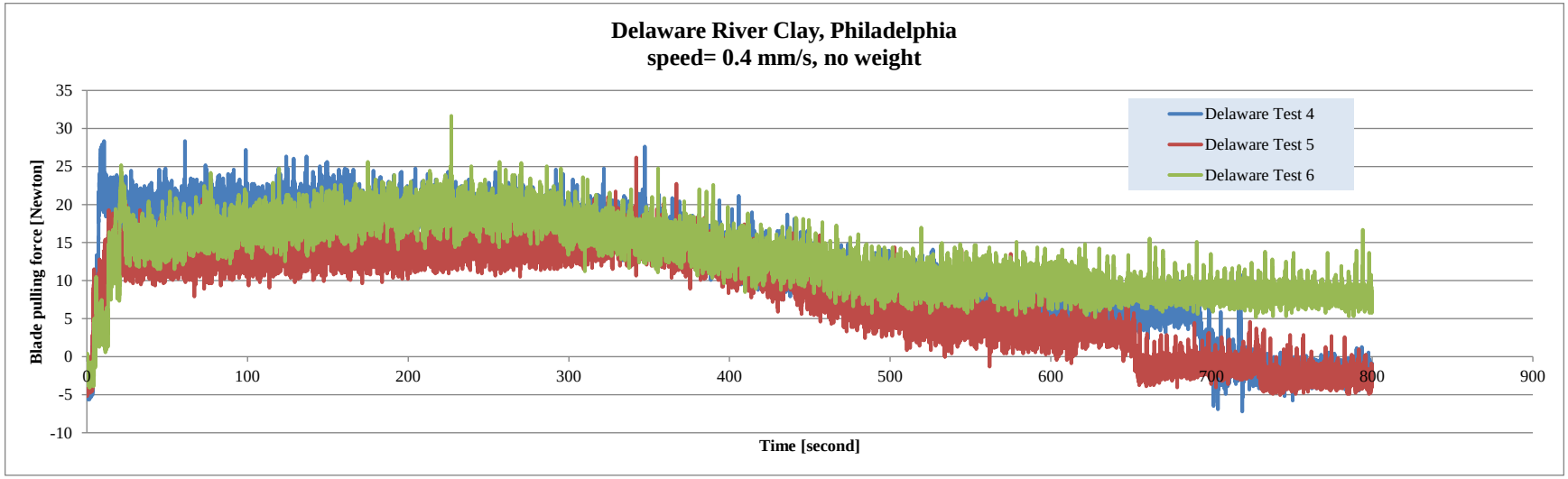
Delaware River Clay, Philadelphia
speed= 0.4 mm/s, no weight
Blade pulling force [Newton]
Time [second]
Delaware Test 4
Delaware Test 5
Delaware Test 6
35
30
25
20
15
10
5
0
-5
-10
0
100
200
300
400
500
600
700
800
900

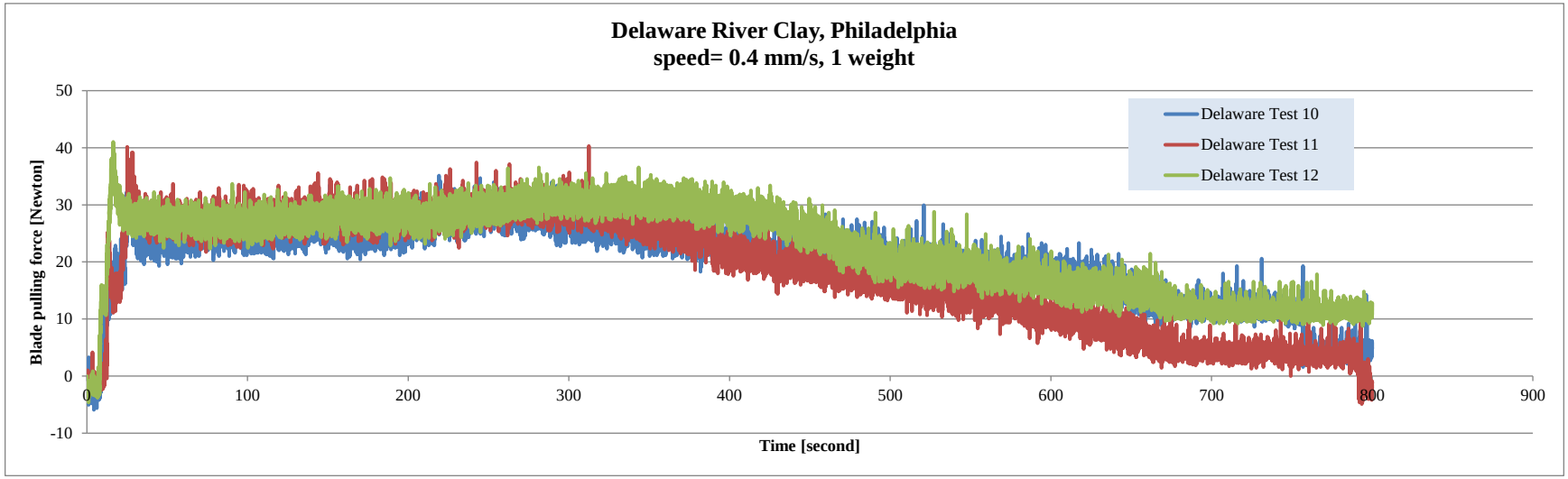
Delaware River Clay, Philadelphia
speed= 0.4 mm/s, 1 weight
Blade pulling force [Newton]
Time [second]
Delaware Test 10
Delaware Test 11
Delaware Test 12
50
40
30
20
10
0
-10
0
100
200
300
400
500
600
700
800
900

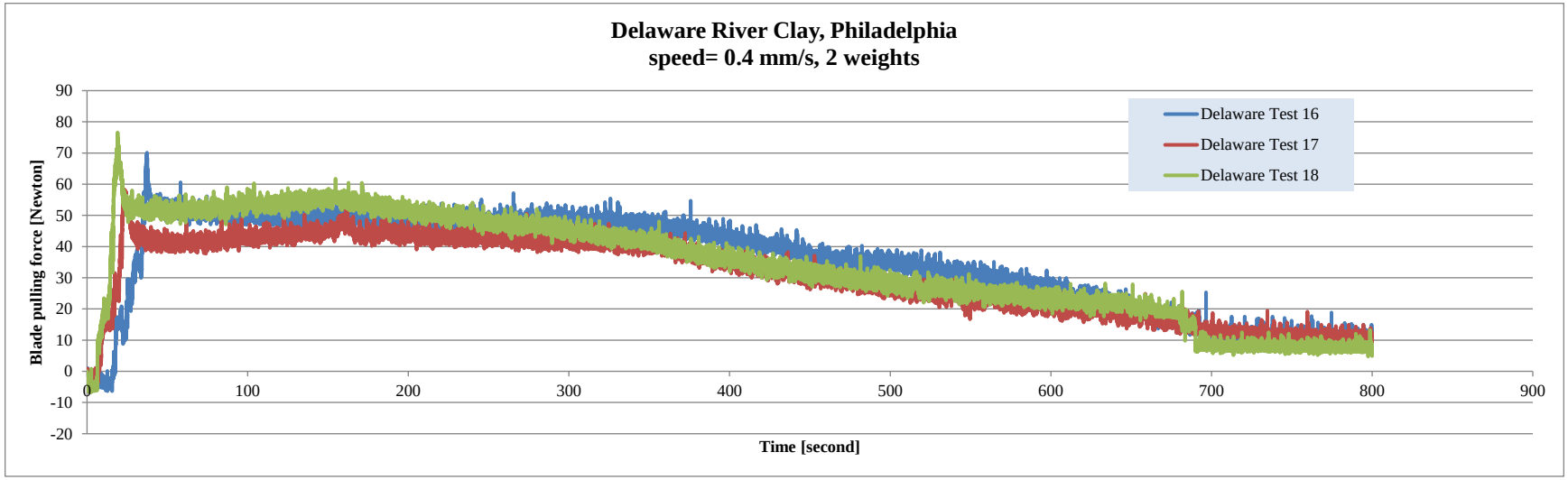
Delaware River Clay, Philadelphia
speed= 0.4 mm/s, 2 weights
Blade pulling force [Newton]
Time [second]
Delaware Test 16
Delaware Test 17
Delaware Test 18
90
80
70
60
50
40
30
20
10
0
-10
-20
0
100
200
300
400
500
600
700
800
900

10.10.2. Freeport grey clay adhesive test set-up graphs

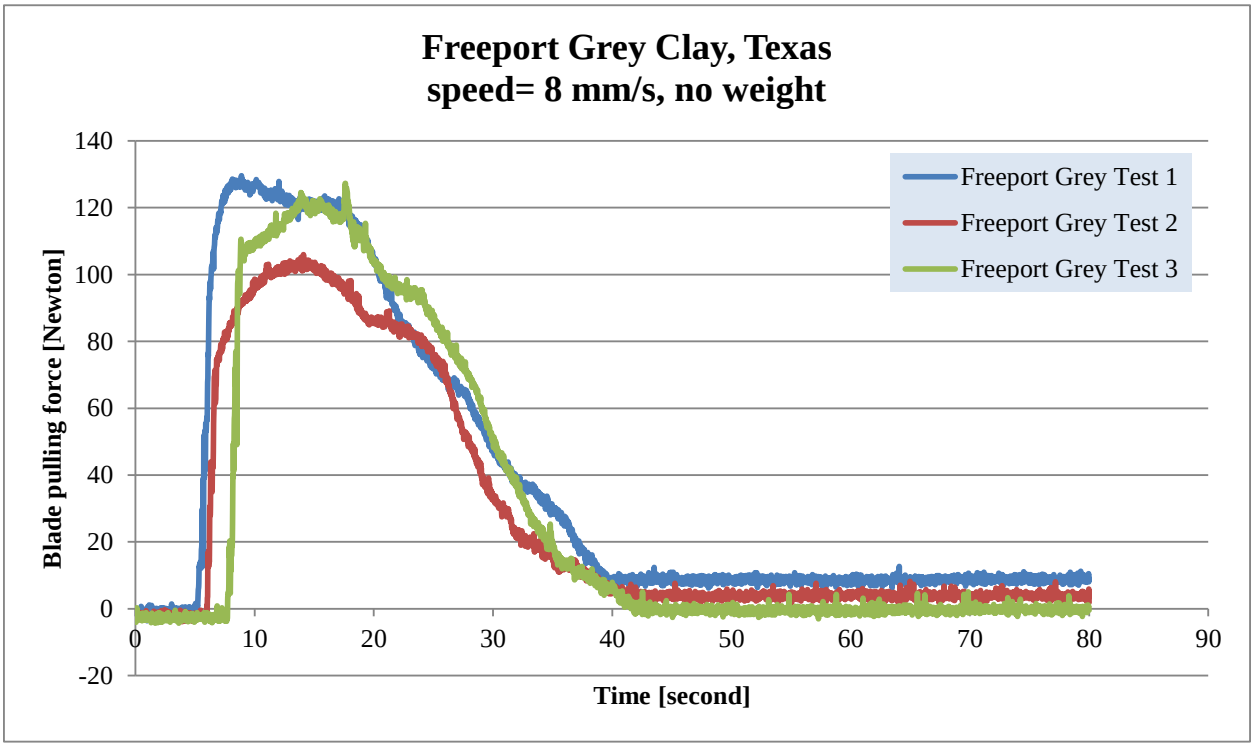

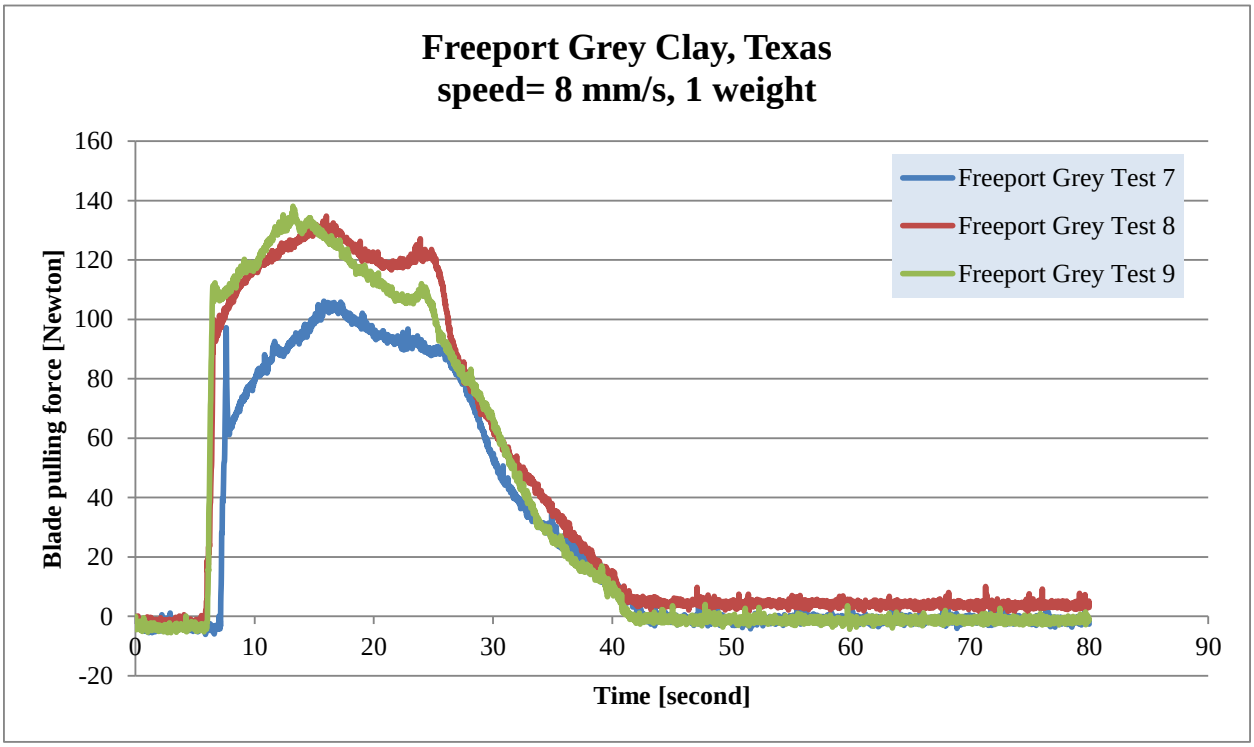

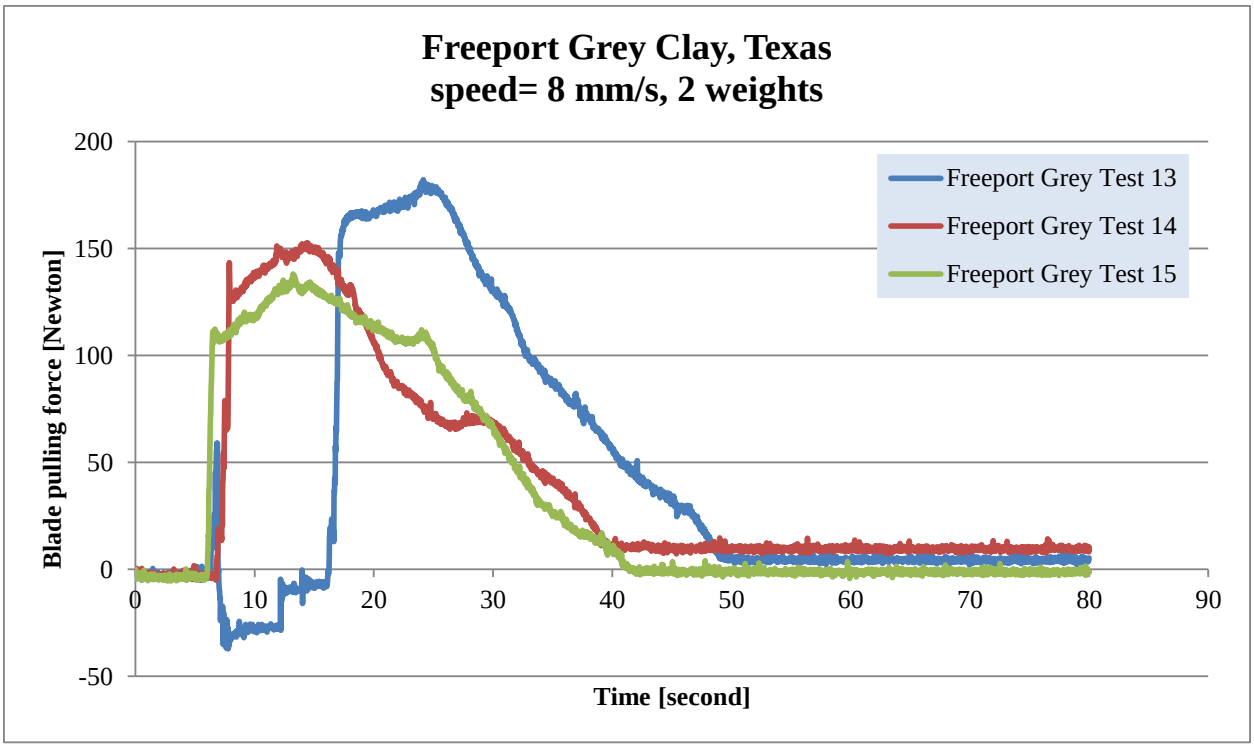
Freeport Grey Clay, Texas
speed= 8 mm/s, 2 weights
Blade pulling force [Newton]
Time [second]
Freeport Grey Test 13
Freeport Grey Test 14
Freeport Grey Test 15
200
150
100
50
0
-50
0
10
20
30
40
50
60
70
80
90

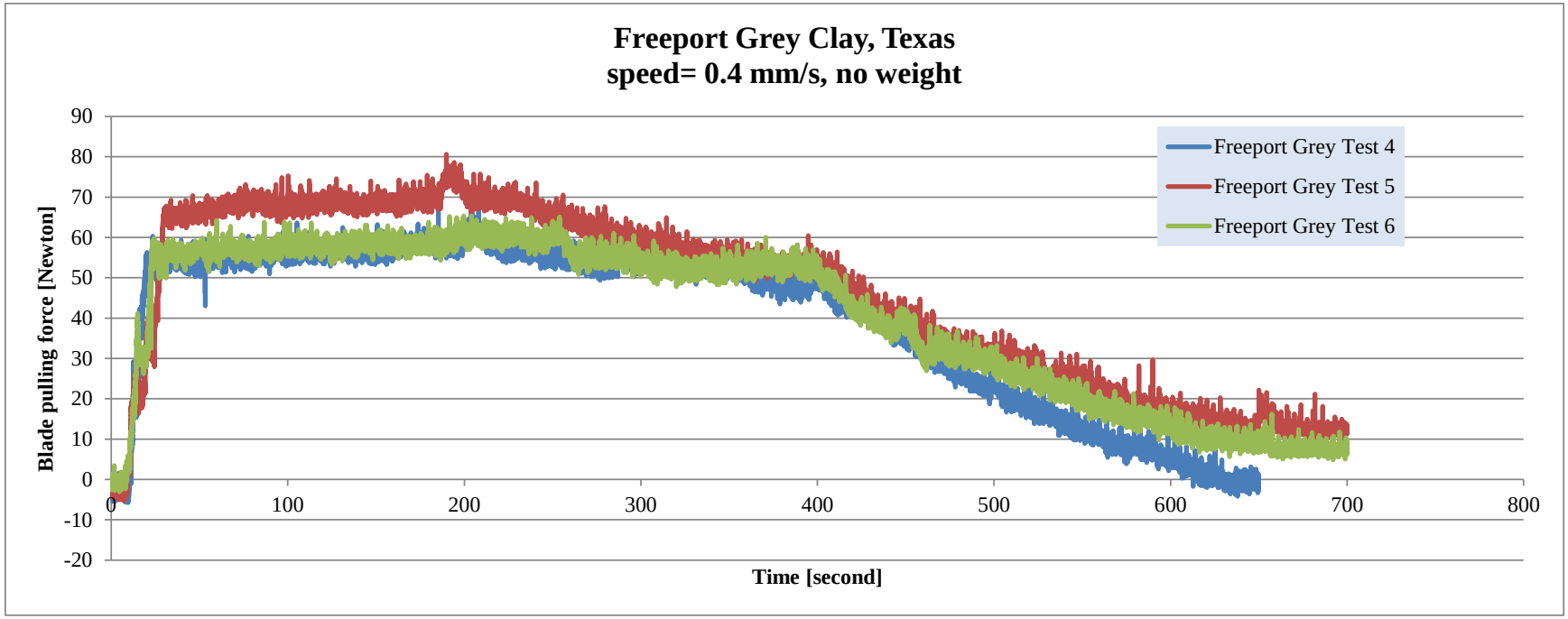
Freeport Grey Clay, Texas
speed= 0.4 mm/s, no weight
Blade pulling force [Newton]
90
80
70
60
50
40
30
20
10
0
-10
-20
0
100
200
300
400
500
600
700
800
Time [second]
Freeport Grey Test 4
Freeport Grey Test 5
Freeport Grey Test 6

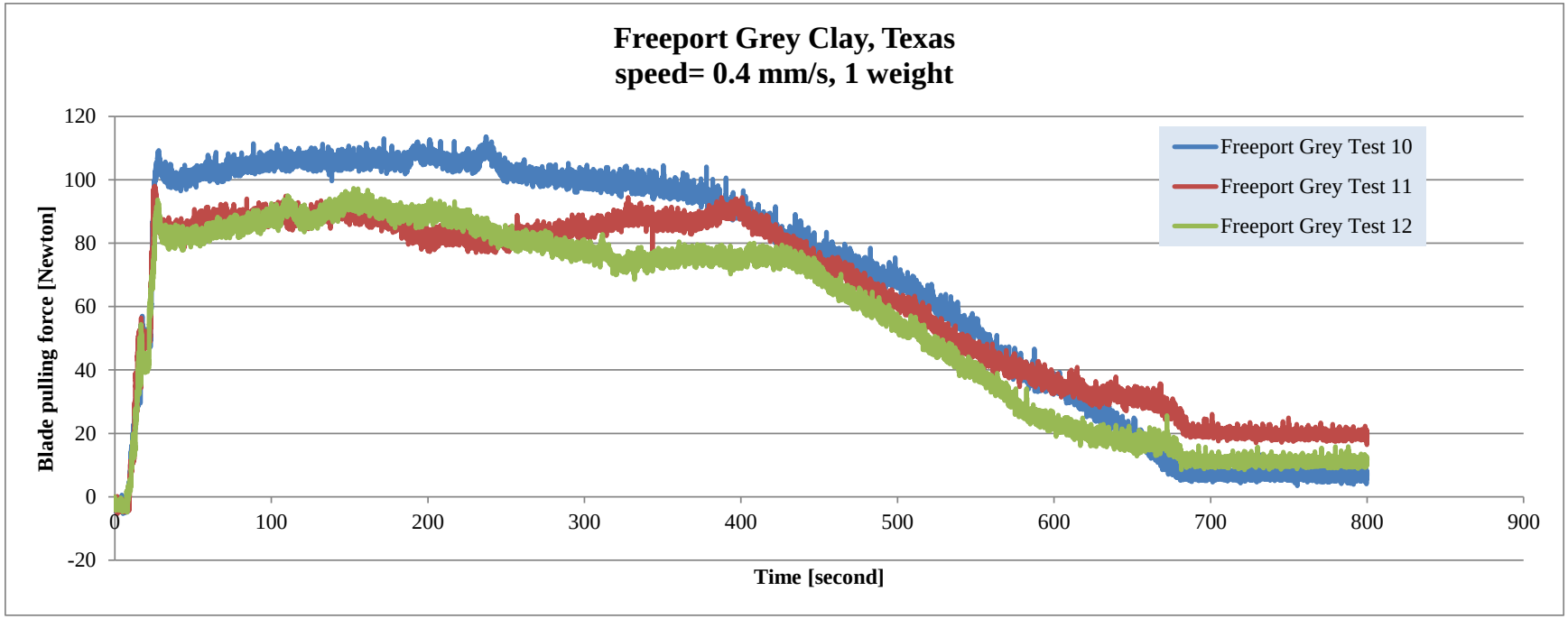
Freeport Grey Clay, Texas
speed= 0.4 mm/s, 1 weight
Blade pulling force [Newton]
120
100
80
60
40
20
0
-20
0
100
200
300
400
500
600
700
800
900
Time [second]
Freeport Grey Test 10
Freeport Grey Test 11
Freeport Grey Test 12

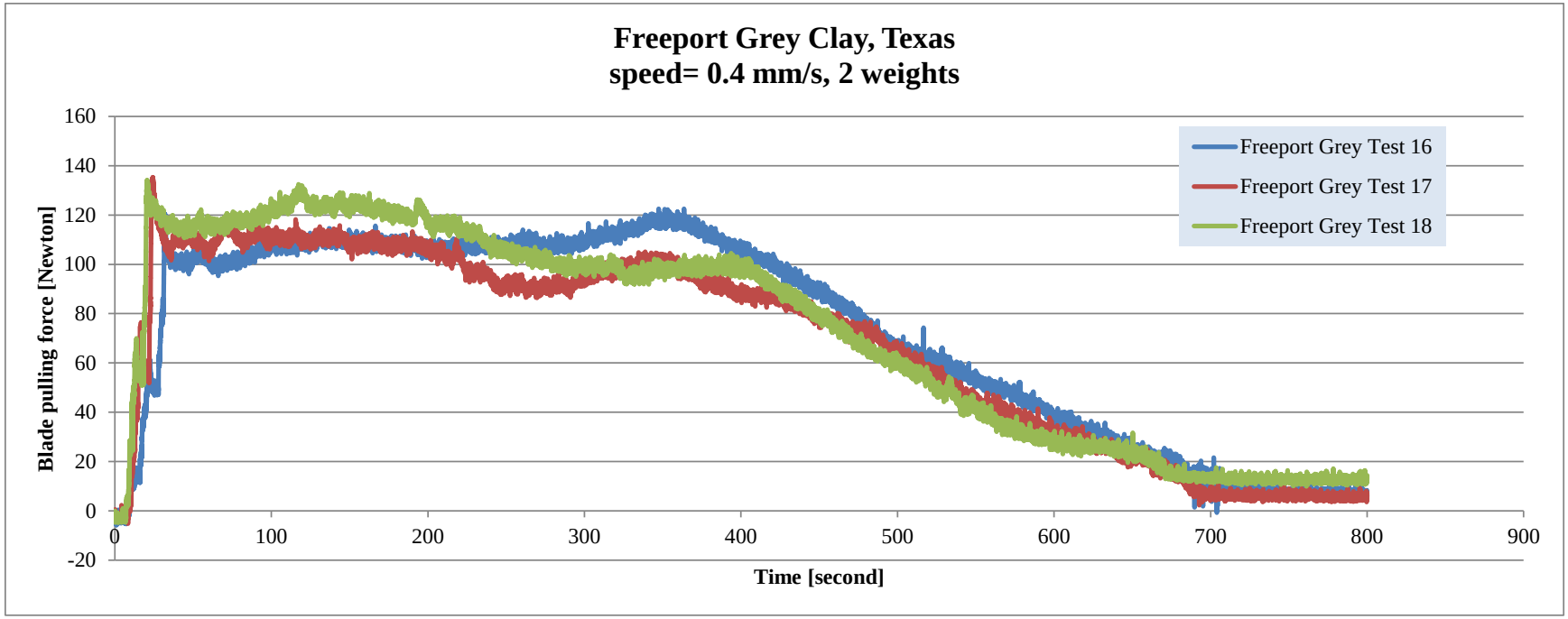
Freeport Grey Clay, Texas
speed= 0.4 mm/s, 2 weights
Blade pulling force [Newton]
160
140
120
100
80
60
40
20
0
-20
0
100
200
300
400
500
600
700
800
900
Time [second]
Freeport Grey Test 16
Freeport Grey Test 17
Freeport Grey Test 18

10.10.3. Freeport red clay adhesive test set-up graphs

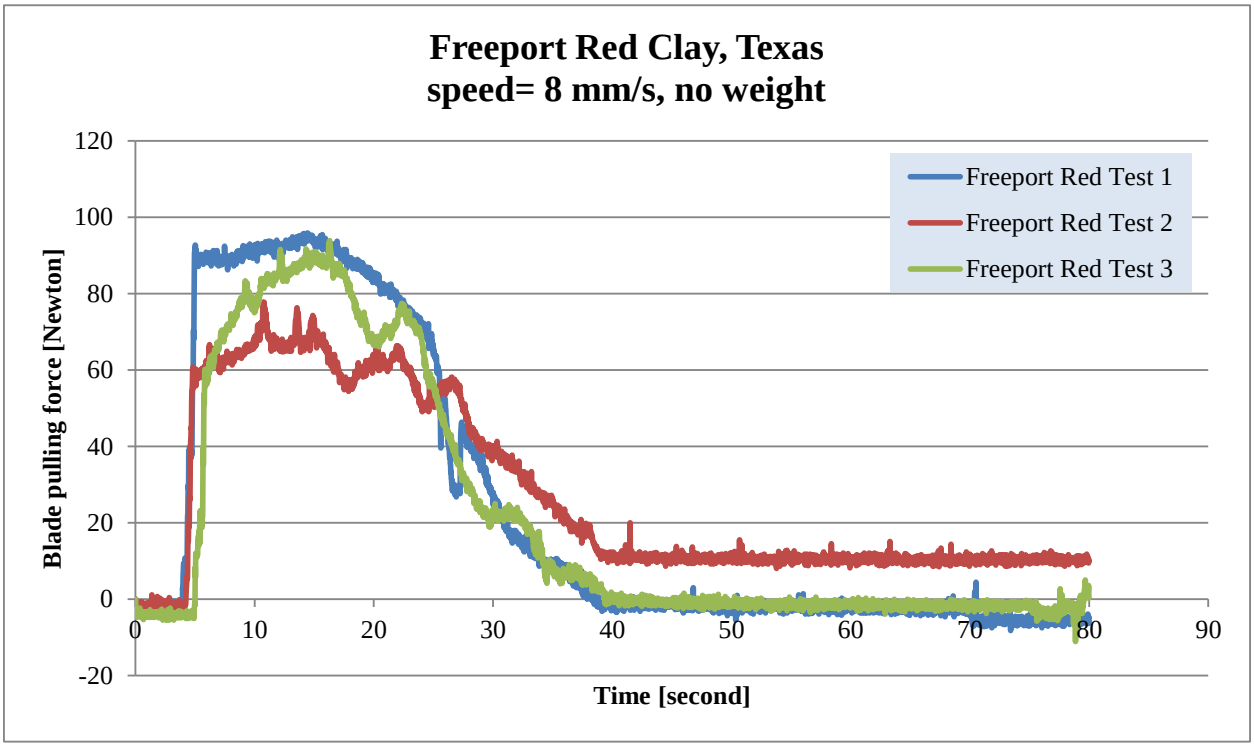

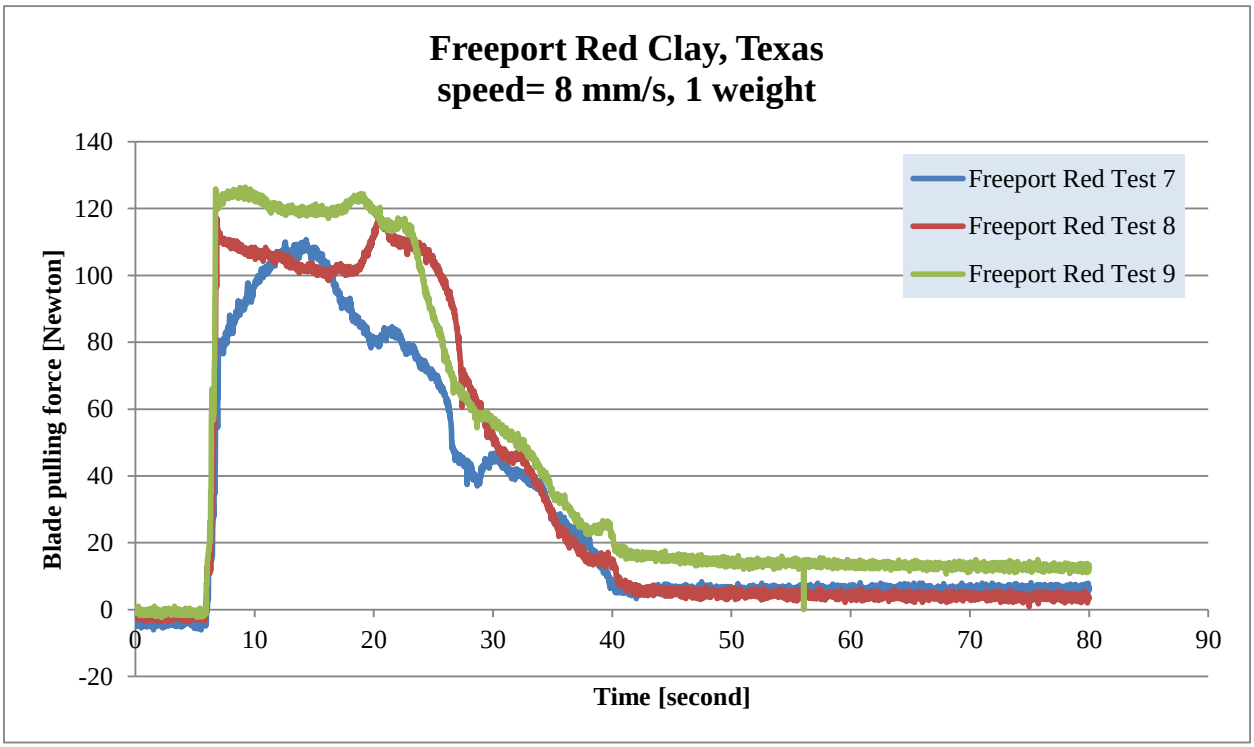

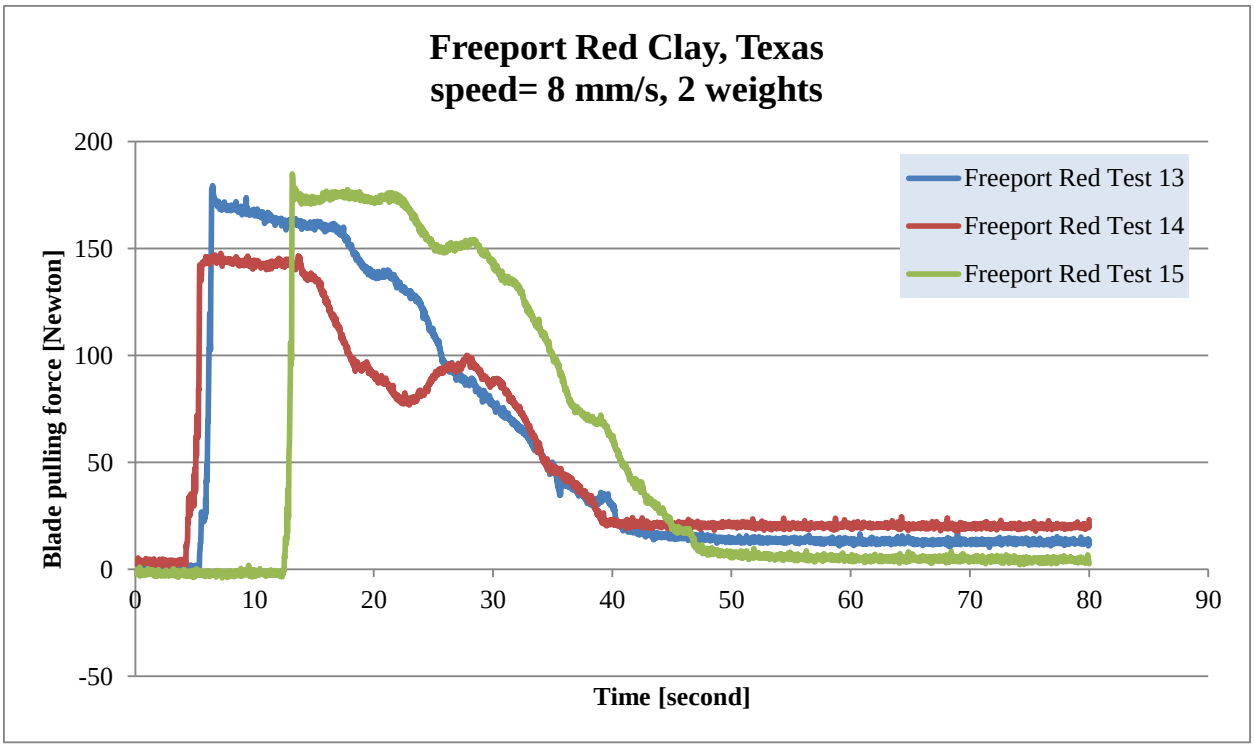
Freeport Red Clay, Texas
speed= 8 mm/s, 2 weights
Blade pulling force [Newton]
200
150
100
50
0
-50
0
10
20
30
40
50
60
70
80
90
Time [second]
Freeport Red Test 13
Freeport Red Test 14
Freeport Red Test 15

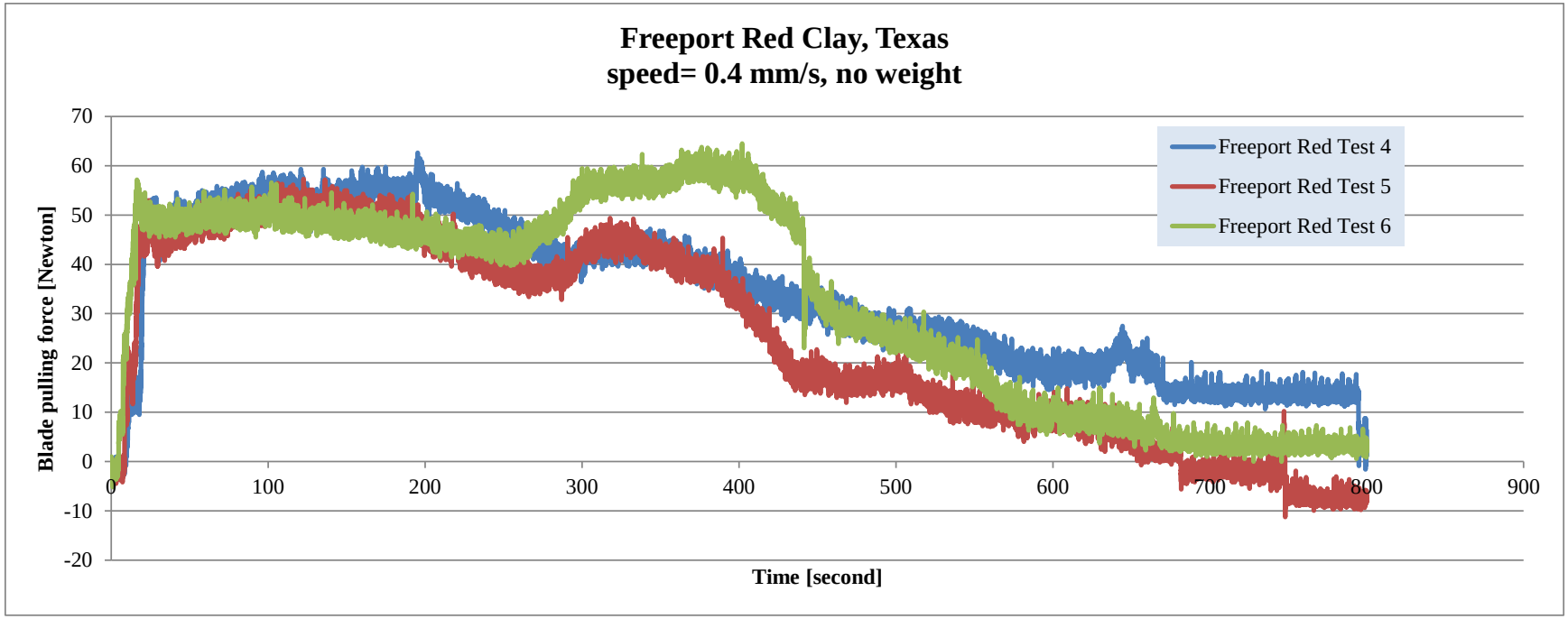
Freeport Red Clay, Texas
speed= 0.4 mm/s, no weight
Blade pulling force [Newton]
70
60
50
40
30
20
10
0
-10
-20
0
100
200
300
400
500
600
700
800
900
Time [second]
Freeport Red Test 4
Freeport Red Test 5
Freeport Red Test 6

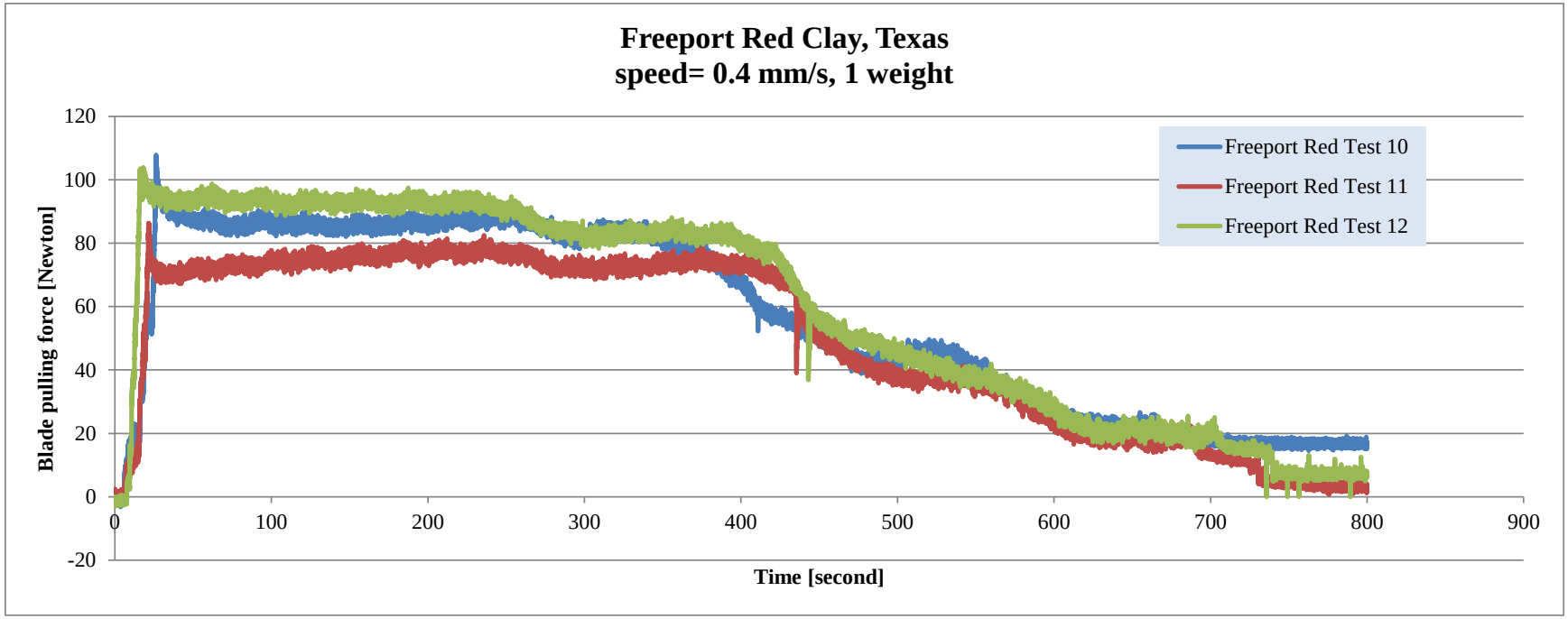
Freeport Red Clay, Texas
speed= 0.4 mm/s, 1 weight
Blade pulling force [Newton]
120
100
80
60
40
20
0
-20
0
100
200
300
400
500
600
700
800
900
Time [second]
Freeport Red Test 10
Freeport Red Test 11
Freeport Red Test 12

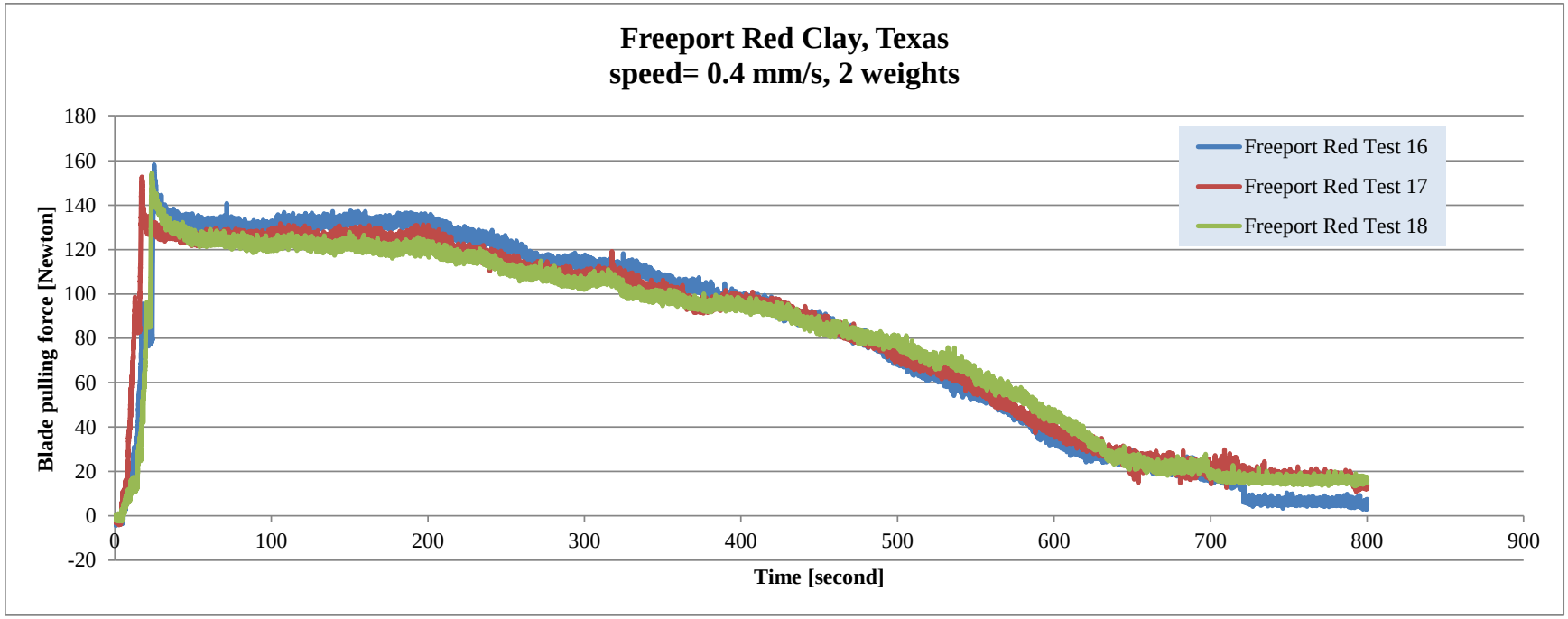
Freeport Red Clay, Texas
speed= 0.4 mm/s, 2 weights
Blade pulling force [Newton]
180
160
140
120
100
80
60
40
20
0
-20
0
100
200
300
400
500
600
700
800
900
Time [second]
Freeport Red Test 16
Freeport Red Test 17
Freeport Red Test 18

10.11. Appendix K

10.11.1. GLX CCS 32 output

Original value	BW	6.57	BW=2	BW=4	BW=6	BW=8	BW=10
	COG	(0.59;2.29)	(0.62;2.17)	(0.65;2.06)	(0.68;2.01)	(0.71;2.01)	(0.74;2.01)
TIME	s	20.33	20.33	20.33	20.34	20.34	20.35
X-LIP	m	0	0	0	0	0	0
Y-LIP	m	-0.21	-0.23	-0.24	-0.26	-0.28	-0.29
SITU PRODUCTION	m^3	2.35	2.59	2.82	3.07	3.31	3.58
WINCH POWER	kW	106.16	116.14	123.9	135.02	141.6	151.82
SPECIFIC ENGERGY	kJ/m^3	507.09	510.91	513.43	515.98	513.41	512.53
PENETRATION DEPTH	m	0.006	0.016	0.025	0.033	0.042	0.05
TOTAL STICKY EFFECT	kN	27	31	34	38	41	45
UPPERBLOCK SPEED	m/sec	0.284	0.289	0.295	0.3	0.306	0.311
LOWERBLOCK SPEED	m/sec	0.066	0.07	0.075	0.08	0.085	0.089
ANGULAR VELOCITY	deg/sec	7.781	7.802	7.837	7.869	7.904	7.934
ROPE FORCE	kN	104	114	122	133	139	149
ARM FORCE	kN	148	162	173	188	197	212
TOTAL MASS	tons	19.709	21.707	23.707	25.707	27.707	29.707
TOTAL VOLUME	m^3	22.433	22.433	22.433	22.433	22.433	22.433

Percentages	BW		BW=2	BW=4	BW=6	BW=8	BW=10
	COG	Original	(0.62;2.17)	(0.65;2.06)	(0.68;2.01)	(0.71;2.01)	(0.74;2.01)
TIME	s	0	0	0	0.05	0.05	0.1
X-LIP	m	0	0	0	0	0	0
Y-LIP	m	0	9.52	14.29	23.81	33.33	38.1

SITU PRODUCTION	m^3	0	10.21	20	30.64	40.85	52.34
WINCH POWER	kW	0	9.4	16.71	27.19	33.38	43.01
SPECIFIC ENGERGY	kJ/m^3	0	0.75	1.25	1.75	1.25	1.07
PENETRATION DEPTH	m	0	166.67	316.67	450	600	733.33
TOTAL STICKY EFFECT	kN	0	14.81	25.93	40.74	51.85	66.67
UPPERBLOCK SPEED	m/sec	0	1.76	3.87	5.63	7.75	9.51
LOWERBLOCK SPEED	m/sec	0	6.06	13.64	21.21	28.79	34.85
ANGULAR VELOCITY	deg/sec	0	0.27	0.72	1.13	1.58	1.97
ROPE FORCE	kN	0	9.62	17.31	27.88	33.65	43.27
ARM FORCE	kN	0	9.46	16.89	27.03	33.11	43.24
TOTAL MASS	tons	0	10.14	20.29	30.43	40.58	50.73
TOTAL VOLUME	m^3	0	0	0	0	0	0

10.11.2. GLY CCS 32 output

Original value	BW	w=2,82	w=2,4	w=2,6	w=2,8	w=3,0	w=3,2	w=3.4
	TBS	s=0=6,8 m	s= -0,5	s= -0,25	s= 0,25	s=0,5	s=0,75	s=1,0
TIME	s	20.33	19.84	20.08	20.55	20.79	21.02	21.25
X-LIP	m	0	0	0	0	0	0	0
Y-LIP	m	-0.21	-0.26	-0.23	-0.2	-0.18	-0.16	-0.15
SITU PRODUCTION	m^3	2.35	2.11	2.23	2.44	2.55	2.64	2.73
WINCH POWER	kW	106.16	92.23	97.37	109.49	144.24	112.31	111.71
SPECIFIC ENGERGY	kJ/m^3	507.09	48682	497.33	518.65	529.23	537.45	545.05
PENETRATION DEPTH	m	0.006	0.02	0.014	0.008	0.002	0	0
TOTAL STICKY EFFECT	kN	27	34	31	26	23	20	18
UPPERBLOCK SPEED	m/sec	0.284	0.311	0.297	0.276	0.268	0.262	0.258
LOWERBLOCK SPEED	m/sec	0.066	0.089	0.077	0.059	0.053	0.048	0.045
ANGULAR VELOCITY	deg/sec	7.781	7.935	7.847	7.719	7.673	7.637	7.612
ROPE FORCE	kN	104	91	96	108	112	111	110
ARM FORCE	kN	148	129	136	153	159	157	156
TOTAL MASS	tons	19.709	19.707	19.707	19.707	19.707	19.707	19.707
TOTAL VOLUME	m^3	22.433	14.018	17.911	25.316	30.453	36.115	42.324

Percentages	**BW**	**w=2,82**	**w=2,4**	**w=2,6**	**w=2,8**	**w=3,0**	**w=3,2**	**w=3.4**
	TBS	**s=0=6,8 m**	**s= -0,5**	**s= -0,25**	**s= 0,25**	**s=0,5**	**s=0,75**	**s=1,0**
TIME	s	0	-2.41	-1.23	1.08	2.26	3.39	4.53
X-LIP	m							
Y-LIP	m	0	23.81	9.52	-4.76	-14.29	-23.81	-28.57
SITU PRODUCTION	m^3	0	-10.21	-5.11	3.83	8.51	12.34	16.17
WINCH POWER	kW	0	-13.12	-8.28	3.14	35.87	5.79	5.23
SPECIFIC ENGERGY	kJ/m^3	0	9500.27	-1.92	2.28	4.37	5.99	7.49
PENETRATION DEPTH	m	0	233.33	133.33	33.33	-66.67	-100	-100
TOTAL STICKY EFFECT	kN	0	25.93	14.81	-3.7	-14.81	-25.93	-33.33
UPPERBLOCK SPEED	m/sec	0	9.51	4.58	-2.82	-5.63	-7.75	-9.15
LOWERBLOCK SPEED	m/sec	0	34.85	16.67	-10.61	-19.7	-27.27	-31.82
ANGULAR VELOCITY	deg/sec	0	1.98	0.85	-0.8	-1.39	-1.85	-2.17
ROPE FORCE	kN	0	-12.5	-7.69	3.85	7.69	6.73	5.77
ARM FORCE	kN	0	-12.84	-8.11	3.38	7.43	6.08	5.41
TOTAL MASS	tons	0	-0.01	-0.01	-0.01	-0.01	-0.01	-0.01
TOTAL VOLUME	m^3	0	-37.51	-20.16	12.85	35.75	60.99	88.67

10.11.3. GLZ CCS 32 output

Original value	Serrated blade	CA=3,5	CA =7	CA =7	CA =7	CA =7	CA =7
	Factor	sb=0	sb=0.9	sb=0.8	sb=0.7	sb=0.6	sb=0.5
TIME	s	20.33	20.33	20.32	20.3	20.28	20.26
X-LIP	m	0	0	0	0	0	0
Y-LIP	m	-0.21	-0.2	-0.22	-0.24	-0.27	-0.31
SITU PRODUCTION	m^3	2.35	2.32	2.58	2.91	3.33	3.9
WINCH POWER	kW	106.16	103.58	103.44	105.06	105.97	109.07
SPECIFIC ENGERGY	kJ/m^3	507.09	483.26	433.13	384.16	335.67	286.75
PENETRATION DEPTH	m	0.006	0.016	0.025	0.035	0.046	0.057
TOTAL STICKY EFFECT	kN	27	25	29	34	40	48
UPPERBLOCK SPEED	m/sec	0.284	0.267	0.27	0.274	0.278	0.284
LOWERBLOCK SPEED	m/sec	0.066	0.052	0.055	0.058	0.062	0.066
ANGULAR VELOCITY	deg/sec	7.781	7.675	7.695	7.719	7.745	7.776
ROPE FORCE	kN	104	102	102	103	104	107
ARM FORCE	kN	148	145	144	147	148	152
TOTAL MASS	tons	19.709	19.707	19.707	19.707	19.707	19.707
TOTAL VOLUME	m^3	22.433	22.433	22.433	22.433	22.433	22.433

Percentages	Serrated blade	CA=3,5	CA =7	CA =7	CA =7	CA =7	CA =7
	Factor	sb=0	sb=0.9	sb=0.8	sb=0.7	sb=0.6	sb=0.5
TIME	s	0	0	-0.05	-0.15	-0.25	-0.34
X-LIP	m						
Y-LIP	m	0	-4.76	4.76	14.29	28.57	47.62
SITU PRODUCTION	m^3	0	-1.28	9.79	23.83	41.7	65.96
WINCH POWER	kW	0	-2.43	-2.56	-1.04	-0.18	2.74
SPECIFIC ENGERGY	kJ/m^3	0	-4.7	-14.59	-24.24	-33.8	-43.45
PENETRATION DEPTH	m	0	166.67	316.67	483.33	666.67	850
TOTAL STICKY EFFECT	kN	0	-7.41	7.41	25.93	48.15	77.78
UPPERBLOCK SPEED	m/sec	0	-5.99	-4.93	-3.52	-2.11	0
LOWERBLOCK SPEED	m/sec	0	-21.21	-16.67	-12.12	-6.06	0
ANGULAR VELOCITY	deg/sec	0	-1.36	-1.11	-0.8	-0.46	-0.06
ROPE FORCE	kN	0	-1.92	-1.92	-0.96	0	2.88
ARM FORCE	kN	0	-2.03	-2.7	-0.68	0	2.7
TOTAL MASS	tons	0	-0.01	-0.01	-0.01	-0.01	-0.01
TOTAL VOLUME	m^3	0	0	0	0	0	0

10.11.4. GLXYZ CCS 32 output

	CA	CA=3,5	CA =7	CA =7	CA =7	CA =7	CA =7	CA =7
	Serrated blade	**sb=0**	**sb=0.9**	**sb=0.8**	**sb=0.7**	**sb=0.6**	**sb=0.5**	**sb=0.5**
	BW	**w=2,82**	**w=2,4**	**w=2,6**	**w=2,8**	**w=3,0**	**w=3,2**	**w=3.4**
	TBS	**s=0=6,8 m**	**s= -0,5**	**s= -0,25**	**s= 0,25**	**s=0,5**	**s=0,75**	**s=1,0**
	BW	**6.57**	**BW=2**	**BW=4**	**BW=6**	**BW=8**	**BW=10**	**BW=10**
Original value	**COG**	**(0.59;2.29)**	**(0.62;2.17)**	**(0.65;2.06)**	**(0.68;2.01)**	**(0.71;2.01)**	**(0.74;2.01)**	**(0.74;2.01)**
TIME	s	20.33	19.91	20.13	20.59	20.81	21.02	21.26
X-LIP	m	0	0	0	0	0	0	0
Y-LIP	m	-0.21	-0.27	-0.28	-0.29	-0.32	-0.6	-0.33
SITU PRODUCTION	m^3	2.35	2.29	3.01	3.96	5.16	6.91	7.16
WINCH POWER	kW	106.16	93.81	115.22	141.28	157.92	189.14	194.86
SPECIFIC ENGERGY	kJ/m^3	507.09	467.49	414.85	400.14	353.06	298.95	307.38
PENETRATION DEPTH	m	0.006	0.038	0.05	0.063	0.078	0.095	0.09
TOTAL STICKY EFFECT	kN	27	36	41	45	53	64	59
UPPERBLOCK SPEED	m/sec	0.284	0.299	0.294	0.279	0.275	0.272	0.262
LOWERBLOCK SPEED	m/sec	0.066	0.07	0.075	0.062	0.059	0.057	0.048
ANGULAR VELOCITY	deg/sec	7.781	7.847	7.82	7.73	7.704	7.693	7.63
ROPE FORCE	kN	104	92	113	139	155	186	192
ARM FORCE	kN	148	131	161	197	220	264	272
TOTAL MASS	tons	19.709	21.687	23.687	25.687	27.687	29.687	29.687
TOTAL VOLUME	m^3	22.433	14.018	17.939	25.316	30.453	36.115	42.324

	CA	ca=3,5	ca =7	ca =7	ca =7	ca =7	ca =7	ca =7
	Serrated blade	sb=0	sb=0.9	sb=0.8	sb=0.7	sb=0.6	sb=0.5	sb=0.5
	BW	w=2,82	w=2,4	w=2,6	w=2,8	w=3,0	w=3,2	w=3.4
	TBS	s=0=6,8 m	s= -0,5	s= -0,25	s= 0,25	s=0,5	s=0,75	s=1,0
	BW	6.57	BW=2	BW=4	BW=6	BW=8	BW=10	BW=10
Percentages	COG	(0.59;2.29)	(0.62;2.17)	(0.65;2.06)	(0.68;2.01)	(0.71;2.01)	(0.74;2.01)	(0.74;2.01)
TIME	s	0	-2.07	-0.98	1.28	2.36	3.39	4.57
X-LIP	m	0	0	0	0	0	0	0
Y-LIP	m	0	28.57	33.33	38.1	52.38	185.71	57.14
SITU PRODUCTION	m^3	0	-2.55	28.09	68.51	119.57	194.04	204.68
WINCH POWER	kW	0	-11.63	8.53	33.08	48.76	78.17	83.55
SPECIFIC ENGERGY	kJ/m^3	0	-7.81	-18.19	-21.09	-30.38	-41.05	-39.38
PENETRATION DEPTH	m	0	533.33	733.33	950	1200	1483.33	1400
TOTAL STICKY EFFECT	kN	0	33.33	51.85	66.67	96.3	137.04	118.52
UPPERBLOCK SPEED	m/sec	0	5.28	3.52	-1.76	-3.17	-4.23	-7.75
LOWERBLOCK SPEED	m/sec	0	6.06	13.64	-6.06	-10.61	-13.64	-27.27
ANGULAR VELOCITY	deg/sec	0	0.85	0.5	-0.66	-0.99	-1.13	-1.94
ROPE FORCE	kN	0	-11.54	8.65	33.65	49.04	78.85	84.62
ARM FORCE	kN	0	-11.49	8.78	33.11	48.65	78.38	83.78
TOTAL MASS	tons	0	10.04	20.18	30.33	40.48	50.63	50.63
TOTAL VOLUME	m^3	0	-37.51	-20.03	12.85	35.75	60.99	88.67